University of Glasgow

Estell, Christopher (2018) *Do erythrocytic miRNA have a function?*
PhD thesis.

https://theses.gla.ac.uk/8899/

Do erythrocytic miRNA have a function?

Christopher Estell
BSc (hons), MRes

Submitted in fulfilment of the requirements for the degree
of Doctor of Philosophy

December 2017

Section of Experimental Haematology
Institute of Cancer Sciences
College of Medical, Veterinary and Life Sciences
University of Glasgow

Acknowledgement

I would like to dedicate this thesis to my family who have stood by me, both financially and emotionally, during my rather protracted university career. Special thanks to my Nan and Grandad, who have no idea what I'm doing, but are happy that I'm happy. You have been stalwarts throughout my life, not just this studentship and I am beyond fortunate to have you in my life. Thanks to my Mother, I can't actually think of the words to put down and instead have a tear in my eye. Thank you, thank you, thank you, thank you. Thanks to Ian for meeting my mum, supporting me and most importantly, welcoming me and my brothers into the family. Thank you Dad and second-mum for all the help during my time at Uni, I doubt I would be here today without your intervention back in the day. Thank you to my GREAT aunt Margaret and Brian who have been beyond generous to me, and for looking after my grandad. Thank you to my sisters, brothers, the fabby one, kitten, Schrody, the lot. Thank you to my beautiful partner Ana, you have been a rock.

I would also like to thank my supervisors for having the patience to have me in your lab for 5 years. A special thanks to Helen who has been beyond generous, thank you Andrew – as it was talking to this gruff curmudgeon during my MRes that I fell back in love with Science. Thank you to Mhairi for taking a chance on a loud mouth. Thank you to the managerial board of the Paul O'Gorman (Tessa, Alison "boo's not as cute as schrody" Michie, Karen [also for the Irish momma hugs], Heather, Vignir, Xu, Helen, Mhairi) for funding me and genuinely making my time at the POG so enjoyable! Thank you Torsten, Angela, Diane, Jean and everyone else I have worked with.

Big shout out to my lab, working with these guys/gals has made my time so much easier, Dr Dr Horne (please stop drawing obscenities on my lap top), Tractor (AKA Ross), Vic, Heather Mo, #POD5 (Mara, Cat, Kai-monster, Jenny, FRIEND, Deem, Jo – I can't wait to see what my celebratory vegetable will be), Jen, Alan. If I've forgotten anyone, it wasn't on purpose, honest!

A final thanks to my Gran, Shirley, who sadly couldn't see me complete this journey.

Author's Declaration

I declare that, except where explicit reference is made to the contribution of others, that this thesis is the result of my own work and has not been submitted for any other degree at the University of Glasgow or any other institution.

Abstract

Despite being translationally null, erythrocytes contain miRNA at concentrations equal to nucleated cells, meaning that of the miRNA found in peripheral blood ~ 99 % is located in red cells. Despite this huge abundance, the literature currently regards erythrocytic miRNA (e-miRNA) as redundant. Data from Hamilton lab challenges this notion as it shows that e-miRNA are stable, maintain a catalytic potential, and have sequence profiles similar across species, indicating conservation. This thesis investigates what the potential function of e-miRNA could be, both within erythrocytes and in other cells. To develop hypotheses, RISC-protein interactions were evaluated unearthing the appearance of an apparently post-translationally modified AGO2; what this modification is, remains to be defined. As part of a homeostatic hypothesis, the idea that e-miRNA may act as a molecular signal and regulate the transcriptome of phagocytosing cells was evaluated. However, it was discovered that e-miRNA are lost as RBCs age, potentially through vesicularisation. The differences between RBC vesicles that occur *in vivo* and those that occur when blood is stored ready for transfusion were evaluated. This highlighted a potential artefact within the literature with regards to what is termed as "microvesicles" (MVs). The clinical concern regarding storage MVs was evaluated through the generation of a phago/endocytosis model, and consistent with recent publications, no mal-effect was observed. This portion of the study highlighted a secondary structure within macrophages that is not a phagolysosome, but does process internalised RBC-MVs.

Contents

List of Tables

List of Figures

.

Chapter 1   **Introduction**

1.1 **Preface**

"the life of a creature is in the blood", Leviticus 17:11

Blood, few biological substances appear to have as much cultural or scientific significance as blood. In ancient times, it is rumoured that the Egyptians bathed in blood due to its perceived regenerative properties, while Vikings supposedly drank the blood of their victims from skull cups to imbue them with the strength of the fallen. While these practices, if ever true, have fallen into antiquity, some beliefs have not - clearly shaping societies through the generations. For example, Melihah is the Jewish tradition of removing blood from fresh meat. This practice, carried out due to passages within Leviticus and Deuteronomy, is still performed today. Indeed, blood is central to the practices of other religions, with the same passages responsible for Jehovah's Witnesses refusing blood transfusions. Out with religion, blood is still in societies general conscious with ancient phrases such as "blood is thicker than water", "it's in his/her blood", "hot blooded", "blood ran cold" still used. In fact, socially, blood has had somewhat of a renaissance, from the blood drinking vampires that appear in the Twilight saga, to the Blood Riders of the Khaleesi Daenerys Targaryen.

Unsurprisingly, with the cultural significance that blood has, there has also been acute scientific interest. Possibly the earliest "report" of blood, that while misguided, may be anchored in fact, was by Hippocrates, a proponent of Humorism. He believed that bodily fluids were comprised of four humors: black bile, phlegm, yellow bile and blood; imbalances of which, lead to morbidity. Fåhræus, discoverer of the erythrocyte sedimentation rate, noted that when blood was allowed to settle, diseased blood separated differently from healthy[1]. Healthy blood was observed to separate slowly, meaning that coagulation occurs when platelets are interspersed with erythrocytes. However, in certain conditions (different infectious diseases were evaluated, Westergen looked at tuberculosis infections) erythrocytes were found to sediment faster than normal and reach the bottom of the tube before clotting could occur[2]. This meant that the fibrin clot would agglutinate the slower sedimenting leukocytes (instead of erythrocytes) and the clot would appear grey / white, not red. He speculated that the black

sediment (deoxidised haemoglobin), blood (erythrocytes), anaemic clots (clotted leukocytes) and plasma were the origin of Hippocrates humors. Over time, Humorism waned, although the link between blood and life continued, with early haematological work focusing on transfusion. The earliest recorded human transfusion was performed by Jean-Baptiste Denis in the 16th century and amazingly involved lambs blood[3]. Xenotransfusions were soon banned, and though transfusion research continued over the centuries, it wasn't before the discovery of blood groups in 1901 by Karl Landsteiner that they started to become safer[4].

In 1843, the first leukocytes were observed by microscope[5]. This led to our understanding that, at a cellular level, blood is heterogeneous, allowing research to focus on individual cell types. Possibly due to their abundance, red blood cells (RBCs) have been extensively studied throughout the years. Indeed, so extensive is the research, and limited their *modus operandi*, that one may be forgiven for thinking they no longer hold any secrets. So it was surprising, that in 2006 Rathjen *et al.* reported the presence of micro RNA (miRNA) within mature erythrocytes[6]. This was surprising as ostensibly miRNA regulate translation, something that does not occur within mature erythrocytes[7]. Further characterisation by the Hamilton Lab (unpublished) revealed that these miRNAs had catalytic potential, were highly abundant and were apparently conserved across vertebrata (discussed later in Figure **13**). All of which suggested a function for these miRNA, and served as the foundation for this thesis. However, before the aims of this project are discussed, the main biological players found herein will be discussed.

1.1.1 Non-coding RNA (ncRNA)

As the name indicates, non-coding (nc) RNA are a family of RNAs that are not translated, separating them from their coding counterparts: messenger RNA (mRNA). The ncRNA family is much larger than its coding counterpoint and is involved in a plethora of different functions.

1.1.1.1 Ribosomal RNA

Ribosomal RNA (rRNA) is the most abundant RNA within a cell, comprising ~80-90 % of its total RNA. Mammals have 4 main rRNA, the 28s, 18s and 5.8s rRNAs, which are transcribed by RNA polymerase I, while the 5s rRNA is transcribed by

RNA polymerase III; two mitochondrial rRNAs (12s and 16s) are also present[8]. The "s" stands for Svedberg, which is a measure of sedimentation speed, meaning rRNAs are named after their size. The 4 main rRNAs, together with ribosomal proteins, come together to form ribosomes within the cytoplasm. Ribosomes comprise of "large" and "small subunits", with the large subunit containing the 5s, 5.8s and 28s rRNAs, and the small subunit, the 18s species only[8]. In Mammalia, the main function of rRNA appears structural, while in prokaryotes the 16s rRNA recognises the Shine-Dalgarno sequence within mRNA and plays a role in translation initiation[9].

1.1.1.2 **tRNA**

Transport RNA (tRNA) is another species of abundant (4-10 %) ncRNA within a cell. There are ~ 513 nuclear tRNA genes within the human genome, which are responsible for binding amino acids (aa), and binding to triplet-codons within translating mRNA[10]. tRNA are transcribed as primary transcripts that undergo maturation before forming the classic cloverleaf configuration (Figure 1). While in the nucleus tRNA nucleotidyltransferases add a non-templated CCA motif to the 3' end[11]. The nucleotide immediately prior to this motif (N73), in addition to the anti-codon sequence, is recognised by one of 20 aminoacyl transferases, which covalently attach its specific aa to the terminal adenosine[12]. "Charged" tRNA, aa bound tRNA, then interact with Eukaryotic Elongation Factor 1 A-1 (EF1A), position themselves at the ribosomal entry site (A-site) and bind to the appropriate mRNA codon, allowing for translation to occur[13].
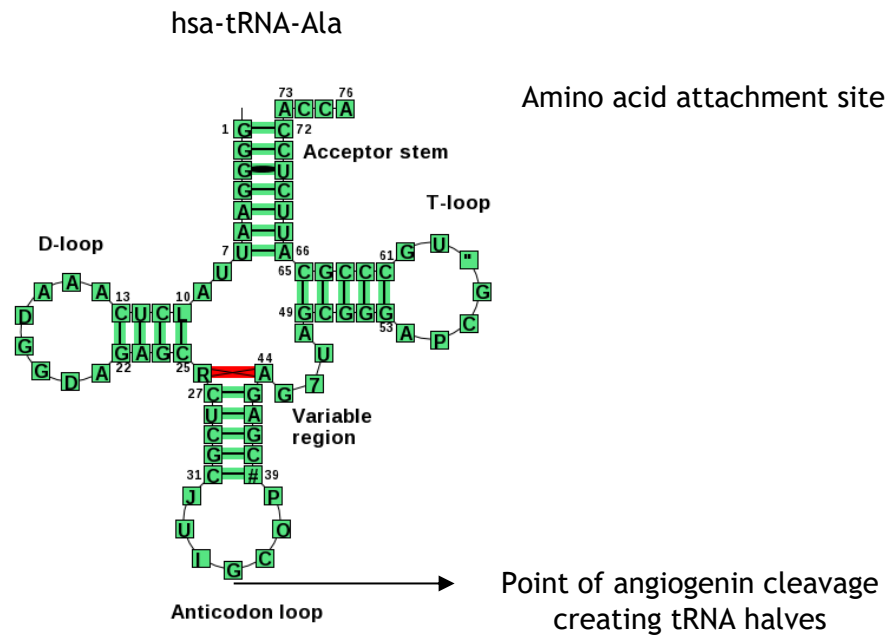
Figure 1: Sequence and secondary structure of human alanine tRNA.
Sequence ID from tRNA database (University of Leipzig) is tdbR00000017, structure was drawn by their software. Non-standard nucleotides represent the following modifications: " = 1-methyladenosine, P = pseudouridine, 7 = 7-methylguanosine, # = 2'0-methylguanosine, O = 1-methylinosine, I = inosine, J = 2'0-methyluridine, R = N2.N2-dimethylguanosine, D = dihydrouridine, L = N2-methylguanosine

1.1.1.3 Long non-coding RNAs

Long (l)ncRNAs are a family of RNAs that are similar to their messenger counterparts, but critically, due to lack of open reading frame (ORF), are not translated. They are arbitrarily classified as being $\geq$ 200 nucleotides (nt) in length, which differentiates them from small ncRNAs[14]. They are mostly transcribed by RNA polymerase (pol) II, and as such share mRNA characteristics: 5' 7-methylguanylate cap, 3' poly(A) tail, contain introns/exons and can undergo splicing[15-17]. Functionally, they are diverse and have been reported to be involved in epigenetic regulation, alternative splicing, transcriptional regulation, post transcriptional regulation, or, act as miRNA sponges[18-22]. This broad range of function make it difficult to ascertain what individual lncRNA do, which is the likely reason so few have been studied mechanistically, although this is changing.

1.1.1.4 Small non-coding RNAs

Contrary to lncRNA, the small non-coding RNA (sRNA) family are $\leq$ 200 nt in length and members include micro-RNA (miRNA), piwi-interacting-RNA (piRNA),

small nucleolar RNA (snoRNA), small interfering RNA (siRNA), y-RNA (Y1, 2, 3 & 5) vault RNA (vtRNA) and small nuclear RNA (snRNA).

snoRNA

snoRNA are a class of sRNA that reside predominantly within the nucleoli of a cell and are involved in site-specific RNA modifications; classically this has been associated with rRNA, but mRNA and snRNA modifications have also been reported[23]. The snoRNA class is split into two types: C/D box snoRNAs, contain highly conserved C (UGAUGA) and D (GUCUGA) boxes at the 5' and 3' end of the RNA, while H/ACA snoRNAs contain a large hairpin structure (H) and a 3' ACA motif[24,25]. When bound as a ribonucleoprotein (RNP) complex, both snoRNAs act as guides to specific RNA positions, allowing for 2'O-methylation or pseudouridylation to occur[26,27]. As ever, there are oddities, with snoRNA U85 RNPs possessing both pseudouridylation and 2'O-methylation abilities due to them containing both C/D and H/ACA boxes[23]. RNAs targeted by snoRNAs are predicted based on sequence complementarity, although this has limitations, as so called "orphans" exist where no targets can be predicted, suggesting either novel targets or redundancy[28].

snRNA

snRNA are a class of sRNAs that, when bound to proteins to form snRNPs, constitute either the major or minor spliceosome, which mediates mRNA maturation within the nucleoplasm[29]. As with snoRNA, snRNA are divided into two categories: Sm-class (U1, U2, U4, U4$_{atac}$, U5, U7 and U12) and Lsm-class (U6 and U6$_{atac}$). The Sm-class has a 3' stem loop, a 5' trimethylguanosine cap, and conserved Sm sites (AAUUUUUGG) that bind Sm proteins, while the Lsm-class, has a 5'-monomethylphosphate cap and a 3' uridyl tale that binds Lsm proteins[30]. Each snRNP is bound by 7 core Sm or Lsm proteins and is referred to as heteroheptameric; notably, U7 binds 5 of the core Sm proteins as well as 2 unique Sm members. snRNPs then bind together to form the major spliceosome, which is comprised of U1, U2, U4, U5 and U6 RNPs along with additional proteins (e.g. members of the *PRPF* family), or the minor spliceosome, which is comprised of U4$_{atac}$, U5, U6$_{atac}$, U11 and U12[30]. These large multiunit complexes facilitate splicing, with the RNA components of individual snRNPs either recognising 5' (U1)

or 3' (U2) splice sites, or recognising and binding other snRNPs (U2-U6)[31,32]. Greater than 95 % of splicing is carried out by the major spliceosome, which recognises so called "U2 introns", mRNAs with 5' intronic splice site GT/AG motifs, while the minor spliceosome, recognises U12 introns (5' AGC/CA); U7 snRNPs act individually to process histone mRNA[33-35].

<u>yRNA</u>

In humans, there are four yRNAs (Y1, Y2, Y3 and Y5) that are ~100 nt in length, are structured as stem loops and bind both La and Ro60 proteins to form RNPs[36]. The exact function of yRNA or the yRNPs is unclear, however, the most accepted theory is that yRNAs act as molecular chaperones for Ro60 and La, or, aid in their localisation[37,38]. When not bound to yRNA, Ro60 and La have been reported to recognise and bind misfolded / erroneous RNA, leading to their turnover[39,40]. Additional reports suggest that yRNA themselves, and not Ro60, play a role in DNA replication, although the mechanism of this has not been revealed[41-43]. Finally, in multiple studies, yRNA have been found to form fragments following stress[44]. At present there is no known function for these fragments, and while other small RNAs have been reported to enter the miRNA pathway (tRNA / snRNA), yRNA fragments do not associate with Argonaute (AGO) and are not capable of silencing luciferase constructs[45,46].

<u>piRNA</u>

Of all the ncRNA discussed, piRNA are the most analogous to the subject of this thesis (miRNA) as they are small (26-31 nt), bind a member of the AGO family (PiWi clade), carry a 3 prime 2'O methyl modification (unlike miRNA) and are involved in silencing[47,48]. However, unlike miRNA, piRNA are thought to be germline specific where they act to silence transposable elements; notably, at recent meetings, piRNA functioning within somatic tissues was discussed, but at the time of writing has not been published. Another difference between miRNA and piRNA is there genomic location. For example, hundreds of miRNA genes are dispersed throughout the genome, while in drosophila, piRNA map to only a few key locations. The largest of which (240 kb) is thought to be responsible for ~ 30 % all piRNA and the 15 largest loci responsible for up to 70 %; this is all the more astounding as there are reported to be ~ 13,000 unique piRNA within drsophila[49,50].

piRNA biogenesis has not been fully elucidated and review of the literature appears to show species-specific differences. However, consistently, there are two biogenesis pathways. In the primary pathway, large piRNA transcripts are fragmented by the endoribonuclease Zuchini, 5' ends recognised by a PiWi protein (e.g. Aubergine), 3' ends cleaved by Zuchini and / or trimmed before a terminal methyl group is added by the methyltransferase HEN1[51-54]. The secondary pathway was described by Brennecke *et al* as "ping pong amplification", in which specific piRNAs are amplified through interplay between sense and antisense transcripts loaded in AGO3 or PiWi proteins respectively; note that this pathway is commonly described in Drosophila and dmAGO3 is not analogous to human AGO3[50]. With regards to Figure **2**, when transposons are silenced (cleaved) by mature piRNA-PiWi complexes (i), resulting cleavage products can be bound by AGO3(ii). These fragments are trimmed (iii) and modified (iv) to form piRNA like molecules that are derived from the silenced transposon. Processed-fragment-AGO3 RNPs can recognise complementary sequences within primary piRNA transcripts, which it cleaves to form new piRNA substrates (v). The net result is that when a transposon is silenced, its degradative products feedback into piRNA biogenesis, so that piRNAs similar in sequence to the active transposon are generated, thus amplifying silencing potential.
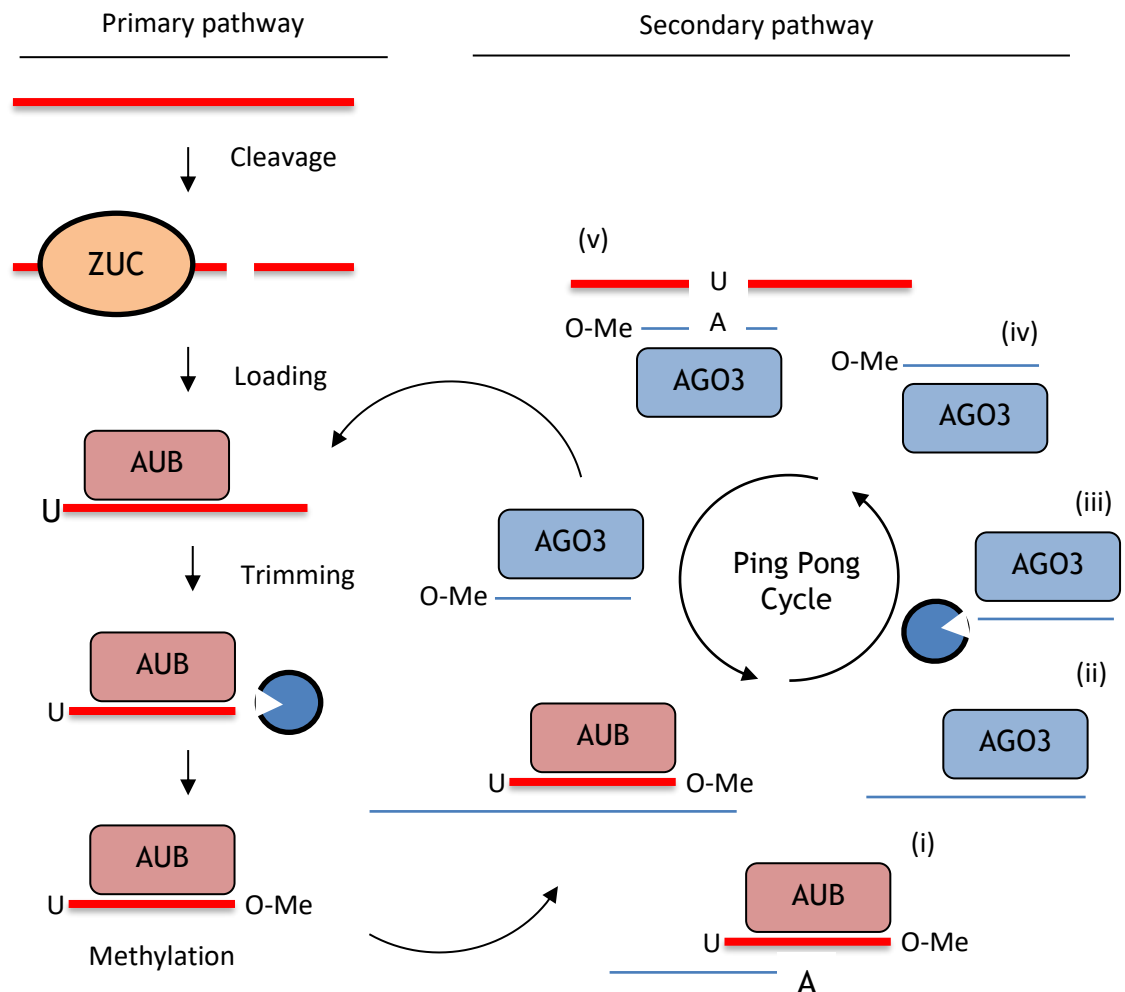
Figure 2: piRNA biogenesis.
Figure was re-drawn from Luteijn and Ketting, description of the pathway can be found in text; AUB = aubergine, Me = methylation, AGO3 = argonaute 3, ZUC = Zucchini[47].

As with miRNA in an RNA induced silencing complex (RISC), piRNA act as guide molecules, facilitating target recognition for post-transcriptional gene silencing (PTGS), or, transcriptional gene silencing (TGS). The simplest mode of action occurs when a piRNP binds through complementary base pairing to a transposable element, which is in turn cleaved through the catalytic action of PiWi[55,56]; note that in these original studies, piRNA are referred to as rasiRNA (repeat associated small interfering RNA). The second mode does not employ endonucleolytic cleavage, and instead relies on transcriptional repression through two epigenetic mechanisms. First, piRNPs are indicated in the formation of heterochromatin, repressing transcription. Although not fully elucidated, PiWi knock outs in drosophila germ cells resulted in a loss of histone-3-lysine-9 tri-methylation (HK39me3), resulting in increased RNA pol II activity at transposon promoters[57,58]. Secondly, in mammals only, piRNA loaded PiWi proteins play a role in the silencing of transposons through methylation of cytosine-glycosine (CpG)

islands located at promoters; the exact mechanism has not been elucidated, but is thought to involve members of the DNA methyltransferase (DNMT3) protein family[59,60].

<u>Endo-siRNAs</u>

Small interfering RNAs (siRNAs) can be split into two distinct classes, those that are endogenous to a cell, and those that are exogenous (shRNA etc). Both are derived from double stranded (ds)RNA, processed by DICER, then loaded into a member of the argonaute (AGO) clade[61]. Unlike miRNA and piRNA they have not been well studied in humans, with most research being performed in worm or fly[62,63]. Nonetheless, existing studies link endo-siRNA to transposon repression and alternative splicing. For example, Chen *et al*. reported that sequenced endo-siRNAs had 100 % complementarity to the 5' LINE-1 promoter and were somehow involved in its methylation, silencing this transposon[64]. In addition, in their model system Ameyar-zazoua *et al*. demonstrated recruitment of AGO complexes to CD44 stalled transcription allowing for alternative splicing to occur[65]. Intriguingly, these two papers demonstrate endo-siRNA functioning within the nucleus, an area where miRNA are also reported to function in a similar manner (Section **1.5.3**).

1.2 **micro-RNA (miRNA)**

MiRNAs are a species of 19 – 24 nucleotide (nt) ncRNA that are highly conserved in plants and Mammalia, playing a pivotal role in post transcriptional gene silencing[1]. Although miRNA were first discovered in the early noughties, effects mediated by their pathway had been observed a decade earlier:

1.2.1 **The history of RNAi and miRNA**

RNA interference (RNAi) is a phenomenon whereby a short RNA (~22 nt), derived from dsRNA, can regulate a gene in a post-transcriptional manner *via* complementary base pairing. Early research involved a lot of overlap, but we now know that RNAi, as coined by Fire *et al*. in 1998, consists of two distinct species of RNA: siRNA and miRNA[66]. The main differences between siRNA and miRNA are summarised in Table 1 and it is thought that siRNA evolved as a means of combating exogenous RNA (viruses), while miRNA only regulate host cell genes[67].

Despite being coined in 1998, RNAi had been observed in plants nearly a decade earlier[68,69]. Two groups were evaluating pigmentation in petunia and were trying to increase this through over expression of chalcone synthase. However, not only was no increase in pigmentation observed, 25-42 % of the transformed plants exhibited a complete abrogation of colour. No mechanism was given, but this phenomenon was observed in other studies also. Mechanistically, RNAi took off with three studies that were published close together. Fire *et al*. reported that RNAi was most efficient when dsRNA was introduced into a system, instead of longer complementary transcripts. This was followed by Hamilton and Baulcombe who demonstrated that it was the sRNAs (~25 nt), not the dsRNA substrate, that were responsible for effecting RNAi and finally by Zamore *et al*. who demonstrated the sRNAs were derived from the dsRNA substrate [66,70,71]. All of which established RNAi as a topic of acute scientific interest.

Table 1: Differences between siRNA and miRNA

	siRNA	miRNA
Origin	dsRNA	Primary-miRNA
Structure	21-23 nt	19-25 nt
Complementarity	Complete	Seed sequence*
No. of Targets	One	Multiple
Mode of action	Direct cleavage	Translational repression, turnover, cleavage

* in rare occurrences, complete complementarity results in AGO mediated cleavage. Relevance of the seed sequence is discussed in Section **1.5**.

The first, of what we now know to be miRNA, were reported in the same edition of Cell in 1993 by the labs of Ambrose and Ruvkun[72,73]. While working in *C. elegans,* they observed three things: (1) lin-4 was not translated but did form two sRNAs (lin-4L [61 nt] and lin-4S [22 nt]); (2) there was an inverse correlation between lin-4 and lin-14 protein levels, and (3) lin-4 RNAs had regions of complementarity within the 3' UTR of the lin-14 mRNA. They both concluded that lin-4 negatively regulated lin-14 *via* an antisense RNA-RNA interaction. However, due to poor species conservation, this finding was thought to be worm-specific. It wasn't until 7 years later that the Ruvkun lab reported on another miRNA, let-7, which was involved in developmental timing[74]. Unlike lin-4, other studies found let-7 to be well conserved, and in 2001, Lee and Ambrose first coined the term miRNA[75]. This lead to an explosion within the field, with studies being published

on miRNA function, miRNA biogenesis, miRNA in disease etc. So what are miRNA and how do they function?

1.2.2 **miRNA nomenclature**

miRbase is a database that archives published sequences for miRNA from all species and serves as a means by which they are annotated; it is currently curated by the Griffiths-Jones lab at the University of Manchester. Unlike traditional genes, miRNAs are named according to a simple convention that was set out by Griffiths-Jones *et al.*[76](Figure 3). In this, the miRNA refers to a mature micro-RNA sequence, while species within the biogenesis pathway are termed pri-miRNA or pre-miRNA, for the primary miRNA transcript or pre-miRNA hairpin, respectively. miRNA are named sequentially in order of discovery, the "first" being miR-1 and the last (current) miR-2588. To differentiate between organisms, a species-specific prefix can be added to afford this specificity. For example, miR-451 from humans is termed *hsa-miR-451,* while the murine homologue is referred to as *mmu-miR-451*; where *hsa* stands for *Homo Sapiens* and *mmu* for *Mus Musculus*. MiRNA that are from the same family have a letter suffix added, for example, miR-30a-c, while miRNA that are encoded at multiple genomic locations have a numerical suffix added, miR-30c-1 and miR-30c-2. As both strands of the miR-duplex can be loaded into AGO to form a functional RISC, a 3p or 5p suffix can be added to state if the miRNA is derived from the 3' or 5' arm: miR-92a-3p. As with everything in biology, there are exceptions: *let-7* (lethal target 7) and *lin* (abnormal cell LINeage) miRNA families were named before the above convention, and are reflective of the phenotype being studied[72,74].
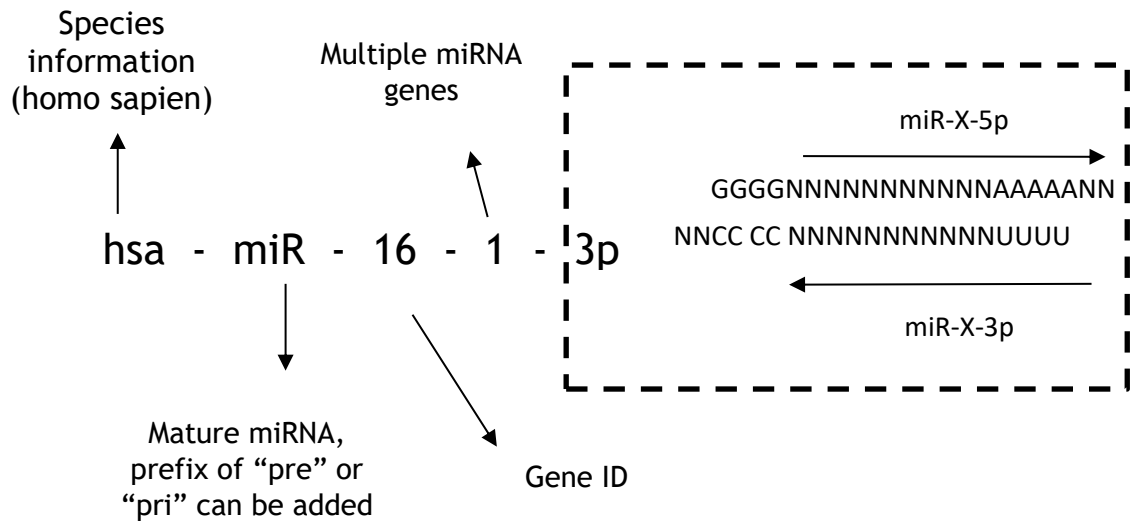
Figure 3: Schematic describing miRNA nomenclature.
The above format is required to gain the sequence for human miR-16 from miRbase.

1.2.3 **An essential molecule**

Soon after their discovery it became apparent the miRNA, as a family, were vitally important, with knock outs of the miRNA biogenesis machinery (*DROSHA*, DiGeorge critical region 8 (*DGCR8*), *DICER* or *AGO2*) proving embryonically lethal[77-79]. Future studies that used conditional knock outs fared little better, with severe defects being reported in all studies. For example, *DICER* or *DROSHA* knockouts in male testes resulted in mature mice being infertile, while *DGCR8* knockouts within neurons or developing renal tubular system resulted in microencephaly or kidney failure, respectively[80-82]. Taken together, this highlights the critical role that miRNA play, both in development and somatic tissues; although this is perhaps not too surprising as these models knocked out the entire miRNA apparatus, not individual miRNA.

With this in mind, specific miRNA(s) have been knocked down with differing phenotypes being observed. For example, loss of the heart specific miR-499 in mice resulted in no obvious phenotype being reported, while the loss of the miR-15a/16-1 cluster resulted in mice developing chronic lymphocytic leukaemia[83,84]. With the number of miRNA within miRbase, there are unsurprisingly more studies than can be referenced in this thesis. Therefore, miRNAs specific to this thesis will be discussed when relevant.

1.3 **miRNA biogenesis**

1.3.1 **miRNA genes**

MiRNA genes can be found intergenically, intronically or exonically, although most are found within the introns of coding mRNA[85]. MiRNAs are transcribed either as individual genes or as part of a cluster where much larger polycistronic transcripts that contain multiple miRNAs are transcribed[86-88]. The majority of miRNA genes are transcribed this way, although interestingly, non-canonical pathways exist where small RNAs can be derived from other ncRNAs (tRNA) and function as miRNAs (discussed in Sections **1.3.3.2**)[89].

1.3.2 **Canonical miRNA biogenesis**

miRNA biogenesis has been well studied within the last 17 years with a wealth of in depth mechanistic detail available[90]. Succinctly put, miRNA are transcribed as large primary transcripts (pri-miRNA) by RNA Pol II, before being cleaved into pre-miRNA by DROSHA. This is exported into the cytoplasm by EXP5, where it is processed into a miRNA duplex by DICER, loaded into a member of the AGO family where it forms a RISC (Figure 4). However, this is an overly simplified version of what occurs, and the process is far more complicated:
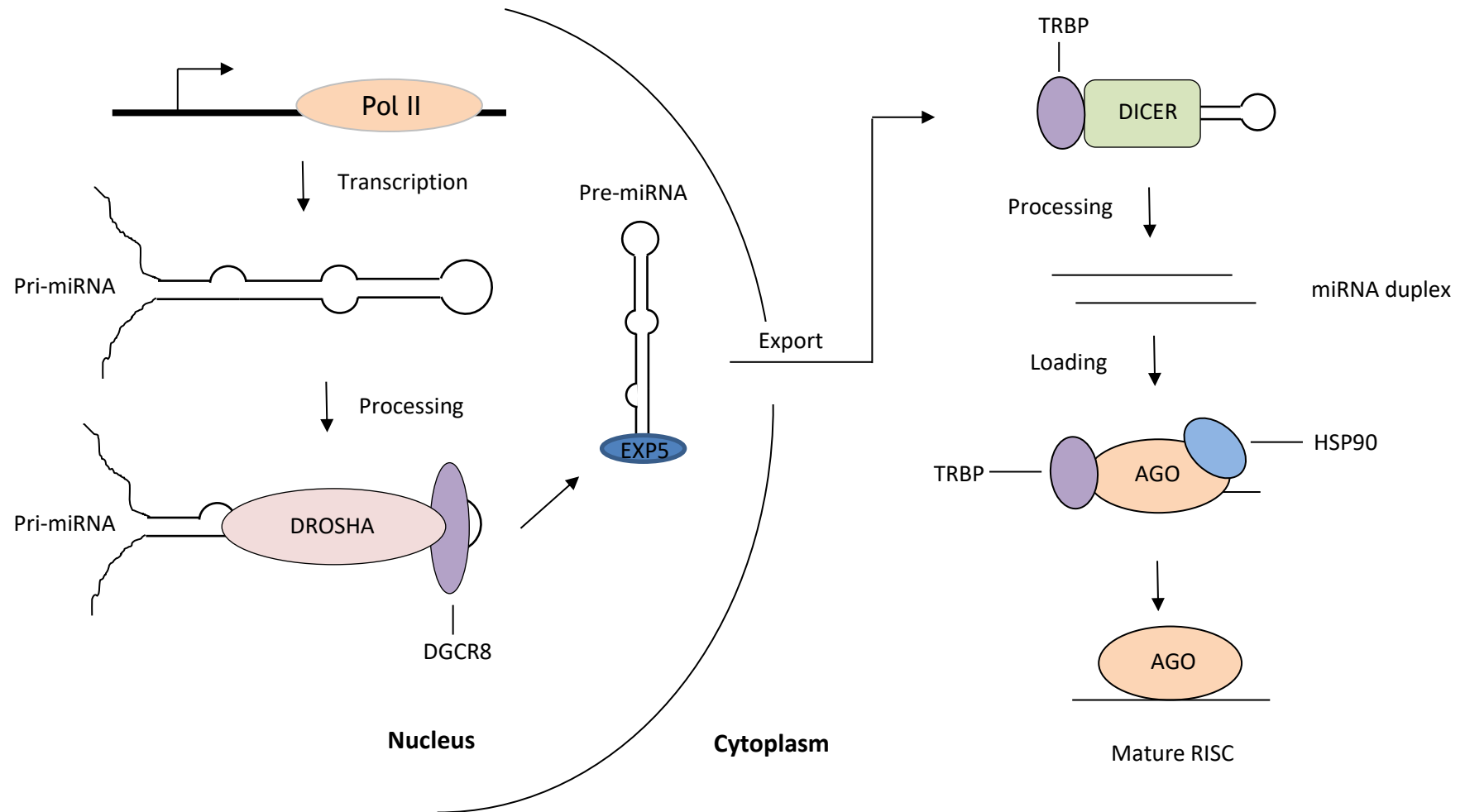
Figure 4: The miRNA biogenesis pathway.
miRNA are transcribed within the nucleus as a primary transcript (pri-miRNA) before being cleaved to form a pre-miRNA by DROSHA/DGCR8, this is then exported into the cytoplasm *via* EXP5. The pre-miRNA is cleaved by DICER/TRBP into a miR-duplex of which one strand is loaded into AGO forming an RNA induced silencing complex (RISC).

1.3.2.1 Pri-miRNA structure, recognition and cleavage

The primary miRNA transcript, as transcribed by RNA Pol II, adopts a distinctive secondary structure (Figure 5), whereby a stem loop is flanked by much longer 5' and 3' ssRNA. The loop portion of the hairpin is termed the apex, while the bottom portion the basal junction; the stem is subdivided into the upper (22 bp long) and lower (11 bp long) regions, which equate to being above or below the site of DROSHA cleavage[91]. Recently, it has also been demonstrated that certain nucleotide motifs are present, with ~79% of human pri-miRNA containing either a 5' UG, a UGUG motif in the apex loop or a 3' CNNC motif[91]. This, in addition to the adopted secondary structure, is the proposed reason for how the microprocessing unit recognises pri-miRNA specifically, and not all dsRNA.

The microprocessing unit is comprised of the type III RNAase DROSHA and its co-factor DGCR8. While both proteins have two dsRNA binding domains, DROSHA's binding capacity is insufficient in isolation for substrate recognition and requires DGCR8[92]. The composition of the microprocessing unit is still unclear, with some studies favouring a cooperative DGCR8 complex comprised of three DGCR8 dimers binding throughout the pri-miRNA, and others suggesting either 4 or 2 DGCR8 proteins being present[81,93,94]. The most recent model involves a DGCR8 dimer interacting with the apical UGUG (Rhed domain) and the upper stem region (dsRNA binding domains), allowing for DGCR8s C-terminus to bind and activate DROSHA, which binds at the ssRNA-dsRNA junction[93]; other studies have also demonstrated that ferric haeme is essential for this process – note that this is in all cells, not just erythropoiesis[95,96]. DROSHA then cleaves the pri-miRNA 11 bp from its basal junction, resulting in a ~65 nt pre-miRNA with a 2 nt 3' overhang[97,98].
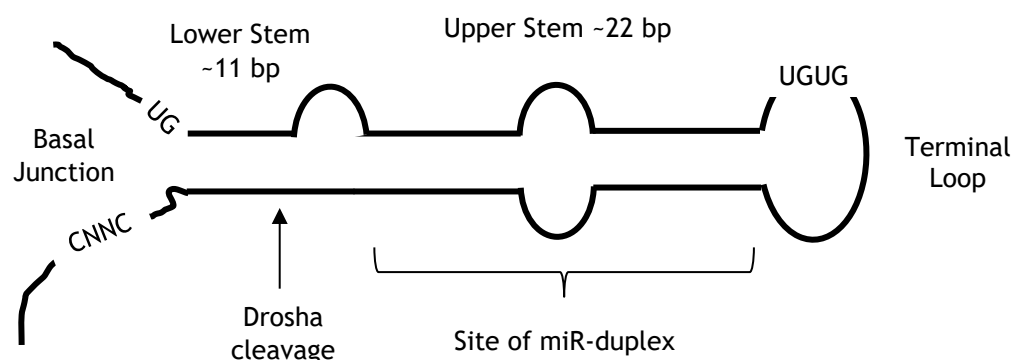
Figure 5: Schematic of a primary miRNA.
The primary transcript comprises of a stem loop structure which is cleaved by DROSHA to give a hairpin of ~100 nt from which a miR-duplex is processed; one strand is then loaded into a member

of the AGO family. The motifs reported by Auyeung *et al* to be present in ~79% of human miRNA are depicted as a nucleotide sequence[91].

1.3.2.2 **Export from the nucleus**

Post processing, pre-miRNA are exported from the nucleus by a combination of exportin 5 (EXP5) and Ran-GTP[99]. Interestingly, the 3' overhang appears to be essential for EXP5 recognition as mutants containing 5' overhangs interacted poorly with EXP5[100]. Okada *et al.* described EXP5-Ran-GTP complex forming a "baseball mitt" structure that binds the pre-miRNA structure that strongly bound the stem and 3' overhang through ionic interactions and hydrogen bonding[101]. When in the cytoplasm, Ran-GTP is hydrolysed and the pre-miRNA released for further processing[99,102].

1.3.2.3 **Pre-miRNA processing**

In mammals, DICER, another type III RNAase, can recognise either the 5' end or the pre-miRNAs 3' overhang, although the prevalence is for the 3' overhang[97,103]. DICER then cuts 21-25 nt from either end, removing the apical loop, resulting in a short miRNA duplex[97]. As with DROSHA, DICER has been shown to interact with two other dsRNA binding proteins: TAR RNA-binding protein (TRBP) and Protein activator of interferon induced protein kinase (PACT), although it's not clear if these are essential as, unlike DROSHA, isolated DICER will cleave pre-miRNA[104,105]. TRBP is thought to modulate DICER cleavage sites, resulting in miRNA duplexes of variable length, potentially playing a role in isomer generation (section **1.3.5**) and while the role of PACT is unclear, *in vivo* knock downs do result in reduced amounts of mature miRNA[105-107].

1.3.2.4 **RISC assembly**

The most recently reported function for TRBP is in the aiding of loading the miRNA duplex into an AGO protein. In this study, Noland *et al.* report that following DICER cleavage, the miRNA duplex is released, then rebound by DICER at a different position[108]. In a manner similar to fly dsRNA binding protein R2D2, TRBP senses strand asymmetry (Figure **6**) and orientates the miRNA duplex within DICER for loading[109]. In humans, a heat shock protein 90 (HSP90) dimer holds AGO proteins in an open conformation, allowing the miRNA duplex to be loaded in an ATP-dependent manner[110]. This is followed by duplex unwinding, whereby the

mature miRNA (guide strand) remains bound to AGO and its complement (passenger strand) is released and degraded; however, how this occurs is unknown. Strand selection is based on 5' stability within the duplex, with the least stable end being chosen as the guide strand and the most stable being degraded (Figure 6)[111]. A RISC is then formed and is able to perform PTGS.

Schematic of a miR-duplex

5'   GGGGNNNNNNNNNNNNNNNNNAAAAANN ⟶ Degraded
3' NNCC CC NNNNNNNNNNNNNNNNNUUUU ⟶ Loaded into AGO

Less stable end
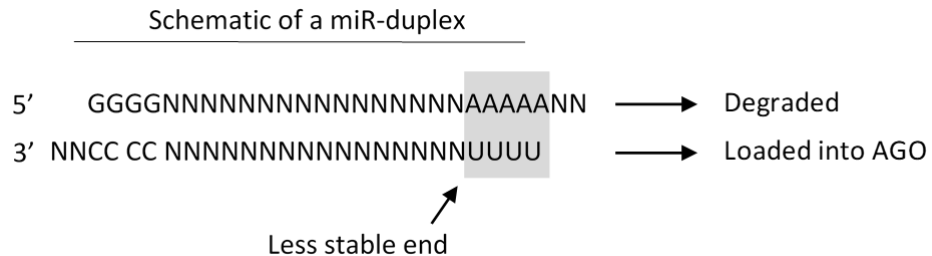
Figure 6: Simplified schematic explaining miRNA asymmetry rule.
The strand selected to be loaded into AGO and form RISC is dependent on the stability of the 5' end, in this case a GC rich region is more thermodynamically stable than a UA (grey) region, meaning the 5' UUUU is loaded into AGO and the 5' GGGG strand is degraded.

1.3.3 Drosha independent biogenesis

In addition to the above, multiple studies have emerged regarding functional miRNAs that are generated out with the canonical pathway. These appear to be largely separated into two main groups, those that do not require DROSHA, and those that do not require DICER: so called DROSHA or DICER independent pathways. Of these two, DROSHA independent miRNA are the most heterogeneous in the way miRNA are formed.

1.3.3.1 mirtrons

The first DROSHA independent miRNA was reported by Ruby *et al.* in 2007, and were termed mirtrons[112]. While analysing their sequencing dataset, they observed 14 pre-miRNA-like transcripts. These transcripts were predicted to fold in the same way as pre-miRNA and were capable of being processed to form functional RISCs. However, these transcripts did not map to miRNA genes, but to small (~56 nt) annotated introns. Two reasons were given why DROSHA was not involved in this process: (1) DROSHA knock downs reduced levels of let-7 members without affecting mature mirtron levels; (2) mapping the short intron sequence past the sequenced 3' and 5' ends revealed sequences that were not complementary, something which is required for DROSHA to bind and cleave pri-

miRNA[98]. Instead of following the canonical pathway, these excised introns are de-branched by a lariat de-branching enzyme, at which point they self-anneal to form pre-miRNA-like transcripts that are able to enter the remainder of the miRNA biogenesis pathway (Figure 7). The mirtrons reported in this study have subsequently been verified in mammals, chicken and rice[113-115].

Since Ruby *et al's*. initial study, the mirtron family has expanded. The original pre-mirtrons were pre-miRNA-like due to their small size and abundant self-complementarity. However, more recently, it has been demonstrated that pre-mirtrons can be much longer. For example, dme-miR-1017 has a 100 nt 3' tail which is trimmed by RRP6 to a canonical pre-miRNA size, before it enters the miRNA biogenesis pathway[116]. In addition, mmu-miR-342 is embedded within a 20 kb intron and while the authors do not elaborate on how it is processed to pre-miRNA size, they do show it is not caused by DROSHA[117].
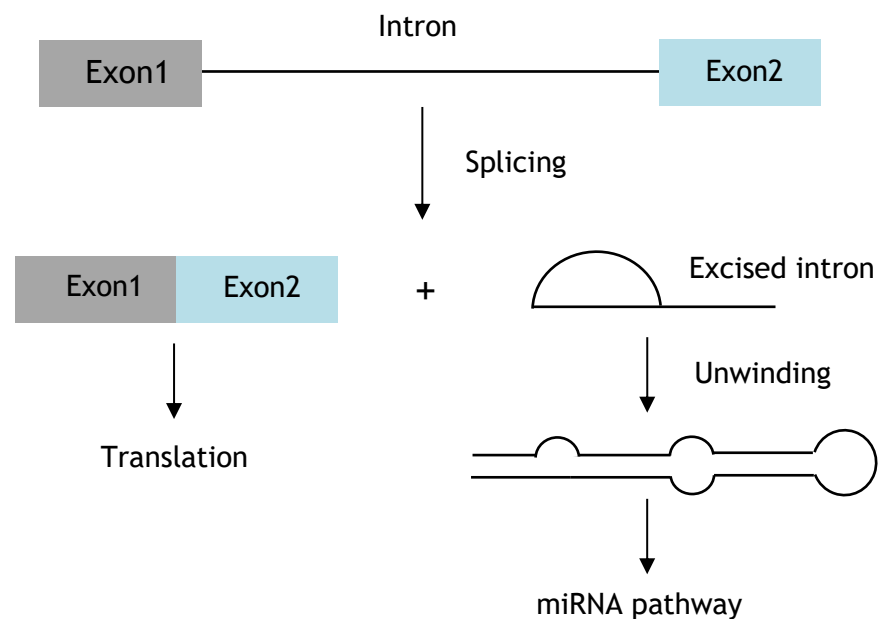
Figure 7: Mirtrons entering the miRNA biogenesis pathway.
Mirtrons are derived from the introns of mRNA. The excised introns, when unwound, have a secondary structure such that it can be recognised as a DICER substrate.

1.3.3.2 miRNA derived from other RNAs

Although not as fully studied as mirtrons, miRNA have also been reported to be derived from other RNA species and not from pre-miRNA. The most commonly reported species from which miRNA-like molecules can be derived is tRNA. Babiarz *et al*. were the first to report of a small RNA derived from the 3'

end of the isoleucine-tRNA (tRNA-ile)[89]. Similar to mirtrons, tRNA-ile could form a secondary structure that made it susceptible to cleavage into a pre-miRNA-like substrate. Multiple other studies have since reported on tRNA fragments (tfRNA) entering the miRNA biogenesis pathway[118,119]. However, the literature appears to be contradictory, Kumar *et al*. report tfRNA are preferentially loaded into AGO1,3,4, but are not generated by the miRNA biogenesis pathway[120] . This contrasts with Hasler *et al*. that report tfRNA are not loaded into AGO at all, as they are prohibited by the Lupus Autoantigen (LA)[121].

Finally, in 2008, Ender *et al*. demonstrated that a ~22 nt RNA derived from the 5' arm of the snoRNA ACA45, loaded into AGO2 and was catalytically active[122]. As with mirtrons, DROSHA was not involved in producing a DICER substrate, but DICER was required for the final stages of miRNA biogenesis. Multiple other studies have reported on the presence of snoRNA derived (sd)-RNA having miRNA similarities[123,124]. However, the abundancies of some of these sdRNAs are barely above background, and / or appear on blots with multiple other unexplained bands. In addition, some miRNA sequences (miR-664a) overlap at snoRNA loci (snoRNA-A36B), meaning it is difficult to ascertain if the mature miRNA was derived from a mature snoRNA, or simply processed from a pri-miRNA that happens to share a snoRNA sequence[123].

1.3.4 **Dicer independent biogenesis**

At present, only miR-451 is thought to be generated in the absence of DICER. Transcription and processing occur as per Section **1.3.2.1-2**, but when pre-miR-451 is transported into the cytoplasm it is not recognised by DICER[125]. Although this lack of recognition was not explained, it was noted that the mature miR-451 sequence extends through the pre-miRNA stem loop and folds back upon itself. This is unlike other miRNA species, and was postulated by Hannon *et al*. to be incompatible with DICER cleavage. Instead, pre-miR-451 is loaded directly into AGO2, which utilises its endonucleolytic capability to cleave the 3' end, forming a 30 nt intermediary. This intermediary is then processed to mature miR-451 when the 3' end is trimmed *via* Poly(A)-specific ribonuclease (PARN), although Tomari *et al*. also demonstrated that this trimming was not required for miR-451 functionality[126]. Interestingly, miR-144, which is co-expressed with miR-451 as a bicistronic transcript, does not require AGO2 cleavage and is formed through

canonical miRNA biogenesis. Note, that while miR-451 biogenesis is unique, it isn't merely an oddity as it is essential for erythropoiesis, with miR-451 knock outs causing severe anaemia[127].

1.3.5 Isomirs

miRNAs that have sequences different to their reported canonical sequence are termed isomirs. DICER or DROSHA misprocessing of pre-miRNAs can result in longer or shorter 5'/3' ends, with these types of isomirs referred to as templated (Figure 8)[128]. In addition, isomirs can also come from non-templated additions and / or changes / edits. For example, poly(A) polymerases and terminyl uridyl transferase can add non-templated A's and U's to 5'/3' ends, while exonucleases like NIBBLER can remove terminal nucleotides[129,130]. Finally, RNA editing, where an adenine deaminase enzyme (ADAR) catalyses the deamination of adenine to inosine - isomirs with this sequence variation are called polymorphic[131].

Sequence data reveals that the most abundant isomirs are 3', both in terms of read number (mass) and variability (number of additions/deletions); 5' and polymorphic isomirs are the next most common, respectively, although they represent a small proportion overall[132,133]. The main reason for this is thought to be due to the way in which miRNA interact with AGO. For example, studies have shown that a miRNAs 5' end is bound deep within AGO's structure, meaning it is unable to be recognised by modifying enzymes. The 3' end however, is thought to be accessible, meaning that it is more susceptible to non-templated additions and / or trimming, which is reflected by the higher amount of 3'-isomirs present in sequence data. It is important to note, that although isomirs exist, within sequencing data sets, the canonical miRNA is usually the most abundant.

Figure 8: Schematic explaining the different types of isomirs.
Isomirs can be templated, i.e. they have the same sequence +/- X of the pre-miRNA, non-templated, i.e. have a uridine or adenine added or polymorphic, which can arise from a single nucleotide polymorphism (SNP) or an A-I edit by ADAR.

<u>But what's the point?</u>

If isomirs make up such a small amount of the miRome, then are they relevant? The short answer is yes, but there are not enough studies at present to detail to what extent they are relevant, or, if all isomirs are. For example, as miRNAs work through their seed sequence, which is present at the 5' end, 3' edits of one or two nucleotides aren't thought to affect this[90,128]. As 3'-isomirs are the most abundant, then it doesn't appear that the bulk of isomirs bear an altered mRNA target repertoire[132]. It is important to note that non-templated additions at the 3' end will affect miRNA activity. As non-templated Us or As promote miRNA turnover or stability, respectively; these modifications will stabilise or attenuate translational repression[134,135]. These are not thought to affect what a miRNA will target, and at present, no studies report a 3'-isomir having different mRNA targets to its canonical miRNA.

Although much rarer than their 3' counterpart, 5' isomirs are often reported to have altered mRNA targets. Unlike a 3'-isomir, any addition/deletion at the 5' end would change the way the miR binds AGO, ultimately shifting the seed sequence. For example, Dibb *et al*. demonstrated that a single 5' nucleotide removal from miR-9 meant that it gained an ability to repress *DNMT3B* and *NCAM2*, although it lost the ability to regulate *CDH1*[136]. In another study, a 5' U addition caused miR-34 / 449 to lose the ability to target *ARHGDIB*, *ARHGAP1* and *RRAS*[137]. However, it is important to note that this phenomenon is not an 'either-or' event. In both studies, the canonical miR sequence was detected along with the 5'-

isomir. Indeed, the canonical sequence was responsible for 80-90% of the sequence coverage, indicating that if genuinely biologically relevant, isomirs represent target augmentation, rather than a whole scale change. Indeed, computational analysis from both studies indicates that with the addition of isomirs, the candidate mRNA pool for a specific miRNA could grow by more than 100 targets; as these pools can already be quite large, validation of this will be challenging.

1.4 **Argonaute proteins**

The second component of the RISC complex are argonaute proteins (AGO). AGOs belong to a larger family of proteins, also termed argonautes, which are split into two clades: Ago and Piwi. Both clades bind small RNAs, with the AGO clade restricted to miRNA/siRNA binding and the PIWI clade binding piRNAs[138]. In addition to small RNA binding, the argonaute family of proteins are defined as containing a PAZ (PIWI-ARGONAUTE-ZWILLE) and a PIWI (P-element Induced WImpy testis) domain (Figure 9). The PAZ domain is perhaps the most important, as along with the middle section (MID domain) of an AGO protein, acts to bind and keep small RNAs in place. The 3' end of the small RNA inserts into a binding pocket within the PAZ domain, whereby it is stabilised by stacking against a phenylalanine (P292)[139]. The 5' terminal phosphate is essential for miRNA loading within the MID domain, whereby it is stabilised by binding a magnesium ion[140]. In addition, a conserved tyrosine (Y529) within this pocket can undergo phosphorylation, and studies show that point mutation of this residue strongly reduces miRNA binding[141]. The PIWI domain is similar in structure to the endonuclease RNase H, but this function appears largely redundant in the AGO clade, as only AGO2 maintains any catalytic   activity[142].
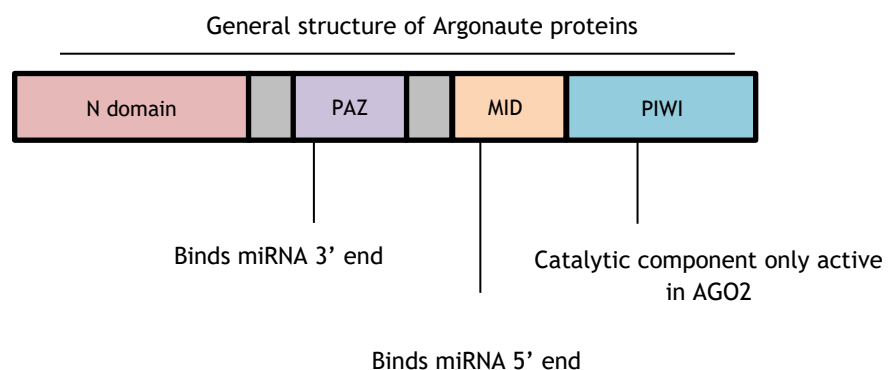
Figure 9: Cartoon of the domains within AGO proteins.
The AGO family is split into two clades, PIWI and AGO – all of which contain the domains above.

1.4.1 **Argonaute 1 – 4**

As only the AGO clade bind miRNA, the subject of this study, the PIWI clade will not be discussed in further detail. In humans, the AGO clade comprises of 4 members: AGO1-4[138]. Within mammalia, it is not immediately clear what the functional relevance of having four AGO proteins is. For example, although the study by Daub *et al.* showed a tendency for miR-222 and miR-223 to preferentially form a RISC with AGO1, the remaining miRNAs sequenced appeared to associate with all AGO members in roughly equal amounts[143]. On the other hand, although Yi *et al.* also reported that each AGO protein bound a near identical pool of miRNA (based on ID), the majority of miRNA present (as a mass) were found associated with AGO2[144]. Taken together, the idea that miRNA can be loaded into any AGO protein, but appear to prefer AGO2, over 1,3 and 4, would indicate some redundancy in the AGO clade. However, genetic studies of AGO3 and 4 demonstrated that this was not the case, as they were required for *Alu* RNA-guided mRNA decay or spermatogenesis, respectively[145,146]. Furthermore, tissue expression analysis reveals that all four AGO members were present in each tissue tested[147]. Although clade member bias was reported intra-tissue, with AGO1-2 being the most prevalent, AGO1-4 signatures were not that dramatically different between the tested tissues. Finally, as AGO2 appears to preferentially bind miRNA with 5' terminal U or A, miRNAs with different termini are more likely to bind other members of the AGO clade, which also argues against redundancy[148]; how this fits with 5'-isomirs discussed in Section **1.3.5** is unclear.

Put simply, in humans it is not clear why there are four AGOs; each AGO does not appear to have specific miRNA pools, AGO1-4 are present in all tissues and, with the exception of one AGO2 target mRNA, all appear to function in the same way, which is not the case for other organisms. In planta, the AGO clade consists of 10 members, many of which have specific binding partners and / or functions[149]. For example, heterchromatic siRNA, siRNA that are transcribed from pericentromeric chromatin, associate with *A. Thaliana* (at)AGO4 and 6[150,151]. These are responsible for RNA-directed DNA methylation (RdDM), whereby the RISC complex binds DNA in an RNA-dependent manner, recruits additional proteins (DNA [cystosine-5]-methyltransferases) and promotes cysteine methylation[150]. atAGO1 appears to bind all miRNA and is involved in traditional PTGS[152]. An exception to this is AGO10, which only binds miR-165 and miR-166[153]. Finally,

siRNAs from intergenic regions containing a terminal 5' C residue are preferentially loaded into AGO5[154]. At present, with the exception of miR-451, this preferential RNA binding isn't seen within Mammalia, although this may change with more detailed studies.

1.5 **miRNA mode of action**

Genes targeted by RISC undergo PTGS *via* translational repression, direct cleavage or sequential degradation[90]. However, while there are three main ways in which miRNA regulate mRNA, the overwhelming majority is through degradation (~66 - 90%), with only a small portion (~6 - 26%) thought to be through translational repression[155,156]. While there are large differences in the ways miRNA regulate mRNA, this still forms the function for which they are best known. Although more recently, as discussed below, other modes of action have been reported.

1.5.1 **mRNA destabilisation and degradation**

As mentioned, the most abundant means of regulation by miRNA results in mRNA degradation; for this to occur, RISC must first recognise a specific mRNA. RISC, an RNA protein complex, binds mRNA through Watson-Crick base pairing *via* the "seed sequence"; nucleotides 2-7 at the 5' end of the miRNA[157]. Degradation occurs when RISC binds to the 3' untranslated region (UTR) of target mRNA and AGO recruits the scaffold protein glycine-tryptophan protein of 182 KDa (GW182)[158] (Figure 10). This then interacts with poly(A) binding proteins and recruits the PAN2-PAN3 (Poly(A) specific Nuclease subunit) complex which performs the first stage of deadenylation[159]. PAN2 is the effector unit and it is guided to its poly(A) substrate through a PAN3-GW182 interaction[160]. The second stage of deadenylation takes place *via* a second complex which comprises of 3'-5' exonuclease (carbon catabolite repression 4 protein (CCR4a)), and a scaffold protein (Negative regulator of transcription (NOT1)); why the removal of poly(A) tails requires two stages is unclear[161]. After this, GW182 acts to sequester mRNA within processing-bodies (sites of degradation), where the 5' cap is removed by decapping protein 2 (DCP2) and the RNA degraded by exoribonuclease 1 (XRN1)[162,163] although interestingly, Bhattacharyya *et al*. showed that this is a dynamic phenomenon which can be reversed during stress, and previously

sequestered mRNA can be released from processing bodies (P-bodies) and subsequently translated[164].

Classical AGO2-mediated endonucleolytic cleavage occurs when there is a 100% consensus match between the miRNA and mRNA target. However, there is only one instance (miR-196 / HOXB8) of this occurring in Humans and this phenomenon is primarily observed in Planta[165,166]. Note, the *Rtl1/Peg11* locus is theorised to be regulated via miRNA mediated cleavage, however, while this has been observed in mice and sheep, it hasn't been validates in humans[167].
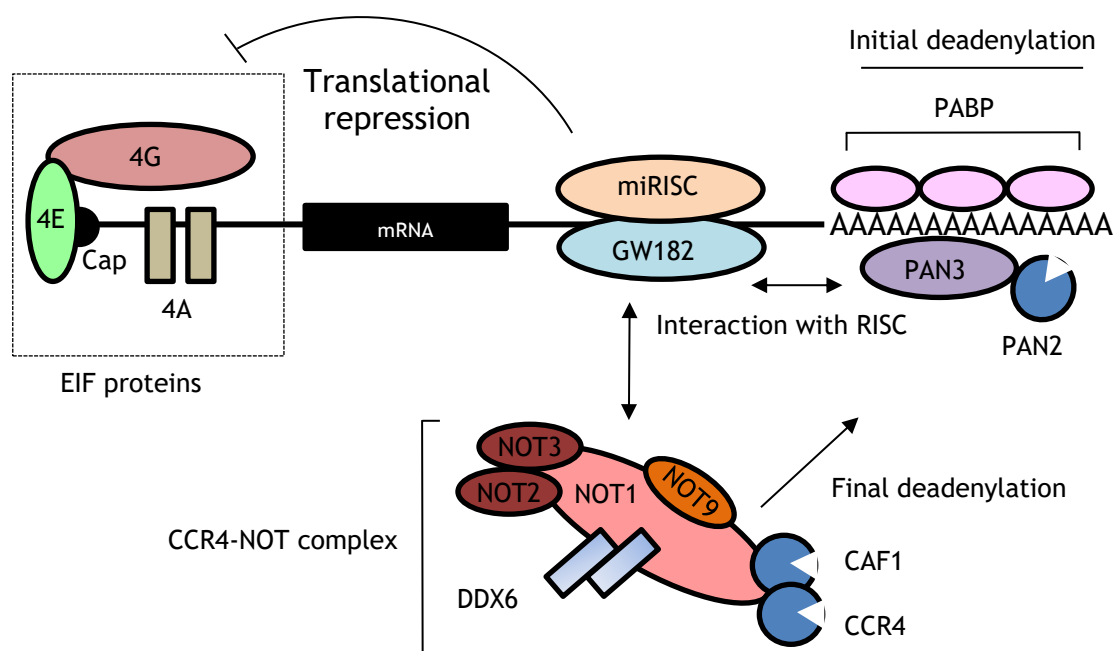
Figure 10: miRNA mode of action.
miRNA regulate translation in two ways 1) mRNA turnover: this occurs in two stages: (A) an initial deadenylation event is catalysed by PAN3-PAN2 which interacts with the RISC-GW182 complex, when the tail is ~ 25 As in length, the PAN complex is replaced by the CCR4-NOT complex which removes the remainder of the Poly(A) tail; (B) the 5' cap is then removed; 2) translation repression: the RISC-GW182 complex interacts with eIF4G, preventing it forming a pre-initiation complex with a ribosome; PAN = PAB1P-Dependent Poly(A)-Nuclease, DDX6 = DEAD-Box Helicase 6, CAF1 = Chromatin Assembly Factor 1 Subunit A, eIF = Eukaryotic translation initiation factor, CCR4 = Chemokine (C-C Motif) Receptor 4.

1.5.2 **Translational repression**

miRNA can also function through translational repression (TR), although as mentioned previously, this is not its dominant mode of action[155]. How this occurs has not been fully elucidated, but is believed to involve cap recognition. First, RISC interacts with both with poly(A) binding proteins (PABP) and the translation initiation factor eIF4e[168,169]. The RISC-eIF4E interaction blocks the

eIF4E-eIF4G interaction, which is required for the formation of the 43s pre-initiation complex[169-171]. Interestingly, although there is no consensus, many publications evaluating TR appear to overlap. For example, Zdanowicz *et al*. suggest that miRNA function through a two-hit model, with TR forming an immediate stop of translation and destabilisation/degradation completing the silencing[172]. This fits well with Eichorn *et al*s. study, where they report that not only is the TR effect weak, but it is only effective at the earliest stages of PTGS[155]. Indeed, some studies corroborate this temporal effect, suggesting a two-hit model may be accurate, while others suggest TR or destabilisation is AGO-specific; note, destabilisation or TR being specific to AGO1 or AGO2, respectively, has only been shown in the fly[169,173].

1.5.3 **Nuclear function**

The vast majority of studies state miRNA function within the cytoplasm, an emerging literature indicates nuclear functions, although these can be contradictory. Firstly, AGO loaded with miRNA have been detected within the nucleus and reported to form multiprotein complexes with typical RNAi members – however protein-complexes weren't found in all studies[174,175]. Gagnon *et al* demonstrated that the profiles of cytoplasmic and nuclear miRNA were similar (75 % overlap), although a separate study indicated that as a mass, the majority of each individual miRNA resided within the cytoplasm[174,176]. Nuclear miRNA are thought to be generated as per Section **1.3.2**, but when a RISC is formed, can shuttle in and out of the nucleus *via* exportin-1 or importin-8[177,178]; an AGUGUU motif present on miR-29b has been linked to shuttling, but this is neither conserved across other nuclear-miRNA, nor is it clear how an AGO-loaded miRNA can be recognised by additional proteins[179].

Functionally, nuclear miRNA are reported to work in numerous ways, with the simplest involving AGO2-mediated cleavage of lncRNA or pri-miRNA[180,181]. Contrary to the situation in the cytoplasm, nuclear miRNA have also been reported to be involved in silencing pre-transcriptionally, not just post. For example, miR-320 was shown to bind to the RNA Polymerase III Subunit D (*POLR3D*) promoter, while miR-10a bound the promoter of Homebox D4 (*HOXD4*)[182,183]. A complete understanding of this is lacking, but both studies report an increase in tri-methyl histone H3 lysine 27 (H3K27me3) at the gene's promoter which was linked to

heterochromatin formation. Note that "proof of concept" studies exist that show a similar phenomenon, and while parities are drawn to these studies, it is worth remembering that they have been designed to the nucleus (siRNA targeting promoters), and not necessarily representative of endogenous miRNA[184].

1.5.4 Heteroclitical modes of action

Interestingly, a number of recent papers have shown miRNAs can have a completely novel function and act as agonists to toll-like receptors (TLR). The TLR family recognise specific exogenous stimuli such as CpG DNA, lipopolysaccharide (LPS) or ssRNA and induce an immune response[185]. In mice, TLR7 recognises viral ssRNA and Lehmann *et al.* showed that aberrantly high cerebrospinal fluid levels of the let-7b miRNA stimulated macrophages and microglia causing neurodegeneration[186]. A few months later, Fabbri *et al.* showed co-localisation of exogenous miRNA binding to TLR8, the human TLR7 homologue, and reported that cancer-derived endosomes containing miR-21/29a induce a pro-metastatic inflammatory response and cachexia[187,188]. Both labs suggested that TLR stimulation is sequence specific, but it was Lehman *et al.* that employed site-directed mutagenesis of the GUUGUGU motif, shared between let-7b and HIV ssRNA40, to demonstrate that stimulation is due to high GU content[186].

1.6 miRNA target prediction

Currently there are 2585 mature miRNAs listed on miRBase V21 and it is thought that these regulate ~ 60% of all protein coding genes[189, 190]; although as isomirs can contain un-templated post-transcriptional modifications within the seed region, this number may well be higher[191]. Biologically, miRNA are involved in the normal function of cells and like protein coding genes can be cell-specific, deregulated in different malignancies or change expression in response to different stimuli. For example, *miR-21* is classified as an oncogene and is over-expressed in multiple cancers including acute myeloid leukaemia, glioblastomas and chronic lymphocytic leukaemia[192-194]. A number of studies have verified *miR-21* targets which are predominantly tumour suppressor genes such as phosphatase and tensin homolog (*PTEN)* or programmed cell death 4 (*PCD4)*[195,196]. It is one of the most widely dysregulated miRNAs in cancer and is associated with poor prognosis and metastasis[197]. However, as a single miRNA may target many genes

so may a single mRNA be targeted by multiple miRNAs, making target validation difficult[198]. Indeed, available software algorithms struggle to accurately predict targets and a study by Sethupathy *et al*. demonstrated that there was little consensus in the predicting powers of commonly used packages and that sensitivity of predicted targets could be as little as 1.3%[199]

1.7 Extracellular vesicles

An emerging area of interest within miRNA biology, is their presence within extracellular vesicles (EVs) and their potential to silence genes inter-cellularly. EVs have been studied in a plethora of different cell types and disease models, too many to discuss here[200,201]. Therefore, the sections below will describe EVs in general and aspects of their biology (miRNA) that fit this project, the EVs specific to this project are described in context in Section **1.10**.

1.7.1 What are extracellular vesicles?

EV is an umbrella term which encompasses, exosomes, microvesicles, apoptotic bodies and nanovesicles. There still isn't an exact terminology / definition that is consistently used by all authors, but at present exosomes / nanovesicles are mostly thought of as being 50 – 100 nm in size, while microvesicles (MVs) and apoptotic bodies are ~100 – 1 µm[202]. Another key distinction between exosomes and MVs is their source of origin: exosomes are formed internally, fuse to make larger multivesicular bodies (MVBs), before these MVBs fuse with the cellular membrane, expelling its content (exosomes) out with the cell[203]. In contrast to this, MVs generally shed, bleb or are pinched off directly from the cell membrane[204]. As a result of this, the molecular makeup of these two types of EV can vary, with exosomes being enriched for tetraspanins, while MVs generally reflect the cell of origin[205]. EVs have been regarded as a means for a cell to get rid of waste, artefacts (red cell storage, apoptotic bodies) but also as vectors for intercellular communication. Classically EVs are isolated / enriched *via* differential centrifugation. Low speeds (up to 1000 x G) remove dead cells and debris before a "harder" spin of 18, 000 – 36, 000 x G separates the larger MVs from exosomes. Due to their small size, exosomes remain in suspension during this 18 – 36, 000 spin, but can be subsequently isolated from media / serum *via* ultracentrifugation.

1.7.2 **EVs contain RNAs**

The first report of RNA being laterally transferred between cells *via* MVs was in 2006 by Ratajczak *et al.*[206]. In this study, they observed that murine embryonic stem cell (ESC) MVs contained mRNA for several ESC transcription factors (Oct4, Nanog, stem cell ligand [Scl] and Gata-2). They found that these were transferred into recipient bone marrow Sca-1$^+$/kit$^+$/lin$^-$ cells (LSK), Oct4 was translated, and augmented stem cell expansion. This was closely followed by Valadi *et al's.* study, which showed that mast cell exosomes contained multiple mRNAs, and when using a rabbit reticulocyte lysate, they were capable of being translated. A key difference between this and the previous studys is that this was the first to show the presence of miRNA in exosomes[207]. Since then, multiple other studies have reported the same phenomena, for example, miR-290, miR-291-3p, miR-292-3p, miR-294, and miR-295 were shown to be transferred from murine ESC into fibroblasts, although targets were not evaluated[208]. miR-223 was shown to be transferred between THP-1 (monocyte/macrophage cell line) whereby it negatively affected CCR5 and CD206 expression, although direct silencing was not shown[209]. Through use of a reporter construct, Montecalvo *et al.* demonstrated functional transfer of miR-451 between dendritic cells (DC), although perhaps more interestingly, this study also reported that exosome content changed during DC differentiation[210]. Furthermore, this doesn't appear to be a "cramming" event, with multiple studies showing that exosomes aren't simply a *fac similie* of their parental cell, but instead miRNA loading appears selective[211,212]. A potential reason for this was given recently, whereby sumoylated heterogeneous nuclear ribonucleoprotein A2/B1 (hnRNPA2B) was able to recognise a GGAG motif within the 3' end of the miRNA and selectively package them into exosomes[213]. Finally, more recent studies that employed RNAseq as opposed to a microarray have reported the presence of other ncRNAs (piRNA, snRNA), although the function of these was not evaluated[214]. The idea that EVs can transfer miRNA between different cells and elicit a response forms a key hypothesis that is tested in Chapters 4 - 6.

1.8 **RBC homeostasis**

A cell type that has recently been reported as containing abundant miRNA are mature erythrocytes[6]. Why these relatively simplistic cells require miRNA is

unknown. However, the function of miRNA within haematology, including erythropoiesis has been widely studied.

1.8.1 **Erythropoiesis**

Erythropoiesis is the process in which mature, circulating red blood cells, also termed erythrocytes, are produced. Developmentally there are two modes of erythropoiesis: primitive erythropoiesis, which is detected approximately 16 days after gestation within the yolk sac (YS) and definitive erythropoiesis, which starts in the YS, but ends in the bone marrow where erythrocytes are terminally differentiated from haematopoietic stem cells (HSCs)[215]. Primitive and definitive erythrocytes are very different, with primitive erythrocytes containing different haemoglobins (so called foetal), a nucleus (for a limited time) and the ability for intravascular proliferation[216]. As this is not the case for definitive erythrocytes, the focus of this thesis, the remainder of this introduction will focus on definitive erythropoiesis only.

1.8.1.1 **Definitive erythropoiesis**

Haematopoiesis is the mechanism by which all lineages of blood cells are produced. Pictorially this is classically represented as the haematopoietic tree (Figure 11a), in which all blood cells are derived from a common progenitor (HSC) following step-wise differentiation[217]; a specific time line of erythropoiesis is depicted in Figure 11b. The earliest cells at which specific erythrocyte progenitors can be identified is the burst forming unit erythroid (BFU-E)[218]. They exist at a concentration of ~ 20 – 40 per 10^5 cells within the bone marrow and rapid *in vitro* differentiation on methylcellulose shows they require thrombopoietin (TPO), stem cell factor (SCF), Fms-Like Tyrosine kinase (FLT3) ligand and interlukin 3 (IL-3)[219]. They differentiate to form colony forming unit erythroid (CFU-E) cells which are dependent on fibronectin[220].

a) **Haematopoietic tree**
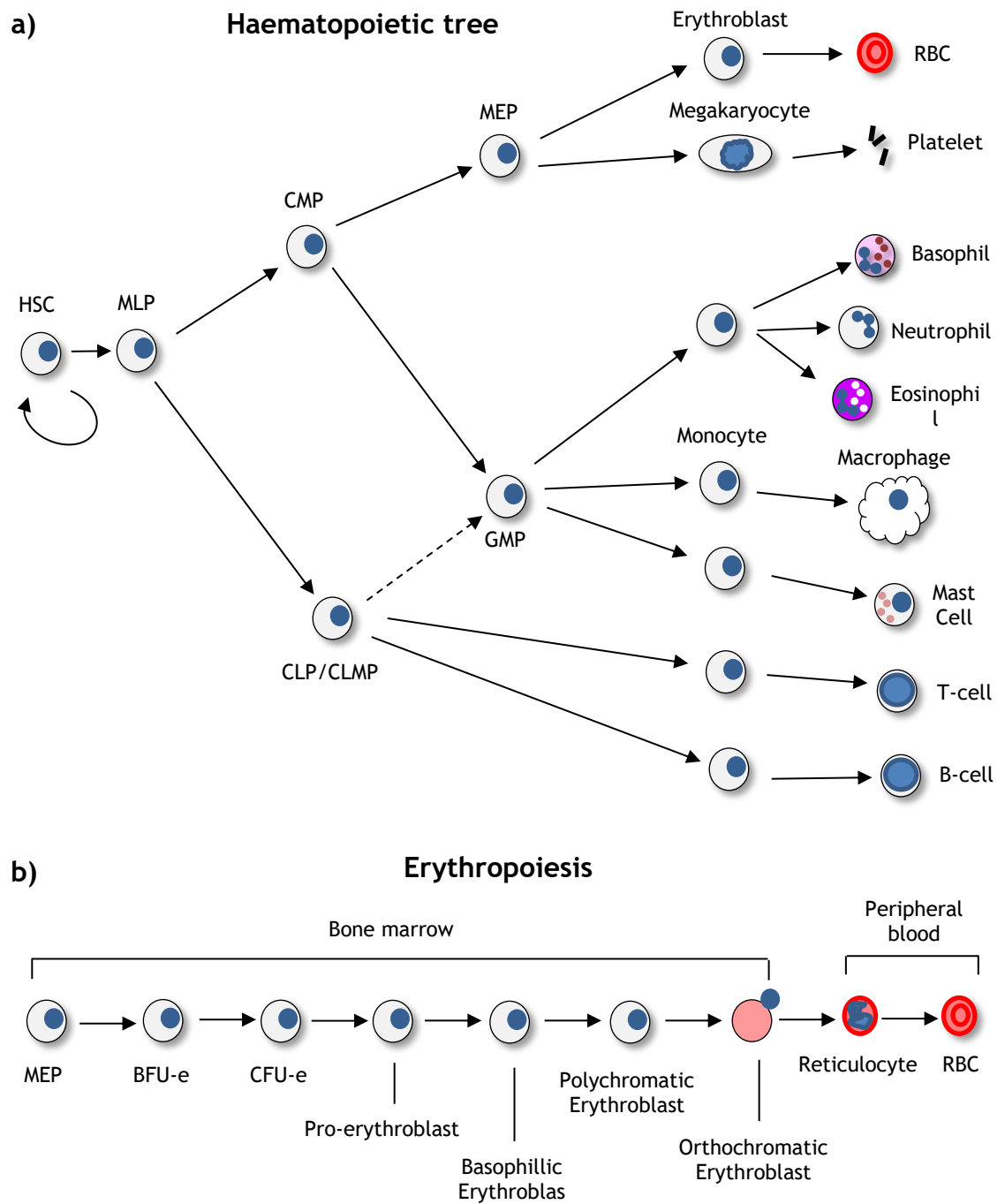
b) **Erythropoiesis**

Figure 11: Schematic describing the haematopoietic tree and erythropoiesis.
a) the haematopoietic tree as re-drawn from Foster *et al.*[221], b) additional detail for erythropoiesis; MEP =megakaryocyte-erythroid progenitor, B/CFU = Blast/colony forming unit, RBC = red blood cell, HSC = haematopoietic stem cell, MLP = multi-lineage progenitor, CLP = common lymphoid progenitor, GMP = granulocyte-macrophage progenitor, CMP = common myeloid progenitor.

Although not required for lineage commitment, erythropoietin (EPO) is required for complete RBC maturation[222]. First, CFU-E respond to EPO through JAK-STAT and PI3K-AKT signalling pathways; perturbation of either results in severe anaemia[223,224]. This results in an increase in proliferation, and expression of glycophorin A (Gly-A). In addition, the erythroid-specific transcription factor Kruppel Like Factor 1 (KLF1) stimulates haemoglobin production, which occurs in

conjunction with increased expression of CD71, the transferrin receptor, responsible for internalising iron[225]. At the same time, a molecular "switch" occurs in which the transcription factor GATA1 is expressed in place of GATA2[226]. Fibronectin is required for the final stages of differentiation, as it promotes shedding of the blast's nucleus: a process termed enucleation[220]. During this time, the blast's chromatin undergoes a histone deacetylase 2 (HDAC2)-mediated condensation[227]. The condensed nucleus then moves towards the cell membrane and a contractile actomyosin ring (CAR) comprised of f-actin and myosin forms between the nascent reticulocyte and condensed nuclei[228]. Then, in a Rac GTPase and Diapahnous Related Formin 3 (mDia2)-dependent manner, the CAR contracts and in a process reminiscent of cytokinesis, the nucleus is extruded[229,230].

Interestingly, all of this takes place within the bone marrow in special units called erythroblastic islands. The centre of this island consists of a macrophage, or nurse cell, which is surrounded by erythroblasts undergoing differentiation[231]. The function of this centralised macrophage appears multifactorial with reports of it promoting enucleation, supplying iron and stimulating proliferation[232,233,234]. The idea that macrophages promote enucleation appears controversial, as multiple studies have shown retinoblastoma (Rb) knock out models result in anaemia, leading to the conclusion that erythroblasts require Rb to undergo enucleation[235]. However, the study by Ivarone et al. suggests a key macrophage function, as they rescued the Rb$^{-/-}$phenotype when Rb$^{-/-}$ erythroblasts were co-cultured with Rb$^{+/+}$ macrophages[234]. More definitive is the belief that macrophages phagocytose and destroy the nuclei once extruded[236]. Finally, GATA1 levels are regulated by direct erythroblast-erythroblast interactions which are facilitated by the nurse cell, although this phenomenon is not fully understood[237]. Note that mature erythrocytes can be differentiated from isolated mononuclear cells (MNCs) in $vitro$ without the presence of supporting macrophages, although this doesn't appear efficient[231].

After enucleation, the anucleate cells (reticulocytes) undergo further maturation whereby organelles (mitochondria) are degraded via autophagy and superfluous membrane proteins (CD71) are removed through endo-exocytosis[238,239]. At this stage, the reticulocyte moves into the circulation where over ~3 days it matures into an erythrocyte[240]. Surprisingly, during this time,

reticulocytes are still translationally active, although this does not persist into mature erythrocytes due to a widespread ribonucleolysis which removes nearly all the RNA[241]. This complex and highly regulated process results in a comparatively simple cell (total proteome of ~2000 in RBCs Vs >10,000 in HeLa cells) whose main purpose is the transport of oxygen; indeed, haemoglobin makes up an astounding 90% of the dry weight of an erythrocyte[242,243].

1.8.1.2 miRNA involved in erythropoiesis

Although the potential function of miRNA within mature erythrocytes is enigmatic, their role in erythropoiesis, due to an abundance of mRNA, is more defined. Multiple studies have profiled miRNAs at different stage of development, compared primitive and definitive erythropoiesis and even looked at miRNA dysregulation in disease (e.g. polycythaemia vera)[244,245]. Functionally, the gross role of miRNA during erythropoiesis is to either prevent, or stimulate differentiation – Table 2 summarises all studies relating to miRNA function during normal, definitive erythropoiesis.

Although the genes being repressed by miRNA are clearly key for erythropoiesis, their functions during differentiation vary. For example, miR-223 negatively regulates LMO2, a key erythropoietic transcription factor[246]. MiR-221/222 and miR-24 were shown to downregulate the expression of Tyrosine-Protein Kinase Kit (*KIT*) and Activin Receptor-Like Kinase 4 (*ALK4*), two surface receptors that bind SCF and ACTIVIN, respectively[247,248]. Both of these receptors have been demonstrated as essential for the proliferation of blasts and their subsequent differentiation, so unsurprisingly, a downregulation of these receptors perturbs erythropoiesis[249,250]. Iron metabolism was disrupted *via* the silencing of *ALAS2*, an aminolevulinate synthase essential for the production of haem, by miR-218[251]. Finally, miR-150 is reported to have multiple targets: firstly, it's a key player in defining lineage commitment, with high miR-150 levels silencing MYB and promoting megakaryopoiesis at the expense of erythropoiesis[252]. Secondly, during terminal differentiation, over expression of miR-150 silenced Erythrocyte Membrane Portein 4.1 (*EPB41*), a key cytoskeletal interactor[253]; however, miR-150 is downregulated during differentiation, so how relevant this study is remains to be seen.

Of the miRNAs that promote erythropoiesis, the miR-144/451 cluster is perhaps the best known. Expression of this cluster is promoted by GATA1. MiR-451, in a feedback loop, then silences GATA2 augmenting the GATA1/2 switch that occurs during erythropoiesis[254]. MiR-451 also plays a role during terminal differentiation as it downregulates 14-3-3ζ, itself, an inhibitor of the transcription factor Forkhead Box O3 (*FOXO3*). Silencing of 14-3-3ζ, allows for the subsequent upregulation of anti-oxidant genes Catalase (*CAT*) and Glutathione Peroxidase 1 (*GPX1*), protecting erythroblasts from oxidative stress[255]. In primitive erythropoiesis, miR-144 regulates embryonic α-haemoglobin expression through targeting Kruppel-like Factor D (*KLFD*), while in definitive erythropoiesis miR-144 silences *RAB14*, itself a negative regulator of erythropoiesis[254,256]. GATA1 appears to be responsible for promoting the expression of several other miRNAs, indeed, the GATA1/2 switch findings above were also found by Wang *et al*. who also reported a silencing of GATA2 by miR-27/24a following GATA1 stimulation[257]. MiR-199b-5p and miR-23a are also GATA1-dependent and downregulate Platelet Derived Growth Factor Receptor (*PDGFRA*) and Protein-Tyrosine Phasphatase 1D (*SHP2*), respectively[258,259].

Finally, miRNA also play a role in regulating other processes during erythropoiesis. For example, Rivikin *et al*. demonstrated that miR-142 KO mice developed erythrocytes with abnormal shape (knizocytes, leptocytes)[260]. Although a direct miR-target was not elucidated, this distinct phenotype was thought to be due a perturbation of F-actin filament arrangement, potentially regulated through Wiskott-Aldrich Syndrome Like (*WASL*) and/or Cofilin 1 (*CFL1*). Enucleation is a distinctive hallmark of erythroid maturation, and it has also been shown to be regulated by miRNA. For example, Zhang *et al*. demonstrated that miRNA expression, for the majority of miRNA species, declined as the cells differentiate. To establish what role these declining miRNA had, they over expressed miR-191, which resulted in a decrease of cells undergoing successful enucleation (~19% Vs 35%). Further work showed this was through inhibition of RIO Kinase 3 (*RIOK3*) and MAX Interactor 1 (*MXI1*), although how they mediate chromatin condensation / enucleation is unclear[261].

Table 2: The function of different miRNA during erythropoiesis

miRNA	Target	Effect	model	Reference
miR-142	Not stated	Regulates actin filament homeostasis	*In vivo* (Murine)	260
miR-144	*KLFD*	Regulates α-globin expression	*In vivo* (Fish)	256
miR-191	*RIOK3 / MXI1*	Regulates chromatin condensation and enucleation	CD34+	261
miR-451	*14–3-3-ZETA*	Protection from ROS	*In vivo* (Murine)	255
miR-125a-5p	*NIX*	Promotes mitophagy	HEL	262
miR-486-3p	*MAF*	Lineage choice (megakaryocyte Vs erythrocyte)	CD34	263
miR-150	*c-MYB*	Lineage choice (megakaryocyte Vs erythrocyte)	CD34+	252
miR-23a	*KLF3*	Promote β-globin expression	K562	264
miR-27a	*SP1*	Promote β-globin expression	K562	264
miR-150	*EPB41*	Inhibits differentiation	CD34 / K562	253
miR-218	*ALAS2*	Inhibits differentiation	K562	251
miR-200a-3p	*PDCD4 + THRB*	Inhibits differentiation	K562 / TF1	265
miR-124	*TAL1 / c-MYB*	Inhibits differentiation	CD34+	266
miR-223	*LMO2*	Inhibits differentiation	CD34+	246
miR-221/222	*KIT*	Inhibits differentiation	CD34+	247
miR-24	*ALK4*	Inhibits differentiation	CD34+	248
miR-23a	*SHP2*	Promotes differentiation	K562 / CD34+	259
miR-27a	Not stated	Promotes differentiation	CD34	257
miR-24	Not stated	Promotes differentiation	CD34	257
miR-199b-5p	*cKIT*	Promotes differentiation	K562	258
miR-156b-5p	*PDGFRA*	Promotes differentiation	K562 / CD34+	267
miR-144	*RAB14*	Promotes differentiation	CD34	254
miR-451	*RAB14 / GATA2*	Promotes differentiation	CD34 / TF1, *In vivo* (Fish)	268

1.8.2 **Mature RBC composition and function**

Mature erythrocytes are a model cell type for those wishing to study cellular deformability or membrane composition, as a result there are a plethora of studies characterising erythrocytes. Early electrophoretic work performed by Fairbanks *et al.* reported six major bands when erythrocyte ghosts (membranes devoid of haemoglobin) were resolved on acrylamide gels. In a move of stunning imagination, the bands were named in the order that they appeared on the gel, from top to bottom (bands 1-6) – names which have stuck to this day[269]. Over the years, the function of these proteins has been established in addition to them being given additional names i.e. band-2 is also known as ANKYRIN. More in depth analyses that Fairbanks *et* al. performed has also revealed that erythrocytes consist of ~1989 proteins[270]. However, the vast majority of this proteome consists of only a few key players, which are discussed below.

1.8.2.1 **Cytoskeleton**

Perhaps one of the most important parts of an erythrocyte is its cytoskeleton, due to the flexibility it affords the cell. In a beautiful study, Liu *et al.* used transmission electron microscopy (TEM) to show the cytoskeletal lattice that forms under the membrane (Figure 12)[271]. Essentially, this image is comprised of repeating units that are made up of long spectrin molecules held together by actin junctions. Spectrin exists as an α (220 kDa) and β (260 kDa) peptide, which coil around each other to form a long (100 nm) filamentous heterodimer $(\alpha,\beta)_2$ (Figure 12-Sp)[272]. Two heterodimers bind head-to-head to form a longer (~200 nm) tetramer[273]. Six to seven of these spectrin chains bind a central actin-troposin-band4.1 complex, forming a hex-heptamer motif, which repeats to create a cytoskeletal mesh (Figure 12-Ac)[274]. This cytoskeleton, observed as "floppy", imbues the erythrocyte with elasticity/deformability[273,275]. For example, Joel Anne Chasis and Narla Mohandas reported a reversible uncoiling of spectrin dimers (becoming longer and linearised) in response to sheer stress, allowing erythrocytes to deform and "squeeze" through narrow capillaries – something essential for the oxygenation of distal tissues[276]. The cytoskeletal mesh is then joined to the membrane at two key points: (1) ANKYRIN, a large adapter protein which

constitutes approximately 5% of the total protein of an erythrocytes membrane, interacts with ß-SPECTRIN and the N-terminus of BAND3 (Figure 12-An)[277]; (2) The ACTIN junction, which binds to Gly-C[278].
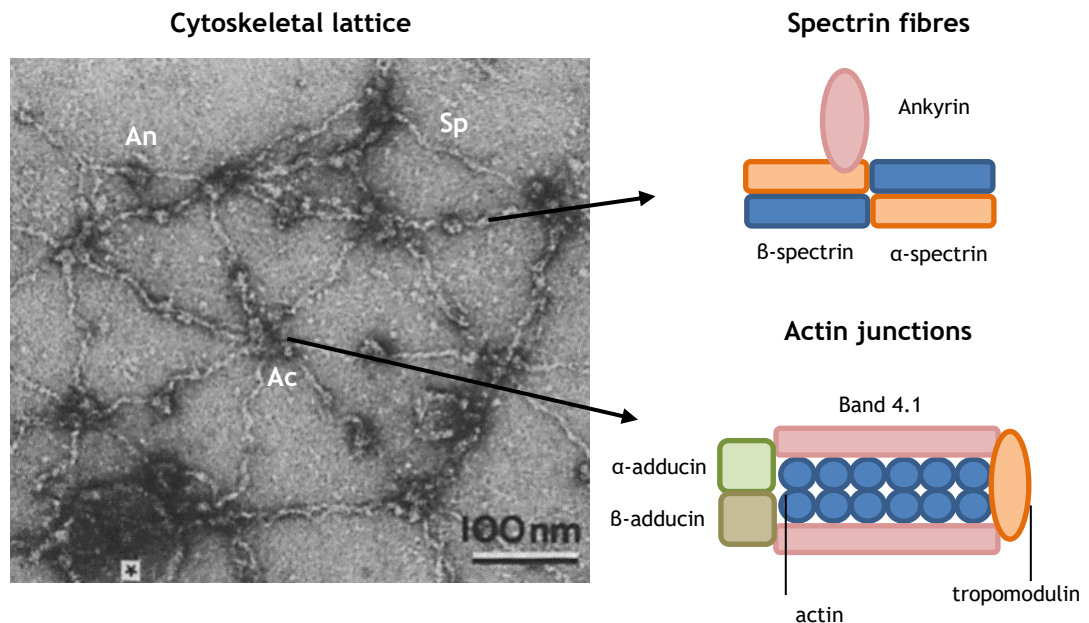
Figure 12: Structure and constituents of the erythrocyte cytoskeleton
TEM image was reprinted from the study Liu *et al.*; cartoons of spectrin fibres and actin junction are based on those from Bennet *et al.*[271,279].

1.8.2.2 Membrane constituents

The transmembrane BAND3 is an oligomeric protein that can form dimers or tetramers, interacting with additional proteins to form large multi-protein complexes[280]. It comprises approximately 15 % of the red cell membrane, is a member of the solute carrier family (SLC) and is responsible for processing carbon dioxide. Carbonic anhydrase, which binds BAND3's C-terminus, converts CO_2 into carbonic acid / bicarbonate ions as it diffuses into the cell, then back to CO_2 when the erythrocyte reaches the lungs[281]. The main function of the N-terminus is to bind ANKYRIN, tethering the cell membrane to the cytoskeleton; it also interacts with glycolytic enzymes and denatured haemoglobin, which is discussed later[282].

Additional proteins that can complex with BAND3 are Rhesus (Rh) proteins, CD47, the glycophorins and P55. The glycophorins (A, B, C) are another highly abundant (2% of total membrane protein) transmembrane protein group, which has two distinct roles. First, Gly-A,B,C carry the MN, Ss and Gerbich blood groups respectively[283]; secondly, in stopping RBC-RBC interactions, which is mediated by the abundant, negatively charged sialic acid post-translational

modifications that they contain[284]. Rh proteins, more commonly known as Rh antigens, comprise the Rh blood group. Interestingly, although there are only two genes (*RHD* and *RHCE*) they are polymorphic which results in the expression of 49 different antigens; absence or presence of *RHD* leads to blood being typed as positive (+) or negative (-) i.e. A+ / A-[285]. CD47 is an integrin binding protein whose role within erythrocyte biology appears to be as a "don't eat me" signal to splenic macrophages, while P55 appears structural[286,287].

1.8.2.3 **Cytoplasmic contents**

Unsurprisingly, the number one constituent of the red cell cytoplasm is haemoglobin. A tetramer consisting of 2-α and 2-ß peptides surrounding an iron-containing porphyrin ring, whose main function is to bind oxygen[243]. So abundant is the HAEMOGLOBIN (Hb), that it consistently caused troubles in proteomic studies and so specific steps were taken to remove it[288]. Using these, proteomic studies have revealed that additional proteins present fall under the following main groups: protective, energy production and turn-over[270].

One of the main challenges faced by erythrocytes is damage caused by oxidative stress[289]. As a result, CATALASE, GLUTATHIONE PEROXIDASE and PEROXIREDOXIN are highly abundant within the cytoplasm and function in converting H_2O_2, a metabolic by-product, into water[290-292]. Although not translationally active, erythrocytes still contain an active proteosomal degradation system and, as a result, contain various ubiquitin ligases[293]. Due to its importance to the central hypotheses of this thesis the data from this study was reviewed extensively, however, AGO2 was not amongst the proteins undergoing proteosomal degradation. Finally, even though mature erythrocytes lose their mitochondria during terminal differentiation, the deformation of the erythrocyte membrane during sheer flow is ATP dependent[294]. As a result, ATP is generated *via* glycolysis and mature erythrocytes contain all enzymes within this pathway.

1.8.2.4 **Discovery of e-miRNA**

The earliest paper to report the presence of erythrocytic-miRNA (e-miRNA), came from Tamas Dalmay's lab who were investigating the presence of short RNAs from *P. falciparum* infected erythrocytes[6]. Although no malarial sRNAs were

observed, an abundant amount of e-miRNA was observed both in normal and infected cells. However, while this is the first mention of e-miRNA, an in-depth review of the literature reveals that AGO2 had been identified 2 years prior[295]. Indeed, while many subsequent proteomic studies have revealed the presence of eukaryotic initiation factor 2c2 (EIF2C2, i.e. AGO2), what is perhaps most interesting about these studies is how abundant AGO2 is in comparison to other erythrocyte proteins[296,297]. For example, none of the referenced studies detect AGO2 just above background, and the most recent, quantitative analysis by Bryk *et al.* put AGO2 within the top 1% of proteins detected at the erythrocyte membrane (28th of 2653 unique proteins detected, when ranked by abundance)[298].

It's somewhat disappointing that these proteomic studies either dismiss the presence of AGO2, or simply ignore it[299,297]. All the more galling are studies that have expressly been set up to evaluate novel erythrocyte protein complexes, then apparently ignore the results. For example, when using blue native 2D electrophoresis, Van Getsel *et al.* identified a clear co-migration pattern between BAND3 and AGO2, but relegated this data to the supplementary and didn't comment upon it[299]. Maybe the name "translation initiation factor", admittedly incongruous in cells without a translational apparatus, deterred these authors. Even studies specifically looking at e-miRNA (not just AGO2), didn't really address their presence as functional, but as an indicator of the translational regulation that occurs during the terminal differentiation[300].

Indeed at the commencement of this study, only one paper looked at the possibility that miRNA in mature erythrocytes were functional[301]. The authors reported that miR-451 is internalised by *P. falciparum* and through its 3' end, covalently attaches to the 5' end of the malarial transcript *PKA-R* – creating a miR-451-*PKA-R* fusion. This prevents 5' capping and subsequent translation, leading to malarial resistance in erythrocytes. Therefore, in their paradigm, the RISC internalised by the parasite uses neither miRNA complementarity, nor AGO-mediated cleavage to elicit its anti-malarial effect. Even if you ignore this, i.e. an evolutionary conserved molecule acting outside of its conserved mode of action, I still have concerns regarding this study.

First and foremost, Lamonte *et al.* only observe this in an artificial system i.e. by adding "naked" oligos to *P. falciparum* in culture. By doing this they are adding non-AGO bound oligos (don't exist) at high amounts (~1×10^6 oligos per cell) which does not represent what occurs naturally within these cells. Indeed, dose may be an issue, as when they add 2 oligos (miR-451 + miR-223) the phenotype measured increases by roughly 50 % i.e. observed parasitaemia of ~75 % (one oligo) vs ~55 % (two oligos). In the same figure, it becomes apparent that this isn't a miR-451 specific phenomenon with other oligos having either the same effect, or none at all.

Although not directly tested, dose may well have an effect within the system of Lamonte *et al*. For example, when they attempt to detect the fusion transcript by sequencing RNA extracted from *P. falciparum* cultured in erythrocytes without additional oligos, the fusion transcript only represented 8 out of 1.5×10^7 reads; indicating it occurs at very low levels. Furthermore, the databases in which they say the fusion transcript is also reported are also suspect. For example, they come from one extended group (Sugano & Watanabe), who use expressed sequenced tags (EST) to cap the 5' end of malarial mRNA prior to cDNA synthesis[302]. There is no mention of how the RNA is extracted from *P. falciparum* other than "standard methods". However, if RNA was extracted from infected erythrocytes, not purified parasites then their extracted RNA would contain e-miRNA. An explanation for this fusion transcript may simply be that, the oligo-ligation event they employ, actually ligates an e-miRNA to the 5' end of a parasites mRNA[303,304]. If my suspicion is correct, then you would expect to obtain other parasite-emiRNA fusions out with of miR-451-*PKA-R*, and you do (Lamonte *et al*. supplementary); including rRNA fusions.

1.8.2.5 Characterisation of e-miRNA

As there was little known about e-miRNA at the commencement of this study, the Hamilton lab set out to characterise them. During this characterisation, they discovered several surprising properties. (1) e-miRNA concentration: using UV spectroscopy, they calculated that e-miRNA is as concentrated as miRNA in nucleated cells, furthermore, short-term culture indicated that e-miRNA are stable despite widespread ribonucleolysis following terminal erythroid differentiation (Figure 13a, redrawn with permission). Due to the huge number of

erythrocytes in the circulation, they calculated that e-miRNA constitute ≥99% of total miRNA within whole blood (Figure 13b). (2) e-miRNA conservation: Illumina sequencing established an e-miRNAome of 470 different miRNAs, while initial phylogenetic analyses indicated conservation across Mammalia (Appendix **1 - 4**). (3) Selective protein retention: western analysis showed that while erythroblasts express AGO1-4, mature erythrocytes contain only AGO2. Indeed, *in vitro* differentiation of CD34⁺ showed the concomitant decrease of AGO1, 3 and 4 while AGO2 showed only a modest decrease (Figure 13c/d). (4) Maintained RISC potential: AGO2 pull downs followed by Northen blots demonstrated that the e-miRNA were present as RISCs. Catalytic potential was demonstrated by incubating radiolabelled bait RNAs (*in vitro* transcripts containing sequences complementary to e-miRNA) in erythrocyte lysates, resulting in predictable cleavage patterns (Figure 13e). This, and other data, was what this project was predicated on, the exact hypotheses of this project are discussed in Section **1.12.2**.

Figure 13: Characterisation of e-miRNA.
a) Total RNA extracted from erythrocytes cultured for 0, 1 and 2 days (to mature residual reticulocytes) then resolved via capillary electrophoresis to compare RNA profiles, miR-451 northern blot serves as loading control; b) small RNA profile of whole blood and leukoreduced blood when

stained with ethidium bromide; c) *in vitro* differentiation of CD34⁺ cells into erythrocytes and subsequent western blots of protein taken at different time points to investigate the retention of AGO proteins during erythropoiesis; d) western and northern blot of protein/RNA extracted from purified erythrocytes from different donors (N1-4); e) Catalytic potential of RISC was evaluated by P32 labelling *in vitro* transcripts containing an e-miRNA reverse complement (or not), then incubating them with an erythrocyte lysate for 1 hour, then resolving samples on an agarose gel.

1.8.3 **RBC senescence**

After reticulocyte maturation, adult erythrocytes course through the body delivering oxygen to tissues for approximately 120 days[305]. During this time, they age and undergo a number of distinctive changes in a process called senescence; notably, erythrocyte senescence is not the same as in other cells[306]. At the end of this process, senescent erythrocytes are recognised by specialist macrophages located within the red pulp of the spleen, turned over and the iron within the haemoglobin recycled[307]. Indeed, this process is essential, with greater than 80% of the iron required for daily erythropoiesis coming from recycled senescent erythrocytes[308]. However, before that can occur, senescing erythrocytes must undergo several biochemical and biophysical cues to be recognised by splenic macrophages.

1.8.3.1 **Gradual deterioration**

First, as there are no definitive stages to erythrocyte ageing, rather a gradual senescence over 120 days, the experimental means by which researchers isolated "old" vs "young" erythrocytes must first be established. A common observation regarding senescent erythrocytes, is that they get denser as they age, although it's not clear where this observation was first made. Nevertheless, the first study to evaluate this *in vivo,* compared the mean corpuscular volume (MCV) of erythrocytes from hypertransfused rats and noted a decrease in MCV between day 0 and day 48 samples[309]. They postulated that increased density of erythrocytes was initially due to water loss, followed by loss of haemoglobin. This observation, that increasing cellular density is proportional to age, has been used by multiple studies in a multitude of different medias (e.g. arabinogalactan, BSA) to separate erythrocytes; at present, Percoll separation appears the most common[310-312]. Concerns raised regarding density gradients (i.e. blood not separating properly, heterogenous fractions etc) appear to have been addressed through more technical studies, whose data corroborate that of the density gradients. In these studies, erythrocytes are biotinylated using a succinimidyl

ester *in vivo/in vitro* and then allowed to age *in vivo*[313,314]. Blood samples are taken at different time points, captured on a streptavidin matrix then analysed.

In gross terms, these studies have revealed that the activity of key enzymes (superoxide dismutase, catalase etc) decrease with age, leading to an accumulation of oxidised proteins – all of which is thought to lead to macrophage recognition[315,316]. Normally haemoglobin cycles through an oxygenated and deoxygenated state, with the deoxygenated state preferentially associating with BAND3[317]. Furthermore, haemoglobin undergoes random autoxidation from the O_2 binding Fe^{2+}, to the non-O_2 binding form Fe^{3+} (methaemoglobin). This autoxidation is associated with the production of superoxide anions, although these are normally processed by superoxide dismutase[318,319]. Increased methaemoglobin membrane association occurs as cells age, which, when coupled with a decrease in enzymatic activity, leads to an increase of oxidised membrane proteins[320,321]. Oxidised haemoglobin covalently binds spectrin, leading to an increased membrane rigidity; while oxidisation of BAND3, or, oxidised-haemoglobin-BAND3 interactions, cause BAND3 clustering[322,323]. BAND3 clustering is an essential part of erythrocyte senescence as it promotes the binding of autologous IgG, something that does not occur in younger erythrocytes[324]. This in turns leads to the deposition of the complement component C3b *via* the alternative complement cascade[325]. Finally, increased cellular rigidity attenuates a senescent cell's ability to pass through the spleen, bringing it in longer contact with red-pulp macrophages, while an age-linked reduction of CD47 allows the cells to be cleared[286].

1.8.3.2 Turnover and iron recycling

Following recognition by splenic macrophages, erythrocytes are internalised and degraded within a phagolysosome[326]. On the face of it, this appears simple, in practice it is far more complex. For example, haem is not degraded within the lysosome, which one would assume to occur along with the rest of the erythrocyte, instead it is exported into the cytoplasm by HAEMRESPONSIVE GENE 1(HRG1)[327]. Here it is broken down into billirubin, Fe^{2+} and CO_2 by HAEME OXYGENASE 1 (HO1)[328]. Following haem catabolisim, the majority of Fe^{2+} is exported into the plasma *via* the membrane protein ferrorportin, while the remaining Fe^{2+} is stored as ferritin; bilirubin is excreted and detoxified by the liver[329,330]. Although the mechanism is not fully understood, haem can also be

broken down within the phagolysosome, with NRAMP1 facilitating Fe^{2+} removal into the cytoplasm[331,332]. <mark>This is particularly important with regards to this project, as it demonstrates two means by which molecules (haem, Fe^{2+}) can exit a phagolysosome, something that would have to occur for e-miRNA, if they were to leave a cell or vesicle and regulate a macrophages transcriptome.</mark>

In addition to recognising senescent erythrocytes, splenic/hepatic macrophages also play key roles in quality control and processing extracellular Hb. For example, following intravascular haemoloysis, haptoglobin (Hp), a plasma expressed scavenger, complexes with haemoglobin (Hb-Hp) allowing its recognition and degradation by $CD163^+$ macrophages[333]. Finally, the narrow nature of the cords of Billroth within the spleen, coupled with rapid circulation, means that erythrocytes are constantly in contact with red pulp macrophages – allowing for quality control. During maturation, incomplete nuclei expulsion can result in small parts of DNA remaining within an erythrocyte (Howell-Jolly body), or, due to oxidative damage/disease, Heinz bodies consisting of denatured haemoglobin can also form. However, in a process known as "pitting", red pulp macrophages can "bite" out these inclusions, returning erythrocytes to the circulation[334,335].

1.9 Blood transfusion

The transfusion of RBCs within hospitals is common with approximately 6000 units required daily in England alone[336]. Although blood transfusions are required by health services globally, the way they are prepared and stored can differ drastically from country to country. As part of this thesis deals with transfusion-associated complications, how blood units are prepared in this country, and differences to other countries, will be discussed.

1.9.1 Blood processing and storage

In the UK, blood units are prepared, stored and managed by the National Blood Transfusion (NBT) service. A blood donation of 450 mL (±10%) is collected from healthy donors into a plastic bag containing 63 mL of the anticoagulant citrate phosphate dextrose[337]. Donations are then passed through two filters: the first removes cellular clumps and fibrin clots, while the second, comprising of polyester or polyurethane, removes $\geq$ 95% of the leukocytes and platelets. The

leuko-depleted, platelet ablated blood is then centrifuged, the plasma removed and the erythrocytes re-suspended in 50 mL of the additive solution Saline Adenine Glucose Mannitol (SAGM); it is then stored at 2-6 °C for a maximum of 42 days. The final specification for blood units within the UK are: volume of 280 – 420 mL, haematocrit of 55 – 75 % and leukocyte count of < $5x10^6$ per unit.

Differences between countries can be major, with leukoreduction not mandated in the US, or subtler, with different formulations or concentrations of additive solutions being used[338]. For example the US uses either AS-1, AS-3 or AS-5, the Japanese use mannitol-adenine-phosphate (MAP), while phosphate-adenine-glucose-guanosine-gluconate-mannitol (PAGGSM) is used in Germany [339]. Although the functions of the individual reagents in these additive solutions is different, the main aim is to prevent eryptosis – i.e. erythrocyte cell death. The glucose is added in excess to what these cells require during storage (3 mmol), ATP improves post-transfusion viability, while mannitol was shown to increase storage by 1 week while also reducing haemolysis[340-342]. As can be seen by Table 3, the formulations of these buffers aren't drastically different and with regards to storage, the benefit of one formulation over the other isn't strikingly clear - although one study has reported that erythrocytes stored in SAGM lose more membrane then those stored in AS-1[343].

Table 3: Composition of different additive solutions used across the globe, redrawn from Sparrow *et al.* 2012[339].

	Licensed RBC additive solutions					
Constituents (mM)	SAGM	AS-1	AS-3	AS-5	MAP	PAGGSM
NaCl	150	154	70	150	85	72
Na2HPO4	-	-	-	-	-	16
NaH2PO4	-	-	23	-	6	8
Citric acid			2	-	1	
Na-citrate	-	-	23	-	5	-
Adenine	1.25	2	2	2.2	1.5	1.4
Guanosine	-	-	-	-	-	1.4
Dextrose (glucose)	45	111	55	45	40	47
Mannitol	30	41	-	45.5	80	55
pH	5.7	5.5	5.8	5.5	5.7	5.7
Anti-coagulant	CPD	CPD	CP2D	CPD	ACD	CPD
Countries used	Europe UK Australia Canada New Zealand	USA	USA Canada	USA	Japan	Germany

1.9.2 The storage lesion

However, regardless of additive solution used, during storage, erythrocytes undergo a variety of morphological and biochemical changes. Biochemically, glycolytic components 2,3-diphosphoglycerate (DPG) and ATP decrease over time[344], while the pH falls due to increased levels of lactic acid[345]. As DPG interacts with haemoglobin, and is critical in the release of oxygen *in vivo*, it was postulated that older blood may not transport oxygen efficiently, although studies have failed to find a clinical link[346]. These biochemical alterations induce morphological changes within RBCs and subsequent vesicularisation[347]. During this time, erythrocytes change from classical biconcave discoids to echinocytes and finally spherocytes. Echinocytes feature multiple membranous arms called spicules from which MVs are released as part of membrane inversion and contraction. Haemoglobin levels within the storage medium increase due to haemolysis, although studies indicate a significant proportion of free haemoglobin is contained within shed MVs[348,349].

1.9.3 **miRNA and the storage lesion**

While miRNAs have been evaluated with regards to the platelet storage lesion as a method to evaluate apoptosis[350,351], only one study has evaluated miRNA during RBC storage. Although miR-96, -150, -196a, and -197 showed an increase in concentration within the storage media, these miRNAs are not readily found within erythrocytes and changes in expression are likely due to contaminating leukocytes that were not depleted; therefore this study is not representative of a UK storage lesion and of limited use[352].

1.10 **RBC-MVs**

Review of the literature indicates that there are three types of extracellular vesicle associated with red cells. These can broadly be thought of as naturally-occurring (i.e. *in vivo*), or, artificial (i.e. those generated through the storage lesion). Description of each are as follows:

1.10.1   **Naturally occurring**

1.10.1.1   **Exosomes**

Erythrocytic exosomes (exRBC) are ~ 0.05 µm in size and are produced by reticulocytes during the final stages of maturation as a means of removing their transferrin receptor (CD71). While this was first reported by Pan *et al*. in 1983, it was their 1985 paper that visualised the mechanism behind this[353,354]. In a particularly elegant study, they probed sheep reticulocytes with anti-CD71 serum, allowed them to mature *in vitro* and analysed them at different time points using immuno-gold TEM. At early time points, CD71 can be seen both on the surface of reticulocytes as well as coating "pits" in the membrane. These pits are internalised, forming exosomes which are subsequently packaged into much larger multivesicular bodies (MVBs) (1 -1.5 µm). These MVBs then fuse with the cellular membrane allowing for EX expulsion (Figure **14**). CD71 recycling is therefore a defined biological pathway, which is different to what occurs during the storage of RBCs.
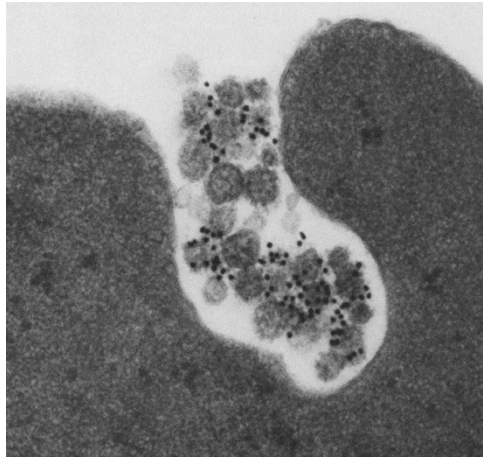
Figure 14: RBC exosome exocytosis.
Figure reprinted from Pan *et al.* dark shape is a maturing erythrocyte, while black dots represent CD71 being excreted on exosomes; earlier pictures in this study show CD71 being internalised and multivesicular bodies forming[353].

1.10.1.2 Microvesicles

The first RBC vesicles detected *in vivo* were reported in 1984, although, as the authors only used TEM and SDS-PAGE analysis of filtered plasma, and did not confirm them immunologically, it is impossible to say if these were truly RBC derived, or from leukocytes / platelets[355]. Nevertheless, Wilkelin *et al.* used this to investigate the possibility that vesicularisation was the means by which RBCs lose ~ 20% Hb as they age[356,357]. The presence of glycated Hb (Hb1c) was confirmed in these MVs and the overall Hb content found to be similar to that of aged RBCs, indicating these MVs came from aged erythrocytes. Later, they reported that MVs were positive for IgG and senescent erythrocyte antigen (clustered BAND3), leading them to hypothesise that the purpose for vesicularisation was to remove pro-phagocytic signals or damaged Hb from RBCs[358].

1.10.2 Artificial

The first erythrocyte vesicle was reported in Nature by Allan *et al.* when they used the calcium ionophore A23187 to produce ~100 nm vesicles[359]. This was repeated in multiple other studies before Lutz *et al.* reported the same phenomenon occurring in artificially aged erythrocytes i.e. stored at 37 °C for > 12 hours without glucose[344]. What is particularly interesting about this study is that vesicularisation was inhibited compared to control: storing erythrocytes in glucose, adenosine, inosine and saline – a very similar buffer to SAGM. It wasn't

until 5 years later that these MVs were reported in stored blood units[347]. Multiple studies have characterised RBC-MVs, both ionophore and storage induced, revealing that they are: (1) spectrin free[344]; (2) have exposed phosphatidylserine[360]; (3) are enriched for stomatin[361]; (4) range from 100-200 nm in size[360] (Figure **15**); (5) contain blood group antigens[362] and (6), increase in number when blood is stored[363]. Indeed, as MVs were found to increase with blood storage, something of clinical interest, multiple studies have now evaluated the effect of these MVs in transfusion. Some of which are discussed below.

Note: at the beginning of this study, there were no reports of miRNA within RBC-MVs (natural or artificial), although supplementary data from a proteomic screen of storage MVs indicated AGO2 (EIF2C2) was not present[296].
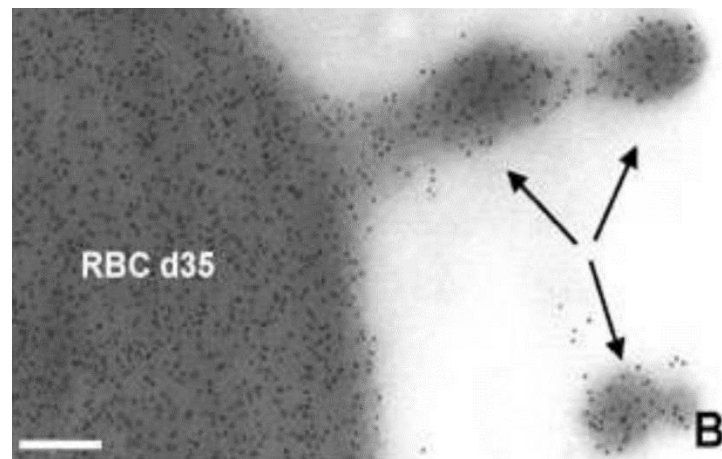
Figure 15: Microvesicles "blebbing" from stored erythrocytes.
Figure reprinted from Kriebardis *et al.* Dark shape represents a stored erythrocyte with a protruding spicule, MVs can be seen "blebbing" from the end; dark dots represent Hbb as visualised by immunogold labelling[364]; scale bar = 0.2 μm).

1.11 Transfusion associated complications

Complications associated with the transfusion of aged RBCs is disputed within the literature - some studies indicate no deleterious effects of transfusion, while others correlate it to morbidity and mortality[365,366,367]. In both types of study, the study group involved trauma patients, ICU patients, and those undergoing coronary surgery. End points include increased mortality, development of deep vein thrombosis, multiple organ failure and increased length of hospital stay or nosocomial infections in patients transfused with "older" rather than "younger" blood. Interestingly some of these studies indicate a dose effect is present. However, while cohorts are generally large and statistically significant,

changes in these studies are modest. For example, Robinson *et al.* evaluated 30-day survival in patients undergoing percutaneous coronary intervention and found that patients receiving high volumes of blood had a higher hazard ratio (HR) (1.26 [95% CI 1.18-1.34], P < 0.001) than those receiving lower volumes[368]. Interestingly, when they evaluated blood $\geq$ 28 days old in comparison to younger units, they observed a HR of 2.4 ± 1.8 versus 3.2 ± 2.4 (P < 0.001). Koch *et al.* compared sepsis, mortality, renal failure and intubation time in patients undergoing heart surgery and found that patients receiving old blood ($\geq$20 days) had an increased risk of complications than those receiving younger blood (25.9% vs 22.4% P = 0.001)[369]. However, in a similar study, McKenny *et al.* found no correlation between blood age and the aforementioned end points; although they did notice a trend between higher transfusion volumes and adverse outcome[370].

It is difficult to compare the results from these studies due to the different statistical methods used, different definitions of "old" or "young" blood and RBC preparations (storage medium etc). In addition, they do not address mechanistic details and the few *in vitro* studies that exist are as conflicted as the clinical observations. For example, Baumgartner *et al.* released two studies in quick succession with different conclusions. In the first study, they demonstrated that RBC storage supernatant potentiated the release of pro-inflammatory cytokines (Interleukin (IL)-1β, IL-6 and tumour necrosis factor alpha (TNF-α)) from LPS-primed peripheral blood (PB)-MNCs and the effect was magnified using the supernatant of older blood units (42 vs 1 day); interestingly leukoreduction attenuates IL-1β release only, indicating one agonist was of white cell origin[371]. Conversely, the following year they released a study that indicated that RBC supernatant had an anti-inflammatory effect and was effective through CD3-primed T_{reg} cells[372]. Something similar was observed by Sadallah *et al*, however, as they didn't use cytokines to differentiate their monocytes, or, phenotype their "macrophages" the data is of dubious value[373]. An additional effect associated with older blood was indicated in a different study where by supernatant from older blood increased the speed of coagulation by 1.5 minutes (P $\leq$ 0.01) compared to the control[374]. The authors speculated that this effect was mediated by RBC-MVs and could be dose-dependent; unfortunately, as they did not quantify the MVs used, dose parity could not be confirmed between experimental arms. This is important as the authors observed different rates of storage lesion deformation

between samples which they suggest was the reason only half their samples exerted a procoagulant response within a 41 day storage period. The disparity in these studies is most likely due to the systems employed, more specifically, how the system is "primed". For example, Baumgartners' LPS model induced a pro-inflammatory response while his CD3 activation induced an anti-inflammatory response. The response phenotype is likely therefore highly complicated, involves cross talk between multiple cell types and may change based on the underlying condition.

Predominantly, the *in vivo* studies identified during this literature review have focussed on transfusion-related acute lung injury (TRALI) and use a "two-hit" murine or rat model[375]. The first hit occurs when animals are primed with LPS, activating pulmonary neutrophils – the second hit occurs with the addition of aged erythrocytes, storage supernatant or MVs. Hod *et al.* showed a marked pro-inflammatory response, an increase in splenic, kidney and free iron levels when transfusing aged blood; mice were also described as moribund and displayed different behavioural characteristics compared to controls[376]. The authors assigned this to extravascular haemolysis by macrophages and the subsequent release of free iron; although IL-6, TNF-α and keratinocyte derived chemokine (KC) levels did not return to control levels following treatment with an iron chelator. Furthermore, they state that this effect is explicit to the RBC portion of a transfusion and not factors released into storage media during the storage legion. This is in contrast to other studies which highlight MVs and not erythrocytes per se as mediating transfusion associated complications. Different mechanistic reasons are also given, with one study citing complement activation *via* thrombin cleavage of C5[377]. The study by Vlaar *et al.* did not speculate on the cause, but rather demonstrated that the inflammation and coagulopathy seen within their experiments could be abrogated *via* the washing of the blood unit and the cause was not due to lysophosphatidylcholine[378]. This distinction was made as it differed to findings from Silliman *et al.*, but as this group neither leukoreduced their blood and transfused human blood into rats their data is of uncertain relevance[379]. No studies definitively identify the cause of the TRALI, but they all demonstrate a pro-inflammatory response in primed hosts after the transfusion of aged RBC products. Of particular interest, is the mild inflammatory response observed within unprimed animals, as this lends credence to the idea that transfusion itself

might be deleterious. These studies sacrificed their animals within 24 hours, precluding the possibility of clinical symptoms (tissue damage) developing over time; to date, no study has evaluated the effect of multiple transfusions or the miRNA found in blood units.

But why does the effect of multiple transfusions have a clinical interest? A clinical condition in which patients are undergoing severe pro-inflammatory responses and can receive mulitple RBC transfusions is graft-versus-host disease (GVHD) which can occur following allogeneic stem cell transplantation (alloSCT). GVHD is a complication that arises when donor T-cells attack recipient tissue. Donor T-cells are responsible for another phenomenon called graft-versus-leukaemia (GVL) effect, where by the graft removes residual cancerous cells[380]. While depleting graft T-cells abrogates GVHD, it also increases the risk of relapse and so, has limited utility. Therefore, a method which reduces GVHD whilst maintaining the GVL response is the holy grail of GVHD research. Grade II - IV acute (a)GVHD develops in approximately 70% of patients following an alloSCT for haematopoietic malignancies and is fatal in approximately 20% of cases[381]. The disease manifests as acute, with symptoms appearing 20 – 100 days post-transplant, or chronic (c), with symptoms appearing after at least 100 days following alloSCT; however, these time frames are not exact and aGVHD can manifest more than 100 days post-transplant[382]. Predominantly, patients who develop cGVHD were previously diagnosed with aGVHD. According to the National Marrow Donor Program, 12% of non-sibling cGVHD patients did not previously have aGVHD (*de novo*), 69% had a gap between onset of cGVHD (interrupted or quiescent) and 19% progressed directly from aGVHD[382].

Acute GVHD pathophysiology is more widely understood than that of cGVHD and it is thought to occur over 3 stages[383]. Host conditioning and inflammation – the first stage where by the patient (host) undergoes myeloblative chemotherapy or total body irradiation in preparation for the graft. This results in the release of the pro-inflammatory cytokines TNF-α, IL-1, IL-6 and damage to the gastrointestinal tract which perturbs the gut micro flora leading to increased exposure to LPS[384]. Host antigen presenting cells (APCs) are thus primed *via* the conditioning regime used and conditioning intensity has been linked to the severity of GVHD. The second stage occurs when donor T-cells are activated by host APCs,

causing them to differentiate. This stage is complicated by the fact that no individual APC has been identified as the *de facto* cell type and stage 2 is likely a balance involving multiple interactions, i.e. CD4 T-cells and host APCs within the gastrointestinal tract[385] or CD8 T-cells and haematopoietic APCs[386]. Indeed, differentiation of T-cells is cytokine-specific and there is growing evidence that particular subsets of T-cells are associated with specific clinical manifestations. For example, differentiation into Th17 following IL-6 stimulation is associated with lung and skin GVHD[387], while Th2 is associated with the skin and liver and is induced by IL-14[388]. The final stage is the effector stage, where by monocytes, natural killer (NK) cells, CD4 T-cells or CD8 cytotoxic T-cells migrate to a specific area and cause apoptosis of neighbouring cells in an antigen-dependent, or antigen-independent manner (CD8 T-cells).

As part of an alloSCT, patients are likely to be transfused with varying amounts of blood. Mean transfusion is ~ 15 units at a rate of 0 – 4 units per week, but this is patient dependent, with some patients not requiring transfusion whereas others, in extreme cases, can reach up to 96 units (personal communication Mhairi Copland). There appear to be no studies investigating either the age of RBCs or the volume of transfused blood exacerbating or being involved in GVHD. A condition called transfusion associated GVHD (TA-GVHD)[389] exists, but it is caused by leukocytes within transfused whole blood and can be stopped by irradiating blood prior to transfusion.

1.12 Project Aims

1.12.1 Summary

When characterising e-miRNA, the Hamilton lab demonstrated that e-miRNA are as concentrated as miRNA from nucleated cells, appear conserved across Mammalia, selectively retain their binding partner (AGO2) at the expense of AGO1, 3, 4, and that erythrocytic RISC complexes maintain a catalytic potential. Taken together, this data indicates a function for e-miRNA, although what this is, is currently unknown. Due to the importance of red cells, both biologically and clinically, we decided to investigate their presence in more detail. As a result, this project investigates questions of homeostasis and transfusion-associated complications.

1.12.2 **Aims and hypotheses**

This project, as with many others, ended up evaluating a question different to what was posed at the beginning. Despite this change in direction, the project did not deviate from the idea that e-miRNA may be functional, it just changed where they may be functioning. With that in mind, even though the three main hypotheses evaluated during this project are summarised below, they were not raised at the beginning of the project and are summarised here for clarity. The reasons for these new hypotheses being raised is detailed in individual chapters after certain data has been generated and interpreted. The aims of the project were as follows:

1.   To determine if e-miRNA play a role within mature erythrocytes that is unrelated to translational regulation;

2.   To determine if e-miRNA lie dormant within erythrocytes but regain their roles as translational regulators in phagocytosing cells;

3   To evaluate how Kupffer-like macrophages respond to an artefact of blood storage: RBC-MVs.

The specific hypotheses behind these aims are:

Hypothesis 1

Establishing interactors with AGO2 using unbiased biochemical analyses

The findings from the Hamilton lab that were elucidated when characterising e-miRNA (Section **1.8.2.5**) lead us to believe that e-miRNA may have a function within erythrocytes. However, as these cells are translationally inert, for e-miRNA to function it must be out with canonical gene silencing. As it is impossible to logically predict what this function may be, an unbiased biochemical approach was used. The unbiased approach of this project involved the isolation of erythrocytic RISCs using biotinylated probes specific to individual e-miRNA. These probes hybridised with the miRNA portion of RISC, before RISC and any interacting proteins were sequestered *via* streptavidin magnetic beads.

Ideally, this would will allow us to establish what the AGO2 portion of RISC interacts with, allowing us to form hypotheses regarding e-miRNA function within erythrocytes.

Hypothesis 2

Evaluating the effect of RBCs or RBC-MVs on the transcriptome of macrophages

Our specific hypothesis is based upon the endpoint of RBC senescence. The life span of a mature erythrocyte is approximately 120 days and during this time it undergoes a variety of morphological and biochemical changes[390]. Firstly, erythrocytes shed a proportion of their membrane through the production of microvesicles (MVs), resulting in cell shrinkage during senescence[355]. Secondly, the oxidative state of erythrocytes increases with age, resulting in the accumulation of oxidised proteins at the cytosolic side of the membrane. This plays a role in the oligomerisation of the membrane protein BAND-3, which in turn promotes the binding of naturally occurring antibodies (nAbs)[322,391]. These "naturally opsonised" RBCs are recognised by splenic macrophages and it is thought this is how macrophages distinguish between senescent and young erythrocytes. Following phagocytosis, the erythrocytes are destroyed and the iron recycled; RBC-MVs are also recycled by macrophages, but this takes place in the liver[392]. As there is no mRNA in RBCs for e-miRNA to regulate, we postulate that e-miRNA, either in erythrocytes or MVs, escape phagolysosomes following ingestion by macrophages and regulate their mRNA in order to maintain homeostasis.

Hypothesis 3

Evaluating the effect of RBC-MVs generated during storage on Kupffer-like macrophages

At the beginning of this project the medical community were split with regards to the negative affect that aged transfusions have on patients[369,370]. *In vitro* studies were also conflicting with some reporting pro-inflammatory effects, and others, anti-inflammatory[371,372]. To date, no study had evaluated the effect of storage MVs on phenotypically relevant macrophages i.e. Kupffer-like cells.

Murine models exist, but these are always primed with LPS before MV/blood/storage supernatant addition. As miRNA have been shown to be transferred between cells in EVs, our hypothesis is any mal-effect that occurs upon transfusion of aged blood products is mediated, in part, by the miRNA-containing vesicles present in the storage lesion.

Chapter 2   Materials and methods

2.1 Buffer compositions

Final concentrations of each reagent included in each solution along with the suppliers are described below:

2.1.1 Protein solubilisation buffer

50 mM Tris-HCL pH 7.5 (Sigma)

150 mM NaCl (NP40, Sigma)

1 % nonidet P40 (Sigma)

10 % glycerol (Sigma)

5 mM ethylenediaminetetraacetic acid (EDTA) (Sigma)

Phosphatase and Protease inhibitor concentrations supplementing solubilisation buffer:

1 mM sodium orthovanadate

1 mM sodium molybdate

1 mM sodium fluoride

40 µg/mL phenylmethylsulphonyl fluoride

0.7 µg/mL pepstatin A

10 µg/mL aprotinin

10 µg/mL leupeptin

10 µg/mL soybean trypsin inhibitor

2.1.2 5 x sodium dodecyl sulphate (SDS) sample buffer

10 % (*w/v*) SDS (Sigma)

Milli-Q ultrapure water

200 mM Tris-HCl pH 6.8 (Sigma)

50 % (*v/v*) glycerol (Sigma)

Bromophenol blue (Sigma)

5 % (*v/v*) 2-mercaptoethanol (Sigma)

2.1.3 1 x SDS-polyacrylamide gel electrophoresis (PAGE) running Buffer

25 mM Trizma base (Sigma)

192 mM glycine (Sigma)

0.1 % (*w/v*) SDS (Sgima)

2.1.4 Silver stain

2.1.4.1 Fixing solution

50 % ethanol (Thermo) (*v/v*) in Milli-Q water

10 % acetic acid (Thermo) (*v/v*) in Milli-Q water

2.1.4.2 Sensitiser solution

1 % ProteoSilver Sensitiser (Sigma) (*v/v*) in Milli-Q water

2.1.4.3 Silver solution

1 % ProteoSilver Silver Solution (Sigma) (*v/v*) in Milli-Q water

2.1.4.4 Developer solution

5 % ProteoSilver Developer 1 (Sigma) (*v/v*) in Milli-Q water

0.1 % ProteoSilver Developer 2 (Sigma) (*v/v*) in Milli-Q water

2.1.5 1 x Tris-buffered saline (TBS) pH 7.5

 20 mM Tris-HCl pH7.5 (Sigma)

150 mM NaCl (Sigma)

2.1.6 1 x Tris-buffered saline NP40 (TBSN)

20 mM Tris-HCl pH 7.5 (Sigma)

150 mM NaCl (Sigma)

0.05 % (*v/v*) NP40

2.1.7 Blocking solutions

2.1.7.1 BSA blocking solution

1 % (*w/v*) bovine serum albumin fraction V (Roche)

1 % (*w/v*) ovalbumin (Sigma)

0.01 % (*w/v*) sodium azide (Sigma)

Dissolved in 1 x TBS pH 7.5

2.1.7.2 Milk blocking solution

5 % (*w/v*) milk (Marvel)

0.01 % (*w/v*) sodium azide (Sigma)

Dissolved in 1 x TBS pH 7.5

2.1.7.3 Goat serum blocking solution

5 % (*v*/*v*) goat serum (Sigma)

0.01 % (*w*/*v*) Sodium Azide (Sigma)

Dissolved in PBS pH 7.5

2.1.8 FACS buffer

1 x PBS *w*/*o* Ca^{2+} or Mg^{2+} (Thermo)

2 % (*v*/*v*) BSA Fraction V (Roche)

0.01 % (*w*/*v*) sodium azide (Sigma)

2.1.9 Vesicularisation buffer

1 x Hanks buffered saline solution (HBSS) pH 7.5 (Thermo)

1 µM calcium ionophore A23187 (Sigma)

2.1.10 RBC fixation buffer

4 % (*w*/*v*) paraformaldehyde (PFA, Sigma)

Dissolved in 1 x PBS pH 7.5

0.2 % (*v*/*v*) glutaraldehyde (Sigma)

2.1.11 General buffers

2.1.11.1 Buffy coat wash buffer

0.5 mM EDTA (Sigma)

2 % human serum albumin (Roche)

Dissolved in 1 x PBS pH 7.5

2.1.11.2   RBC lysis buffer

150 mM NH$_4$Cl (Sigma)

1 mM KHC0$_3$ (Sigma)

.1 mM EDTA (Sigma)

2.1.11.3   RBC wash buffer

4 % BSA Fraction V in PBS *w/v* (Roche)

2.2 Tissue culture

2.2.1 Cell lines

2.2.1.1 Suspension cells

K562[393] (human CML blast crisis, passage 4) and Jurkat[394] cells (human acute T cell leukaemia, passage 6) as purchased from Deutsche Sammlung von Mikroorganisem und Zellkulturen (DSMZ) were cultured in Roswell Park Memorial Institute medium (RPMI) supplemented with 10 % foetal bovine serum (FBS) (Gibco), 4500 mg / L-glutamine, 10 µg / mL streptomycin and 10 units / mL penicillin. Cells were passaged every 48 hours, maintained at 5 x 10^5 cells / mL and cultured at 37 °C in 5 % CO$_2$.

2.2.1.2 Adherent cells

HeLa[395] cells (human cervical adenocarcinoma, passage 15) as purchased from DMSZ were cultured in Dulbecco's modified Eagle's medium (DMEM, Invitrogen) supplemented with 10 % FBS, 4500 mg / L glutamine and 10 µg / mL streptomycin and 10 units / mL penicillin. At 90 % confluency cells were passaged by decanting spent media, washing cell mono-layer twice with PBS, incubating with 2 mL trypsin (Invitrogen) for 5 minutes, neutralising trypsin with 10 mL complete media, spinning at 300 x G for 5 minutes, decanting supernatant, resuspending cells in complete media and seeding in a fresh T25 flask; cells were cultured at 37 °C in 5 % CO$_2$.

2.2.2 Human primary culture

2.2.2.1 Primary samples (buffy coats)

White cell concentrates (buffy coats) were purchased from the Scottish National Blood Transfusion Service (SNBTS). Details regarding donor age, sex etc are confidential and were with-held. All buffy coats were bought within 2 days of processing by SNBTS and MNCs isolated immediately or on the next day.

NOTE: If stored overnight as per SNBTS recommendations, buffy coats were kept at room temperature (RT) to prevent platelet apoptosis.

2.2.2.2 Mononuclear cell isolation

10 mL Histopaque 1077 (Sigma) was dispensed into 50 mL centrifuge tubes (Corning), brought to RT, overlaid with 40 mL buffy coat diluted 1:1 in wash buffer (0.5 mM EDTA, 2 % HSA in PBS), spun at 400 x G for 30 minutes (break off), interface (MNCs) removed, washed twice in wash buffer then enumerated *via* Hemavet MULTI-TROL™ blood analyser.

2.2.2.3 CD14$^+$ cell isolation

Monocytes were isolated from MNCs using CD14 MicroBeads (Miltenyi Biotec). After Hemavet enumeration MNCs containing the desired amount of monocytes were decanted into a 15 mL falcon, spun at 300 x G for 10 minutes, supernatant removed, pellet resuspended with 80 µL wash buffer (WB; 0.5 % human serum albumin in PBS) per 10^7 total cells, probed with 20 µL of CD14 MicroBeads per 10^7 total cells and incubated in the fridge for 15 minutes. Probed cells were then washed with 2 mL WB per 10^7 total cells, spun at 300 x G for 10 minutes, supernatant decanted and pellet resuspended at a concentration of < 10^8 total cells per 500 µL of WB. LS columns (Miltenyi Biotec) were placed in a MACS Separator, wetted with 3 mL WB, before adding labelled cells to the column reservoir and allowing them to flow through *via* gravity filtration. The column was washed three times with 3 mL WB to wash through any unattached cells. To elute the bound monocytes,5 mL of WB was added to the reservoir, plunger placed in the top and cells eluted into a fresh 15 mL falcon. Cells were enumerated *via* haemocytometer and used as required.

2.2.2.4 Monocyte derived macrophage (MDM) differentiation

Isolated monocytes were resuspended in RPMI supplemented with 2 mM glutamine (Invitrogen) and 10 % FBS at a concentration of 1 x 10^6 monocytes per mL. Monocytes were supplemented with 100 ng / mL human granulocyte macrophage colony stimulating factor (h-GMCSF) or human macrophage colony stimulating factor (h-MCSF) (both Peprotech) for M1 or M2 macrophages respectively. Supplemented monocytes were seeded at a concentration of 1 mL / cm^2 in Lab-Tek™ II Chamber Slides™ (Nunc) or Costar® cell culture plates (Corning) and cultured at 37 °C in 5 % CO_2 for seven days; media was refreshed on days 3 and 5. At day 7, media was removed and macrophages polarised using media supplemented with 50 ng / mL lipopolysaccharide (LPS [Invitrogen]) and 20 ng / mL human interferon gamma (h-IFN-γ) (Peprotech), 10^{-7} M dexamethasone (Sigma) or 20 ng / mL IL-4 (Peprotech) for 2 days to achieve a mature M1, M2a or M2c phenotype respectively - macrophages were phenotyped on day 7 and 9 *via* flow cytometry.

Note: A schematic of macrophage generation can be found in Chapter 6 Figure **38a**, macrophages were phenotyped on day 7 and 9 according to Section **2.2.2**.

2.2.3 Murine primary culture

All experiments were performed in accordance with the local ethical review panel, the UK Home Office Animals Scientific Procedures Act, 1986 and UKCCCR and NCRI guidelines. Animals were kept in regulated facilities, monitored daily, and all experiments were carried out in compliance with UK Home Office guidelines. Femurs, hips and tibias were collected from wild type C57BL/6 mice by Mrs Karen Dunn.

Bone marrow cells were extracted using pestle and mortar, filtered through a cell strainer, washed with wash buffer (2 mM EDTA, 5 % FBS in PBS) three times, pelleted, incubated in RBC lysis buffer (150 mM NH_4Cl, 1 mM $KHC0_3$, 0.1 mM EDTA) for 5 minutes (RT) to remove RBCs. 5 x 10^6 bone cells were seeded in 10 cm petri dishes in DMEM supplemented with 10 % FBS, 2 mM glutamine, 10 μg / mL penicillin / streptomycin and 100 ng / mL mMCSF for 7 days; media was refreshed on day 5.

2.2.4 Phagocytosis

2.2.4.1 Whole RBCs

With ethical approval (Section **2.11**), whole blood was drawn with consent from healthy volunteers as per Section **2.5.1** and processed as per Section **2.5.2** to give purified erythrocytes. These were counted by haemocytometer and then added at a ratio of 10 erythrocytes per macrophage and left overnight.

Note: In order to maintain sterility, all manipulations were performed in a class II hood and the cellulose / cotton wool used in leukodepletion (Section **2.5.2.2**) was first sterilised with alcohol.

2.2.4.2 RBC-MVs

RBC-MVs were quantified as per Section **2.3.2** and 2.575 µg of MVs per 0.8 cm^2 were added directly to cultured macrophages and left for different periods of time.

2.3 General

2.3.1 Protein preparation

3×10^6 cells were pelleted at 450 x g for 5 minutes, washed 3 times with ice cold PBS, suspended in 90 µL protein solubilisation, incubated on ice for 30 minutes then spun at 12,000 x g (4 °C) for 5 minutes to remove cellular debris, supernatant decanted and retained in fresh plastic ware.

2.3.2 Protein quantification

Proteins were quantified using the Quick Start™ Bradford Protein Assay (Bio-Rad) against a 7-point standard curve (0, 2.5,5, 7.5, 10, 15 and 20 µg / mL) prepared using a BSA standard (Bio-Rad) according to manufacturers instructions. Samples were measured using a Spectramax M5 plate reader (Molecular Devices).

2.3.3 Nucleic acid quantification

1.5 µL of sample (RNA, DNA etc) was pipetted onto the lower pedestal of a NanoDrop 1000 spectrophotometer and quantified based on the samples absorbance at 260 nm.

2.3.4 RNA extraction

2.3.4.1 QIagen

RNA was extracted from 2 x 10^6 cells using an RNeasy® Plus Micro Kit (Qiagen) according to manufacturers' instructions.

2.3.4.2 Trizol

200 µL of packed RBCs, or RBC-MVs prepared as per Section **2.8.1**, were homogenised in 1 mL or 500 µL of Trizol respectively. A tenth volume of 1-Bromo-3-chloropropane (BCP, Sigma) was added, samples vortexed for 1 minute, spun for 10 minutes at 12, 000 x G, upper phase (aqueous) decanted, 3 µg of tRNA was added as a carrier, then 1 volume of isopropanol (Sigma) was added and the RNA precipitated in the freezer over-night. The following day samples were spun at 21, 000 x G for 30 minutes, supernatant decanted, pellet washed with 1 mL of 70 % ethanol twice, then air dried and re-suspended in DEPC treated water.

Note: carrier tRNA was not used when extracting nucleated cells.

2.3.5 Nucleic acid precipitation

A tenth volume of 3 M sodium citrate (pH 5.5, Sigma) was added to a sample along with 1 volume of isopropanol and the nucleic acid precipitated on ice for 30 minutes. Samples were spun at 21, 000 x G for 30 minutes, supernatant decanted, pellet washed with 1 mL of 70 % ethanol twice, then air dried and re-suspended in DEPC treated water.

2.4 Molecular

2.4.1 Reverse transcription

2.4.1.1 Oligo dT reverse transcription

cDNA was prepared by incubating 250 ng total RNA, 50 µM OligoDT (IDT) and 10 mM dNTPs (Bioline) at 65 °C for 5 minutes, cooling reactions on ice for 2 minutes, adding 200 units of SuperScript® III reverse transcriptase (Invitrogen), 1 x First Strand Buffer (Invitrogen), 1 mM dithiothreitol (Invitrogen), 40 units RNAseOUT™ (Invitrogen), then incubating at 50 °C for 60 minutes followed by an enzyme inactivation step (70 °C for 15 minutes).

2.4.1.2 miRNA reverse transcription

A reverse transcription primer pool was prepared by dispensing 5 µL of each TaqMan® MicroRNA Assays RT primer (Applied Biosystems) into a 1.5 mL eppendorf and making it up to 500 µL with TE buffer. cDNA was prepared by incubating 3 µL total RNA with 6 µL RT primer pool, 0.3 µL dNTP (100 mM) (Bioline), 150 units MultiScribe reverse transcriptase (Applied Biosystems), 1.5 µL RT buffer (Applied Biosystems) and 1.2 µL water, incubating samples on ice for 5 minutes, 16 °C for 30 minutes, 42 °C for 30 minutes and 4 °C for 5 minutes.

2.4.2 *In vitro* transcriptions (IVT)

T7 oligo (5 µM, Sigma) and template oligo (5 µM, Sigma), containing reverse T7 promoter sequence, were allowed to hybridise at 37 °C for 5 minutes. For each 10 µL reaction, 2 µL of 5 X buffer (ThermoFisher), 1 µL each of 1 mM ATP, GTP, UTP, 1 µL of 1 mM biotin-14-CTP (ThermoFisher), 1 µL T7 RNA polymerase (ThermoFisher), 1 µL annealed template oligo, 2 µL water, mixed and allowed to reverse transcribe at RT for 30 minutes. Template oligo was digested with 1 µL of TurboDNAse (ThermoFisher) for 10 minutes at RT, RNA probe was diluted with 40 µL of 50 % deionised formamide (Sigma).

2.4.3 PCR

All primers used within this project are detailed in Appendix **5 & 6.**

2.4.3.1 End point PCR

End point PCR was performed using PCR Master Mix (2X) (ThermoFisher). To 1 μL of cDNA, 1 μL of 1 μM forward and reverse primer mix, 12.5 μL PCR Master Mix (2X) and 10.5 μL water was added, dispensed into 8-tube PCR strips (ThermoFisher) then amplified using a Techne TC-412 with the conditions below:

Step	Time	Temperature (˚C)
Initial denaturation	1 min	95
Cycle (x 40)	30 sec	95
	30 sec	60
	1 min	72
Final extension	10 min	72
Hold	∞	4

2.4.3.2 SYBR green qPCR

qPCR was performed using SensiFAST™ SYBR® Hi-ROX (Bioline). To 1 μL cDNA, 1 μL of 0.4 μM forward and reverse primer mix, 5 μL 2x SensiFAST SYBR® Hi-ROX Mix and 3 μL water was added, mixed and dispensed into a MicroAmp® Optical 384-Well Reaction Plate (Applied Biosystems) then amplified using a 7900HT Fast Real-Time PCR system (Applied Biosystems) with the conditions below:

Step	Time	Temperature (˚C)
Polymerase activation	2 min	95
Cycle (x 40)	5 sec	95
	10 sec	60
	5 sec	72
Melt curve	∞	4 - 95

2.4.3.3 miRNA qPCR

miRNA were detected by probe based qPCR using TaqMan® MiRNA Assays (Applied Biosystems). To 1 μL of 1:10 diluted pre-amped material (Section **2.4.4.1**), 0.5 μL of a specific TaqMan® MicroRNA assay (Appendix **8**), 5 μL TaqMan® Universal Master Mix II (no UNG) and 3.5 μL of water was added, mixed and dispensed into a MicroAmp® Optical 384-Well Reaction Plate (Applied Biosystems) then amplified using a 7900HT Fast Real-Time PCR system (Applied Biosystems) with the conditions below:

Step	Time	Temperature (°C)
Polymerase activation	10 min	95
Cycle (x 40)	15 sec	95
	60 sec	60

2.4.3.4 Universal probe library qPCR

qPCR was performed using FastStart Taqman Probe Master (Roche) mastermix. To 1 μL cDNA, 1 μL of 7.2 μM forward and reverse primer mix, 10 μL 2 x FastStart Taqman Probe Master mastermix, 1 μL of 10 μM LNA probe and 7 μL water was added, mixed and dispensed into a LightCycler® 96 well-plate (Roche) and amplified using a LightCycler® 480 with the conditions below:

Step	Time	Temperature (°C)
Polymerase activation	10 min	95
Cycle (x 40)	10 sec	95
	30 sec	60
	1 sec	72
Cooling	30 sec	4

2.4.4 Fluidigm analysis

2.4.4.1 Pre-amplification

To increase sensitivity, low abundance genes were "pre-amped". First, a primer pool was prepared by adding 1 μL of a forward / reverse primer (100 μM) for each gene of interest and making it up to 200 μL with TE buffer (Invitrogen). 1.25 μL of cDNA was then pre-amped by adding 1 μL of Multiplex PCR MasterMix (Qiagen), 0.5 μL pooled primer and 2.25 μL water then amplified using a Techne TC-412 with the conditions below:

Step	Time	Temperature (˚C)
Hot-start	15 min	95
Cycle (x 40)	30 sec	95
	90 sec	60
	90 sec	72
Final extension	10 min	72
Hold	∞	4

2.4.4.2 Exo I nuclease digest

Unincorporated primers were removed by adding 1.4 μL water, 0.4 μL exonuclease I (NEB) and 0.2 μL exonuclease I reaction buffer to each sample and incubating them for 30 minutes at 37 ˚C then heat inactivation of the enzyme performed for 10 minutes at 80 ˚C.

2.4.4.3 Flex Six IFC Gene Expression

Samples underwent qPCR on Flex Six microfluidics chips (Fluidigm) using the Biomark HD™ (Fluidigm) system. 10 X assays were prepared by adding 0.15 μL of 50 μM forward and reverse primer mix for each gene of interest, 1.35 μL TE buffer and 1.5 μL of 2 X Assay Loading Reagent (Fluidigm) per inlet required. Sample pre-mixes were prepared by adding 1.5 μL SoFast EvaGreen® Supermix with low ROX (Bio-Rad), 0.15 μL Flex Six Delta Gene Sample Reagent (Fluidigm) and 1.35 μL of *exo I* treated pre-amp sample per inlet. 150 μL of control line fluid was added to both chips accumulators, then the chip was primed using an IFC HX

controller (Biomark). Post prime, 3 µL of 10 X Assay were added to the appropriate assay inlets and 3 µL Sample Pre-Mix was added in triplicate to the appropriate sample inlets. The chip was loaded using the IFC HX controller (Fluidigm) then analysed using a BioMark HD™ (Fluidigm) with the conditions below:

Step	Time	Temperature (˚C)
Hot-start	10 min	95
Cycle (x 35)	15 sec	95
	60 sec	60
Melt curve	∞	4 - 95

2.5 Blood processing

2.5.1 Venepuncture

With ethical approval (Section **2.11**), peripheral blood was collected in K$_3$EDTA, sodium heparin or buffered sodium citrate coated / containing Vacutainers® (Becton Dickonson) by a clinician and used within 1 day.

2.5.2 RBC purification

2.5.2.1 Platelet ablation

1 mL whole blood was diluted in 9 mL wash buffer (4 % BSA (*w/v*) PBS), centrifuged at 150 x G for 10 minutes and platelet rich plasma removed; RBC pellet was resuspended in 10 mL WB and re-centrifuged to remove residual platelets.

2.5.2.2 Leukodepletion

Leukodepletion was performed using a modified protocol from Blume *et al*[396]: Cotton wool was packed into the barrel of a 20 mL syringe, overlaid with 0.5 g of α-cellulose (Sigma) and wetted by allowing 10 mL PBS to flow through *via* gravity. Platelet free blood was diluted 1:10 in WB, overlaid onto the wetted α-cellulose and allowed to pass through *via* gravity filtration, the column was then washed with 10 mL WB (Appendix 9). Flow through containing leukodepleted RBCs was

retained, spun at 1000 x G for 10 minutes, resuspended at normal concentration (3.6 - 6 million erythrocytes / µL) and analysed *via* Hemavet MULTI-TROL™ blood analyser (Drew Scientific) to confirm leukodepletion (Appendix 10); RBCs were processed this way throughout the duration of this project.

2.5.3 Percoll gradients

BSA and 20X HEPES buffered saline was added directly to Percoll to a final concentration of 133 mM NaCl, 4.5 mM KCL, 10 mM HEPES pH 7.4, 4 % (*w/v*) BSA. Buffered Percoll was diluted with dilution buffer (DB; 4 % BSA *w/v* in 1 X HEPES buffered saline, pH 7.4) to final densities of 1.06, 1.07, 1.08, 1.09 and 1.1 g /L, discontinuous gradients were prepared by carefully layering 2 mL of each preparation on top of each other in 15 mL centrifuge tubes. 5×10^8 RBCs from above were made up to 500 µL with DB, layered on the gradient, spun at 1000 x G (4 °C) for 30 minutes in a Sigma 4K15 with swing arm rotor (brake off). RBCs were separated into 5 distinct layers which were harvested, washed twice with DB then analysed as discussed in text.

2.5.4 Erythrocyte membrane manipulations

2.5.4.1 Preparing red cell membrane

RBC membrane were prepared using a modified protocol from Dodge *et al.*[397] Briefly, 5 mL of compact RBCs were lysed using 30 mL ice cold 20 mOsm sodium bicarbonate buffer (pH 7.4 [Sigma]), membrane pelleted at 21, 000 x G for 30 minutes (brake off), supernatant decanted and membrane washed with 30 mL lysis buffer; this was repeated until the membrane were white. Membrane preparations were used at this point or processed as outlined in section **4.4.2**.

2.5.4.2 Preparing AGO2 concentrates

RBC membranes were resuspended in PBS and incubated on ice for 5 minutes, pelleted at 21, 000 x G for 30 minutes (brake off), supernatant retained and concentrated using an Amicon® Ultra 3000 molecular weight pin column (Merck Millipore); concentrated samples were quantified as per Section **2.3.2** and used as discussed.

2.6 Electrophoresis

2.6.1 SDS-PAGE

2.6.1.1 Casting acrylamide gels

All protein samples were resolved using the Mini-PROTEAN Tetra Cell gel system (Bio-Rad). Resolving gels were prepared according to Appendix **13**, poured into a 0.75 mm gel cassette, overlaid with Milli-Q water and allowed to set for 15 minutes. Stacking gels were prepared as per Appendix **13**, water removed from the gel cassette, 2 mL of stacking gel added on top of the resolving gel, a 15 well comb placed in the cassette and the gel allowed to set for 15 minutes.

2.6.1.2 Running acrylamide gels

Protein samples were diluted in SDS sample buffer (final concentration 1 x with 5 % beta-mercaptoethanol [Sigma]) and denatured at 95 ˚C for 15 minutes. Cast gels were placed in a sandwich clamp assembly, then in a Mini PROTEAN electrophoresis cell, 200 mL of 1 x SDS running buffer was poured into the outer chamber and the inner chamber filled. Gel comb was removed, empty wells flushed with 1 x SDS running buffer using a 10 mL syringe. Up to 20 μL of sample was loaded per well, along with 5 μL of PageRuler™ Plus Prestained Protein Ladder (ThermoScientific); unused wells were filled with an equal volume of 1 x SDS sample buffer. Samples were run at 90 volts for 15 minutes then 180 volts for 35 minutes, or until the bromophenol blue ran off the end of the gel.

2.6.2 Western blot

Post SDS-PAGE, proteins were transferred to a Protran® nitrocellulose membrane (Whatman) using a semi-dry method. Membranes were blocked (5 X block in TBS = 5 % (*w/v*) BSA Fraction V (Roche), 1 % (*w/v*) Ovalbumin (Sigma), 0.01 % (*w/v*) Sodium Azide (Sigma)), probed with primary antibodies (Appendix **11**) overnight, washed 3 x TBSN, probed with HRP conjugated secondary antibodies (Appendix **12**), washed 3 x in TBSN, 2 x in TBS and incubated with Immobilon™ Western Chemiluminescent HRP substrate (Millipore). CL-XPosure™ (ThermoFisher) film was exposed and developed using the SRX-10A developing system (Konica Minolta).

Note: For low abundance proteins signal was visualised using the SuperSignal™ West Femto Maximum Sensitivity Substrate kit (ThermoFisher)

2.6.3 Staining

2.6.3.1 Coomassie

Post electrophoresis, acrylamide gels were rinsed in 50 mL of deionised water for 10 minutes three times. After the final wash, water was decanted and the gel immersed in 50 mL Coomassie Brilliant Blue R-250 Staining Solution (Bio-Rad) and left to stain for 1 hour at RT with agitation. Post stain, Coomassie was decanted and the gel washed with deionised water until any background was removed.

2.6.3.2 Silver stain

Post electrophoresis acrylamide gels were fixed in 50 mL fixing solution for 1 hour, washed with 50 mL of 30 % Ethanol for 10 minutes, washed with 100 mL deionised water for 10 minutes, sensitised in 50 mL of sensitising solution for 10 minutes, washed twice in 100 mL of deionised water for 10 minutes, equilibrated in 50 mL of silver solution for 10 minutes then washed with 50 mL deionised water for 1 minute. Wash was removed and the gel developed in Developer solution until the bands were clearly visible at which point development was stopped by adding 5 mL ProteoSilver Stop Solution and incubating for 5 minutes. Gels were then washed with 100 mL of water and dried according to Section **2.6.4**.

2.6.4 Gel drying

Post stain, gels were rinsed with 50 mL deionised water, drained, then equilibrated in 35 mL Gel-Dry™ Drying Solution for 5 minutes. 1 cellophane sheet was wetted in Gel-Dry™ Drying Solution and placed on the DryEase® Gel Drying Frame, equilibriated gel placed on top, then covered with a final cellophane sheet. The remaining drying frame was placed on top, secured in place with plastic clamps, stood on its feet and the gel allowed to dry overnight.

2.6.5 Agarose gel electrophoresis

0.5 – 2.5 % *w/v* agarose (Web Scientific) tris/borate/EDTA (TBE [Gibco]) gels were prepared by melting agarose in TBE using a microwave, then pouring the molten agarose into a casting tray (Bio-Rad). Samples were diluted in 5 x GoTaq® Reaction Buffer (Promega), resolved using a PowerPack™ (Bio-Rad), post stained in 0.5 µg / mL ethidium bromide / TBE solution then visualised using a Chemidoc XRS (Bio-Rad) or a FLA-5000 imaging system (FujiFilm).

2.7 Flow cytometry

2.7.1 Exosome calibration

Megamix-Plus SSC beads (Biocytex) were used to calibrate a BD FACs Canto™ II before use. 50 µL of beads were dispensed into 200 µL of 0.2 µm double filtered HBSS, vortexed, and used to change instrument forward scatter (FSC) and side scatter (SSC) voltages; voltages were adjusted until all Megamix beads (0.16, 0.2, 0.25 and 0.5 µm) were visible on a FITC-H Vs SSC-H dot plot. Signal height (H) was used for all parameters and parameter data was collected on a logarithmic scale.

2.7.2 Staining

2.7.2.1 Internal staining

RBCs, Jurkat and K562 cells were processed as per Section **2.9.1.1**, then analysed using a FACs Canto™ II (Becton Dickinson).

2.7.2.2 Cell surface staining

5×10^5 cells were pelleted, washed in 2 mL of FACs buffer (PBS with 2 % FCS and 0.02 % sodium azide) and resuspended in 100 µL of PBS. Cells were probed with conjugated antibodies (Appendix **12**), incubated in the dark for 10 minutes, washed twice with PBS, resuspended in 200 µL PBS and analysed using a BD FACs Canto™ II (Becton Dickinson).

2.7.2.3 MV staining

5 μL of cleared plasma, pelleted MVs or RBC-MVs were added to 100 μL of 0.2 μm double filtered HBSS, probed with antibodies from Appendix **11**, left to stain for 10 minutes in the dark, then analysed using a BD FACs Canto™ II.

2.7.2.4 Cell viability

5×10^5 cells were pelleted, washed in 2 mL of FACs buffer then resuspended in 100 μL HBSS. Cells were probed with 5 uL of Annexin-FITC in the dark for 15 minutes, washed twice with HBSS, resuspended in 100 μL HBSS and analysed using a FACs Canto™ II (Becton Dickinson); 100 μL of 300 nM DAPI solution was added to cells 1 minute prior to analysis.

All data analysis was performed using FlowJo® V10 (FlowJo LLC).

2.8 MV isolation and preparation

2.8.1 Artificial RBC-MV generation

200 μl of leukodepleted compact RBC pellet was added to 1 mL of Vesicularisation Buffer (1 μM ionophore [A23187 – Sigma] in HBSS) and incubated at 37° C for 2 hours to induce vesicularisation; samples were inverted to mix every 30 minutes. Samples were spun at 1000 x G to pellet RBCs, supernatant removed and re-spun at 3000 x G for 15 minutes to pellet debris. Cleared supernatant was spun at 21,000 x G for 15 minutes, supernatant removed and MV pellet washed twice with 0.2 μm HBSS then resuspended in 0.2 μm filtered HBSS for further analysis.

2.8.2 *Ex vivo* RBC MV isolation

Blood taken as per Section **2.5.1**, or from buffy coats purchased from the SNBTS, was spun at 500 x G for 15 minutes to pellet cells, plasma harvested, spun twice at 1000 x G for 20 minutes, then observed under light microscopy to ensure it was clear of cells or debris. Cleared plasma was then spun at 21, 000 x G for 30 minutes, supernatant discarded, pellet washed with 1 mL of HBSS then resuspended in 100 μL of HBSS.

2.8.3 Fluorescent sorting of MVs

50 µL of cleared plasma was probed with 1 µL of 1/10 diluted Gly-A APC conjugate for 10 minutes in the dark on ice, diluted with 300 µL double filtered HBSS and sorted by Miss Jennifer Cassels using a FACSAria™ IIu (Becton Dickinson); instrument was calibrated using Megamix-Plus SSC beads (Biocytex).

2.9 Microscopy

2.9.1 Immunofluorescence

2.9.1.1 RBCs, Jurkat and K562 cells

1 µL of leukodepleted RBCs, or 1×10^6 Jurkat / K562 cells, were fixed in 0.2 % glutaraldehyde / 4 % paraformaldehyde [PFA] (*v/v*) at RT for 10 minutes, washed in 0.1 M glycine twice, then incubated in 0.1 M glycine for 30 minutes (RT) to block unreacted aldehyde groups. Fixed cells were permeabilised for 10 minutes with 0.1 % Triton, blocked in 10 % goat serum for 10 minutes, probed with primary antibodies from (Appendix **11**) overnight at 2-8 °C, washed 5 times with 0.1 % Triton, probed with secondary antibody (Appendix **12**)for 1 hour at 2-8 °C then washed 5 times with 0.1 % Triton. Probed cells were allowed to adhere to poly-L lysine (Sigma) coated slides for 1 hour at 2 – 8 °C, washed twice with water to remove non-adherent cells then visualised by fluorescent microscope or FACs.

2.9.1.2 HeLa cells and bone marrow-derived macrophages (BMDM)

HeLa cells and BMDM were fixed in 4 % PFA for 10 minutes (RT), washed three times with PBS, permeabilised with 0.1 % Triton, blocked with 10 % goat serum for 1 hour, probed with primary antibodies from (Appendix **11**) overnight at 2-8 °C, washed 3 times with 0.1 % Triton, probed with secondary antibodies from (Appendix **12**) for 1 hour, washed 3 times with 0.1 % Triton, stained with DAPI (1:10,000 dilution) for 1 minute, washed twice with water, then visualised by fluorescent microscopy.

2.9.1.3 Monocyte derived macrophages

Macrophages grown on Lab-Tek® II 8 well chamber slides (Nunc) were permeabilised pre-fixation with 0.15 % digitonin (Sigma [*v/v* PBS]) for 1 minute at

RT, digitonin carefully removed and cells fixed in 4 % PFA (*w/v* PBS) for 10 minutes. Fixed cells were washed 3 times with PBS, further permeabilised with 0.15 % digitonin for 10 minutes, blocked for 1 hour with 5 % goat serum (*v/v* PBS), probed with antibodies from (Appendix **11**) overnight at 2-8 °C, washed 5 times with PBS, probed with secondary antibodies (Appendix **12**) for 1 hour at 2-8 °C then washed 5 times with PBS. When specified in text, cells were stained with 165 nM phalloidin-TRITC (Invitrogen) for 30 minutes at RT and washed twice with PBS. All cells were stained for 1 minute with 200 µL of 300 nM DAPI solution at RT, 8 well chamber removed, slide air dried, 1 drop of mounting media (10 % *w/v* Mowiol® 4-88 [Polysciences Inc] in 4 % glycerol *v/v* 0.1 M Tris pH 8.5) added to slide surface and a coverslip added and sealed with nail varnish. Cells were visualised as below.

2.9.2 Light microscopy

All light microscopy images were taken using an Olympus CKX41 microscope with a U-CMAD3 ColorView camera (Olympus).

2.9.3 Image acquisition and editing

All images were taken using an inverted fluorescence microscope (Olympus IX51) with an F-view II 12-bit digital camera (Olympus UK Ltd) at the stated exposures; images were processed using Image J software (National Institute of Health).

2.9.4 TEM

MVs were prepared as per Section **2.8.1**, pellet resuspended in 50 µL of 4 % paraformaldehyde then analysed by Miss Margaret Mullin from the University of Glasgow using an Tecnai T20 (ThermoFisher).

2.10 Pull downs

2.10.1   Antibody mediated

100 µg of RBC membranes prepared as per Section **2.5.4.1** were cross linked with (dithiobis(succinimidyl-propionate)) (DSP, Thermo) for 30 minutes at RT;

crosslinking was stopped by incubating reactions with Tris (final concentration 50 mM) at RT for 15 minutes. 3 µg of appropriate primary antibody (Appendix 11) was added to crosslinked samples and incubated overnight with inversion at 4°C. 50 µL protein G sepheraose (GE healthcare) was washed with PBS, resuspended in 50 µL PBS, added to reactions and incubated with inversion for 3 hours at 4°C. Reactions were pelleted at 14, 000 x G for 10 minutes, supernatant removed, slurry resuspended with 1 mL of 0.1 % (*v/v*) Triton x-100 PBS then pelleted at 14, 000 x G for 10 minutes; washing was repeated 5 times. Slurry was resuspended in 100 µL of 1 x SDS buffer (with 5 % 2-mercaptoethanol), heated to 95°C for 5 minutes, pelleted at 14, 000 x G for 10 minutes, supernatant retained and analysed as per Section **2.6.1**.

2.10.2   RNA dependent

Streptavidin paramagnetic beads (NEB) were decanted into a 1.5 mL Eppendorf, sequestered using a magnet and washed twice with PBS-T (1 % (*v/v*) Tween 20). 100 pmol of biotinylated 2'-O-methylated (2-OM) oligos (sequences detailed in Appendix 1) were added per 10 µL of beads and allowed to capture with inversion for 10 minutes at RT. Bead-oligo complex was sequestered, washed 3 times with PBS-T, resuspended in 1 volume of PBS, blocked with 40 pM free biotin (Sigma) per 10 µL beads before being sequestered again, washed 3 times and resuspended in 1 volume of PBS. 100 µL bead-oligo complex, or blocked bead only, was added to 7 mL of membrane eluate and incubated at 37 °C with rotation for 1 hour. Beads were sequestered, supernatant discarded, beads washed 5 times with PBS-T, resuspended in 40 µL 5 X SDS loading buffer and eluted at 95 °C for 5 minutes. Samples were analysed by gel electrophoresis.

2.11 Ethics

Informed consent, in accordance with the declaration of Helsinki and with Greater Glasgow and Clyde NHS Trust Ethics Committee approval, was granted from healthy donors before peripheral blood was taken.

NHS Greater Glasgow & Clyde. West of Scotland Research Ethics Service REC No: 15/WS/0077.

Chapter 3   Approaches to identify novel functions of e-miRNA

3.1 Introduction

Erythrocytes are highly specialised cells that have one major function: the constant delivery of oxygen to body tissues and removal of CO_2. Their bi-concave shape has evolved to increase cell surface area, while their distinctive red hue is caused by abundant haemoglobin, the metalloprotein responsible for binding oxygen. Erythropoiesis itself is an inexorable drive to create cells that are as efficient in their primary function as possible, with cellular contents extraneous to this function being removed. For example, during terminal differentiation, erythrocyte precursors eject their nucleus and organelles, and undergo widespread ribonucleolysis[238,241]. Although this maximises the amount of haemoglobin present, it also means that no further translation occurs. It is therefore surprising to discover that mature erythrocytes contain an abundant amount of key translational regulators: micro-RNA (miRNA)[6].

However, the data discussed in depth in Section **1.8.2.5** that was generated from the Hamilton lab appears to challenge this notion. Briefly, it was demonstrated that erythrocytic miRNA (e-miRNA) are as concentrated as miRNA from nucleated cells, appear conserved across Mammalia, selectively retain their binding partner (AGO2) at the expense of AGO1, 3, and 4 during erythropoiesis, and that erythrocytic RISC complexes maintain a catalytic activity. Taken together, this data indicates a function for e-miRNA, although what that might be is currently unknown.

While miRNA are widely reported within the literature to modulate multiple different pathways, mechanistically this is all achieved in the same way: translational repression. Therefore, as RBCs contain no mRNA, establishing a function for e-miRNA within erythrocytes requires one to consider possibilities outside of the canonical miRNA-mRNA paradigm. At this stage, specific hypothesis testing is challenging as it is not clear how e-miRNA relate to the routine function of an erythrocyte. For example, how could an RNA guided ribonuclease affect oxygen transport, or play a role in glycolysis?

In the absence of an obvious cellular role, a reasonable approach is to identify proteins with which AGO2s interact in erythrocytes, then form hypotheses based on those interactions. Therefore, the Hamilton lab performed AGO2 pull-downs to establish what interacts with AGO2. As a result, the first portion of this PhD focused on testing the validity of this pull-down/proteomic data to identify genuine AGO2 interactors.

3.2 Results

3.2.1 Validation of previous proteomic data

The Hamilton lab had previously performed proteomic analysis of AGO2 pull-downs to establish candidate interactions (Table 4). Positive pull-downs were performed using αAGO2 (4G8) and analysed by mass spectrometry; αAGO4 was used as a negative control as AGO4 is not present within erythrocytes (Figure **13**). All candidates reported have a P-value $\leq$ 0.05, are enriched in the AGO2 Vs AGO4 pull-down at a ratio $\geq$ 1:70 (control Vs specific); typical contaminants (IgG subclasses, keratin) have been removed.

Table 4: Protein candidates from the Hamilton Lab proteomics studies.

Protein ID		No. of peptides per pull-down		
Name	Gene	AGO2	AGO4	Ratio
Argonaute 2	AGO2	70	1	1:70
Fibrinogen-beta	FIB-B	8	0	0:1
Host cell factor	HCFC1	6	0	0:1
Fibrinogen-gamma	FIB-G	5	0	0:1
Zinc alpha glycoprotein	AZGP1	5	0	0:1
Coiled-coil and C2 domain containing protein	CC2D1A	4	0	0:1
BAND3	SLC4A1	2	0	0:1
Heat shock protein 40	DNAJB4	2	0	0:1
Thioredoxin	TXN	1	0	0:1
Bone morphogenetic protein	BMP2	1	0	0:1
Galectin-7	LGALS7	1	0	0:1

BAND3 was chosen as the first candidate AGO2 interactor for two reasons: (1) it is a membrane protein and initial work demonstrated AGO2 associates with the erythrocyte membrane (personal communication Andrew Hamilton); (2) proteomic data reported by Van Wijk *et al*. also suggested a BAND3-AGO2 interaction[299]. To test this interaction, reciprocal pull-downs using antibodies to either AGO2 or BAND3 were performed. Initial data had indicated that the AGO2-membrane interaction was unstable in diluted protein solutions in PBS (personal communication Andrew Hamilton). Therefore, to stabilise protein-protein interactions, RBC lysates were cross-linked with dithiobis-succinimidyl propionate (DSP). As DSP cross-linking is reversible in the presence of a reducing agent (ß-mercaptoethanol), it is possible to evaluate cross-linking efficiency *via* non-reducing SDS-PAGE (Figure **16a**). Cross-linked lysates were unable to penetrate a 7.5 % acrylamide gel when not reduced (lane 2), but retained the profile of fresh lysate (lane 1) when ß-mercaptoethanol was added (lane 3), indicating samples had undergone crosslinlinking. Western blot analysis of pull-downs indicated that the correct protein was isolated with each specific antibody above IgG controls (Figure 1b). However, probing each blot with the reciprocal antibody failed to indicate any AGO2-BAND3 interactions; although weak AGO2 signal is present within the BAND3 pull-down, its intensity is that of the IgG control, indicating a non-specific interaction. ==The signal for BAND3 in Figure 16 is very weak, although in my opinion it does appear as though there is a faint band present – a longer exposure time should have been used to establish this.==

The next candidate AGO2 interactor chosen was fibrinogen. Although fibrinogen is a plasma protein, it was highly represented in the proteomic data. It was also reasonable to propose AGO2 might have a plasma-based target. Firstly, because there is no obvious intracellular function for AGO2s; and secondly, intravascular haemolysis is a feature of normal vascular physiology which increases due to exercise, mechanical trauma and infectious disease[398]. Thus, the contents of erythrocytes are normally found circulating extracellularly to some extent. It was possible that the AGO2-FIBRINOGEN interaction suggested by the pull-down/proteomic data reflected a normal interaction of AGO2 released from erythrocytes with FIBRINOGEN (FIB) that had adsorbed to the outside of the RBCs used in lysate preparation. Due to how critical the coagulation cascade is, which involves FIB, this interaction was explored.

To evaluate any potential AGO2-FIB interaction, a sample enriched for AGO2 was prepared as per Section **2.5.4.2**. As FIB is a plasma protein, 100 µL of human plasma was spiked with different amounts of AGO2 concentrate and allowed to

interact for 1 Hr on ice; FIB pull-downs were then performed and eluates probed with αAGO2/αFIB (Figure 1c). From this experiment, it was impossible to evaluate how much FIB was isolated as FIB is ~ 55 kDa in size and resolves at the same location as an IgG heavy chain (IgH) on a gel. The observed band on the FIB blot is most likely IgH as the bead only control (αFIB absorbed) contained this band. Note the two middle controls appear to only have a faint IgH presence, this is an artefact caused by high IgH presence. High IgH presence recruits a high amount of secondary-HRP, as HRPs turn brown when oxidised (visibly present on membrane), a likely explanation for the lack of ECL signal is due to the HRP becoming inactive (oxidised). Probing these samples with αAGO2 did not result in any AGO2 being observed; note that the AGO2+ve is a western blot control. This shows that the western blot worked, but no AGO2 was present in the samples.

Closer analysis of the proteomic data indicated that identified FIB was of mouse origin rather than human. As the antibodies used in these pull-downs were raised in mouse and were not purified, but crude ascites preps, it was thought that FIB was a contaminant present in the Ab stock - even though pull-downs were performed with protein-G conjugated magnetic beads, which should have removed *FIB*. To test this, the stock Abs were resolved on a gel, blotted and probed with α*FIB,* which detects both murine and human FIB. Note, all AGO Ab stocks, kindly donated by Mikiko Siomi were resolved, in addition to a commercially available, purified mAGO2 Ab. Figure 1d shows that FIB is present in the stock AGO2 Ab used for the pull-downs in addition to the F6 AGO3 clone; no FIB was observed in the commercial mAGO2 stock. As the Ab stocks are contaminated, it means the previously generated proteomic data is not reliable; therefore, pull-downs using a different method were pursued to identify an AGO2 interactor.

a) Ensuring that RBC lysate was cross-linked

b) Band3 does not associate with AGO2

c) Fibrinogen does not associate with AGO2

d) Stock AGO Abs are contaminated with fibrinogen
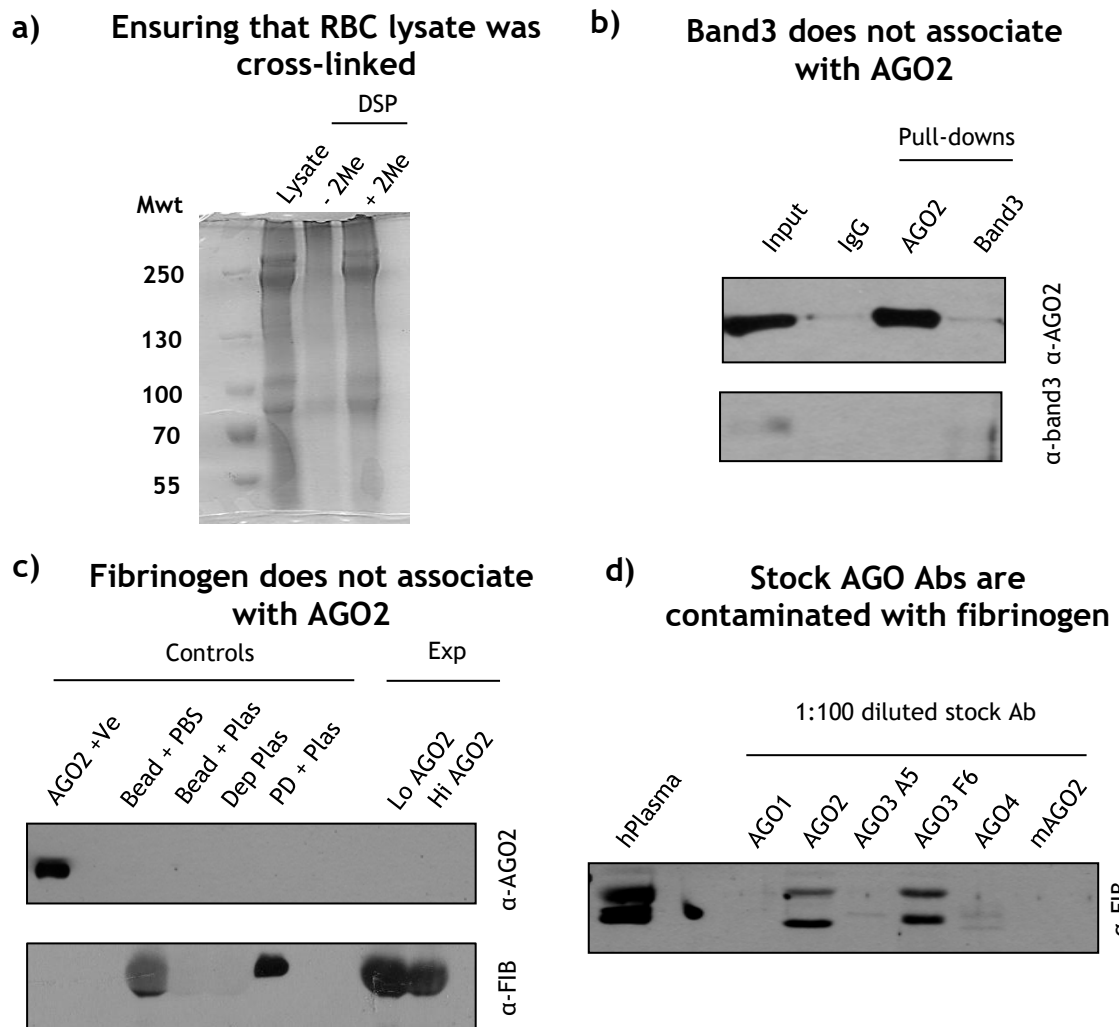
Figure 16: Proteomic candidate interactors with AGO2 are confounded by impure antibody solutions.
a) Lysates were prepared from erythrocytes cross-linked in the presence of DSP and resolved on a 7.5 % acrylamide gel in the presence or absence of 2-Mercaptoethanol then stained with coomassie blue; b) cross-linked erythrocyte lysates from (b) were immunoprecipitated with α-AGO2 / α-BAND3 then probed with the reciprocal antibody via immunoblot; c) Plasma was spiked with low (5 µL) or high (50 µL) AGO2 concentrate, incubated for 30 minutes then pulled down with α-AGO2 or α-FIB then probed with the reciprocal antibody via immunoblot; d) All non-purified stock Abs were diluted 1:100 with PBS and probed with α-FIB via immunoblot. Note, Ab +ves = concentrated eluate (AGO2) or 1:100 diluted plasma (FIB) and are technical controls.

3.2.2 Investigating AGO2-protein interactions *via* 2-O-methyl pull-downs

Before AGO2-protein interactions were evaluated it was decided to optimise certain areas that could increase the sensitivity of future methodologies. For example, ensuring the starting sample was enriched for AGO2, and/or reducing the amount of haemoglobin.

3.2.2.1 **Method for enriching AGO2**

Previous data from the Hamilton lab demonstrated that AGO2, unlike in nuclear cells, associates with the erythrocyte membrane. This interaction is maintained despite hypotonic lysis with 1 mM HEPES and subsequent washing, but can be interrupted by PBS in dilute solutions of the lysate. To reduce potential background, this finding was used to prepare a protein sample enriched for AGO2 and depleted for haemoglobin (Hb), the most abundant erythrocyte protein. Figure **17a-i** details the methodology of producing an AGO2-enriched solution. To increase concentration, but minimise disruption of interactions, samples taken at each stage were concentrated through a 3 kDa centrifugal filter column (Amicon). To determine the degree of loss of AGO2 at each step, an equal volume of each sample was analysed by immunoblot using αAGO2. The vast majority of AGO2 remained in association with the membrane fraction through several washes, and was found within the final eluate (Figure **17b-ii**); note that some AGO2 is found within the lysis and wash 1 sample, but none is observed in washes 2 -5, indicating that this interaction is robust.

3.2.2.2 **Method for depleting Hb**

While hypotonic lysis with 1 mM HEPES greatly reduced the amount of Hb present in the membrane eluate, a substantial amount remained bound as the pellet retained a pinkish hue. This also appeared to bind to streptavidin beads used in subsequent pull-downs (data not shown). As a high degree of Hb-bead binding would manifest as a false positive, in addition to obscuring genuine strep-bio interactions, an improved method of Hb depletion was developed. Packed RBCs were lysed with 1 mM HEPES (comparator), 20 mOsm sodium bicarbonate, 20 mOsm monosodium phosphate buffer with or without 1 mM EDTA and washed until no further Hb was visually being removed. Membranes lysed with HEPES, sodium bicarbonate-EDTA and phosphate buffer-EDTA all visually retained Hb following washing, while those lysed with sodium bicarbonate and phosphate buffer without EDTA did not (Figure **17b**). These new buffers did not affect the AGO2-membrane interaction as membrane samples analysed by western blot showed the presence of AGO2 pre-elution, but not post (Figure **17c**). Comparing the protein profiles of the membrane eluate to RBC lysis indicated the preparation of a sample containing numerous membrane and cytoskeletal proteins (Figure

17d); this sample, termed AGO2-eluate from here, was used in pull-downs to evaluate proteins interacting with AGO2.

a) (i)   AGO2 associates with red cell membrane

Hypotonic Lysis

Spin and wash (x5)

Release AGO2 with PBS

Lysis buffer

PBS

AGO2 in solution

AGO2 bound to RBC membrane

RBC membrane

(ii)

L   W1 W2 W3 W4 W5   E

130
100
70
55

α-AGO2

L = lysis
W = wash
E = eluate
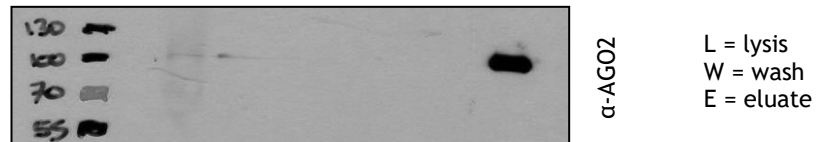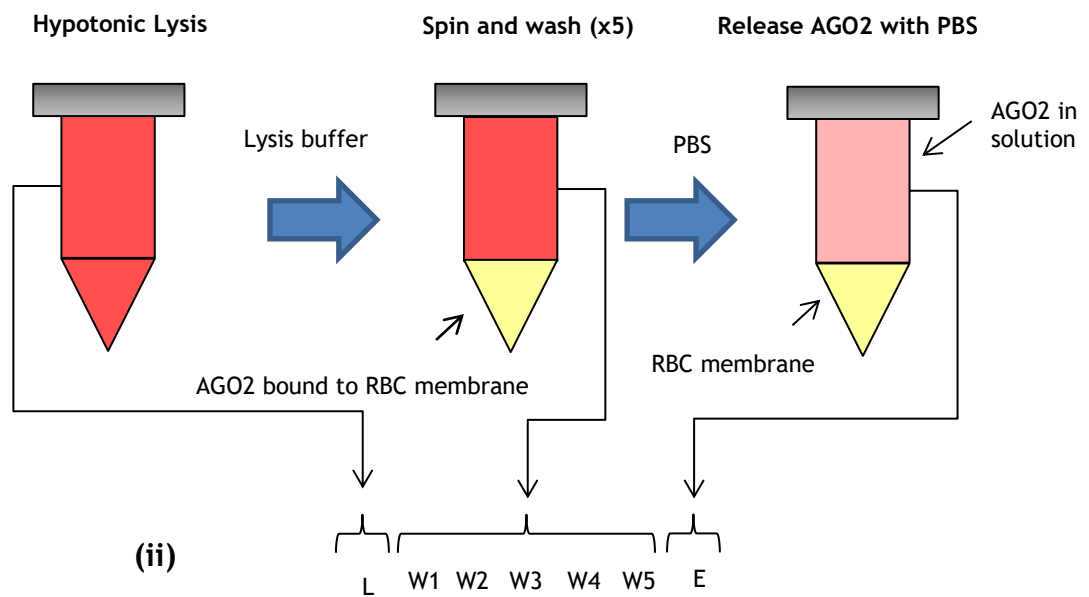
b)   NaBi or Pho remove most Hb from RBC ghosts

Membrane pellet after wash 5

H   NaBi   NaBi-EDTA   Pho   Pho-EDTA
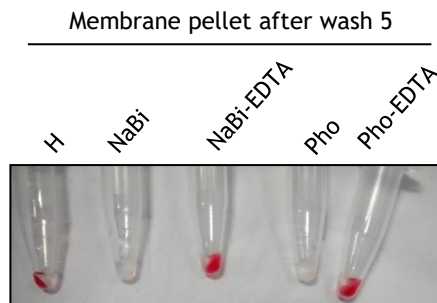
c)   Lysis buffer type does not affect AGO2 membrane association

Pre-PBS   Post-PBS

H NaBi Pho   H NaBi Pho

α-AGO2
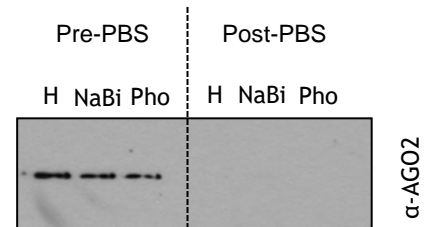
d)   Eluate is enriched in membrane proteins
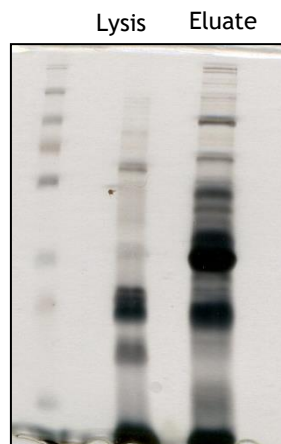
Lysis   Eluate

Figure 17: AGO2 associates with the red cell membrane.
a) (i) Schematic detailing how to prepare RBC ghosts; (ii) 5 mL lysis (L), wash (W) and eluate (E) samples concentrated to 300 μL using a 3 kDa MWt spin column and probed with α-AGO2 *via* immunoblot (5 μL loaded); b) RBC ghost pellets following five washes with 1 mM HEPES (H), 20 mOsm Sodium Bicarbonate (NaBi) or 20 mOsm Phosphate (Pho) buffer; Ghosts were also prepared with 20 mOsm NaBi / Pho in the presence of 1 mM EDTA (E); c) membrane samples lysed using different methods and probed with α-AGO2 pre- and post-PBS elution; d) protein profiles for AGO2-eluate and lysis concentrate as visualised by silver stain; 5 μL AGO2 eluate and 5 μL 1:100 diluted lysis loaded.

As the antibodies used in pull-downs had previously been shown to be contaminated, pull-downs using an alternative method were employed on the AGO2-eluate sample. This methodology was adapted from the protocol generated by Simard *et al.*[399] Briefly, RNA probes *in vitro* transcribed (IVT) in the presence of biotin-16-UTP, or, 2'O-methylated RNA oligos (2'OM) containing a 5' biotin motif that are complementary to specific e-miRNA are allowed to hybridise to the miRNA component of RISC, before being isolated using streptavidin magnetic beads; probe sequences are detailed in Appendix **7** (Figure **18a**). Note that in the beginning both IVT and commercially synthesised probes were used. However, due to the comparative ease of using 2'OM, these were pursued in further work

Initial optimisation was performed to reduce the considerable background of the bead-only control (Figure **18b**). Surprisingly, it was discovered that high background was due to the nature of the agitation used when incubating bead-only controls in AGO2-eluate. Agitation that resulted in continuous sample inversion (rotator) caused the beads to clump, presumably due to proteins becoming denatured and precipitating. This was quite surprising, but it is believed to be analogous to the thickening of an egg white post whisking (i.e. protein denaturation caused by mechanical stress). On the other hand, gentle agitation (roller) resulted in no clumping and significantly less background. Although comparatively lower, pull-downs using IVT probes still resulted in high background, with an e-miRNA specific probe (miR-451) having less signal than the bead-only control (Figure **18c**). Blocking beads with free biotin abrogated residual background, indicating non-specific interactions were *via* streptavidin (Figure **18d**).
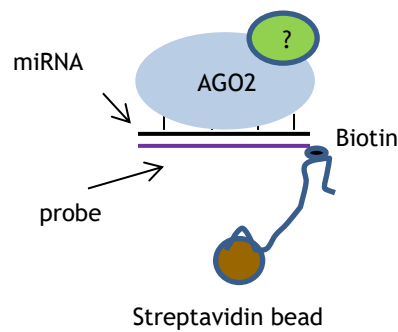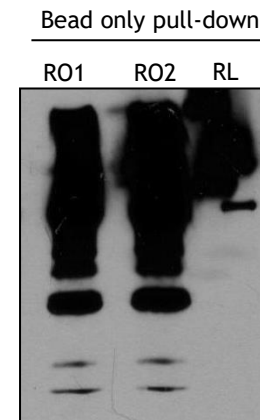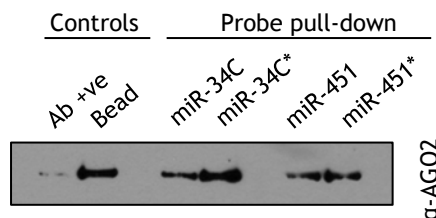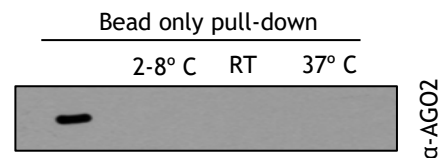
Figure 18: Optimising a RISC pull-down strategy using 2'O-methyl probes.
a) Schematic detailing how 2'O-methyl pull-downs work, the sequences of all probes used are detailed in Appendix **7**; b) Immunoblot detailing high background due to sample agitation strategy causing bead clumping (RO = rotary agitator with inversion, RL = roller, note two different types of RO were used; c) 2'O-methyl pull-downs of AGO2 concentrate using positive (miR-451), negative (miR-34C) and bead only controls; d) Blocking beads with 40 pM free biotin prior to sample incubation removes background, temperature was also investigated but had no discernible effect. Note, Ab +ve = concentrated AGO2 eluate and is a technical control. Note, IVT probes were allowed to hybridise to RISC, then pulled down with beads, or, probe coupled beads pulled down RISC directly (*).

Pull-downs using e-miRNA-specific oligos resulted in similar high molecular weight protein profiles (6 % gel) with two protein bands visible at ~ 100 kDa and ~120 kDa (Figure **19a** – red brackets); an oligo complimentary to EBER3, a small ncRNA found in cells infected with Epstein-Barr virus (EBV), was used as a non-specific oligo control. Interestingly, low molecular weight profiles (15 % gel) differ between capture oligos, with miR-16 having a doublet band at ~ 18 kDa; profiles are consistent between experiments (N=5). Transferring these samples to a membrane and probing with αAGO2 indicate the band seen at ~100 kDa is AGO2, which matches the predicted size of 97 kDa (Figure 4b (i). Note that AGO2 is observed in the EB3 negative control. With the data provided here it is unclear whether this is a non-specific interaction between the EB3 probe and e-miRNA due

to high GC content (52%), or, whether unloaded AGO2 is recognising and binding the probe as per a small RNA. Note that this would most likely have to be through the 3' end of the probe, *via* the PAZ domain, as the 5' end of the probe contains a biotin motif (not a terminal phosphate) and is bound to magnetic beads, making it unlikely to be recognised by the mid/PIWI domain.

Although the proteomic data mentioned previously is suspect, the AGO2-BAND3 interaction it suggested was also reported by Van Wijk *et al*.[299] Even though the reciprocal pull-downs in Figure **16c** suggested no AGO2-BAND3 interaction, as a final test the 2'OM samples were probed with αBAND3 as the observed higher molecular weight band in Figure **19a** is similar to the predicted size of BAND3. However, probing with αBAND3 indicated that this was not the higher molecular weight band observed by silver stain (Figure **19b(ii)**). Failure to detect this band by western blot was not believed to be a sensitivity issue as the doublet band observed in Figure **19a** is visible when stained via Coomassie, a method less sensitive than immunoblot. The low molecular weight doublet observed when pulling down with miR-16 (Figure **19a** – red circle) is not Hb-beta (Figure **19b(iii)**), or likely to be the alpha Hb chain, as the alpha and beta chains are the same size. A potential explanation for why this doublet band is seen with miR-16 pull-downs only is that AGO2 interacts with different proteins, depending on the miRNA cargo it is carrying.

To ensure that the high molecular weight band in Figure **19a** was a robust interaction, the stringency of the pull-down washes was increased. Increasing the NaCl concentration of the wash buffer (0.25 - 1 M) to reduce non-specific protein interactions did not affect the high molecular weight band (Figure **19c**), indicating this interaction was robust. Probing these samples for AGO2 confirmed that AGO2 was still present and undiminished in intensity, demonstrating, as expected, the stringent washes did not affect AGO2 pull-downs. Interestingly, a secondary band sometimes observed when probing with αAGO2 was reduced in signal following the higher stringency washes (Figure **19c** – black arrow). This was taken as evidence that the stringency washes were working and removing non-specific interactions. Samples were re-run, stained with Coomassie and the band in Figure **19c** marked with a star was excised and sent for mass spectrometry (MS) analysis. Note, that only the top band was sequenced as it was the only consistent, prominent, band

visible when performing these pull downs. As we were looking for what AGO2 interacts with, and Figure 19b identified the bottom band as AGO2, only the top band was sequenced.
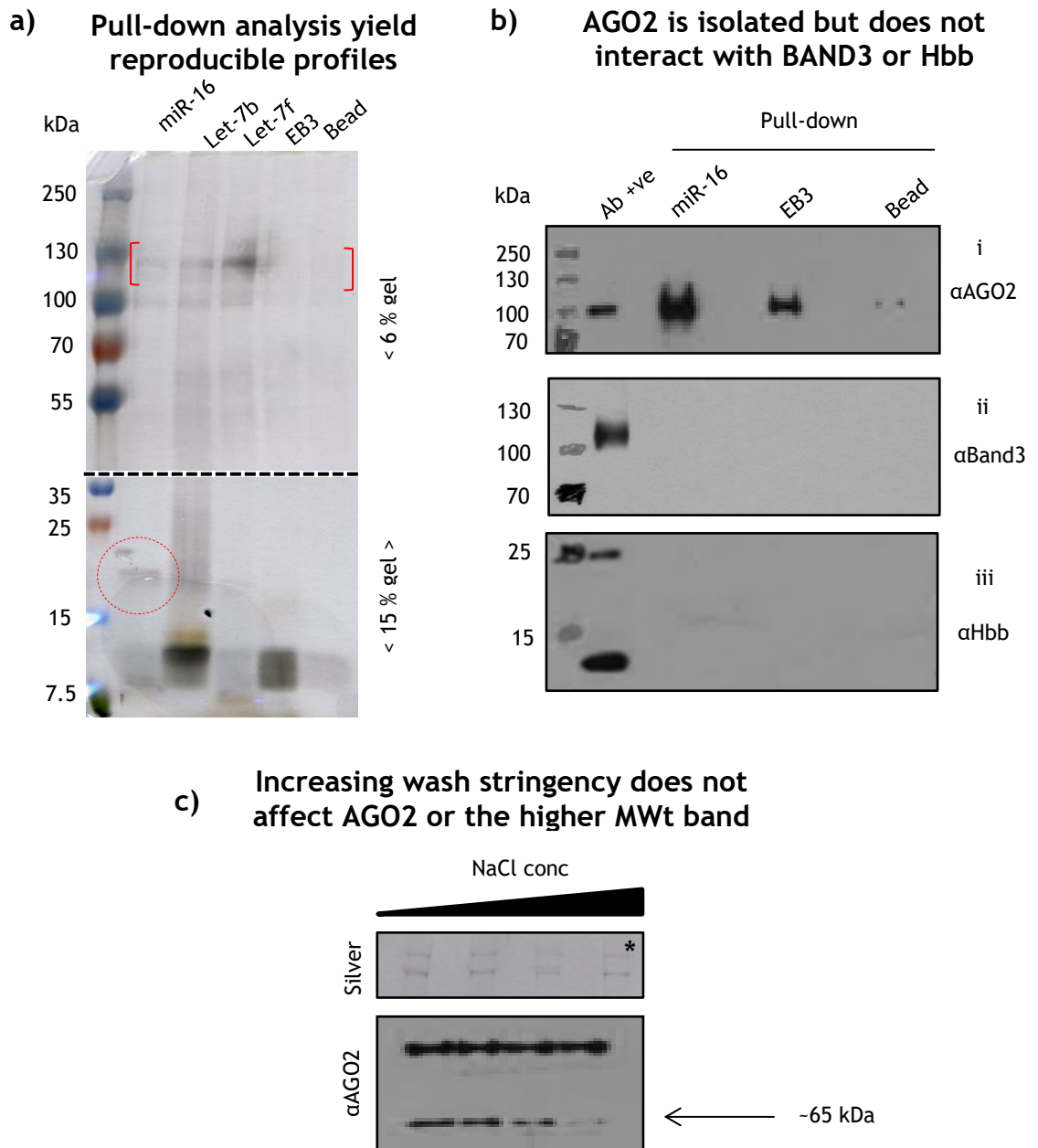
Figure 19: Analysis of 2'O-methyl based pull-downs results in a reproducible protein profile.
a) Protein profiles for RISC pull-downs using 2'O-methyl probes that are e-miRNA specific (miR-16, let-7b, let-7f), not present (EB3) or bead only controls, an equal volume of each sample was loaded; b) Analysis of pull-down samples *via* immunoblot using α-AGO2, α-BAND3 or α-Hbb antibodies; c) Western and silver stain analysis of samples pulled down and washed using 0.25. 0.5, 0.75 or 1 M NaCl in PBS-T (1% (*v/v*) Tween-20), an equal volume of each sample was loaded. Note, Ab +ve = concentrated eluate (AGO2), RBC membrane (BAND3) or 1:100 RBC lysis (Hbb) and are technical controls; profiles generated in 4a were performed more than 4 times. Red brackets and circle are discussed in text.

The higher molecular weight band was identified as AGO2, with a Mascot probability score of 494 (Table 1); additional sequencing results were either not significant, keratin, a known MS contaminant or significantly below the size of band excised (Appendix **14**).

Table 5: Top 7 hits for the high molecular weight band as reported by MS.

Name	Score	Mass
protein argonaute-2 isoform 1 [Homo sapiens]	494	97146
keratin 1 [Homo sapiens]	307	66027
type II keratin subunit protein, partial [Homo sapiens]	259	52757
unnamed protein product [Homo sapiens]	197	59492
keratin 6B, isoform CRA_a [Homo sapiens]	107	59874
Chain B, Crystal Structure Of S-Nitroso-Nitrosyl Human Hemoglobin A	105	15865
epidermal cytokeratin 2 [Homo sapiens]	103	65825

3.3 **Discussion**

The overarching hypothesis of this project is that e-miRNA have a function and are not just artefacts of maturation. This chapter focused on the hypothesis that within erythrocytes e-miRNA have a novel function out with canonical miRNA silencing. To elucidate what this function could be, proteins interacting with the AGO2 portion of RISC were investigated.

3.3.1 **Proteomic validation**

Two candidate AGO2 interactors highlighted by previously generated proteomic data were evaluated, neither were verified. An AGO2-FIB interaction appears to be an artefact caused by an impure Ab preparation as murine FIB was found within the stock Abs used for the AGO2 IPs (Figure **16e**). Although an AG02-BAND3 interaction was suggested by Van Wijk *et al.* this was also not verified (Figure **16c**)[299]. It is not believed that any potential AGO2-BAND3 interaction is being perturbed due to the IP procedure (cell lysis), as samples were successfully cross-linked with DSP prior to isolation (Figure **16b**). In addition, DSP cross-linking was not used on the samples sent for MS by the Hamilton lab, indicating this precaution wasn't required. Furthermore, the AGO2-BAND3 interaction was also not reported by Speer *et al.*, the only published study to have performed an AGO2-IP in erythrocytes, indicating that the AGO2-BAND3 interaction is not genuine[400]. Comparing the data generated in Speer's study to that generated by the Hamilton lab reveals only one protein in common: Phosphofructokinase (PFK). As this was reported by two independent sources it is entirely possible that this is a genuine interaction. The reason why this was not evaluated at the same time as FIB / BAND3 interactions was that this study had not yet been published. As this project had already moved onto a different hypothesis by the time of publication of the Speer paper, and as it's not clear how e-miRNA would play a role within glycolysis, this avenue was not pursued / revisited.

3.3.2 **Generating a miRNA pull-down protocol**

2'O-methyl based RISC pull-downs have successfully been employed by Sonenberg *et al.* when studying the recruitment of *CAF1/CCR4* by RISC[401]. As there are few nucleic acids within mature erythrocytes, using a probe-based pull-down

should theoretically result in low background due to a lack of material to cross-react with. Indeed, using this method routinely isolated AGO2 above the non-specific probe controls (Figure **19a, b**). The protein profiles of RISCs isolated with different miRNA are very similar, with a band ~ 20 kDa larger than AGO2 consistently being detected. Although it was possible to sequence the entire 2'O-methyl pull-down (specific Vs nonsense probe) and establish which proteins were enriched, due to the reproducibility and robustness (Figure **19c**) of the observed high molecular weight protein, this band was excised and sequenced. This resulted in the excised band being identified as AGO2 (Table **5**) and not an interacting protein. Note that AGO1 was also identified within the mass spec data, although the predicted size of 97 kDa is smaller than the band excised at ~ 120 kDa making it impossible for it to be the identified band. In addition, western blots in Figure 13d demonstrate that AGO1 is not present in mature erythrocytes, meaning that the mass spec data in this instance is incorrect.

3.3.3 **AGO2 doublet and modifications**

This high molecular weight AGO2 (hmwAGO2) band runs ~ 20 kDa higher than predicted, indicating a modification, or, a splice variant. Two splice variants of AGO2 are reported on NCBI and uniprot: the major isoform, which has a mass of 97 kDa and is detected by the 4G8 Ab (Figure **19b**) and a second isoform which has a predicted molecular mass of 93 kDa. This second isoform is not what is observed in Figure **19a** for two reasons: (1) hmwAGO2 band has an estimated size of 125 kDa and runs above the major isoform, not below, as it would have to if it had a mass of 93 kDa; (2) Uniprot notes that there is no experimental evidence of this second isoform existing. While this doesn't preclude the possibility of an unreported splice variant, a more likely explanation is that hmwAGO2 has been post-translationally modified in some way.

```
001  MYSGAGPALA PPAPPPPIQG YAFKPPPRPD FGTSGRTIKL QANFFEMDIP KIDIYHYELD
061  IKPEKCPRRV NREIVEHMVQ HFKTQIFGDR KPVFDGRKNL YTAMPLPIGR DKVELEVTLP
121  GEGKDRIFKV SIKWVSCVSL QALHDALSGR LPSVPFETIQ ALDVVMRHLP SMRYTPVGRS
181  FFTASEGCSN PLGGGREVWF GFHQSVRPSL WKMMLNIDVS ATAFYKAQPV IEFVCEVLDF
241  KSIEEQQKPL TDSQRVKFTK EIKGLKVEIT HCGQMKRKYR VCNVTRRPAS HQTFPLQQES
301  GQTVECTVAQ YFKDRHKLVL RYPHLPCLQV GQEQKHTYLP LEVCNIVAGQ RCIKKLTDNQ
361  TSTMIRATAR SAPDRQEEIS KLMRSASFNT DPYVREFGIM VKDEMTDVTG RVLQPPSILY
421  GGRNKAIATP VQGVWDMRNK QFHTGIEIKV WAIACFAPQR QCTEVHLKSF TEQLRKISRD
481  AGMPIQGQPC FCKYAQGADS VEPMFRHLKN TYAGLQLVVV ILPGKTPVYA EVKRVGDTVL
541  GMATQCVQMK NVQRTTPQTL SNLCLKINVK LGGVNNILLP QGRPPVFQQP VIFLGADVTH
601  PPAGDGKKPS IAAVVGSMDA HPNRYCATVR VQQHRQEIIQ DLAAMVRELL IQFYKSTRFK
661  PTRIIFYRDG VSEGQFQQVL HHELLAIREA CIKLEKDYQP GITFIVVQKR HHTRLFCTDK
721  NERVGKSGNI PAGTTVDTKI THPTEFDFYL CSHAGIQGTS RPSHYHVLWD DNRFSSDELQ
```

```
781  ILTYQLCHTY VRCTRSVSIP APAYYAHLVA FRARYHLVDK EHDSAEGSHT SGQSNGRDHQ
841  ALAKAVQVHQ DTLRTMYFA
```

Figure 20: Mass spec coverage of the AGO2 sequence is low (23%).
The amino acid sequence of AGO2 (NP_036286.2) with the peptides sequenced by mass spec mapped to it and highlighted in red. P = hydroxylation site, S + Y = phosphorylation site, K = sumoylation site, dashed box = 4G8 Ab immunising peptide.

As hmwAGO2 was not detected by the 4G8 AGO2 Ab it suggests that any post-translational modification must be in the region of the immunising peptide (amino acid 1 – 148, n-terminus). Although the identification of AGO2 is statistically significant, MS data (highlighted in red) only covers 23 % of the reference AGO2 amino acid sequence (black, [Figure **20**]). In addition, MS data only correlates to 22 % of the 4G8 immunising peptide, meaning the likelihood that the modification lies on a sequenced peptide is low. Indeed, although cursory, analysis performed by Glasgow Polyomics indicates that these three peptides bear no modification. What this modification is, or, its relevance to e-miRNA function, is unclear. That said, the modifications AGO2 is reported to undergo and the relevance of that to this project are discussed below.

3.3.3.1 **Sumoylation**

Small Ubiquitin-like Modifier (SUMO) proteins are a form of post-translational modification whereby a SUMO protein (SUMO 1 – 4) is ligated to an amino acid motif: KXE[402]. The effect of this modification is protein dependent, but has been reported to fall into three main categories: (1) prohibiting protein function; (2) stimulating protein-protein interactions; and (3) affecting a protein's 3D conformation[403]. Dejean *et al*. demonstrate that AGO2 can undergo sumoylation (Sumo 1, 2/3) at L402 and report that it promotes AGO2 turnover. Analysis of this paper shows that an AGO2-SUMO1 modification, when visualised by western blot, bears a striking resemblance to the profile observed in Figure **19a**[404].

However, there are multiple reasons for suggesting that this is not the cause of hmwAGO2. First, the key effectors in sumoylation are *RANBP2*, *UBC9* and *SAE2* – none of which are present within erythrocytes[270]. Therefore, if hmwAGO2 was due to sumoylation, it would have had to occur prior to terminal differentiation. So, even if this was sumoylation, and the observed AGO2 was being turned over, only a proportion of the total AGO2 observed in erythrocytes is hmwAGO2, meaning the remaining AGO2 wasn't being turned over. Second, although Dejean

et al. investigated, they were unable to detect AGO2-sumoylation *in vivo*, even in conditions that are known to promote this modification (i.e. γ-irradiation, arsenic); Indeed, all AGO2-SUMO data shown in their paper is from an induced system. For example, recombinant AGO2 was isolated and incubated in a mixture containing all sumoylation key effectors, or, these key effectors were over-expressed in a cell line. Although this proves that AGO2 can indeed undergo sumoylation, due to their difficulty detecting this modification *in vivo* one must ask if it is biologically relevant. With this in mind, it is not apparent how this report is relevant to the function of e-miRNA. Note that 2'O methyl pull-down samples were probed for SUMO1, 2/3 *via* western blot, and while the result was negative, it was not possible to generate a suitable SUMO positive control. As there are insufficient technical controls for this western, it is not shown.

3.3.3.2 **Hydroxylation & Poly(ADP-ribose)**

Another two AGO2 modifications are hydroxylation, at P700, and poly-ADP-ribosylation, which are linked to AGO2 stability and stress, respectively[405,406]. However, neither of these modifications could cause the mobility shift responsible for hmwAGO2; poly-ADP-ribosylation results in a protein smear when observed by western and hydroxylation doesn't have enough mass to shift a protein 20 kDa. Therefore, these modifications are not the cause of hmwAGO2.

3.3.3.3 **Ubiquitination**

A common post-translational modification that AGO2 undergoes, and which has been widely studied, is ubiquitination[407]. So far, AGO2 ubiquitination is associated with turnover, although if this was true for e-miRNA, we would expect an "AGO2-ladder" caused by poly-ubiquitination to be visible – this is not observed. Furthermore, a study by Goodman *et al.* investigated proteosomal degradation in mature erythrocytes. While they found active 20S proteasomes within mature RBCs, none of the identified proteins degraded was AGO2[293]. Taken together this indicates that the hmwAGO2 modification is not poly-ubiquitination.

3.3.3.4 **Phosphorylation**

Mobility shifts of proteins are commonly caused by phosphorylation, personal communication Dr Richard Burchmore (Head of Glasgow University

Proteomics). However, why a protein becoming phosphorylated could cause an apparent mobility shift of ~20 kDa is unclear. Nevertheless, consulting the literature reveals multiple reports of AGO2 being phosphorylated. For example, it is reported by Weaver *et al.* that AGO2s S387 phosphorylation plays a role in RISC being sorted into exosomes[408]. However, S387 (Figure **20**, red S highlighted in blue) is present on a peptide sequenced by MS and analysis of the data shows that our sample was not phosphorylated.

Meister *et al.* report that phosphorylation of Y529 plays a role in miRNA binding. However, review of this paper shows no indication of any mobility shift on western blots they performed[141]. Two reports studying AGO2 phosphorylation do contain western blots that have AGO2 profiles similar to the silver stains in Figure **19a**; although the study Mendell *et al.* can be discounted as the size shift observed is induced *via* the use of a phospho-tag assay[409]. The study that reported S387 phosphorylation was published in 2008, where Graves *et al.* showed that phosphorylation at this site was required for p-body sequestration. Analysis of this paper reveals the presence of an AGO2 doublet similar to that in Figure **19a**. This wasn't the cause of the mobility shift however, as inducing phosphorylation only increased the amount of WT AGO2 observed by western blot, not hmwAGO2; this doublet was not remarked upon by the authors[410]. Although phosphorylation doesn't appear responsible for hmwAGO2, it is interesting that this doublet is observed within the literature. Indeed, in-depth analysis of the literature demonstrates that this doublet has been observed multiple times, even sequenced, but has not readily been explained[411].

3.3.3.5 hmwAGO2 summary

The post-translational modifications that AGO2 is known to undergo have been discussed above and are unlikely to be responsible for hmwAGO2. Therefore, hmwAGO2s modification is either completely novel, or, at a residue hitherto unreported. As hmwAGO2 is only a proportion of the total AGO2 observed within an erythrocyte it raises certain questions: Is this observation relevant to the question at hand? Why is only a proportion of AGO2 modified? Is this a dynamic interaction, and if so what causes it? To further confound this issue, even though hmwAGO2 was never observed by either the 4G8 or 11A9 antibodies during the first 15 months of this studentship, the first western blot performed on density

gradient erythrocytes revealed the presence of hmwAGO2 (Figure **28a**)! While this apparent contradiction was frustrating, it did rule out the possibility that hmwAGO2 was caused by the 2'O methyl probe remaining bound to e-miRNA as the samples analysed in Figure **28a** had no probe present. As there was no discernible pattern for when hmwAGO2 would be observed, and it was not believed to be relevant to the question of e-miRNA function, establishing the hmwAGO2 modification was not pursued.

3.3.4 **Conclusion**

The aim of this chapter was to establish what AGO2 interacts with in an erythrocyte, in order to glean information regarding its potential function. However, while two methods of pull-down were performed, no interaction was verified / discovered. This data does not preclude a potential of e-miRNA retaining a function within erythrocytes, but it is difficult to speculate, and thus test, what this could be. Due to the difficulty in evaluating novel functions of e-miRNA within erythrocytes, and the time spent, this hypothesis was no longer pursued. Instead, a second hypothesis, the results of which are reported in Chapter **4**, was generated.

Chapter 4   Do e-miRNA function within different cells?

4.1 Introduction

<u>New hypothesis:</u>

e-miRNA lie dormant within red cells, but regain their functionality as translational regulators when senescent RBCs are removed from circulation by splenic macrophages.

This specific hypothesis is based upon the endpoint of RBC senescence. The life span of a mature erythrocyte is approximately 120 days and during this time it undergoes a variety of morphological and biochemical changes. Firstly, erythrocytes shed a proportion of their membrane through the production of MVs, resulting in cell shrinkage during senescence[356]. Secondly, the ability of erythrocytes to deal with free radicals decreases with age, resulting in the accumulation of oxidised proteins at the cytosolic side of the membrane. This plays a role in the oligomerisation of the membrane protein BAND3, which in turn promotes the binding of natural occurring antibodies (nAbs)[317,391]. This "natural opsonisation", coupled with a loss of the "don't eat me signal" CD47, is how it is thought macrophages distinguish between senescent and young erythrocytes, allowing the phagocytosis of old or damaged cells only.

Following phagocytosis, internalised erythrocytes are consumed by phagolysosomes, although surprisingly, not everything that is internalised undergoes degradation. For example, haem, the porphyrin ring bound by globin, is exported into the cytoplasm where it is degraded by HO1 releasing iron. The iron is then stored within the cell, or, exported by FER into the plasma where it can be internalised *via* CD71^{+} erythroblasts in the bone marrow, forming new haemoglobin. While this allows for the massive recycling of cellular iron, it is also a means by which cellular components exit a phagolysosome – something that must occur if e-miRNA are to function within a macrophage.

So, why would a macrophage export e-miRNA from a lysosome and not simply transcribe new miRNA? Our hypothesis is that e-miRNA act as a molecular signal, regulating a macrophages transcriptome to maintain homeostasis. With this in mind, the continual delivery of e-miRNA from erythrophagocytosis would allow the host cell's transcriptome to be regulated dynamically; the more material phagocytosed, the more "X" is dampened, while a lack of material being phagocytosed allows a cell to return to its basal phenotype. In order for this dynamic regulation to occur, *de novo* transcription of miRNA would not be required. However, before candidate genes are identified, the idea that e-miRNA escape phagolysosomes, like haem, must first be tested.

In order to test this hypothesis a xenomodel, where by human erythrocytes where incubated with murine macrophages was developed. A xenomodel model was chosen due to the 4G8 Ab only detecting human AGO2. This meant that murine AGO2 (endogenous in macrophages) would not be detected, potentially allowing the detection of human AGO2 egressing from RBC to macrophage. However, a potential weakness to this model is that it's impossible to verify if murine macrophages are recognising human RBCs in a manner similar to that of senescent murine RBCs, or are simply recognising them as foreign material. That said, xenomodels are routinely used within the literature to evaluate the phago / endocytosing of RBCs by macrophages. For example, Wellek *et al*. used a cross species model to examine the impact of different immunoglobin subclasses on phagocytosis, while Knutson *et al*. used rat RBCs and murine macrophages to evaluate the effect of ferroportin on iron release[412,329]. Finally, Steinberg's group co-cultured human erythrocytes with murine peritoneal macrophages when evaluating binding mechanisms[413,414]. As these models had been used successfully to evaluate erythrocyte biology, they were pursued here.

The data during the first part of this chapter was generated while testing this hypothesis. However, the majority of the data herein, was generated from a second hypothesis (detailed later) that was formed due to observations from the initial testing.

4.2 **Results**

To test this hypothesis, a cross species model was established; where murine bone marrow derived macrophages (BMDM) were incubated with human RBCs (hRBCs) and IF for AGO2 performed. This methodology took advantage of an AGO2 Ab that is specific to the human isoform only. As all cells contain AGO2 and miRNA, any AGO2 detected by this Ab following phagocytosis could only come from the hRBC; this could then be co-localised with other markers. First, BMDM were generated from wild type C57BL/6 mice in the presence of m-MCSF. After 7 days, macrophages were phenotyped by FACs (CD14+ / F4/80+ - Figure **21a**), then co-cultured with human erythrocytes for 1 hour. To discriminate whether erythrocytes were internalised, or bound to the cell surface, BMDM were treated with a hypotonic wash for 5 minutes; those not internalised were lysed, while those phagocytosed were not (Figure **21b**). To allow the BMDM to recover from the cold hypotonic shock, they were placed back in the incubator for 1 hour prior to performing IF. To ensure that IF is possible on internalised material, BMDM were probed for the presence of hRBCs using the presence of αBAND3 (Figure **21c**). Although a 'no RBC control' is missing (i.e. macrophages only probed with αBAND3) no cross-reactivity of the BAND3 Ab can be seen i.e. BAND3 signal coincides with the RBCs visible by white light and is not present in macrophages. As biconcave RBCs can readily be detected within BMDM, this indicates the suitability of this methodology to detect internalised material; note that these macrophages were not polarised at day 7 and are therefore M0 in character. The next stage was to see if hAGO2 could be detected with this system.
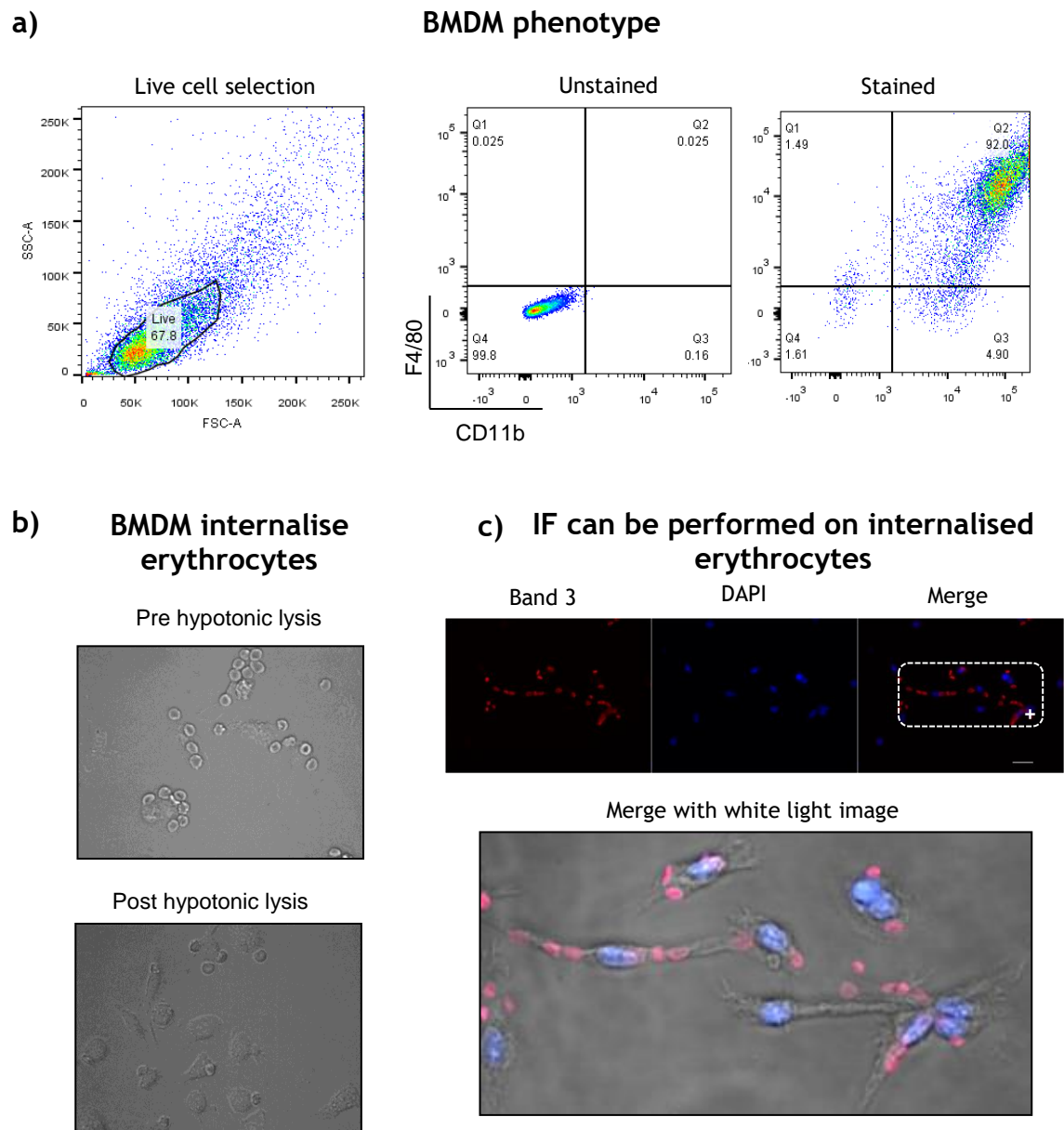
Figure 21: Phenotyping murine bone marrow derived macrophages and using them to phagocytose human erythrocytes.
a) After seven days of culture in 100 ng / mL mMCSF mature macrophages are dual positive for CD11b and F4/80; b) macrophages are incubated with erythrocytes for 1 hour then treated with a hypotonic lysis buffer (150 mM NH4Cl, 1 mM KHC03, 0.1 mM EDTA), non-internalised cells are lysed while internalised cells are not; c) immunofluorescence of phagocytosed erythrocytes using α-hBAND3 merged with a white light image. Scale bar = 20 µm.

Using the above cross species model, RBC phagocytosing BMDM were probed for hAGO2 with the 4G8-AGO2 Ab. Figure **22a** shows that while the *BAND3* Ab does not cross react with BDMD, the AGO2 Ab does, as indicated by the large degree of green staining observed in the no RBC control (red arrow). Although the 4G8 Ab highlights the presence of RBCs in the experimental arm, the background in the negative control is too high, meaning no conclusions about hAGO2 could be drawn. This background was not improved with different blocking methodologies (i.e.

increased blocking time, block concentration, or block type (serum, BSA etc), so a second AGO2 Ab was purchased: the 11A9 clone, which has also been shown to be human specific[415]. However, although the background was greatly reduced when using this Ab, no hAGO2 was detected either within RBCs, or, being released into the cytoplasm of BMDM (Figure **22b**). The 11A9 clone is suitable for IF, as in HeLa cells it co-localises with GW182 (a known AGO2 interactor), highlighting presumed p-bodies (Figure **22c**). During BMDM / RBC incubation, it was observed that only a small proportion of RBCs were internalised. Physiologically, only senescent RBCs (sRBCs) are phagocytosed by splenic macrophages[416]. Considering this, the following questions were raised: If the internalised RBCs are senescent, is it possible they simply no longer contain AGO2, or, is the IF protocol not optimal?

a) IF for hAGO2 in BMDM using the 4G8 Ab results in non-specific signal
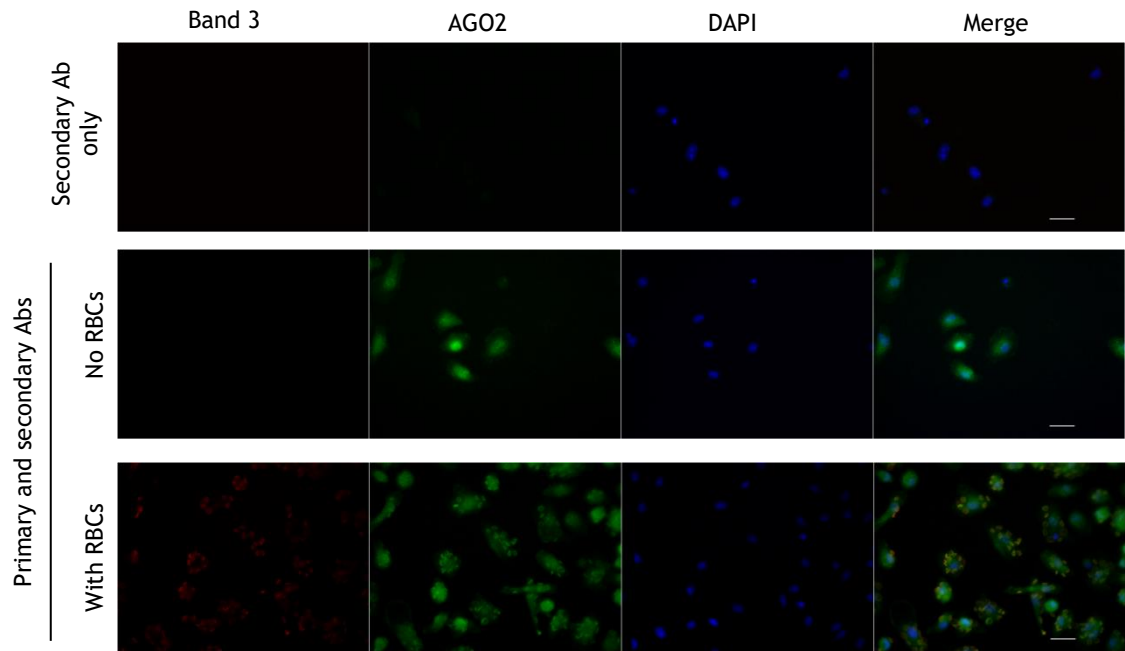
b) The 11A9 Ab does not detect hAGO2 in internalised erythrocytes
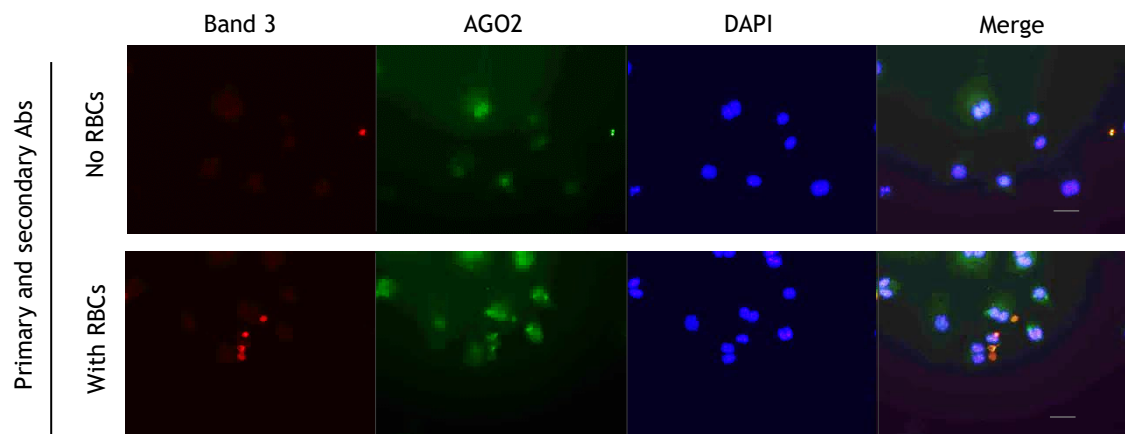
c) The 11A9 Ab can detect p-bodies in HeLa cells
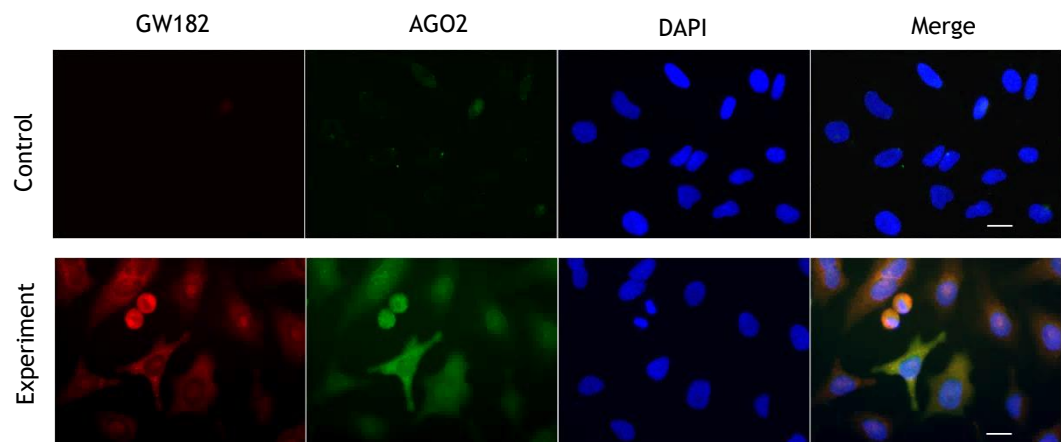
Figure 22: hAGO2 cannot be detected in erythrocytes but can be detected in HeLa cells.
a) BMDM incubated with 6 RBCs per macrophage for 1 hour, washed with hypotonic lysis buffer then probed for α-hBAND3 or α-hAGO2 (4G8); b) Repeat of experiment from (a) but using a different hAGO2 Ab (11A9 clone); c) HeLa cells are probed with α-hAGO2 (11A9) or α-GW182 to detect putative p-bodies. Scale bar, a), b) = 20 µm, c) = 10 µm.

Previous work by the Hamilton lab has shown that e-miRNA levels are stable following 3 days of culture *ex vivo*, while tRNAs and rRNAs are not (Figure **13**). However, this does not preclude the possibility that e-miRNA are lost during the 120 day lifespan of an erythrocyte. IF on bulk erythrocytes would allow this question to be addressed, as if AGO2 levels are variable, then one would expect to see varying degrees of AGO2 positivity in a single field of vision. Conversely, if AGO2 is maintained, then all erythrocytes should demonstrate the same level of positivity. In addition, pursuing this question would allow the optimisation of an AGO2 IF protocol that could be used with the BMDM assay, and, would be a means to verify the AGO2-membrane interaction reported in Chapter 3 Figure **17a.**

Protocol development was problematic due to the fragility of erythrocytes - cells lysed in ethanol, methanol, acetone, 2 – 4 % PFA; blood smears were also evaluated, but erythrocyte morphology was lost post fixation (data not shown). Cells incubated in 0.5 % PFA survived fixation but lysed upon the addition of any permeabilising agent (triton, NP-40 etc); increased fixation times did not reverse this trend. Note that acrolein, which has been reported as suitable for RBC fixation, caused mild lysis; although this was not as high as the complete lysis observed with PFA or solvents. There was no way to ascertain if this was a selective lysis of the most aged / fragile cells, or, a lysis of all RBCs, regardless of age. As the main experiment was to evaluate the potential of differing AGO2 abundancies based on cell age, this method of fixation was not suitable as it was not clear which cells were being lysed. Erythrocytes were successfully fixed using a 0.2 % glutaraldehyde / 4 % PFA mix; no cell loss or morphological change were observed.

To ensure that this protocol was suitable for IF, cells were probed for both membranous (BAND3) and cytoplasmic (Hbb) proteins – BAND3 was exclusively membranous, while Hbb was largely cytoplasmic (Figure **23a**). However, when probed with either the 4G8 or 11A9 antibody, AGO2 was not detected (even at a 1:50 primary Ab dilution). Changing the permeabilisation agent from 0.1 % Triton, to NP-40, SDS, methanol or saponin had no effect on the detection of AGO2 (data not shown). To increase the sensitivity of the AGO2 IF, signal amplification was attempted. This is an enzyme-mediated reaction, whereby horseradish peroxidase, in the presence of H_2O_2, catalyses the reduction of a fluorophore-

tyramide conjugate into a highly reactive radical that labels proteins in the immediate vicinity (Figure **23b**). However, the background in controls without primary or secondary Ab were very high (Figure **23c**). This is presumably due to haemoglobin acting as a pseudo-peroxidase, making this technology incompatible with erythrocytes[417].

a)

Detection of erythrocyte proteins and AGO2 *via* IF

b)
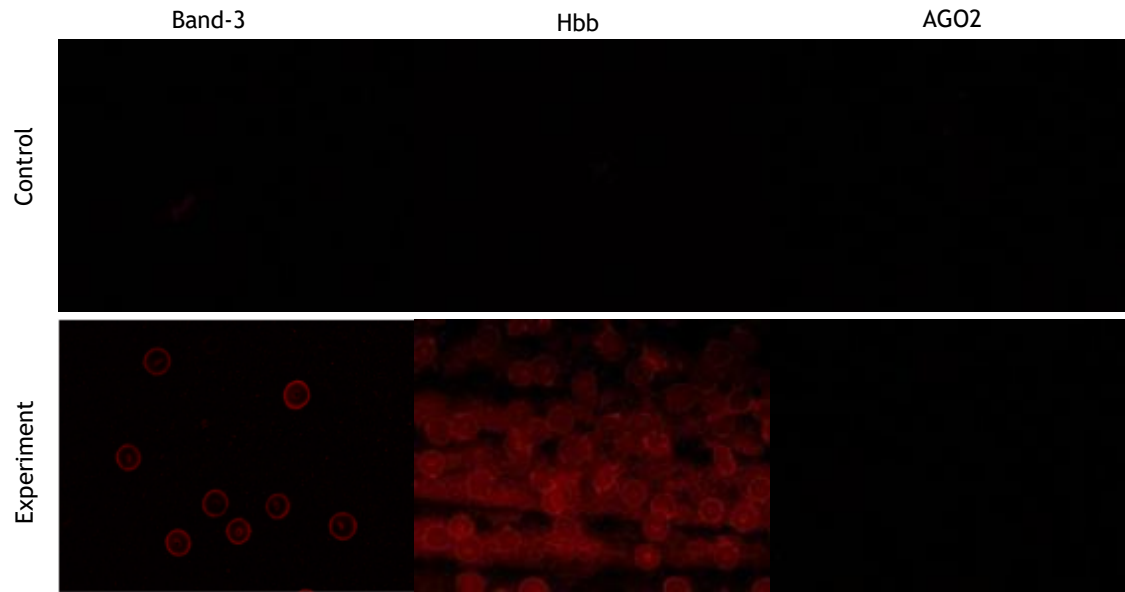
Tyrmaide signal amplification schematic
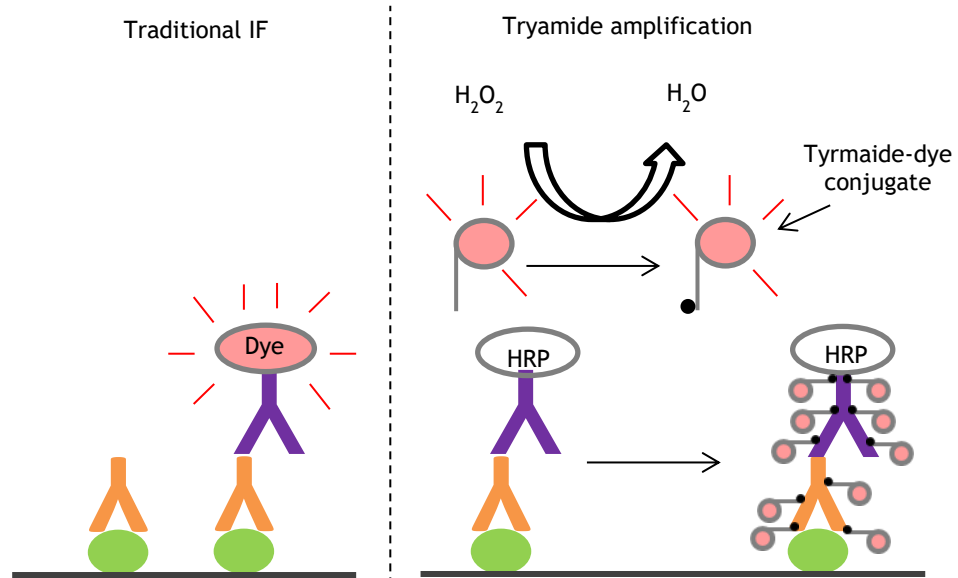
c)

Haemoglobin acts as a pseudo-peroxidase
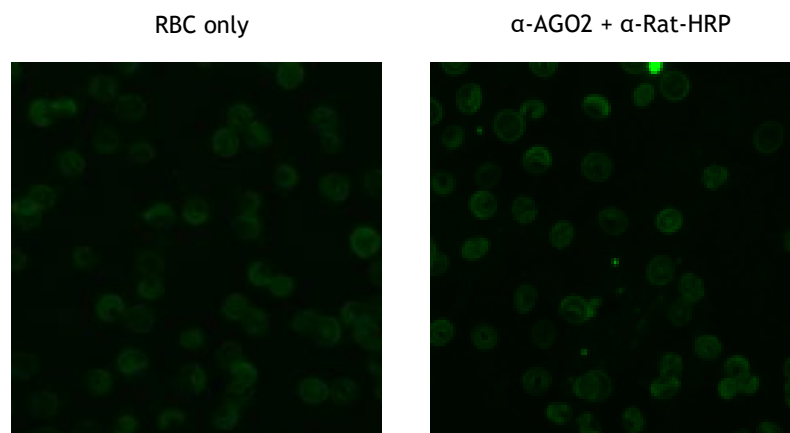
Figure 23: AGO2 cannot be detected in erythrocytes *via* IF.
a) Erythrocytes fixed in 0.2 % glutaraldehyde / 4 % PFA (*v/v*), permeabilised with 0.5 % triton and probed for membrane proteins (α-BAND3), cytoplasmic proteins (α-Hbb) or α-hAGO2 (clone 11A9); b) Schematic depicting how tyramide signal amplification works; c) Tyramide signal amplification of erythrocytes in the presence or absence of HRP conjugates.

A reason for not detecting AGO2 by IF may still be one of sensitivity. Due to having photo multiplier tubes, which amplifies detected signal, flow cytometry is more sensitive than epifluoresence-based IF. The protocol developed above was therefore used to evaluate the levels of AGO2 in erythrocytes by FACs. To ensure that the 11A9 antibody, and the above protocol, were suitable for FACs, AGO2 was first detected in KCL22 and Jurkat cell lines (Figure **24a**). Probing erythrocytes for AGO2 resulted in a modest fluorescent shift (Figure **24b**). Fluorescence peak analysis indicated a mean fluorescence of 137.3 RFU in unstained compared to a stained fluorescence of 199.7 (P = 0.039) (Figure **24c**). However, based on this shift, AGO2 could only be detected in 3.1 % (± 0.7) of erythrocytes, unlike the 100 % of KCL22 or Jurkat cells. Ostensibly, this data suggests that AGO2 levels in erythrocytes are low. Indeed, evaluation of AGO2 levels by western in erythrocyte membranes and KCL22 / K562 cells showed that AGO2 was more readily detected in the nucleated cells (Figure **24d**). While the numbers of cells analysed in Figure **24d** indicate a 100-fold increase in abundance of AGO2 in nucleated cells versus erythrocytes, one has to take into consideration cell volume. For example, the mean volume of a K562 cell is 2030 μm^3, while the volume of a red cell is ~ 60 μm^3, 33 times smaller than the nucleated cell. This suggests that the levels of AGO2 are more comparable than the western in Figure 4d suggests[418,419]. As AGO2 is readily detectable by immunoblot, this method was used to evaluate levels of AGO2 in erythrocytes that had been separated by age using a density gradient.

a) Detection of AGO2 in translating cells using the 11A9 Ab
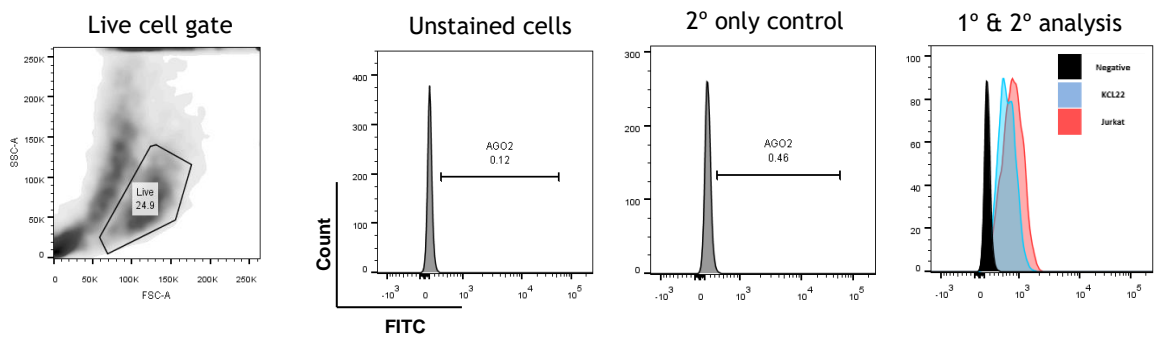
b) Detection of AGO2 in bulk RBCs as per a)
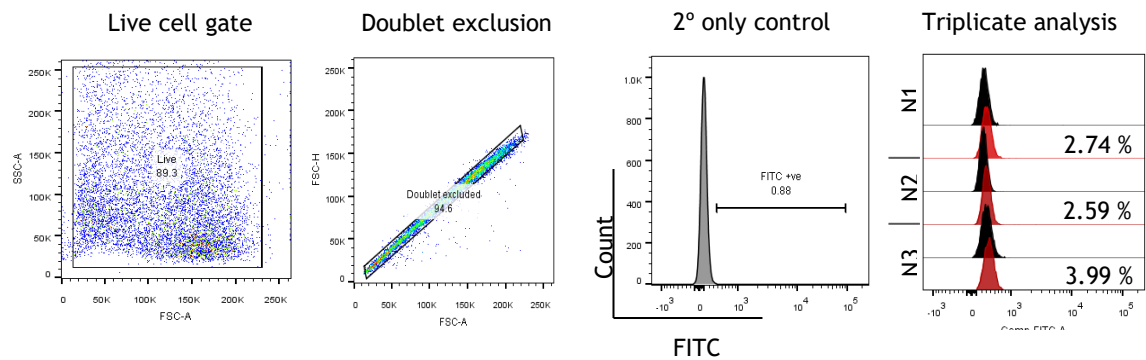
c) Statistical analysis of AGO2 MFI shift
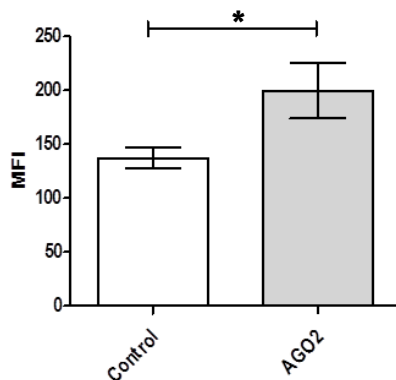
d) AGO2 is more readily detectable in cell lines than RBCs

No. of cells dissolved in SDS and directly loaded

Cell lines = 0.5, 1 and 1.5 x 10^5

RBCs = 0.5, 1 and 5 x 10^6
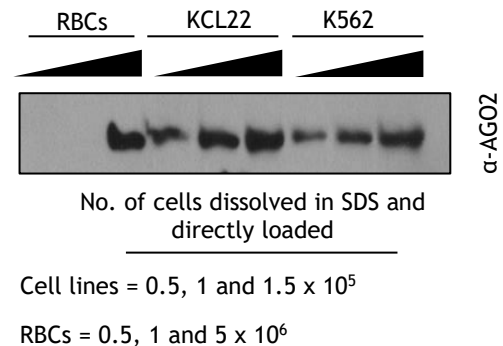
Figure 24: Investigating if erythrocytes maintain e-miRNA using FACs.
a) Establishing the 11A9 Ab can be used to detect AGO2 by FACs by probing the nucleated Jurkat and KCL22 cell lines; b) Detecting low levels of AGO2 in fixed and permeabilised erythrocytes using the 11A9 Ab (N=3); c) two tailed students T-test reveals the fluorescent shift in 11A9 probed cells compared to FITC conjugated secondary only control is significant; d) Cells counted by haemocytometer were blotted and probed for α-AGO2 to establish relative levels of AGO2 between nucleated cells and cell lines; note, for RBCs, the cell number indicates the number of cells ghosts were prepared from.

Erythrocytes have a lifespan of 120 days and exhibit various markers that can be used to identify young (CD71^{+}) or senescent (IgG^{+}) RBCs[391]. Erythrocytes also become smaller and denser as they age, making it possible to separate out

different ages of erythrocytes using percoll density gradients[310] (Figure **25a**). Separating 5×10^8 purified erythrocytes on a 5-point density gradient (1.06 – 1.1 g/L) results in a distinct banding pattern (Figure **25b**). To assess purity, each fraction was harvested, washed, and re-purified on a separate gradient. As can be seen in Figure **25c**, fraction 1 (F1) and F5 both re-separate to form distinct bands, indicating that each fraction is an enrichment of cells at a specific density (age), rather than an absolute population. From three separate experiments, representing the number of cells from each fraction as a percentage of total number of cells, shows that the majority of cells are within F3-4 (Figure **25d**). Based on these numbers, the least dense (0.42 %) and densest (4.75 %) fractions make up the minority of erythrocytes; as these should represent the reticulocyte (~0.5 % of peripheral RBCs) and senescent population (low due to constant splenic attrition), this indicates that the gradient is working and that most RBCs are "middle aged". However, before AGO2 levels are analysed, age-based fractionation needs to be verified.

a) Schematic of RBC ageing

CD71

Microvesicles?

Autologous IgG

≥ 3 days

Day 3 - 120

Cell age

b) RBCs can be separated by age (density)

RBC diluent
1.06 g / L
1.07 g / L
1.08 g / L
1.09 g / L
1.10 g / L

Fraction 1
Fraction 2
Fraction 3
Fraction 4
Fraction 5

c) Each fraction represents an enrichment of cells not purity

Fraction 1 Fraction 5

RBC diluent
1.06 g / L
1.07 g / L

RBC diluent
1.09 g / L
1.00 g / L

d) Youngest and oldest cells comprise the smallest proportion of peripheral RBCs

Propotion of yield (%)

Fraction 1 Fraction 2 Fraction 3 Fraction 4 Fraction 5

Figure 25: Establishing a density gradient methodology to separate erythrocytes based on their age.
a) Reticulocytes exist in peripheral blood as CD71^{+} cells for 3 days before maturing into erythrocytes. As they age, they grow smaller due to loss in membrane caused by vesicularisation, before autologous IgG binds to clustered BAND3 and acts as a recognition signal to splenic macrophages; b) Typical profile of erythrocytes separated on a five point percoll density gradient; c) Re-fractionation of F1 and F5 to assess purity; d) Each fraction was isolated, counted by haemocytometer, and plotted as a proportion of the total number of cells recovered (percentage of overall yield [N=3]).

Although it is possible to separate RBCs using a 5-point density gradient, it is not practical. This is caused by the gradient's sensitivity to any disturbance caused by the operator or centrifuge. Therefore, different gradients were tested to see if they separated blood as previously observed. A 3-point gradient of 1.06, 1.08 and 1.1 g/L was found to produce a similar profile as per Figure **25d** with one less band i.e. very young, middle aged and very old fractions. In addition, a gradient difference of 0.2 g/L between gradient points instead of the 0.1 g/L in Figure **25b** made the gradients easier to pour and more resistant to disturbance. Therefore, this gradient was used in further experiments as it was believed sufficient to answer the question of whether RBCs maintain AGO2 as they age.

Using these improved gradients, FACs was employed to analyse each fraction for different markers to see if these fractions represented differentially aged cells. Analysis of F1-4 scatter profiles indicated that the cells were getting smaller (as measured by FSC) as they got denser (Figure **26a**). Overlaying the scatter profiles of F1 and F4 (ringed red and blue) show that there is a clear shift to the left, indicating F4 (oldest) cells are smaller than F1 (youngest) (Figure **26b**); this is consistent with the idea that erythrocytes get smaller as they age[347]. As old and young populations of erythrocytes bear different markers, it should also be possible to use FACs to confirm these populations are enriched for different ages of cells.

a) Representative scatter profiles of pure and fractionated erythrocytes
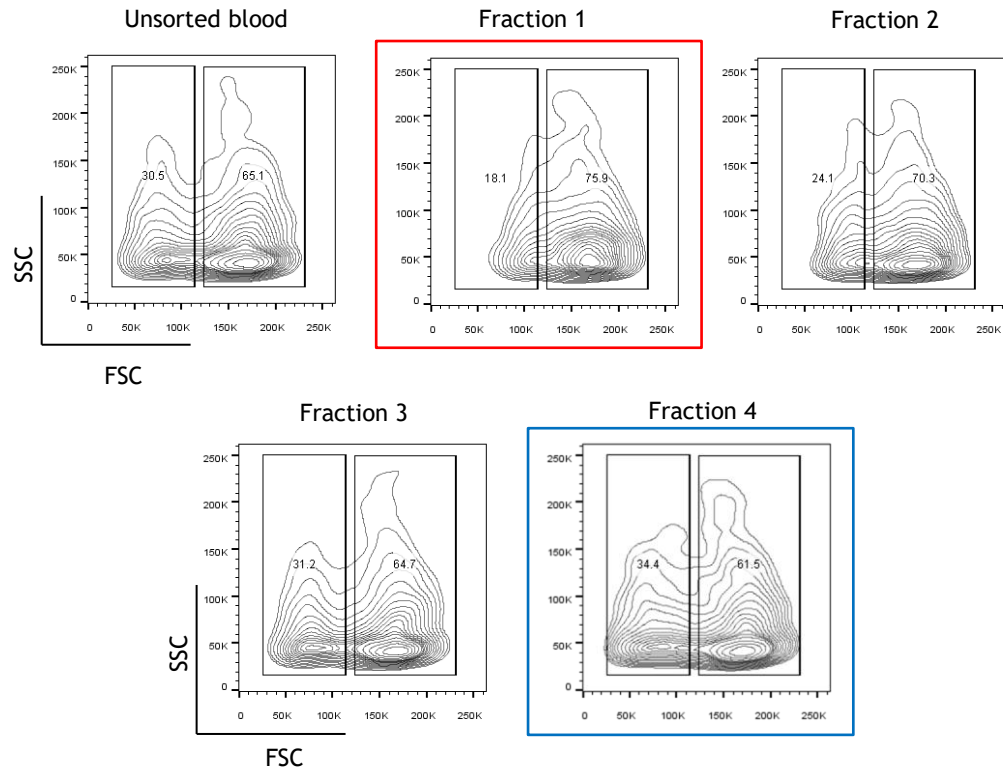
b) Overlaying the scatter profiles of the least (F1) and most (F4) dense cells from a)
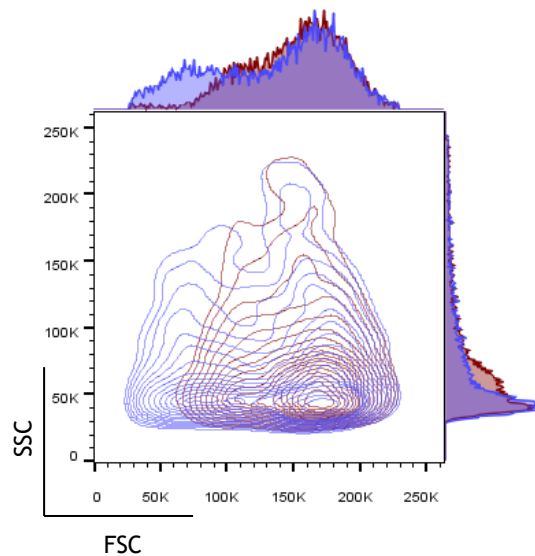
Figure 26: Verifying that blood fractionation reflects cell age; part 1.
a) Representative scatter profile of F1-4 and whole blood, red (F1) and blue (F4) bordered plots represent the youngest and oldest cells respectively; b) Overlaying the highlighted scatter profiles from (a) demonstrates that F1 cells (purple) are larger (FSC-A) than F4 cells while granularity (SSC-A) is unchanged.

CD71, the transferrin receptor, was used as a marker for reticulocytes, while anti-human IgG was used as a marker of senescent erythrocytes, due to them binding autologous IgG as they age. CD71$^+$ reticulocytes were found to be enriched in F1 only, verifying that this is the youngest fraction (Figure **27a**). Enrichment

analysis of three independent experiments is displayed in Figure **27b**. A students T-test revealed that only F1 had a statistically significant increase of reticulocytes, when all fractions were compared to unfractionated blood. Different probes were used unsuccessfully to verify the presence of membrane-associated IgG in F4. This included two different anti-human IgG clones (BD – G18-145, Sigma – F4512) and a protein-A-FITC conjugate; the BD clone, caused a significant change in erythrocyte scatter profile and was not suitable, while the protein-G conjugate displayed low specificity. To ensure that the negative signal wasn't a technical issue due to IgG being lost during processing, F4 was exposed to h-IgG by incubating it in autologous serum for 30 mins, then probing for bound IgG; none was detected (data not shown). As leukodepletion involves the filtration of RBCs through a cellulose column, it is possible that the most senescent RBCs are remaining on the filter, either due to being physically stuck, or, interacting with Fc receptor-expressing immobile leukocytes. However, analysis of cells eluted from the membrane indicated that this was not the case (data not shown). However, the distinct banding patterns seen in Figure **25b**, coupled with F1 being enriched in reticulocytes and F4 cells being smaller than F1 cells indicate this method is enriching erythrocytes of different ages.

a) Representative analysis of CD71⁺ expression on fractionated cells
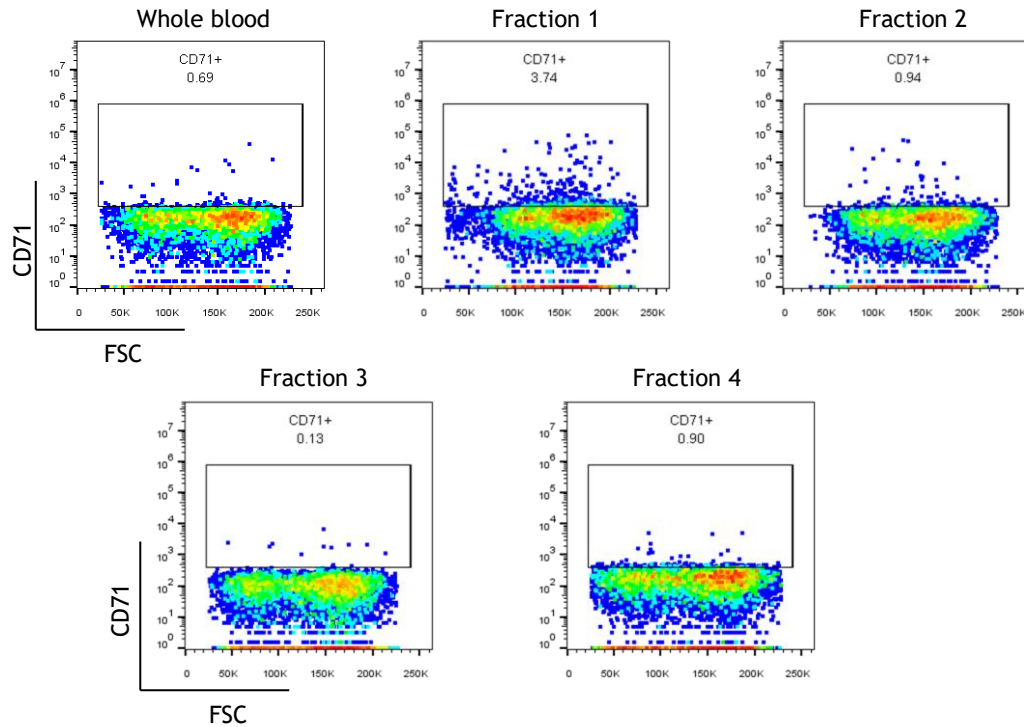
b) Amount (%) of CD71⁺ reticulocytes in each fraction
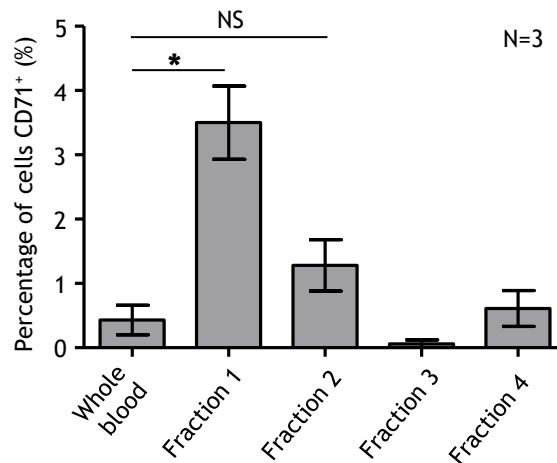
Figure 27: Verifying that blood fractionation reflects cell age; part 2.
a) Establishing CD71⁺ reticulocyte levels in whole blood (basal) and fraction 1 – 4 *via* FACs; b) Amount (%) of CD71⁺ cells present in each fraction from three independent experiments, one tailed students T-test was used to test for significance.

These gradients were then used to answer the question of whether AGO2 is maintained as RBCs age. Cells were harvested from each fraction, washed to remove percoll then enumerated by haemocytometer. Presumably due to donor variability, blood samples yielded a different number of cells per band, although the pattern observed in Figure **25b** remained. As a result, while the number of cells between donors varied, cells per fraction for a single donor were the same. For example, fractions 1-4 for sample 1 had 1 x 10⁶ cells analysed per fraction,

sample 2 had 1.3×10^6 and sample 3 had 0.62×10^6 analysed. RBC ghosts were prepared for each fraction and probed with αAGO2 (11A9) as displayed in Figure **28a**. As F2 and F3 represented the majority of cells present (equivalent of F3+4 in Figure **25d**), which have been classed as "middle aged", only F3 was analysed as the samples of interest were F1 and F4; i.e. the youngest and oldest cells. Note, the high molecular weight band observed in Chapter One is present in samples 1 and 2, but not sample 3. This experiment was the first time that the AGO2 doublet was detected by western, and there is no obvious indication why this is the case. Densitometry of all three samples indicates that AGO2 is decreasing as RBCs age, with an average of 54.6 % (± 22.4 %) AGO2 lost from cells between F1 and F4; note as the larger band had been identified as AGO2, where present, both bands were quantified.
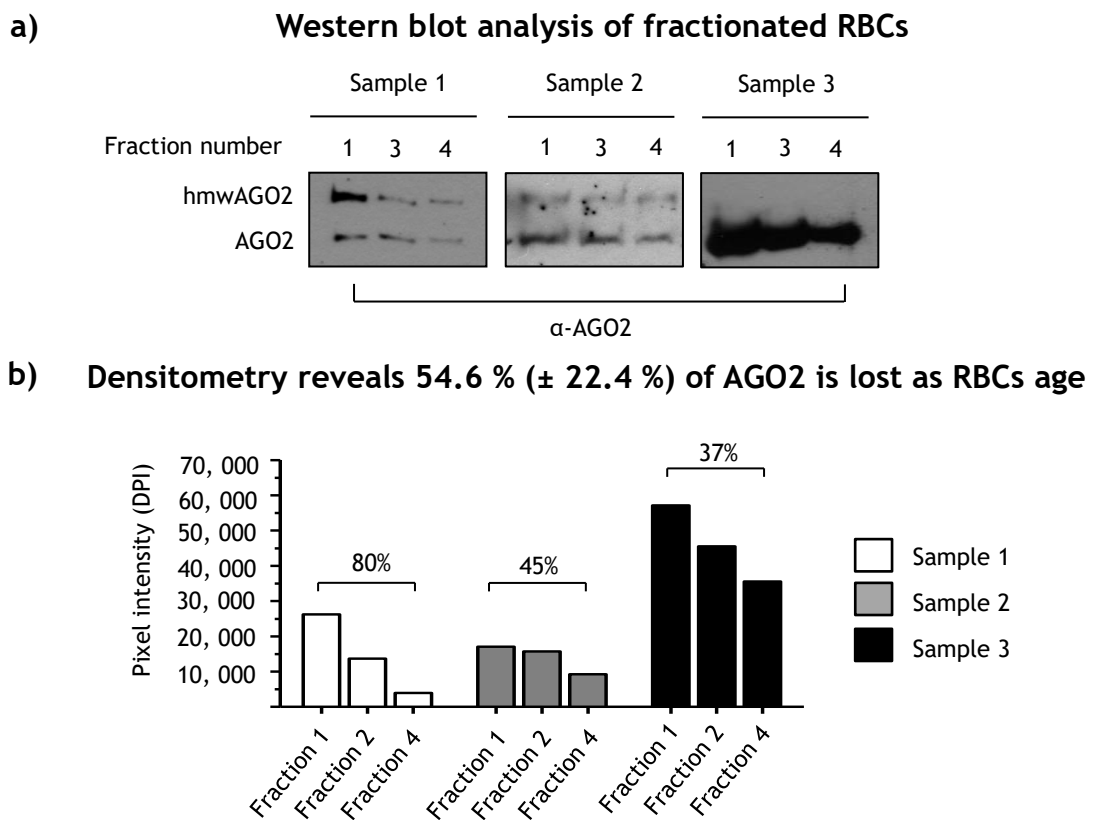
Figure 28: AGO2 is lost as RBCs age.
a) Ghosts from an equal number of erythrocytes (as counted by haemocytometer) from each fraction are probed with α-AGO2, blots are from three independent experiments b) Densitometry for each blot in a) as calculated using ImageJ, percentages represent decrease in signal intensity from fraction 1 to fraction 4, 54.6 % loss of AGO2 is an average from three experiments while ± 22.4 % is the standard deviation.

4.3 **Discussion**

The aim of this chapter was to investigate the ability of e-miRNA to modulate the transcriptome of a phagocytosing cell. However, difficulties in detecting AGO2 in endo/phagocytosed cells led this research question changing to a more simple: do erythrocytes maintain AGO2 as they age?

4.3.1 **Failure to detect AGO2 by IF**

AGO2 was not detected in erythrocytes by IF (Figure **22a**), and the positive fluorescent shift detected by FACs, although significant, was modest (Figure **24b**). The fix and perm strategy used during this study detected both cytoplasmic and membranous proteins, suggesting its suitability for AGO2 detection (Figure **22a**). Furthermore, it was demonstrated in Figure **22b** and by Siomi *et al.* that the 11A9 or 4G8 Ab, respectively, is suitable for the detection of AGO2 by IF[415,420], while Figure **24a** demonstrates that the 11A9 Ab is suitable for AGO2 detection *via* FACs. AGO2 is readily detectable by immunoblot and the relative sensitivities between nucleated cells and erythrocytes are similar, when taking into account cell volume (Figure **24d**), indicating abundance isn't an issue.

Indeed, abundance isn't the problem as during this study, two other studies, using primary Abs different to those used here, published IF images of AGO2 in erythrocytes[421,422]. Intriguingly, both studies show AGO2 to be membrane associated as suggested in Chapter 3 and not cytoplasmic. Fix and perm strategies between these two studies and that reported in Section **2.9.1** are similar. Both employ aldehyde fixation, but at slightly different concentrations – 4 % PFA with 0.007% glutaraldehyde[421] or 0.5 % acrolein[422]. Acrolein wasn't used in this study due to the small amount of lysis it caused, nevertheless, in light of this study, this fixation method was evaluated coupled with the 11A9 Ab, but no AGO2 was detected (data not shown). As the methodologies between the studies are similar it suggests something else is occurring. As the 11A9 and 4G8 Ab can detect AGO2 in nucleated cells, it suggests that in erythrocytes the epitope recognised by these Abs is being masked. It is not clear what is causing this occlusion, but, as AGO2 is membrane associated in erythrocytes, it can be speculated that it is either this proximity to, or interaction with, the membrane that is responsible.

Analysis of the data sheets / publications for all 4 AGO2 antibodies suggests where this interaction / occlusion is taking place (Figure **29**)[415,420]. The immunising peptide for the 4G8 Ab is the first 148 amino acids (aa) from the N-terminus of AGO2. However, as it is published as not detecting mAGO2 and is instead hAGO2 specific, the epitope recognised by this Ab must be within the first 35 aa, as this is the only region with sequence variability between human and mouse; this is the same region the 11A9 Ab is raised against[415]. The 2E12-1C9 Ab from Abnova was raised against an epitope 378 aa long from the C-terminus, while the C34C6 Ab (Cell Signalling Technologies [CST]) peptide is not specified. CST have been contacted regarding the sequence of the immunising peptide, but are unwilling to disclose it. However, considering C34C6 cross reacts with human, murine, rabbit and monkey AGO2, the immunising peptide cannot be within the first 47 aa of the N-terminus as this is not conserved in rabbit. As it appears there is no epitope overlap between the two studies successfully detecting AGO2 and this one, it suggests epitope masking / occlusion is why AGO2 was not successfully detected above, and this occlusion is at the N-terminus.

Mapping immunising peptides to the AGO2 amino acid sequence
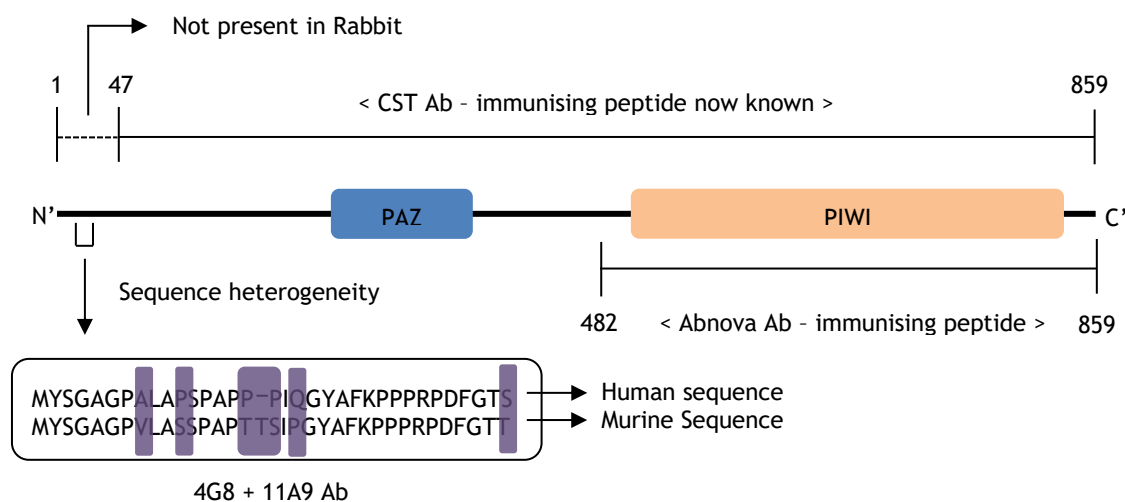
Figure 29: Schematic of the immunising peptides used to raise AGO2 Abs.
hAGO2 is 859 aa in length, immunising peptide regions for the CST and Abnova Abs are shown. m/hAGO2 are highly conserved. Highlighted in purple is the heterogeneous region the 11A9 or 4G8 Ab must bind in order to be human specific.

A simple way of proving if this is the case or not, would be to buy either the 2E12-1C9 or C34C6 Ab and repeat the IF. However, there are two reasons why

this wasn't performed, firstly, budgetary constraints. Secondly, the aim of the experiment was to evaluate AGO2 levels throughout the 120-day life span of an erythrocyte. As this was successfully answered *via* density gradients and western blots, either of these additional Abs were not purchased.

4.3.2 **Reduction of AGO2 as cells age**

Percoll gradients have been successfully used to fractionate erythrocytes based on their density. It has been shown that F1 is representative of the youngest population (increase in CD71^{+} reticulocytes) and that in F4 the cells are comparatively smaller. However, it has not been possible to verify the presence of senescent markers the literature states are present within F4 – specifically, surface bound IgG. Although two different Abs have failed to detect autologous IgG in a variety of samples (whole blood, fraction 4, filter retained blood), a weakness of this experiment is that no positive controls have been used to show these Abs are working as reported. Nevertheless, reticulocyte enrichment and reduction in size is consistent with the literature[322], indicating this methodology is suitable for isolating populations of erythrocytes of different ages.

Analysis of this fractionated blood *via* western blot indicates that AGO2 is lost as erythrocytes age (Figure **28a**). However, there are caveats to this that must be discussed. Loading control: as RBCs lose membrane and haemoglobin as they age, it is not clear which protein can serve as a loading control. The only protein the literature suggests is not lost as RBCs age is spectrin – a part of the cytoskeleton which is resistant to detergent solubility[344,423]. While a loading control is not included in these blots, to address this issue, equal numbers of cells, as counted by haemocytometer, were analysed. AGO2 perturbation: whole RBCs cannot be resolved directly by acrylamide gel, due to poor resolution (Appendix **16**). RBCs must first undergo hypotonic lysis to prepare membranes, a process in which AGO2 could be lost. However, Figure **17a-ii** Chapter 3 indicates that very little AGO2 is lost during lysis and the vast majority remains membrane associated. In addition, there is nothing to suggest that AGO2 would be lost in higher amounts in older versus younger cells, meaning that this consideration is unlikely to affect the blots in Figure **28a.**

It's important to note that AGO2 levels are diminished by 52.4 %, not completely abrogated as cells age. This raises the possibility that e-miRNA are not completely lost during ageing. However, a more likely explanation is that the AGO2 observed in F4 is from younger cells carried through during the gradient, especially as Figure **25c**, demonstrates that the isolated fractions correspond to cellular enrichment, not absolute populations. Furthermore, Speer *et al.* used qPCR to also report that e-miRNA are lost as RBCs age, which is in agreement with the findings in Figure **28b**[400]. Taken together, we believe that e-miRNA are not maintained during the entire 120-day life span of an erythrocyte, meaning that the original hypothesis of e-miRNA functioning within RBCs is false.

<u>Conclusion</u>

It is important to note that none of the data presented above show e-miRNA being turned over, and what occurs to them is unclear. This is interesting as although the paper discussed in Chapter 3, Section **3.3.3.3** detected 20s proteasome-mediated proteolytic degradation within RBCs, AGO2 was not one of the targets identified as being turned over[293]. Unlike any other cell in the body, AGO2 is membrane associated in erythrocytes (Figure **17a-ii**); a membrane that is reported to be lost as RBCs age through vesicularisation[358]. Extracellular vesicles are widely reported within the literature to act inter cellular communicators. To do this they are released by cell A, taken up by a recipient cell (B) and the miRNA they contain modulates the hosts transcriptome. A central hypothesis to this studentship, which is detailed in the introduction to this chapter, is that e-miRNA modulate a phagocytosing cell's transcriptome. As it appears that e-miRNA are lost as erythrocytes age, it is unlikely that this occurs during the phagocytosis of senescent RBCs by splenic macrophages. However, it is possible that an RBC-MV could act as a vector, transferring e-miRNA to distant cells, where they can regain their function as translational regulators; this hypothesis is pursued in Chapter 3.

.

Chapter 5   Do RBC-MVs contain e-miRNA?

5.1 Introduction

It is widely accepted within the literature that erythrocytes get smaller as they age, partly due to membrane lost through vesicularisation[357,424]. The density gradients in Chapter 4 demonstrate that AGO2 is lost as erythrocytes age. As AGO2 has been shown to be membrane associated, it is tempting to speculate that as the erythrocyte membrane undergoes vesicularisation, AGO2 is lost concomitantly. Extracellular vesicles (EVs), either exosomes (EXs) or MVs, have been shown by multiple studies to be able to transfer their cargo to recipient cells, where importantly, it has elicited a function[425]. For example O'Connell *et al.* demonstrated that dendritic cells (DCs) could transfer miR-155 *via* EXs to neighbouring DCs, where it repressed *BACH1* & *SHIP1* expression resulting in a pro-inflammatory response (IL-6 production) when the cells were challenged with LPS[425].

Review of the literature reveals that there are three types of erythrocyte EV: (1) EXs that are shed from reticulocytes as part of CD71 removal; (2) MVs containing oxidised Hbb that are lost as RBCs age; and (3) MVs found within the "storage lesion" which are shed into the storage media (SAGM) of RBC units stored by the transfusion service. Due to the clinical interest regarding transfusion products, the majority of functional studies have been performed on MVs from the storage lesion. A consistent area of research regarding these MVs is their interaction with thrombin and subsequent effect. For example, two individual studies report that RBC-MVs from storage initiate thrombin generation, while a study from Kurtis *et al.* reported that RBC-MVs caused clotting to occur faster when they measured thrombus formation[374,426,427]. Although this means hypercoagulability could be an unintentional side effect of transfusion, Yeon *et al.* identified this as a potential clinical opportunity[428]. They prepared large quantities of RBC-MVs using high pressure extrusion, then demonstrated a dramatic reduction in both bleeding time and blood loss when transfused into their rat model. Although these MVs are not the same as those found within the storage lesion (they are induced and range from 50 – 2000 nm), the authors suggest that this methodology could be translational, specifically in patients with coagulation disorders.

The exact mode of action regarding how RBC-MVs promote coagulation is unclear, however, the most common factor appears to be exposed phosphatidylserine. This has lead multiple studies to demonstrating that it is responsible for the binding of tissue factor or clotting factors (FXII & FVII) to the outside of an MV, increasing the amount of clotting factors at a thromboses[426,429]. Interestingly it was also reported to decrease thrombin activity by binding protein-S, the co-factor of protein-C, resulting in a anti-coagulatory effect[430]. Although stating conclusions, both studies suggest a roll in the regulation of coagulation by RBC-MVs.

There are also a large number of studies evaluating naturally-occurring RBC-MVs (noRBC-MVs), but by-in-large these are restricted to characterisation and enumeration. For example, noRBC-MVs have been characterised by FACs in multiple studies to reveal that they are GLY-A, CD55, and CD59 positive, expose PS and can carry autologous IgG[358,431]. The first three markers are hallmarks of the noRBC-MV's erythrocytic origin, while PS exposure reflects membrane inversion and the autologous IgG has been suggested as a means by which erythrocytes shed pro-apoptotic markers. Other studies take a different approach and instead compare the levels of noRBC-MVs in healthy individuals, to different disease states. For example, Webster *et al.* estimate there is an almost 10-fold increase in circulating noRBC-MVs in thalassemia patients compared to normal[432].

However, despite a large amount of literature on RBC-MVs, when embarking on this work, no study had evaluated the transfer of e-miRNA, or its potential function. Although e-miRNA functionality is the *raison d'être* of this studentship, before any functional studies could be performed, protocols for RBC-MV isolation first needed to be established. With consideration to published studies and the guidelines set out by Hochberg *et al.*, protocols suitable for the evaluation of RBC-MVs were established[433].

5.2 **Results**

Before establishing if e-miRNA is present in noRBC-MVs, artificial RBC-MVs (aRBC-MVs) were first generated to be tested as a proof-of-concept. In addition, generation of aRBC-MVs allowed the generation of protocols to isolate and analyse MVs; work that had not previously been carried out at the Paul O'Gorman Leukaemia Research Centre. The calcium ionophore A23187 has widely been shown to induce vesicularisation, therefore an adapted method from Limbrick *et al*. was used[434]. Using established methodologies enabled the data we generated to be compared with published data, ensuring that the methodologies used herein were suitable.

Incubating purified RBCs with 1 µM A23187 and 1 mM $CaCl_2$ promotes a morphological change, with cells becoming echinocytic (Figure **30a**). aRBC-MVs are released into the incubating medium and need to be purified from remaining RBCs and extracellular Hbb before analysis. To do this, different strategies of isolating aRBC-MVs were evaluated, including different centrifugation speeds, or the type of precipitation reagent used. The most effective method of isolating aRBC-MVs, as judged by MV pellet size, was through differential centrifugation. A final spin of 21,000 x G was sufficient to form a compact red pellet. As analysis of this pellet by light microscopy revealed no contaminating erythrocytes, it was considered an aRBC-MV pellet.

Flow cytometry has been widely used to characterise EVs[358,431], giving information both on their size, relative to known bead controls, and surface composition. However, due to the small size of EVs, analysis by FACs can be problematic due to the instruments not having the resolution to distinguish between EVs and noise. Therefore, Megamix-Plus SSC FITC conjugated beads were used to ensure the BD FACs Canto II could resolve sub-micron particles. Double filtered (0.2 µm) HBSS was used to establish background (Figure **30b-i**) and its scatter profile was qualitatively different to that that of the bead standard (Figure **30b-ii**). This bead mix, contains 4 different sizes of beads, which resolve as individual FITC+ populations, demonstrating the Canto's ability to resolve sub-micron particles. MV samples are qualitatively different to HBSS control, as demonstrated in Figure **30b-i** and Figure **30c-i**, indicating MVs had been isolated. In addition, they appear positive when probed with an Annexin-FITC conjugate

(Figure **30c-ii**), demonstrating that the putative aRBC-MVs have exposed PS on their surface. Probing MVs with an Annexin-FITC conjugate demonstrated that approximately 60 % of the MVs are positive for PS (Figure **30d**); this is caused by membrane inversion during MV formation and the above data are consistent with the literature regarding RBC-MVs[364,427].
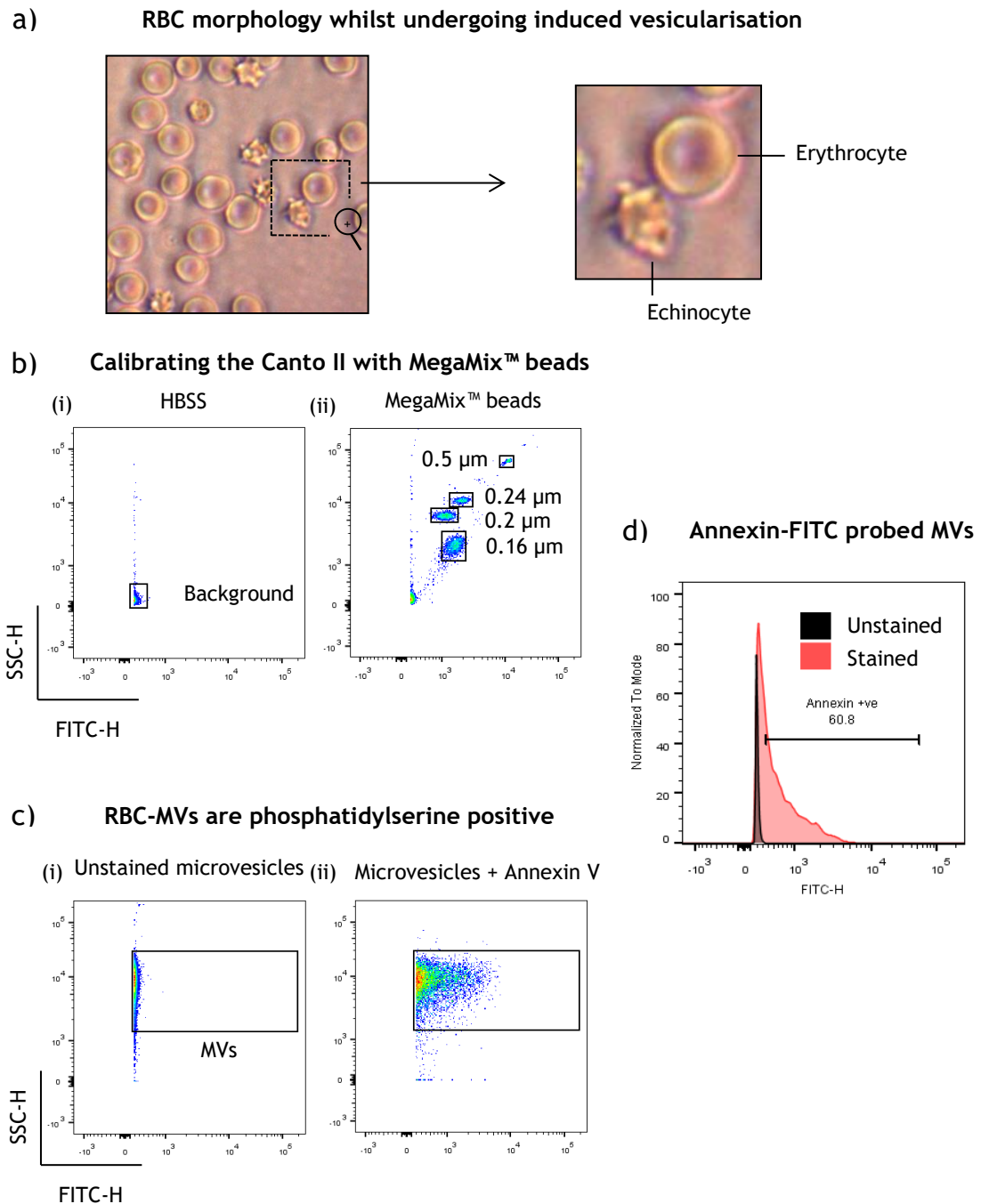
Figure 30: Generation and analysis of RBC-MVs *via* FACs.
a) Morphology change of erythrocyte to echinocyte following incubation with 1 µM A23187; b) Calibration of a FACs Canto II using MegaMix™ SSC beads (i) scatter profile of 0.2 µm filtered HBSS (instrument background) (ii) scatter profile of MegaMix™ SSC beads in HBSS; c) (i) unstained RBC-MVs in HBSS, or, (ii) stained for 20 minutes with 1:100 Annexin-FITC conjugate; d) Histogram overlaying the FITC (phosphatidylserine positivity) signal of the unstained and stained MVs from (c).

Further validation that these putative aRBC-MVs were genuine was sought by verifying their size. Analysing the scatter profile of the MegaMix beads allowed each individual population to be gated then plotted as a SSC-H histogram. Note that while SSC-H is usually a measure of granularity, due to the way the Canto II is designed, and the small size of EVs, it is the parameter recommended by the manufacturer for estimating size. Using FlowJo software, it is possible to overlay these SSC-H histograms in order to produce a "ruler", by which aRBC-MV size can be estimated (Figure **31a**). Using this approach, aRBC-MVs appear to be slightly smaller than 0.2 μm in size (Figure **31b**), however, this is an estimate based on a visual comparison to beads and was therefore verified by transmission electron microscopy (TEM) (Mrs Margaret Mullen, University of Glasgow). The first TEM analysis performed resulted in an "amorphous mass", with what appeared to be aggregated aRBC-MVs (Figure **31c-i**). This was caused by particulates in the 4 % PFA used to fix the MVs. Filtering the PFA removed all particulates (as observed by FACs) and resulted in the observation of individual vesicles (Figure **31c-ii, iii**). TEM revealed that the vesicles were largely uniform in size (~0.2 μm) and shape (circular), verifying the sizes estimated by FACs in Figure 31b. Some discrepancies in shape and size were observed (Figure **31c-ii** white arrow), however the overall distribution appears homogenous.
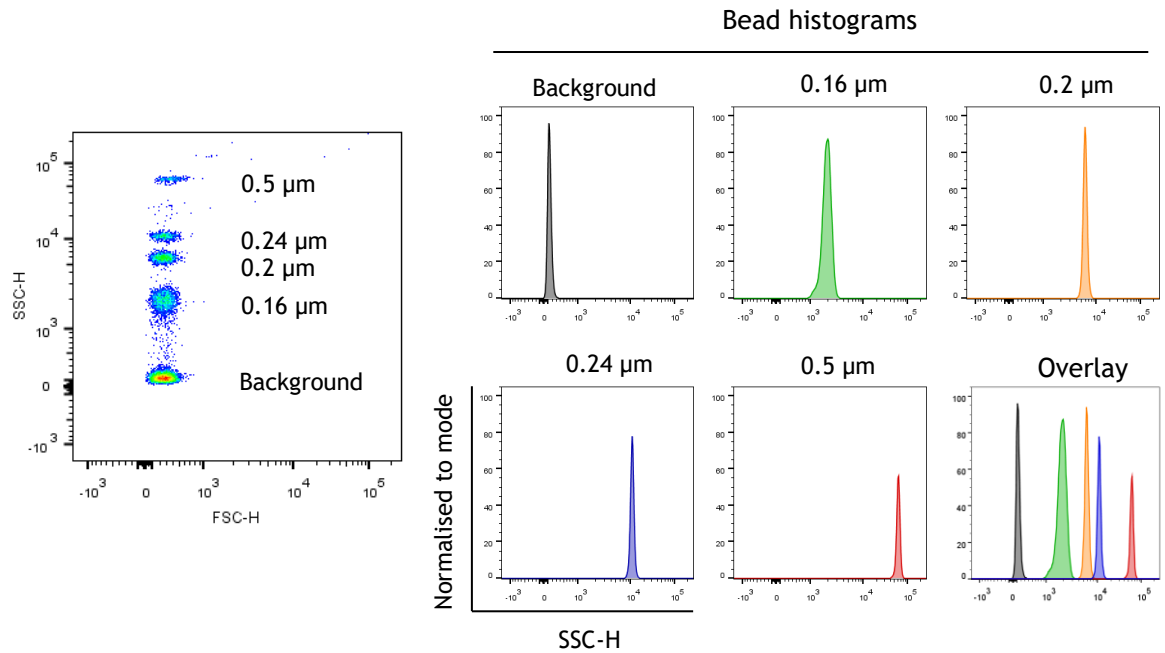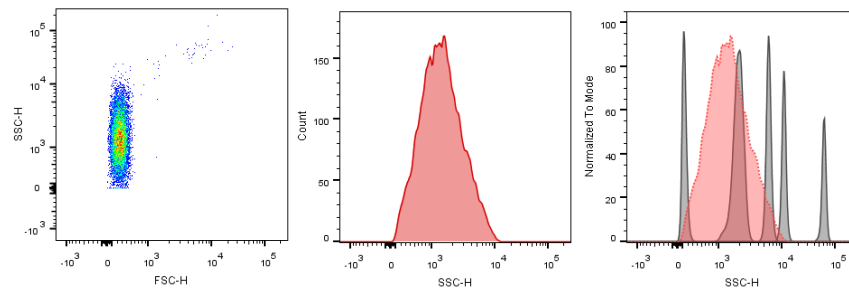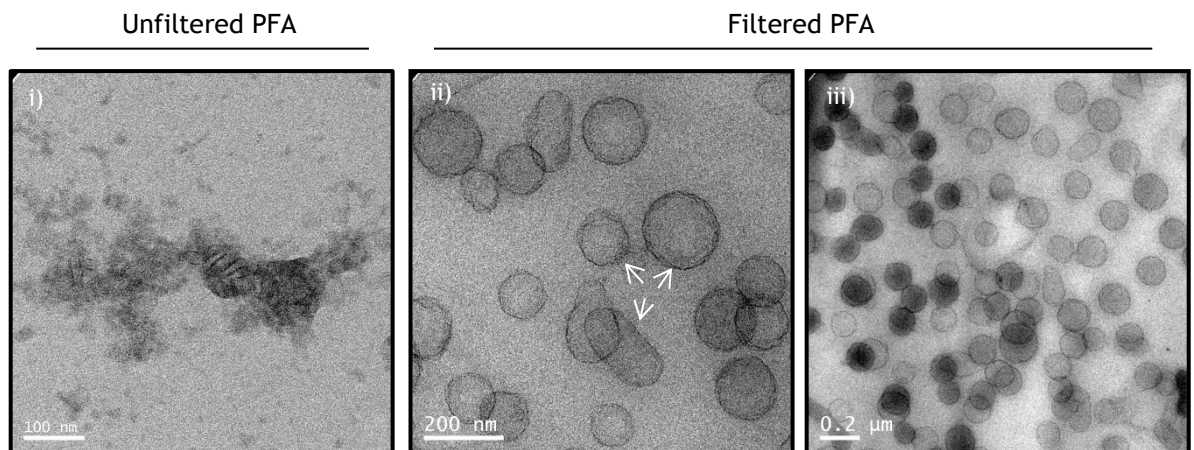
Figure 31: Ionophore induction of vesicularisation results in a homogenous population of RBC-MVs that are ~0.2 µm in size.

a) Individual bead populations are gated, plotted as SSC-H histograms then overlain in FlowJo® to create a "size-ruler" which RBC-MVs can be compared; b) The SSC-H histogram of RBC-MVs in HBSS are plotted against the "ruler" from (a), RBC-MVs have an approximate size of ~0.18 µm as compared to beads; c) TEM of RBC-MVs in unfiltered 4 % PFA (i), TEM of RBC-MVs in 0.2 µm filtered 4 % PFA. Note (ii, iii), all TEM images were captures using an FEI Tecnai T20 by Mrs Margaret Mullin (University of Glasgow).

As aRBC-MVs are derived from erythrocyte membranes, it is possible, using SDS-PAGE, to establish any selective loss/gain of protein within MVs by resolving erythrocyte membranes pre- and post-vesicularisation and comparing their protein profile to aRBC-MVs (Figure **32a**). There are few differences between the erythrocyte membrane pre- or post-vesicularisation, although the profile of the MVs is qualitatively different. As the MVs are self-contained they contain more Hbb than the membranes which have been prepared through hypotonic lysis (white dashed box). In addition, MVs appear enriched for a protein (red circle) in comparison to the membrane preps; this may be stomatin, which has been shown to be enriched on aRBC-MVs[361]. In addition, there are protein bands that are lost upon vesicularisation (black arrows), although these do not appear on the MVs. As Hbb appears to make up the majority of an RBC-MV proteome a different strategy was used to evaluate its protein composition. Although silver stain is a more sensitive stain than Coomassie, just changing the staining method would result in a disproportionate staining in favour of Hbb. Therefore, to get a better estimation of protein profile, aRBC-MVs were re-run, allowing the Hbb to run off the end of the gel. The lower abundant proteins were then visualised *via* silver stain (Figure **32b**). Blotting 20 µg of the same samples, then probing with specific Abs, reveals that unsurprisingly, aRBC-MVs contain erythrocyte markers BAND3 and GLY-A; in addition, probing with αAGO2 indicates the presence of e-miRNA (Figure **32c**).

a)   **Protein profile of RBCs pre / post vesicularisation and MVs**
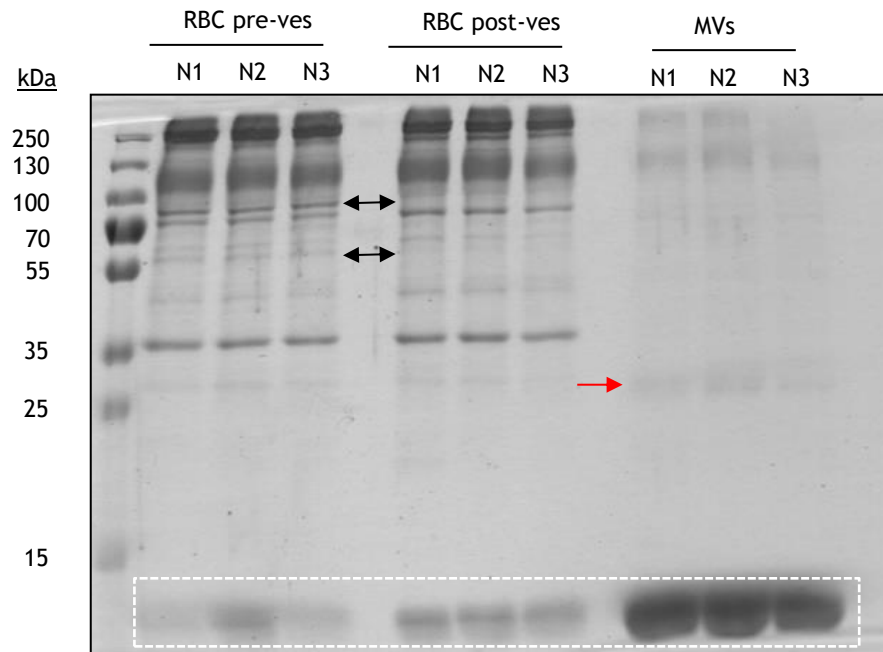
b)   **Silver stain of MVs**   c)   **Immunoblot of MVs**
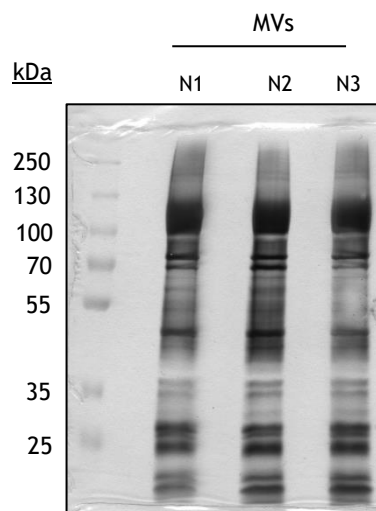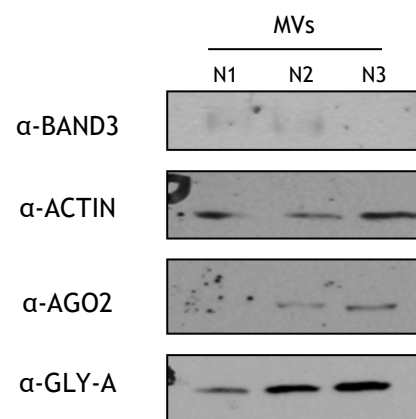
Figure 32: RBC-MVs contain AGO2 and have a protein profile different to RBC membranes.
a) Resolving 20 µg of RBC ghosts pre- and post-vesicularisation compared to 20 µg of aRBC-MVs on a 12 % acrylamide gel and staining with Coomassie; b) Silver stain of 40 µg aRBC-MVs as resolved on a 12 % acrylamide gel; c) Immunoblot of 20 µg aRBC-MVs.

Although AGO2 is present within aRBC-MVs, a western blot doesn't detail which e-miRNA are present. Therefore, qPCR was used to evaluate the presence/absence of three e-miRNA, previously reported to be abundant within RBCs (FIGURE **13**, Appendix **1**). As mature miRNA are small and lack a poly(A) tail it is not possible to use oligo DT or random hexamers to prepare cDNA. A stem loop primer (Applied Biosystems), specific to a single e-miRNA (Figure 4a) was used along with the High-Capacity cDNA Reverse Transcription Kit (Applied Biosystems) to reverse transcribe mature e-miRNA species. Note, this

methodology was used instead of the poly(A) tailing methodology employed by Qiagen, as the Applied Biosystems method has a higher degree of specificity afforded to it through the use of *Taq*man probes. Representative amplification plots observed for e-miRNA extracted from whole erythrocytes and aRBC-MVs are detailed in Figure **33b**, while Figure **33c** confirms the presence of mir92a, mir451 and mir486 in aRBC-MVs. Note, it is unclear what can be used as a control within aRBC-MV, therefore the results reported are the mean raw CT values from three independent experiments run in technical triplicate.
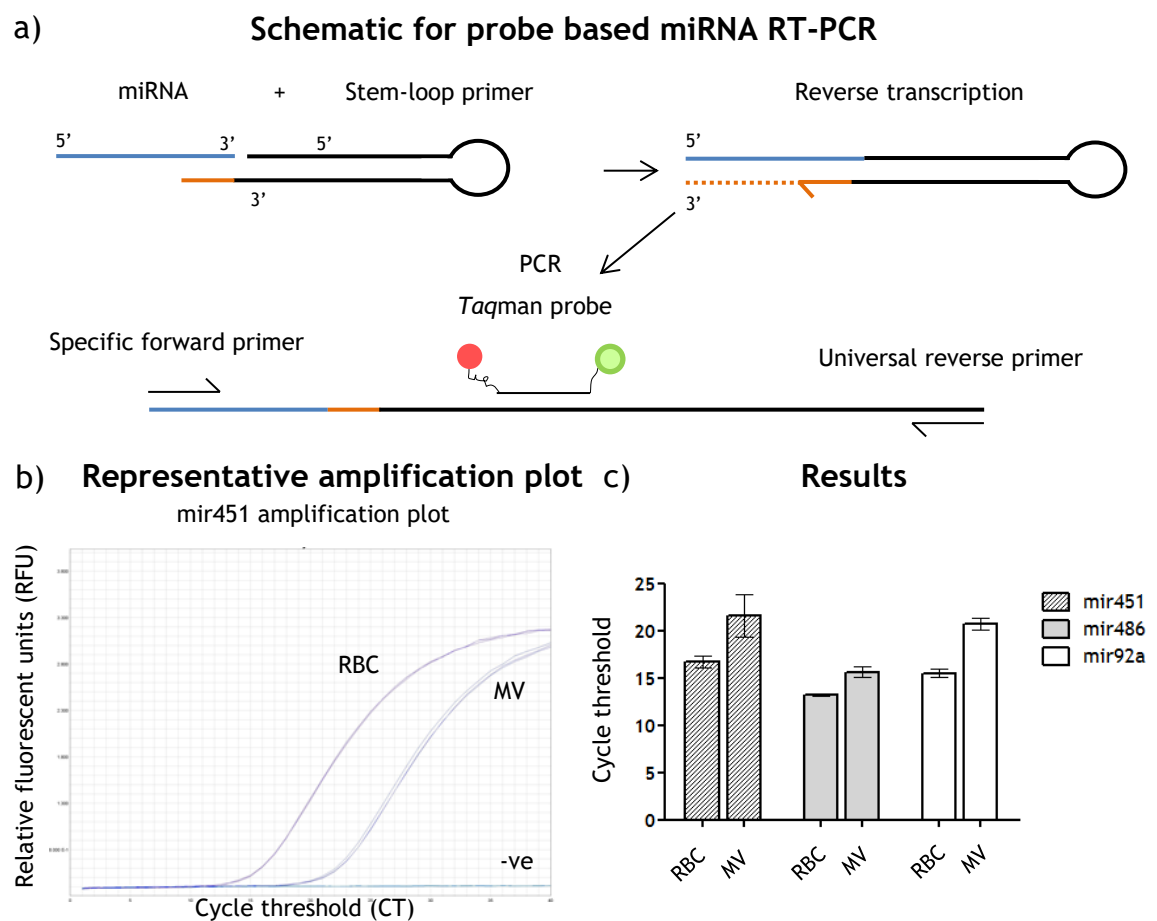
Figure 33: RBC-MVs contain miRNA.
a) Schematic representation of the miRNA luciferase assay; b) Schematic for the Applied Biosystems methodology of miRNA RT-qPCR that utilises a stem loop primer and *Taq*man probe; c) Representative qPCR sigmoidal curves for miRNA isolated from whole RBCs and RBC-MVs; d) Quantification of miR-451, miR-486 and miR-92a in whole RBCs and RBC-MVs, N=3 with all samples analysed in technical triplicate.

As a proof of concept, aRBC-MVs have been shown to contain e-miRNA, the next stage was to verify if this occurs in noRBC-MVs. At present, there is no consensus regarding how blood is to be taken, with the guidelines stated by Hochberg *et al.* recommending that isolation should be tailored to the MV of interest[433]. Therefore, from the same volunteer, 5 mL of blood was drawn via

venepuncture into BD vacutainers containing different anticoagulants (citrate, heparin, and EDTA) or into a pro-coagulation vacutainers to generate serum (Serum Tubes [BD]). Cells were separated from the plasma via low speed centrifugation until the isolated plasma was clear of any contaminating cells when observed by light microscopy. As a protocol for MV isolation had not been optimised, plasma was analysed directly to see whether it contained a population of RBC-MVs and where they lay in relation to the size markers. 5 µL of each sample was probed directly with αGLY-A/Annexin and analysed by FACs for the presence of noRBC-MVs (Figure **34a**). Only blood collected in EDTA tubes contained a distinct population that was dual positive for GLY-A and PS, (Figure **34a** – red boxes). Back gating on this dual positive population and overlaying it with MegaMix beads to estimate size, revealed that putative noRBC-MVs are larger than aRBA-MVs (Figure **34b**). To ensure that this population was genuine, and not an EDTA artefact, EDTA was spiked into 1 mL of citrate/heparin blood and serum, at a final concentration of 10 mM and incubated for 5 minutes at RT. This time point and EDTA concentration was chosen to mimic the final EDTA concentration in a vacutainer and the duration that samples were kept at RT before processing i.e. how the blood was handled that gave the results in Figure 5a. The addition of EDTA had no effect on blood anticoagulated with citrate, heparin or serum prepared with Serum Tubes, indicating that the GLY-A peak observed is not induced by EDTA (Figure **34c**). As blood collected in EDTA vacutainers contains a distinct population of GLY-A+ submicron vesicles, this was decided as the optimal means of collecting blood for the study of noRBC-MVs.

a) Effect of different anti coagulants on RBC MVs

b) RBC MVs Vs SSC beads

c) GLY-A peak is not an EDTA artefact
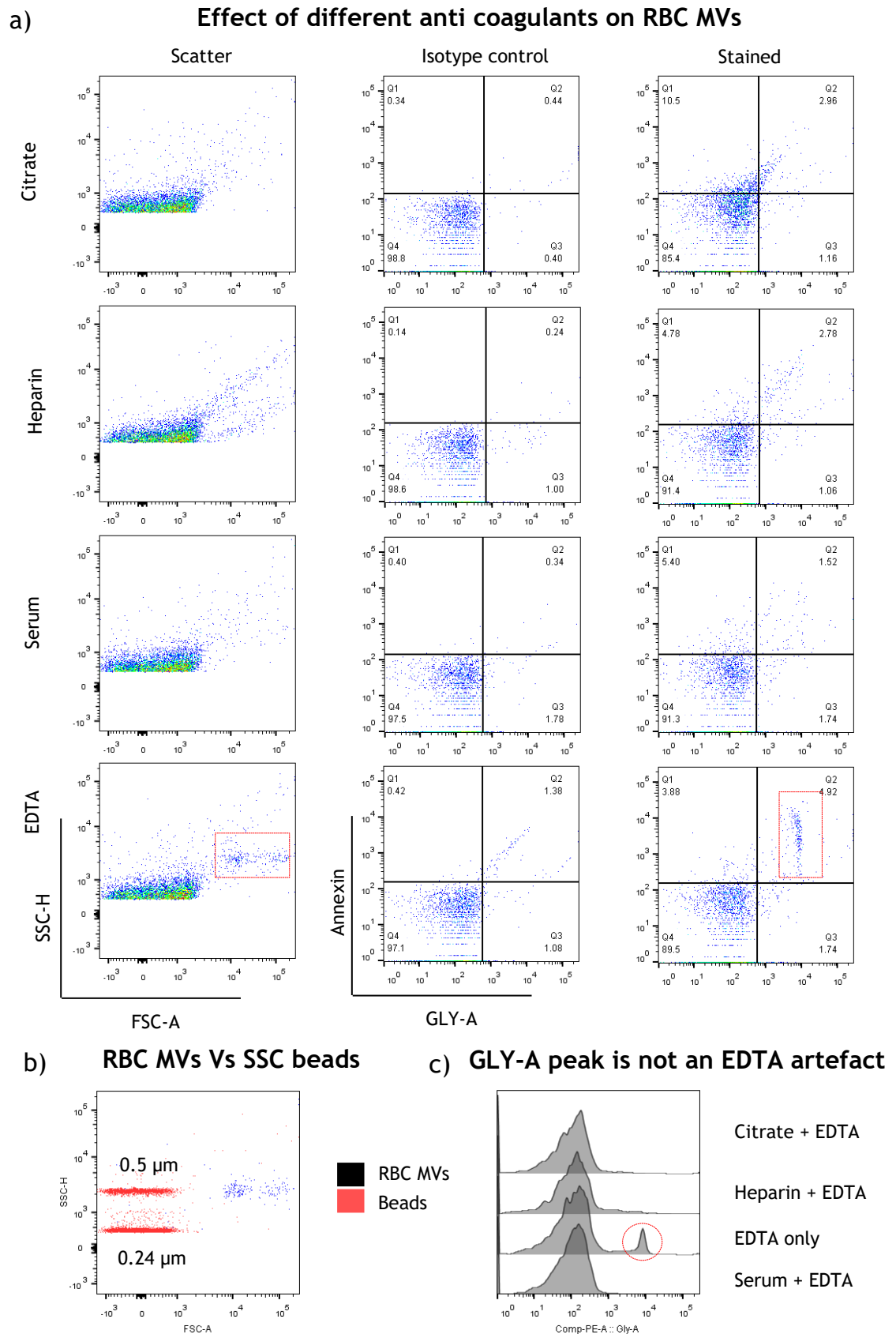
Figure 34: Use of EDTA as an anticoagulant when collecting blood results in a distinct population of small GLY-A positive particles.

a) 5 mL venous blood was collected from the same volunteer in K_3EDTA, 0.105 M sodium citrate, sodium heparin or clot activation BD vacutainers, MV-containing plasma was isolated, stained for CD41a and Gly-A then analysed *via* FACs; b) Using the same voltages as (a) scatter profiles of MegaMix™ beads and RBC-MVs are overlain using FlowJo® to estimate size; c) EDTA was spiked into 1 mL of blood collected in citrate or heparin vacutainers or non-treated blood (phlebotomy performed using a 21-gauge needle and syringe), incubated for 5 minutes at room temperature, and

then MVs were isolated and analysed as per (a). Note, final concentration of spiked EDTA was 10 mM.

Before noRBC-MVs can be evaluated by western blot or qPCR for the presence of e-miRNA, they must first be separated from EXs, or, plasma borne miRNA. As exosomes (50 – 100 nm) are smaller than MVs (100 – 1000 nm) differential centrifugation is widely used to separate one from the other[435]. However, it became apparent when using this approach, that unlike aRBC-MVs, putative noRBC-MVs are highly resistant to centrifugation and remain in plasma, even after being centrifuged at 21,000 x G for 30 minutes (Figure 6a). Some noRBC-MVs are observed in the pellet (5.8 % of total events), but more than double (14.4 %) remain in suspension (Figure **35a** – highlighted). However, as there were no platelet-MVs (CD41a+) in the plasma post centrifugation, it was considered possible to separate noRBC-MVs from exosomes based on size exclusion. To achieve this, plasma from EDTA blood was spun through a 0.45 µm spin column, then analysed by FACs. Figure **35b** demonstrates that the noRBC-MVs are not only retained in the spin column, but are enriched ~20 fold from that observed in plasma. In addition, the process appears efficient, as no noRBC-MVs are present in the flow through.
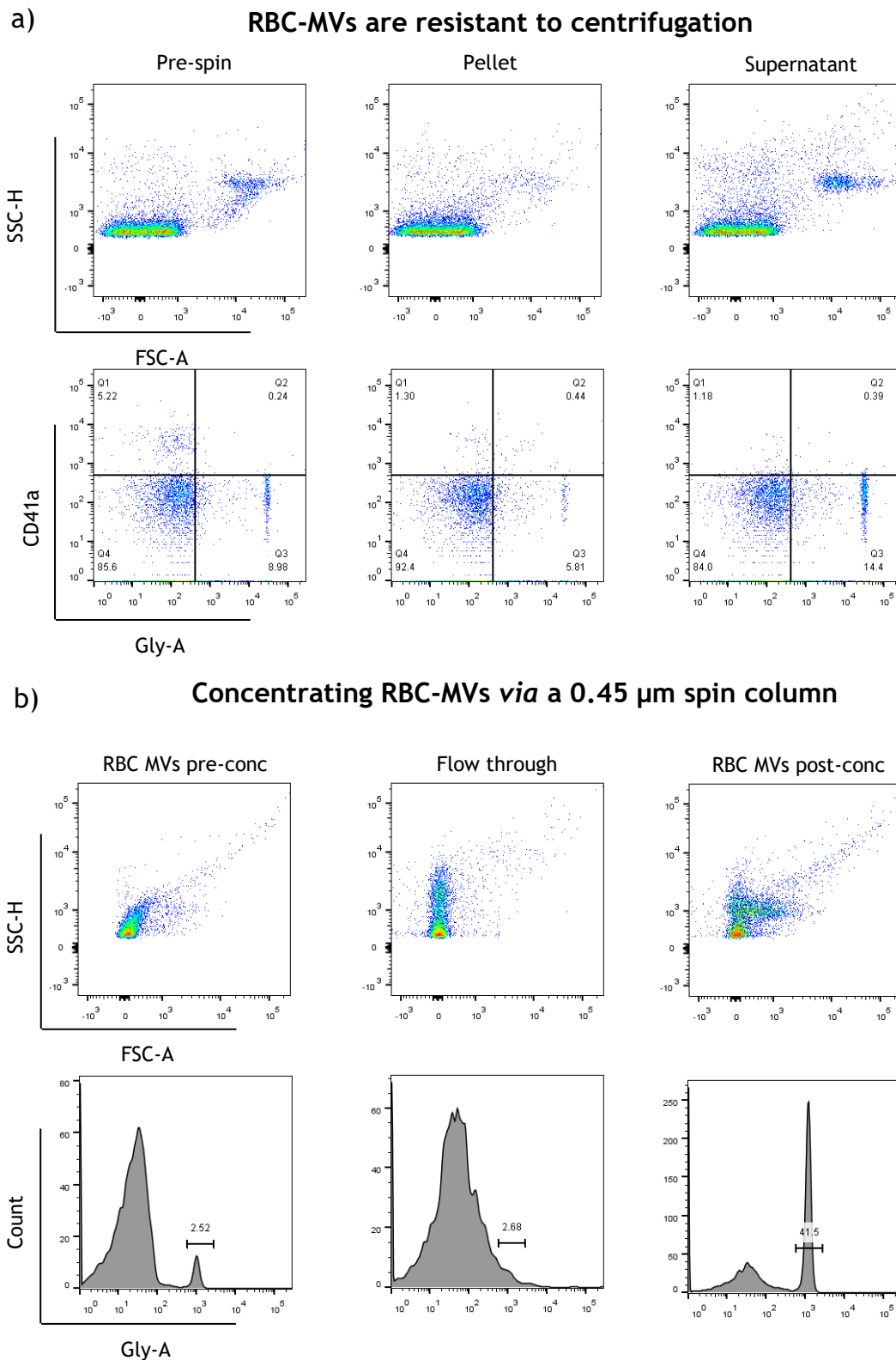
Figure 35: *Ex vivo* RBC-MVs are resistant to centrifugation and can be collected in a 0.45 µm spin column.
a) 500 µL EDTA plasma was centrifuged for 30 minutes at 21,000 x G, supernatant, pellet and plasma pre-centrifugation was stained with CD41a, GLY-A and analysed *via* FACs; b) 500 µL of EDTA-plasma, prepared as per Section **2.8.2**, was spun through a 0.45 µm cellulose acetate spin column (Costar®), reconstituted in 100 µL of HBSS, stained for GLY-A then analysed *via* FACs – an equal volume of column flow through was analysed with samples pre- and post-enrichment.

At this stage, a method of enriching putative noRBC-MVs appeared to have been generated. Part of the process used to verify the presence of aRBC-MVs was

TEM, therefore, noRBC-MVs were isolated as per Figure **35b** and sent for TEM analysis. While waiting for the results of the TEM analysis, additional work was undertaken. Although noRBC-MVs can be concentrated *via* a spin column, the number of events recorded by FACs was low. While AGO2 can be seen by western blot in aRBC-MVs, the bands observed are weak and require a 20 μg of protein (Figure **32c**). Due to this poor sensitivity, functional assays were investigated instead.

With the aim of visualising noRBC-MV phagocytosis in real-time, MVs were labelled with CFSE (Figure **36a**); note the FACs data shows a single population of CFSE positive events that co-stain with GLY-A, verifying erythrocyte origin. These putative noRBC-MVs were then co-cultured with macrophages for 24 hours. Next day, analysis using live fluorescent microscopy unexpectedly revealed the presence of ~4.5 μm CFSE +ve particles in each well. Analysis of the original noRBC-MV sample used to inoculate these macrophages revealed the presence of similar sized fluorescent particles, indicating they were present when originally added to the macrophages (Appendix **17**). The presence of these particles was unexpected as all MV preparations were visually observed by light microscopy to ensure there were no contaminating cells or debris. These particles have now been observed multiple times, and in order to illustrate the point made above, a specific experiment was performed. Isolated RBCs or noRBC-MVs were probed with GLY-A-PE, or stained with CFSE respectively; this separately labelled both population red or green. Both populations were spiked together in approximate 1:1 ratios, then observed by fluorescent and white light microscopy (Figure **36b**). Using this approach, both populations were visible by fluorescence, but only the RBCs were visible by white light. Note that the debris visible in Figure **36b** was kept, as this acted as a means to immobilise noRBC-MVs. This was important, as unlike RBCs, noRBC-MVs do not sediment, making visualisation challenging. Although these CFSE particles are not visible by white light, there still may be two populations present: a noRBC-MV population that was observed by FACs, in addition to a larger population observed by fluorescent microscopy.

To evaluate if two GLY-A+ populations exist, the original MV prep was re-analysed by FACs. To ensure a second, larger population wasn't missed by previous FACs analysis, the sample was re-analysed using the original, MV optimised

settings, along with those specific for erythrocytes. Analysis of RBCs using voltages optimised for erythrocyte analysis resulted in an expected scatter profile (Figure **36c-i**); this profile is the same as observed in Chapter 4 when analysing density gradients. However, analysis of the noRBC-MV preparation co-cultured with macrophages reveals no large population present (Figure **36c-ii**). The only events observed are particles too small for analysis at these voltages (Figure **36c** – red circle). To date, all size estimations have been made in comparison to MegaMix beads, while accurate for aRBC-MVs (Figure **31**), the same might not be true for noRBC-MVs. Therefore, voltages were changed so that whole erythrocytes, platelets and noRBC-MVs could be analysed in the same window. Purified RBCs and platelets were probed for GLY-A (erythrocytes) or CD41a (platelets), positive events gated *via* histogram and the scatter profiles for each overlain using FlowJo to estimate size (Figure **36d**). This allows the comparison of putative noRBC-MVs to whole cells, including their cell of origin. Comparison reveals, as expected, whole erythrocytes are larger than platelets, while the noRBC-MVs are smaller than both, which is in concordance with the size estimate when compared to MegaMix beads (Figure **34b**).

Why a second, larger population, is visible by fluorescent microscopy is unclear. This is not explained with the TEM analysis, as the results failed to detect either noRBC-MVs or large particles (Figure **36e**). Instead, a high amount of filamentous and clumped material was observed. Circular shapes were observed, but these were not like the aRBC-MVs observed in Figure **31c-ii**. It is unclear what these images represent, but they do not appear to represent MV profiles.

a) **CFSE labelled MVs**

b) **Microscopy of labelled RBCs spiked with labelled noMVs**

Red channel (RBCs) Green channel (MVs)

White light Merge

Debris

c) **Analysis of MVs using RBC settings**

RBCs MVs

d) **Size comparison of MVs**

RBC MVs

Platelets (1-3 µm)

RBCs (6-8 µm)

e) **TEM of *ex vivo* RBC MVs**

0.5 µm 1 µm
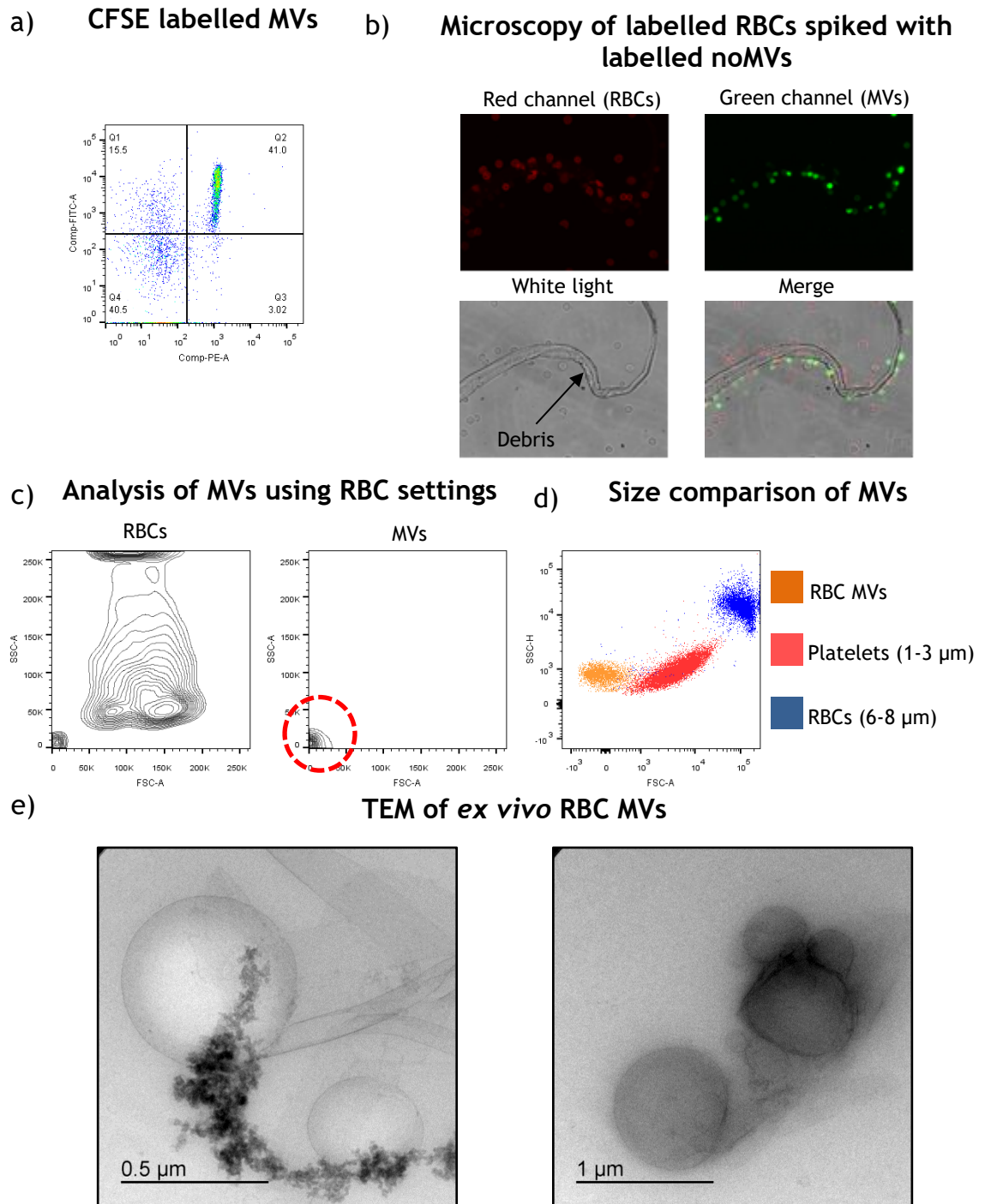
Figure 36: *Ex vivo* RBC-MVs are larger than they appear when analysed *via* FACs.
a) *Ex vivo* RBC-MVs were stained with 5 µM CFSE for 30 minutes, co-stained for GLY-A and analysed *via* FACs; b) Isolated RBCs and noRBC-MVs were stained with GLY-A-PE (red) or CFSE (green), mixed together in equimolar concentrations and visualised *via* fluorescent and white light microscopy; c) Using voltages suitable for whole cell analysis, RBCs and *ex vivo* RBC-MVs were analysed *via* FACs; d) Using the same voltages, RBC-MVs, RBCs and platelets were gated *via* histogram using GLY-A or CD41a positivity and overlain using FlowJo®; e) TEM analysis of RBC-MVs as analysed in panels a-d. Note, all TEM images were captures using an FEI Tecnai T20 by Mrs Margaret Mullin (University of Glasgow). Arrow in b) highlights debris.

In case an artefact had been introduced via the handling described in Figure **35b**, a different methodology of noRBC-MV isolation was employed – FACS. NoRBC-MVs were sorted based on GLY-A positivity using an Aria cell sorter (BD), resulting in a highly concentrated and pure population of noRBC-MVs (Figure **37a**). Isolated

noRBC-MVs were compared to MegaMix beads, demonstrating the sorted population was approximately 0.5 μm in size (Figure **37b**). However, analysis of this sorted population by fluorescent microscopy again revealed particles that were much larger than indicated by FACs (Figure **37c**). In addition, TEM analysis of this sorted population failed to verify the presence of noRBC-MVs (Figure **37d**). These results are discussed in depth below.
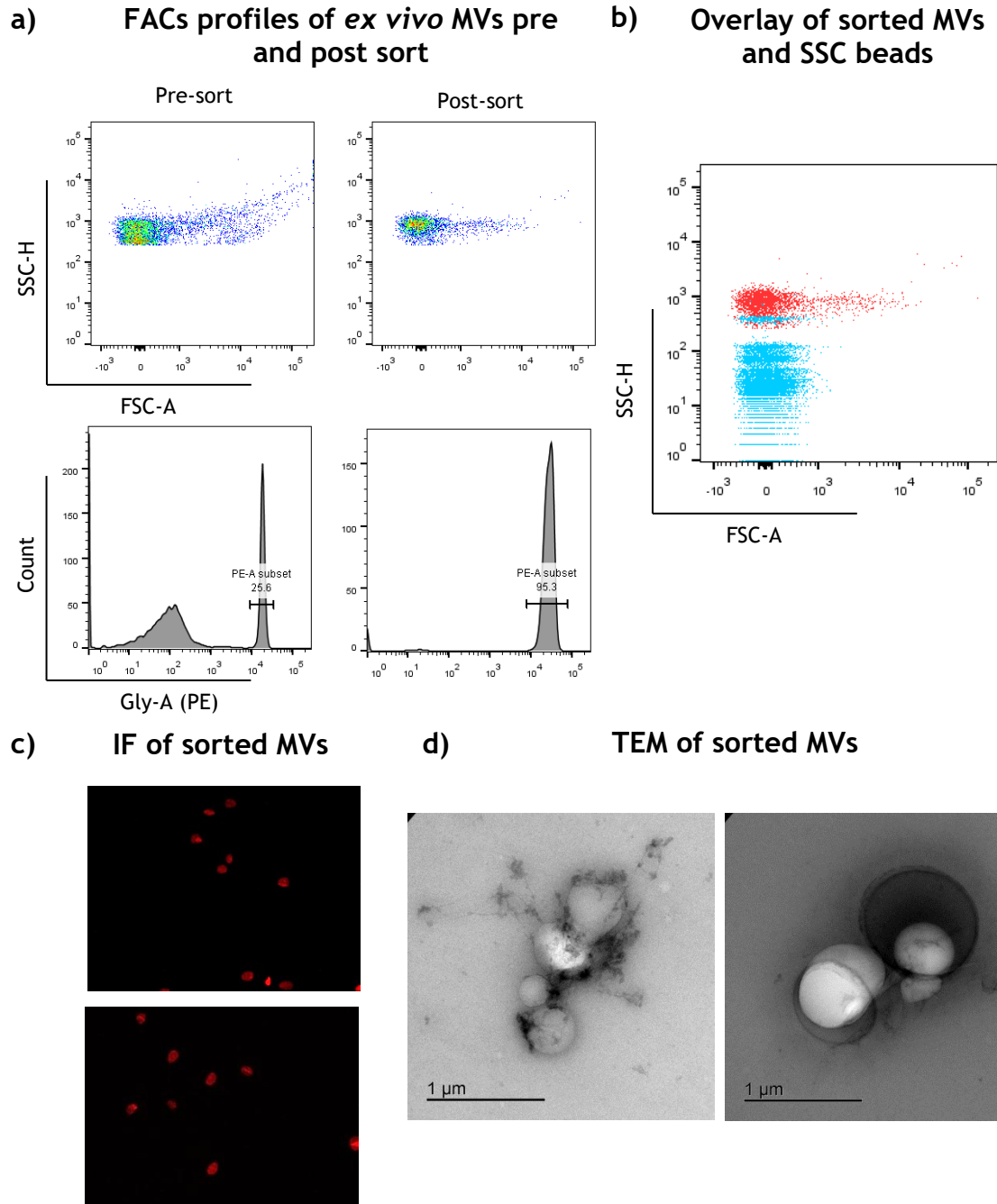
Figure 37: *Ex vivo* RBC-MVs are not MVs but instead damaged membrane.
a) EDTA plasma was stained for GLY-A, and RBC-MVs sorted using a BD FACs Aria III by Miss Jennifer Cassells; scatter profiles and Gly-A histograms of samples pre and post sorting are shown; b) Using the same voltages, profiles for sorted RBC-MVs and MegaMix beads are generated and overlain using FlowJo®; c) GLY-A+ events sorted from (b) visualised via fluorescent microscope; d) TEM analysis of GLY-A+ events from (b). Note, all TEM images were captured using an FEI Tecnai T20 by Mrs Margaret Mullin (University of Glasgow).

5.3 **Discussion**

The aim of this chapter was to evaluate if the vesicles produced during erythrocyte senescence contain e-miRNA – allowing us to test the hypothesis that vesicularisation is the method by which erythrocytes lose AGO2 as they age, Chapter 4 (Figure **28**). If proven correct, it would raise the possibility that RBC-MVs could act as vectors, and transfer e-miRNA between different cells; allowing us to test a central hypothesis of this study:

e-miRNA lie dormant within red cells, but regain their functionality as translational regulators when they are removed from circulation by splenic macrophages.

5.3.1 **aRBC-MVs**

As EVs are challenging to work with due to their small size and no established EV protocols exist at the Paul O'Gorman Leukaemia Research Centre, initial work was carried out using induced RBC-MVs. This allowed EV protocols to be developed and, as a proof-of-concept, establish if RBC-MVs can contain e-miRNA. Widely published protocols for MV induction were used and resulted in a population of vesicles that bore all the hallmarks of aRBC-MVs – sub-micron size (Figure **31b**, Figure **31c**) and exposed PS (Figure **30c**). Analysis by western blot demonstrated the presence of red cell markers (BAND3, GLY-A), while AGO2 was also found (Figure **32c**). The presence of e-miRNA was confirmed for three individual miRNAs (miR92a, miR451, miR486) by qPCR (Figure **33b**), proving the concept that RBC-MVs can contain miRNA. The next stage was to establish if the findings of this artificial system are relevant to what occurs *in vivo*.

5.3.2 **NoRBC-MVs**

As per the guidance published by Hochberg *et al.*, different methods of collecting blood were evaluated and revealed EDTA to be the optimal anti-coagulant for the study of noRBC-MVs (Figure **34a**)[433]. This conclusion was drawn as it was the only methodology that revealed particles that were not only of GLY-A/Annexin positive, but also appeared as a distinct and tight population when analysed by FACs. Indeed, comparison of the data generated in Figure **34a** is

consistent with multiple studies also evaluating noRBC-MVs, suggesting that what we were looking at was genuine[358,431].

Discrepancies, between this study and the literature, became apparent when methods for isolating noRBC-MVs from plasma were being optimised. This optimisation resulted in the finding that the majority of noRBC-MVs remained in suspension, despite extended centrifugation at high G-forces (Figure **35a**). This was incongruous for two reasons: (1) aRBC-MVs, which are at least half the size of noRBC-MVs, are readily pelleted at these forces (Figure **31**); (2) there is no mention of this within the literature. A potential explanation for the latter is that, in all the studies evaluating isolated noRBC-MVs, none look at the efficiency of the isolation i.e. no study evaluated the plasma pre- and post-centrifugation. It was only by performing this analysis in Figure **35a** that it became apparent that noRBC-MVs are centrifugation-resistant, and the majority remain in suspension. Note that although a small amount of noRBC-MVs were present in the pellet, increased centrifugation times, or re-spinning depleted plasma did not remove the centrifugation-resistant population. The degree of centrifugal resistance was not established, for example, ultracentrifugation at higher speeds may pellet the population of noRBC-MVs. However, the purpose of this experiment was to establish a technique which only purifies noRBC-MVs and ultracentrifugation would also isolate EX, therefore it was not pursued.

The main discrepancy came with the revelation that putative noRBC-MVs were much larger than they appeared by FACs (Figure **36a/b**). This observation was not an artefact of isolation as "noRBC-MVs" were prepared by two different methods which yielded the same phenomenon (Figure **37c/d**). Indeed, the sorting experiment confirms the small "noRBC-MVs" observed by FACs are one and the same as the large particles observed *via* fluorescent microscopy. To date, this observation has not been reported by any study; what they are, the cause of the size discrepancy and its relevance to the literature is discussed below.

5.3.2.1 **What are these particles?**

Although it is not known definitively what these particles are, it is not thought that they are experimental artefacts. For example, it is not possible for this to be an artefact induced by FACs, as analysis of unsorted stocks, or samples

not analysed by FACs, show the same large particles to be present. It is unlikely that these large particles are MV aggregates, as if so, they would be visible by FACs (Figure **36c**) and TEM (Figure **36e** and **37d**), which they are not. Furthermore, if aggregates, one would expect particles to exhibit heterogeneity in size, morphology and complexity. However, the images in Figures **36e** and **37d** do not display this and instead show these particles to be relatively homogenous in size, regular in shape (circular), smooth (not complex) and singular (not discontinuous or "grape" like). Although conjecture, at present, there appears only one explanation that accounts for what is being observed: these large particles are erythrocyte ghosts, or, damaged erythrocyte membranes. Ghosts are RBCs that have undergone lysis but have reformed, retaining some of the original morphology of erythrocytes[436,437]. They are so called due to their ethereal (ghost-like) nature when visualised i.e. translucent, not red. Indeed, evaluation of multiple papers demonstrates, that while visible, RBC ghosts are not easy to detect by white light and are usually highlighted in various publications, or have been visualised using special conditions. This is similar with Figure **36b** where the large particles observed in this study are not readily detectable *via* white light but only following fluorescent staining.

5.3.2.2 Why is there a discrepancy between methods?

If these particles are ghosts, or ghost-like particles, this would explain the morphology observed in Figure **36b** and the GLY-A positivity in Figure **36a**. It was observed in Chapter 4 that PFA fixation causes erythrocytes to lyse, if a ghost, they may also have a sensitivity to PFA fixation, which may be a reason the TEM images in Figure **36e** are so "messy" and do not detect them. Part of an erythrocyte's characteristics is its ability to deform in order to "squeeze" through small capillaries. For example, Branemark *et al*. demonstrated that RBCs (measured at 7 μm) were able deform in order to fit through a capillary with a diameter of 4 μm[438]. This deformability is a potential explanation for the discrepancy observed between the fluorescence microscopy and the FACs. When observed by microscopy there is no force exerted on these particles, so they adopt their natural "relaxed" conformation. When analysed by FACs they are under flow conditions, where a force is being exerted this may cause them to deform and contract.

This is not an unreasonable suggestion as intact erythrocytes have been shown to dramatically change morphology depending on the conditions they are in. For example, by changing the shear force, Schonbein *et al.* demonstrated that erythrocytes could adopt multiple different morphologies, specifically, elongation as they "tank treaded"[439,440]. This and other morphological changes have been observed in multiple studies, and the effect cell deformation has on scatter detection by FACs is unclear. Work was performed to establish if flow rates could affect the "size" of these particles by changing the flow rate of the cytometer (data not shown). Although the particles did not appear to change in size, the experiment was crude. For example, it is only possible to change the flow rate between low, medium and high, which corresponds to a flow rate range of 10 – 120 µL / min. The forces exerted at these rates are not stated and low flow may already be causing these particles to deform/contract. Indeed, as referenced above, RBC deformation/contraction has been observed both *in vivo* and *in vitro* under flow conditions, that ghosts are more susceptible to external forces than intact RBCs is not unreasonable. Although this idea has not been proven, this observation by itself raises multiple questions:

5.3.2.3 Why has this not been seen before?

There are currently 21 studies evaluating noRBC-MVs - why has this phenomenon not been reported before? The most likely reason for this is that the scope of most studies is one of characterisation. This study was to evaluate function, which is why these noRBC-MVs were CFSE labelled and this size discrepancy identified. Most studies rely on FACs to characterise their noRBC-MVs and there is no reason for them to perform fluorescent microscopy – meaning this observation has simply been missed. Indeed, on the face of it, when it comes to the distribution and FACs profiles, these studies largely agree with each other and the data in Figure **34a/36c**[360,441-443]. This means it is easy to draw parity to other studies and overlook any discrepancies. In addition, a lot of studies, especially earlier ones, are missing critical controls. For example, the FACs study by Larson *et al.* omitted their gating strategies, while the study by Sewify *et al.*, despite being based on FACs, showed no gating strategies, dot plots or histograms, just tabulated counts[444,445]. In addition, the vast majority of noRBC-MVs studies do not use a non-FACs based technique to verify the population of interest are indeed MV[446]. This is surprising as TEM is the gold standard in EV research and is routinely

used to verify EV presence. One of the few studies to perform TEM on noRBC-MVs was performed by Willekens *et al.* however, as they pelleted whole plasma, which does not discriminate from other MVs present, the verification is of limited use[357].

5.3.2.4 **Is this discrepancy genuine and is it relevant?**

Although the combined evidence in this chapter indicates that this observed discrepancy is genuine, it has not definitively been proven that the small particles observed by FACs are the same as the large ones observed by microscopy. However, due to the relevance of this observation to so many studies, it warrants further investigation. The idea that the shear force exerted on these particles during FACs causes deformability is plausible, but untestable. A collaboration with Prof Thomas Franke from the School of Engineering (University of Glasgow) has been established, but work has not been completed. The Franke group combines microfluidics and microscopy to observe the deformation of erythrocytes under different flow conditions. Applying their technology with the question at hand would allow a subtler manipulation of flow parameters than afforded by the Canto II and discussed above. If the hypothesis is correct, then it should be possible to detect any particle deformation in real-time simply by changing the flow rate. Unfortunately, erythrocyte deformation is observed by microscopy, which is not compatible with these particles due to difficulty in observing them by this method (Figure **36b**). At present the microscope in this Franke laboratory is not fluorescent, but is in the process of being upgraded/replaced, meaning that this is a viable option to pursue with future experiments.

For absolute clarity, it is not the position of this author that all functional "noRBC-MV" studies are erroneous. For example, "noRBC-MVs" are generally associated with pro-coagulation properties[374,426]. This may well be accurate, as the artificial particles prepared by Ahn *et al.*, which are more similar in size to the "noRBC-MVs" observed above (range of 50 nm – 3000 nm), do positively affect coagulation[428]. These ghost-like particles may well be relevant in different conditions as suggested by multiple studies. However, as this study was to evaluate noRBC-MVs, and ultimately compare their properties to aRBC-MVs, then this phenomena is not applicable to this study.

5.3.2.5 **What does it mean for this project**

As it was not possible to purify noRBC-MVs, they were no longer pursued. Instead, as aRBC-MVs have been verified (Figure **30 & 31**) and shown to contain miRNA (Figure **32 & 33**) they were used as an alternative source. In the context of the original question, ionophore induced MVs were termed artificial, however, these MVs have been shown to be almost identical to the MVs produced when blood units are stored by the transfusion service[447], making them an ideal source for the rest of this study. Although an artefact caused by prolonged storage, they are genuine and there is a clinical interest in the reports that link aged blood products to side effects post RBC transfusion. Therefore, using an aRBC-MV model not only allows the transfer of e-miRNA to be established as a proof-of-concept, it also allows a clinical angle to be pursued. The next stage of this investigation was to establish an aRBC-MV endo-phagocytosis model to pursue this aim, which is detailed in Chapter **4.**

Chapter 6 **Generation of an RBC-MV endo-phagocytic model**

6.1 **Introduction**

The main purpose of this project was to explore the possibility that erythrocytic microRNA (e-miRNA) had a novel function within mature erythrocytes. To evaluate this, work in Chapter 3 attempted to establish what AGO2 interacts with in RBCs. However, candidate interactors suggested by previous proteomics (BAND3, FIB) could not be verified, while AGO2 pull-downs performed by this student identified only a higher molecular weight AGO2, not any interacting proteins. Through the use of density gradients in Chapter 4, it was demonstrated that AGO2 was lost as erythrocytes age. As e-miRNA are membrane-associated, and RBCs are postulated to lose membrane *via* vesicularisation during aging, it was hypothesised that e-miRNA loss coincided with vesicularisation. Although e-miRNA were detected in induced MVs, proving the concept, noRBC-MVs could not be detected in plasma, precluding our ability to verify our initial hypothesis (Chapter **3**). As it is possible to use the clinically relevant aRBC-MVs as a proof-of-concept for e-miRNA transfer, it was decided to pursue both the e-miRNA and a clinical angle at the same time. The clinical relevance of aRBC-MVs is as follows:

The transfusion of RBCs within hospitals is common with approximately 6000 units required daily in England alone[336]. However, during storage, erythrocytes undergo a variety of morphological and biochemical changes. Biochemically, glycolytic components 2,3-DPG and ATP decrease over time, while the pH falls due to increased levels of lactic acid[344,345]. During these biochemical changes, erythrocytes change from classical biconcave discoids to echinocytes and finally spherocytes. Echinocytes feature multiple membranous arms called spicules from which MVs are released into the storage medium[347]. These MVs are transfused along with the blood unit and are reported to increase in number the longer a unit is stored[448].

Complications relating to the age of transfused RBC units, or the breakdown products they contain, have been hotly debated within the literature for decades. Some studies indicate these factors have no deleterious effects on patients, while

others correlate it to increased morbidity and mortality[369,370]. The most recent meta-analysis used a Grading of Recommendations, Assessment, Development and Evaluations (GRADE) approach to score multiple different studies based on the validity and strength of the data[449]. They report, with moderate degrees of certainty, that transfusion of aged cells is not linked to mortality[450]. However, they were less confident with the link between transfusion and nosocomial infection or adverse events e.g. acute transfusion reactions, seizures, renal or urinary events. While they report that aged cells do not cause adverse events, this is reported with only low degrees of certainty. Furthermore, a limitation/concern the authors raised in this study, is that it does not address the number of transfusions received. This is especially important as multiple studies, even those that report no side effect regarding the transfusion of aged cells, suggest a dose effect may exist[370].

A confounding factor for all meta-analyses are the multiple different variables that exist between studies, e.g. enrolment criteria (age, disease), blood processing (whole blood versus leuko-depleted), blood storage media (SAGM, MAP) etc. In addition, these clinical trials usually have particularly binary end points e.g. death. While undoubtedly important, this can make studies black and white, when transfusion effects may be more nuanced. On the other hand, using adverse events as end points i.e., increased hospital stay, inflammation, risk of nosocomial infection etc. is very broad, meaning any subtle side effect caused by transfusion may be lost.

A different, and less biased methodology, is to remove the pre-set end points and objectively observe what occurs upon transfusion. As it is known what occurs to RBCs during storage, it is possible to isolate a storage artefact of interest and evaluate how "x" cell/patient responds. MVs were chosen as they have been shown to accumulate during storage and in other models have been shown to cause or be associated with symptoms of disease/inflammation[421]; in addition, work detailed within Chapter 3 has already enabled us to fully characterise erythrocyte-derived MVs. As it has been reported that RBC-MVs localise within Kupffer cells following transfusion[392] – we asked the relatively simple and unbiased question: How do macrophages respond to RBC-MVs?

6.2 **Results**

To evaluate the response of macrophages to RBC-MVs, macrophages were first generated through the *in vitro* differentiation of CD14^{+} peripheral blood monocytes. As detailed in Figure **38a**, CD14^{+} monocytes from peripheral blood (small scale) or buffy coats purchased from the SNBTS (large scale) were isolated using magnetic microbeads (Miltenyi). With a media change at day 3 (D3) and D5, isolated monocytes were differentiated in the presence of recombinant human (rh)GM-CSF or, rhM-CSF for seven days to generate M0 macrophages; different cytokines were used at this stage as it was reported that differentiation with GM-CSF resulted in a stronger M1 phenotype, while M-CSF produced a stronger M2 phenotype[451]. M0 macrophages, generated with either GM-CSF-M0 (gM0) or M-CSF-M0 (mM0), were phenotyped *via* FACs for the presence of M1 (CD80, CD86) and M2 (CD206, CD163) markers to get a baseline reading (Figure **38b**). gM0 macrophages are chimeric and possess M1 and M2 markers, while mM0 markers appear more phenotypically distinct with most cells being dual positive for M2 markers with only a low expression of M1 markers.

a) Macrophage generation schematic

b) Representative macrophage phenotype at day 7
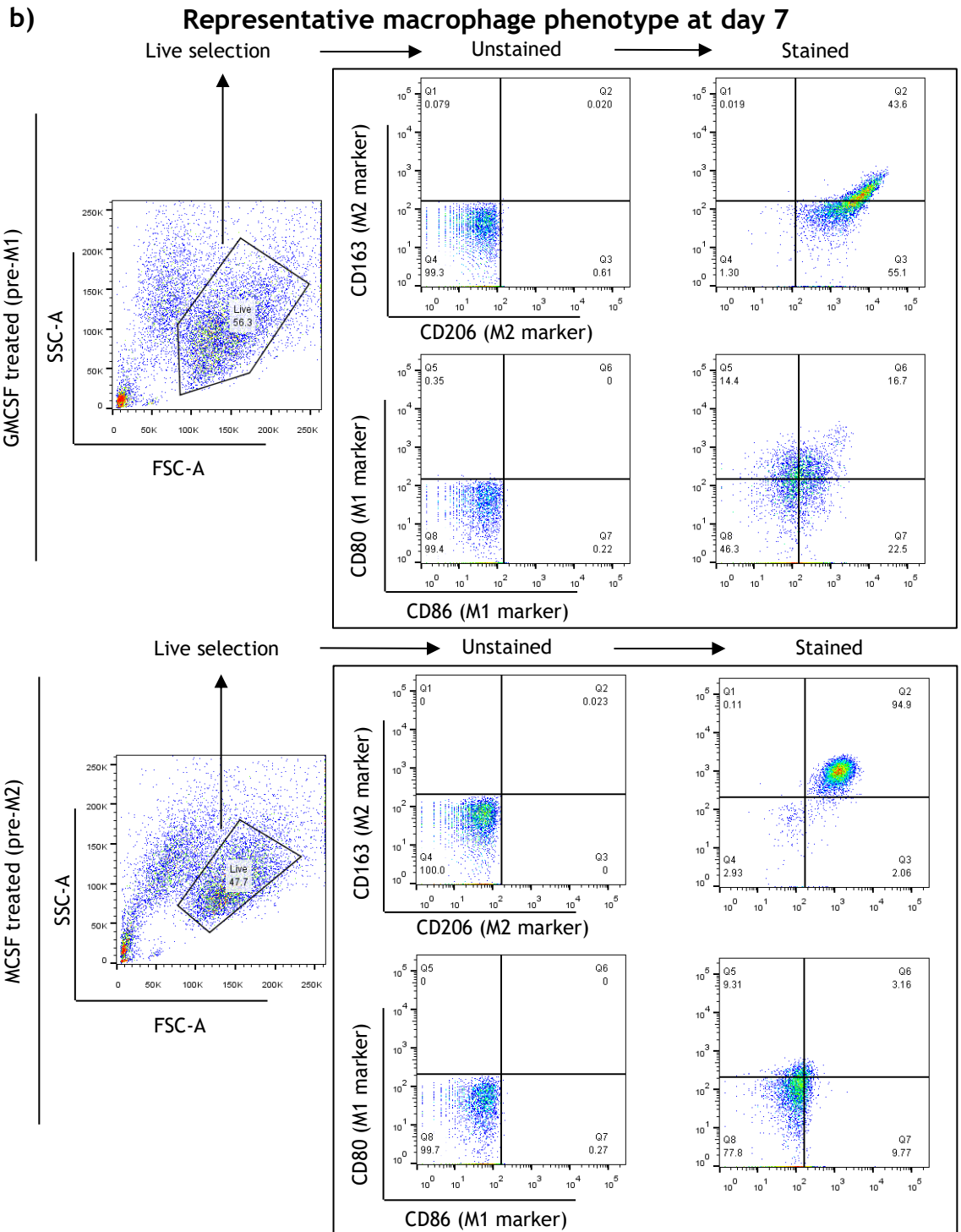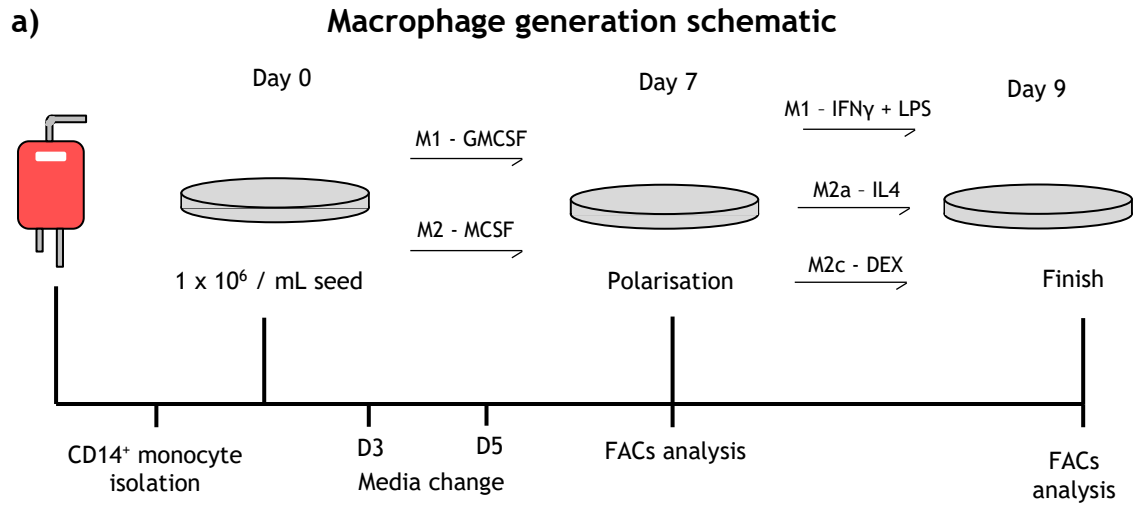
Figure 38: Generation of macrophages from isolated CD14⁺ monocytes.
a) Purified CD14⁺ monocytes are incubated with rhGM-CSF or rhM-CSF (100 ng/mL) for 7 days then polarised towards an M1, M2a or M2c phenotype for two days using IFN-γ (20 ng/mL) + LPS (50 ng/mL), IL-4 (20 ng/mL) or dexamethasone (2 x 10⁻⁷ M) respectively; b) Representative FACs results when phenotyping macrophages for M1 (CD80/CD86) or M2 (CD163/CD206) markers at D7.

Macrophages were polarised towards an M1 (inflammatory) or M2 (tissue repair) phenotype to mimic the transfusion of patients with, or without an underlying inflammatory condition i.e. graft versus host disease (GVHD) or surgery. These broad phenotypes were chosen because, as macrophage phenotype corresponds to function, it is possible that these two phenotypes may respond differently to RBC-MVs; as both are clinically relevant, both were evaluated. M1 macrophages were generated through polarisation of gM0 macrophages with IFN-γ and LPS to achieve macrophages with a pro-inflammatory phenotype. "Alternatively" activated macrophages (M2) were generated through the polarisation of mM0 macrophages with IL-4 or dexamethasone (DEX) to generate macrophages with a tissue repair phenotype. Following 2 days polarisation, macrophages were again phenotyped for M1 and M2 markers *via* FACs – representative FACs plots for macrophages polarised with IFN-γ + LPS, IL-4 or DEX are detailed in Figures **39a-c**. gM0 polarised macrophages have a strong M1 phenotype, with all cells dual positive for CD80 + CD86 (M1 markers), but only ~12 % dual positive for CD206 + CD163 (M2 markers). Interestingly, IL-4 polarised macrophages resulted in ~ 40 % macrophages being chimeric (dual positive for M1 and M2 markers), while DEX dampened this M1 response and maintained the M2 phenotype (Figure **39d**). As IFN-γ + LPS or DEX polarised macrophages appear to be phenotypically distinct, they were used in the following sections.

a) Representative phenotype of mature M1 macrophages
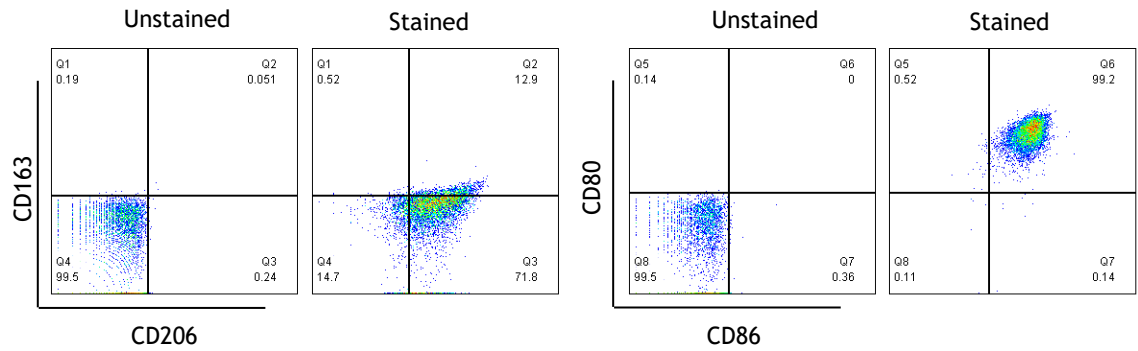
b) Representative phenotype of mature M2a macrophages (IL4)
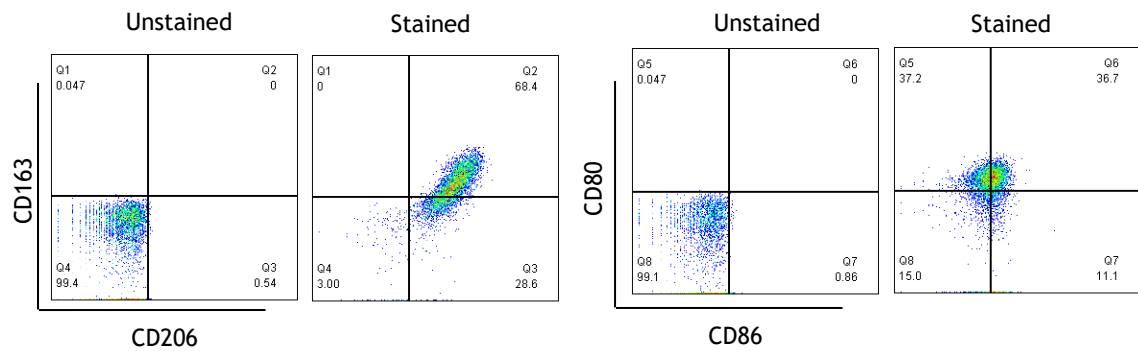
c) Representative phenotype of mature M2c macrophages (DEX)
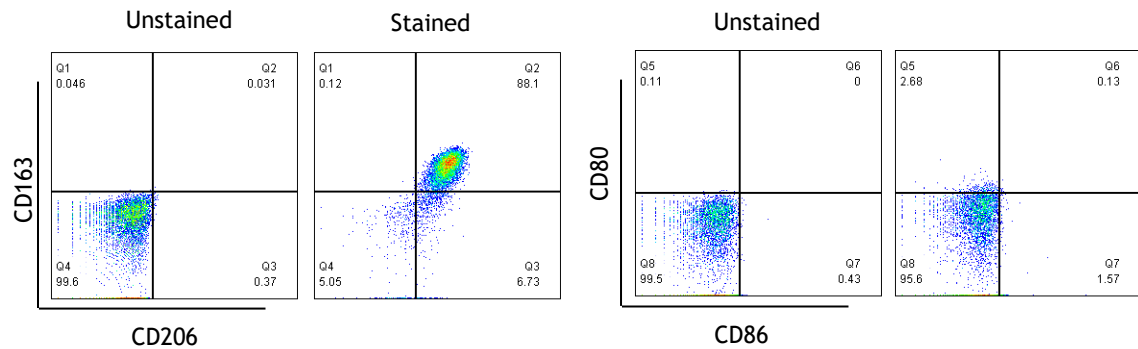
d) IL4 generates chimeric macrophages

Number of macrophages dual positive for M1 or M2 markers
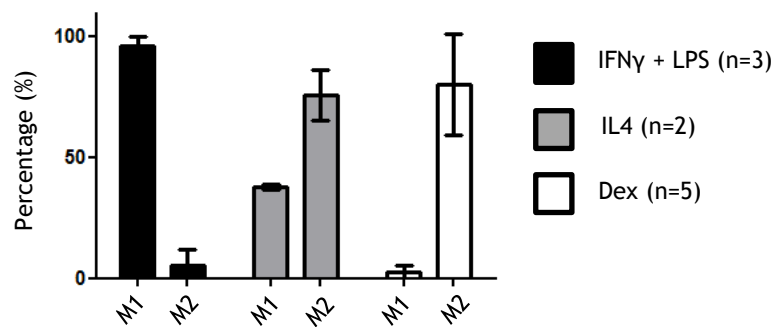
Figure 39: IL-4 treatment generates chimeric macrophages while DEX treatment stimulates a pure M2 phenotype.
a - c) Representative FACs results when phenotyping polarised macrophages (D9) for M1 or M2 markers; d) Average number of macrophages dual positive for M1 or M2 markers after 2 days polarisation (D9).

In addition to generating a strong M2 phenotype, DEX treatment has been reported to induce the expression of *HO1* and *FER* in monocytes. These two proteins are responsible for the breakdown of haem and export of recycled iron respectively; two essential components of erythrocyte turnover. Comparison of gene expression levels between mM0 and DEX treated macrophages revealed that *HO1* was not induced, while *FER* showed a ~ 150-fold increase (Figure **40b**); note, although DEX did not induce *HO1*, it was highly expressed (CT = 19). This data, coupled with Figure **39c**, demonstrates that not only does DEX polarisation result in a strong M2 phenotype, but this phenotype appears primed for erythrocyte turnover and matches the profile of hepatic/splenic macrophages[452]. A caveat of DEX treatment is its potential toxicity with one report indicating it being toxic to macrophages[453]. However, 48 Hr treatment of macrophages with DEX did not appear to cause cell death (Figure **40c**). This conclusion was drawn, as while there was a low amount of cell death (10 % ± 9 %; N=3), there was no shift in Annexin staining (3.83 % ± 0.5 %; N=3) which would be indicative of DEX inducing cell death. The profile displayed in Figure **40c** is binary, the cells are either dead (dual positive for DAPI and Annexin) or alive (negative for both).

Additionally, DEX treatment results in macrophages that are morphologically distinct from M1 macrophages (Figure **40d**). At D7 gM0 macrophages are amoeboid in shape while mM0 cells are more fibroblastic. Following polarisation, the morphology for both phenotypes changes, M1 cells become fibroblastic and M2 cells become amoeboid; this morphological distinction is consistent with what was observed by Porcheray *et al.*[454]. Having established the differentiation of monocytes to cells resembling features of Kupffer-like macrophages (klM) and macrophages (M1) bearing an inflammatory phenotype, the next step was to evaluate if they interacted with RBC-MVs.
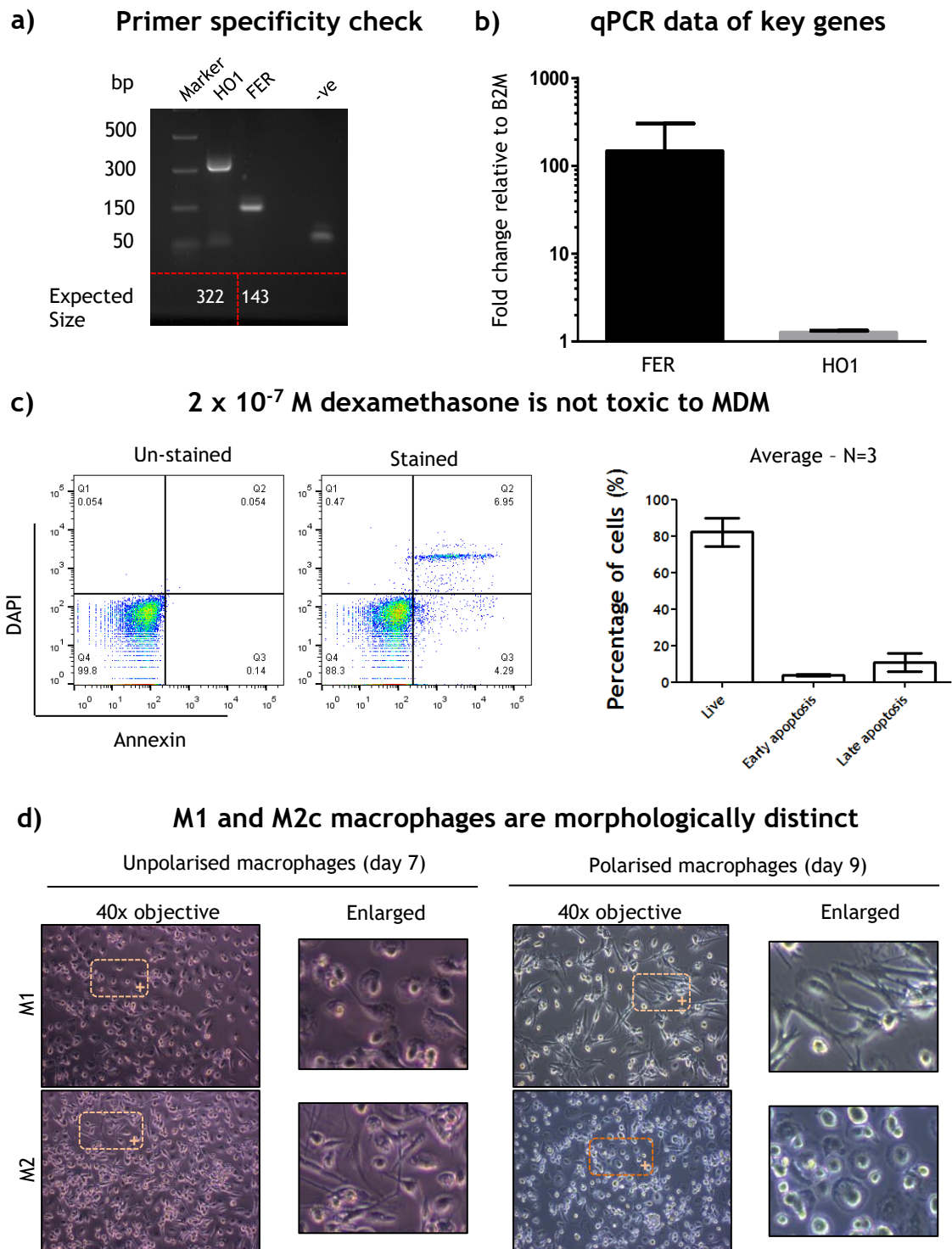
Figure 40: DEX polarisation generates macrophages that are Kupffer-like and does not cause cell death.

a) Agarose electrophoresis of PCR products generated using haem oxygenase-1 (*HO1*) and ferroportin (*FER*) primers reported by Vallelian. F *et al*[55] – BLAST predicted amplicon sizes are in white; b) Fold enrichment of *HO1* and *FER* of D9 macrophages (DEX polarised) versus unpolarised macrophages – expression normalised against *B2M* and fold change calculated using 2^-ΔΔCt (N=2); c) Apoptosis analysis of macrophages polarised with DEX (D9) using Annexin-V FITC and DAPI – average number of live (dual negative), early apoptotic (Annexin-V+) and apoptotic cells (DAPI+ and Annexin-V+) plotted on a bar graph; d) Representative white light images of live M1 and M2 macrophages at D7 and D9.

A common method of evaluating the interaction of EVs with "X" cell of interest is to stain EVs with a lipophilic dye e.g. PKH26[456]. However, labelling with this method was highly degrading to RBC-MVs, and thus not suitable for future applications (Appendix **16**). Therefore, a different method to determine RBC-MV macrophage interactions was employed: immunofluorescence for Hbb. Although this method is comparatively longer than using PKH26, it has two advantages over the previous technique: (1) Specificity; Hbb is not expressed in macrophages, meaning that any Hbb signal detected by IF could only come from internalised RBC-MVs. (2) A concern of lipophilic dyes such as PKH26 is that they may be released during phagic processing, where they may non-specifically stain a cellular organelle, resulting in false positives. An additional concern raised regarding the PKH26 method of labelling is that it introduces foreign matter into the vesicle of interest and there is no way of controlling how this affects vesicle recognition/internalisation/processing. As IF detects RBC-MVs post any RBC-MV macrophage interaction, this concern is eliminated.

To mimic blood being transfused into a patient with either underlying inflammation (GVHD), or those with no underlying inflammation (e.g. surgery patients), RBC-MVs were added to M1 and klM macrophages and allowed to interact overnight. The Hbb antibody (Santa Cruz) was first tested for non-specific staining and results indicate that it does not react with the no RBC-MV control, demonstrating its suitability to detect RBC-MVs (Figure **41a-i**). With the addition of RBC-MVs, M1 macrophages do not appear to interact with RBC-MVs (Figure **41a-iii**). mM0 macrophages appear to interact with RBC-MVs in a non-specific manner, as indicated in the diffuse appearance of Hbb within these cells (Figure **41a-ii**). This contrasts with the klM macrophages which contain a large amount of internalised Hbb that appears highly concentrated within a more defined area of the cytoplasm (Figure **41a-iv**). This is particularly interesting as the FACs profile of mM0 and klM macrophages are very similar – with high expression of CD163, CD206 and low expression of CD80, CD86 (Figure **38b** Vs Figure **39c**); why this may affect RBC-MV internalisation is unclear, but is discussed later.

a) M2 macrophages strongly internalise RBC-MVs

b) Enlarged images from (a)
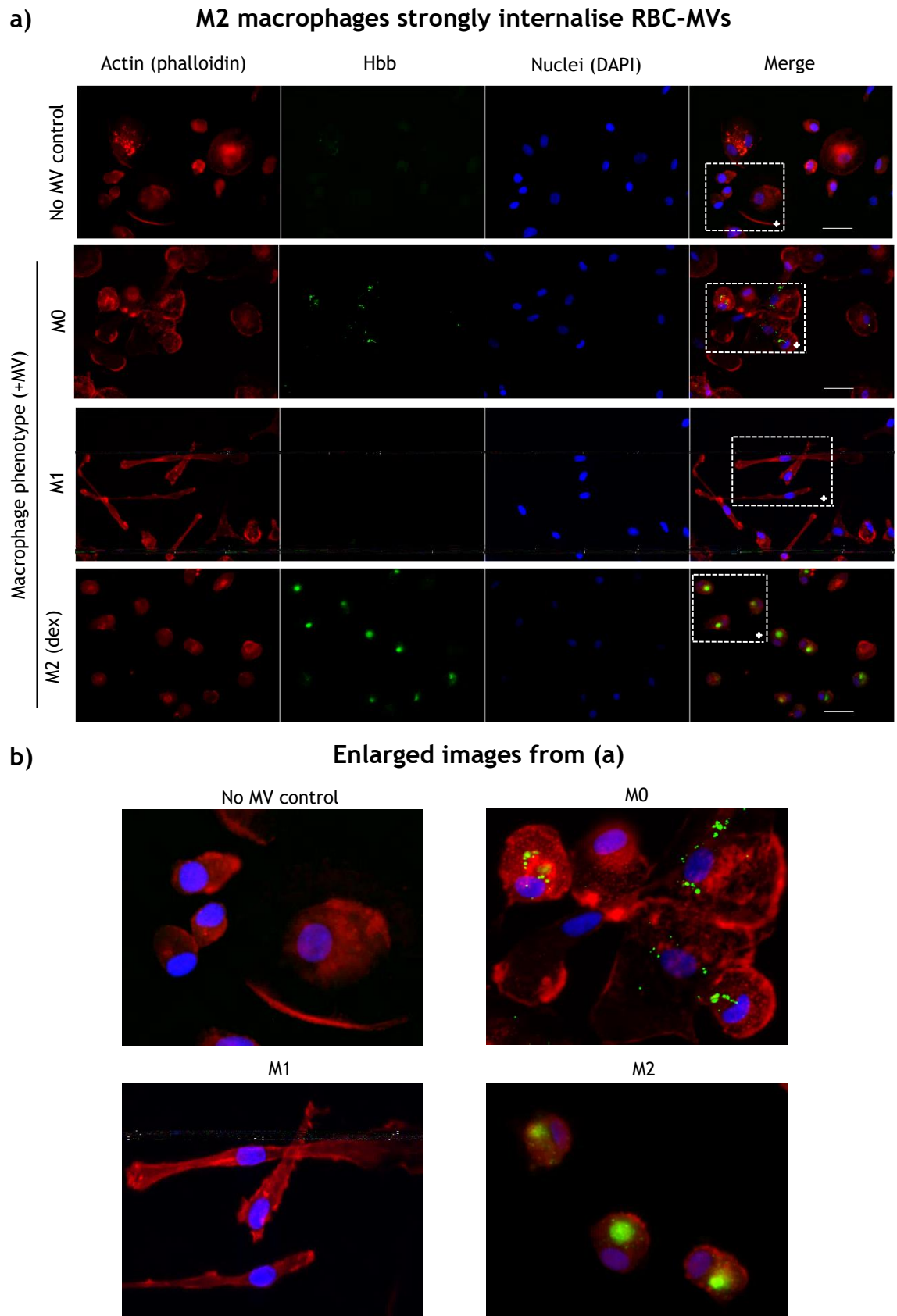
Figure 41: RBC-MVs are preferentially internalised by kIM.
a) M0, M1 or hl macrophages were incubated with 2.5 µg of RBC-MVs overnight, fixed and permed, then probed for actin (phalloidin) haemoglobin-β (α-Hbb) or DNA (DAPI) then visualised *via* epifluorescence; b) Sections highlighted in (a) were digitally enlarged to see the distribution of signal more clearly; Scale bar = 50 µm.

The inability of M1 macrophages to internalise RBC-MVs is not due to these cells being defective as they readily internalise fluorescently labelled *E. coli* BioParticles® (Invitrogen, Figure **42a**). Conversely, the presence of Hbb within klM is an active endo-phagocytic process and not RBC-MVs fusing with macrophages membranes. This can be concluded as the inhibition of actin-rearrangement with cytochalasin-D abrogates Hbb signal, meaning that RBC-MVs are actively taken up by the cell (Figure **42b**). Furthermore, the likelihood that the Hbb signal is an artefact and not from genuine RBC-MVs is low, as the Hbb signal co-localises with BAND3 – another RBC-MV marker that is not present within macrophages (Figure **42c**).
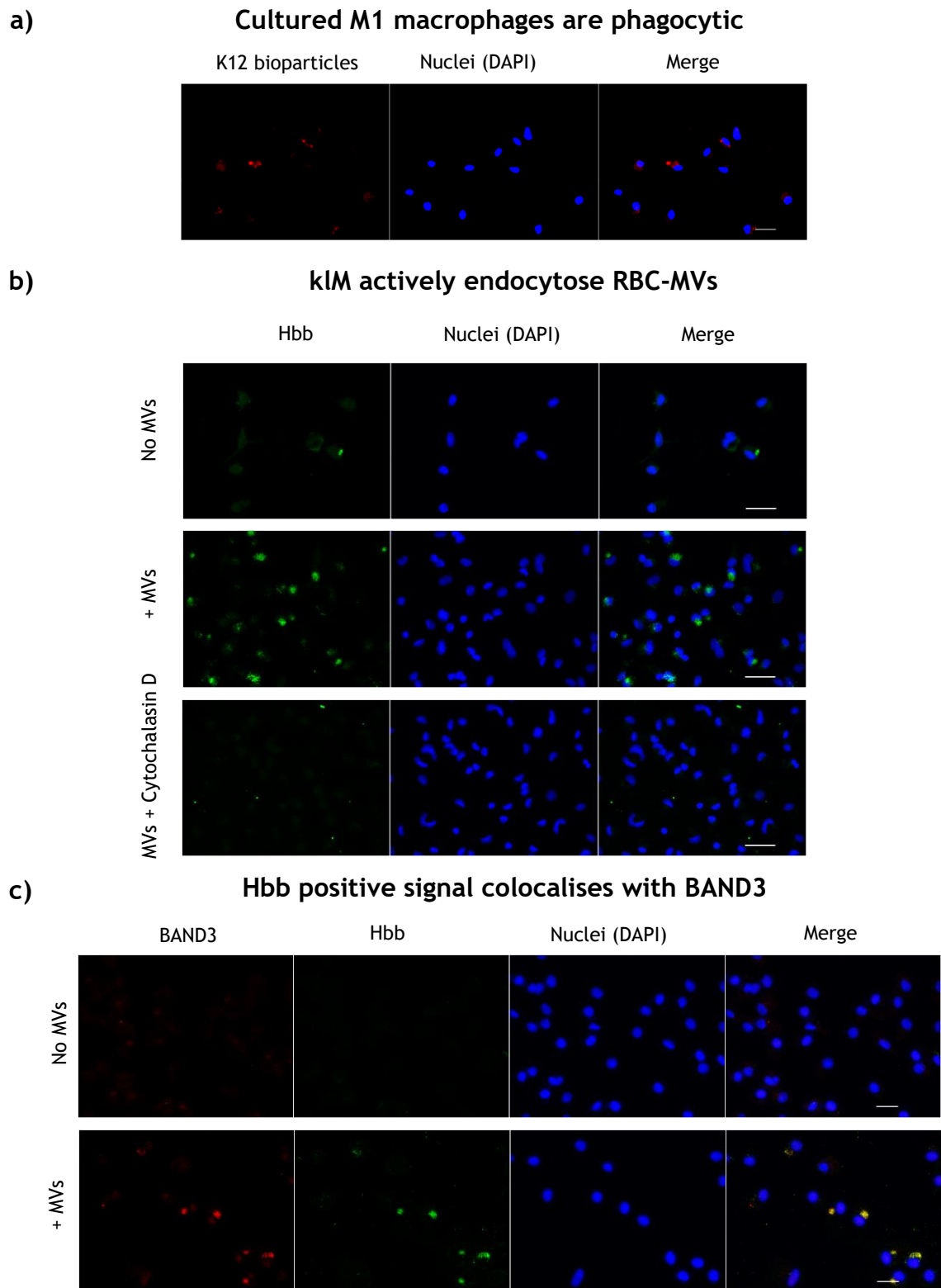
Figure 42: Failure of M1 macrophages to internalise RBC-MVs is not due to a functionality defect while kIM actively endocytose RBC-MVs.
a) M1 macrophages where incubated with 9 x 10⁶ K12 BioParticles overnight then visualised *via* epifluorescence; b) kIM were incubated with 2.5 μg of RBC-MVs overnight in the presence or absence of 0.2 μg / mL cytochalasin-D then probed with α-Hbb and visualised *via* epifluorescence; c) kIM were incubated with 2.5 μg of RBC-MVs overnight then probed with α-Hbb and α-BAND3 then visualised *via* epifluorescence. Scale bar = 20 μm.

While RBC-MVs can readily be detected within klM macrophages after an overnight incubation, this does not detail how quickly they are recognised and internalised. To establish the dynamics of this process, a time course was carried out where IF was performed on macrophages that had interacted with RBC-MVs for 0.5, 1, 2, 5, 6 and 24 Hrs (Figure **43**). To enable comparison, all images were taken at the same exposure as the overnight control – 2 seconds; in addition, the brightness and contrast settings between the images were kept the same. Furthermore, as all macrophages were grown on LabTek II 8-well chambered slides, imaging bias was avoided by imaging each condition *via* several fields of view in the same approximate well area – i.e. images taken randomly in the top left, top right corner, bottom left, bottom right corner and the well centre. Qualitatively, the signal distribution between 6 Hrs and overnight is similar: both show concentrated Hbb within the cytoplasm, although the concentration appears more intense in the overnight sample. Quantitatively, there is more Hbb present within the overnight sample than there is in the 6 Hr incubation, little internalisation is observed at 4 Hrs and none is observed with the shorter incubation times (0.5, 1 and 2 Hrs).

RBC-MVs are visibly internalised after 4 hours
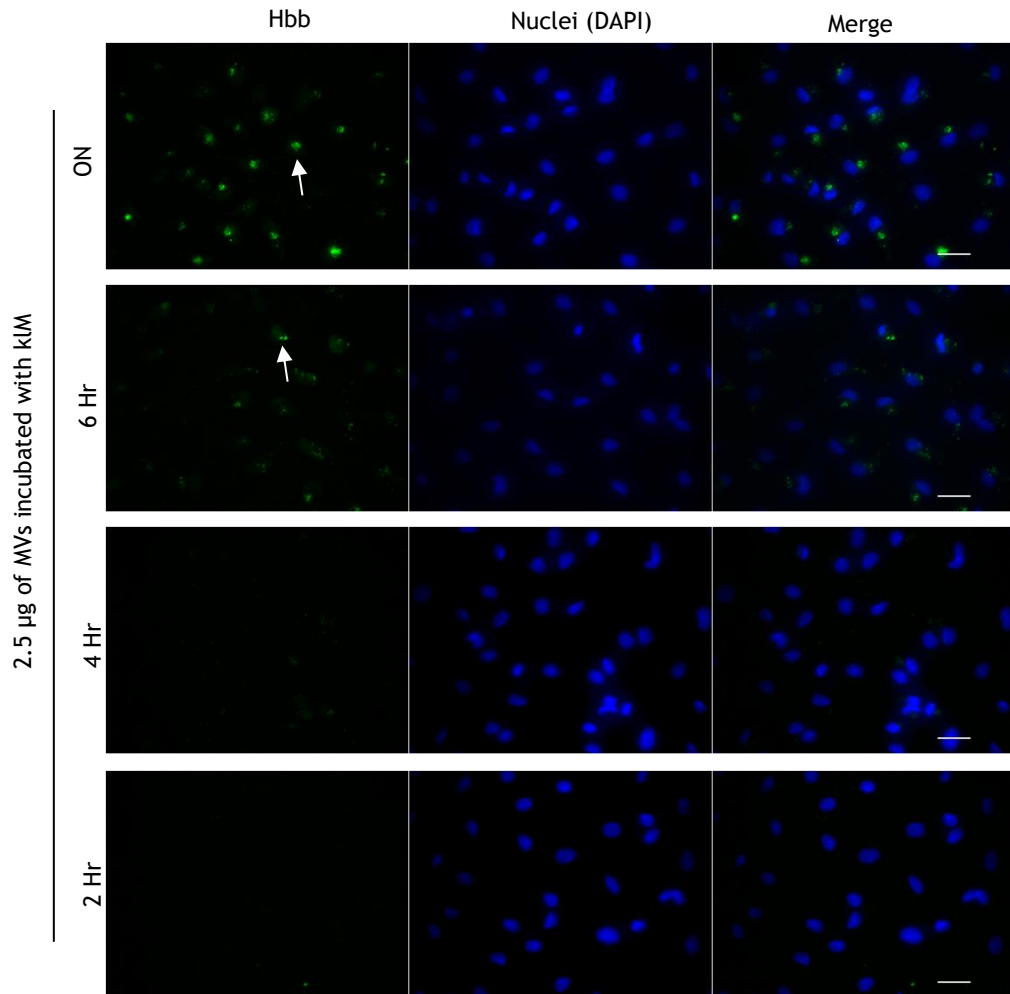
Figure 43: RBC-MVs are visually internalised within macrophages after 6 hours as depicted by Hbb staining.
kIM were incubated with 2.5 µg of RBC-MVs overnight, for 0.5, 1, 2, 4 and 6hours, probed with α-Hbb and visualised *via* epifluorescence. Exposure time settings between samples were kept constant. ON; overnight. White arrows highlight RBC-MVs. Scale bar = 20 µm.

To establish what occurs to the Hbb distribution following longer incubation periods, the incubation time was extended to 48 and 72 Hrs (Figure **44a**). There appears little difference either qualitatively or quantitatively regarding the Hbb distribution or intensity in macrophages at the longer time points. Hbb signal continues to be visible within the cytoplasm, but there is no apparent increase at later time points. As it is not clear if the Hbb seen at 24 Hrs is the same as the Hbb observed 72 Hrs, i.e. RBC-MVs were internalised but not processed, a chase experiment was performed (Figure **44b**). During this experiment, macrophages were pulsed for 24 Hrs with RBC-MVs; a time point where Hbb could easily be detected by IF. The media and residual RBC-MVs were removed and macrophages washed thoroughly, given fresh media and allowed to process/respond to the

internalised MVs for a further 24 to 48 Hrs. After a 24 Hr chase, nearly all previously detectable Hbb signal was lost – indicating that the macrophages were either digesting, processing, or excreting these RBC-MVs. As these macrophages appear to have an erythrocyte turnover phenotype (splenic-like), it was concluded that the most likely explanation was that the RBC-MVs were being degraded.
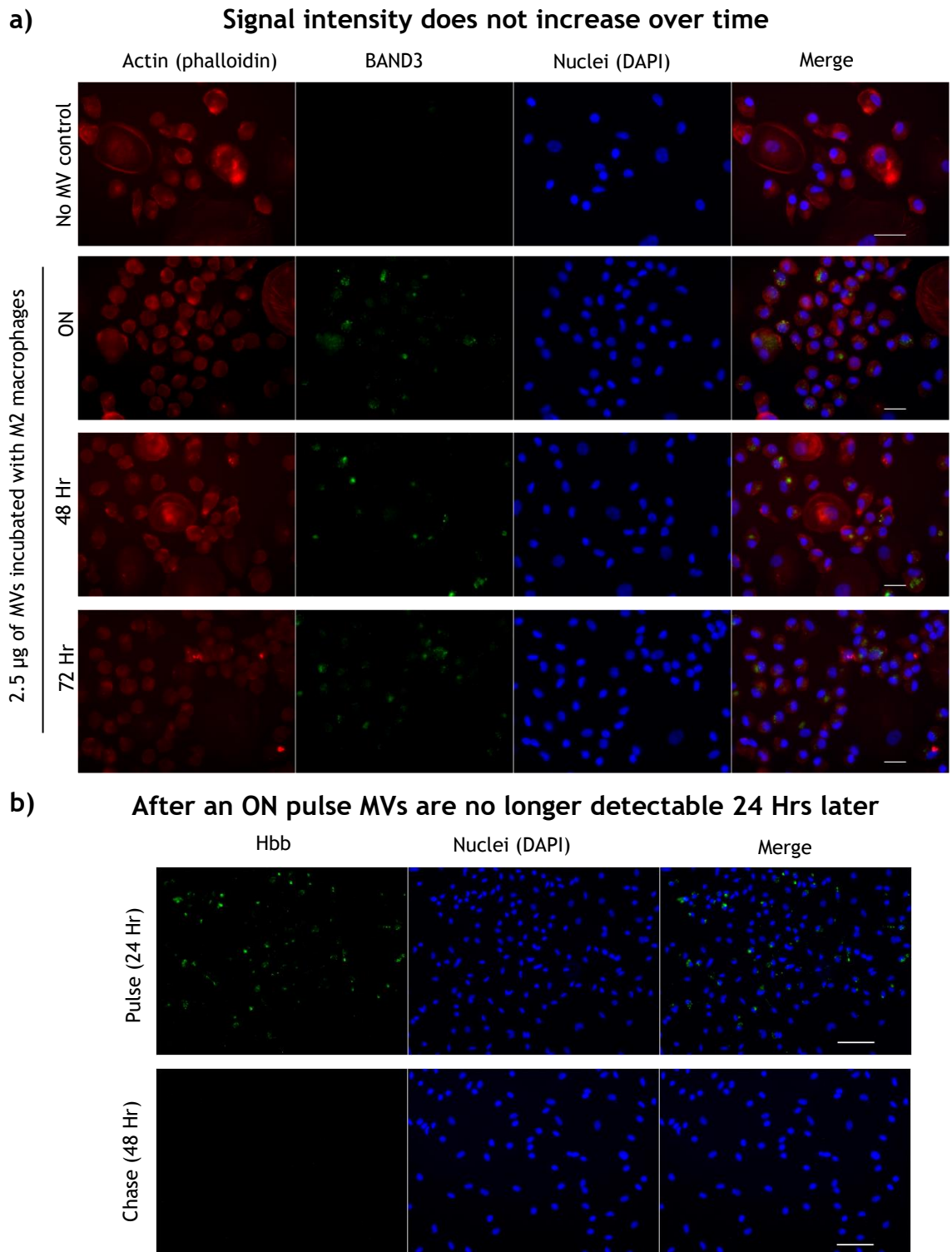
Figure 44: Increasing incubation times does not result in an increase in internalised RBC-MVs.

a) kIM were incubated with 2.5 µg of RBC-MVs for 24, 48 or 72 Hrs, probed with α-Hbb then visualised *via* epifluorescence – exposure times between experiments were identical. b) kIM were incubated with 2.5 µg of RBC-MVs for 24 Hrs, washed, refreshed with new media and incubated for a further 24 hours before being probed with α-Hbb and visualised *via* epifluorescence. ON; overnight. Scale bar a) = 20 µm, b) = 50 µm.

One of the key points of interest for transfusion-related problems is that of dose: does an increase in transfusion number, or amount of transfusion artefacts, positively correlate with adverse events? With that in mind, an experiment was performed where differing amounts of RBC-MVs, as quantified by Bradford, were incubated with a set number of macrophages. Doubling the dose of RBC-MVs from 2.5 to 5 µg results in a modest increase in Hbb signal observed by IF (Figure **45**). However, increasing dose again by 5-fold (25 µg) does not result in a further increase of Hbb signal (Figure **45**). Although there is a slight increase in signal observed when doubling the dose, there does not appear to be a linear relationship between dose and signal. Further increasing this dose does not affect signal, indicating equilibrium between uptake and processing has been reached; macrophages were incubated with lower amounts of MVs, but they were not readily detected, suggesting the 2.5 µg dose is the limit of detection for this system.
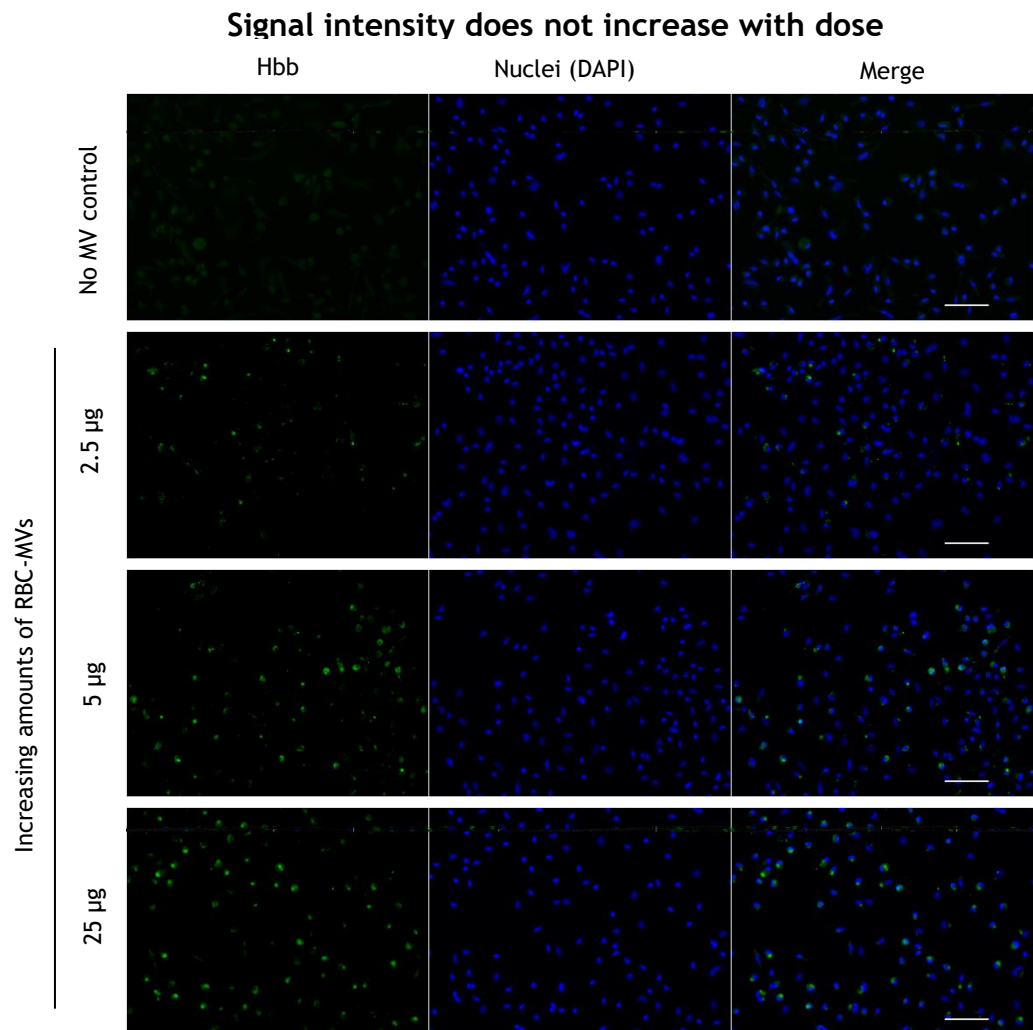
Figure 45: RBC-MV internalisation has a maximum MV dose
kIM were incubated with 2.5, 5 or 25 µg of RBC-MVs for 24 Hrs, probed with α-Hbb then visualised *via* epifluorescence – exposure times between experiments were identical. Scale bar = 50 µm.

To evaluate if MVs were being degraded, different endocytic and phagocytic markers were evaluated to see if they co-localised with the Hbb signal. LC3, a marker of autophagic vacuoles, is reported to be involved not only with canonical autophagy, but also in the turnover of various bacteria[457]. While RBC-MVs are not pathogens, they are still extracellular and how a macrophage responds to them is unknown; therefore, an RBC-MV/autophagosome interaction was evaluated. Although LC3b was readily detected within the cytoplasm, it did not co-localise with RBC-MVs (Figure **46a**). In addition, basal levels of LC3 did not increase, or change localisation (form distinct autophagosomes) when RBC-MVs were present.

When recycled during homeostasis, haemoglobin is broken down into haem (porphyrin ring) and the globin peptides in a phagolysosome. The haem is exported

to the cytoplasm and broken down into biliverdin by HO1, releasing ferrous iron, which is exported and recycled[327,458]. Perls' Prussian blue stain is used to detect iron stores (haemosiderin) in bone marrow trephines and was therefore used to detect haemosiderin in macrophages incubated with RBC-MVs (Figure **46b**). We therefore made use of the expertise of the NHS as this test is routinely performed by the Haematology Department of Gartnaval General Hospital. However, no haemosiderin was detected in macrophages that had been incubated with RBC-MVs. A potential explanation for this is that the haemosiderin present is below the limit of sensitivity of the assay, or, the iron is present as ferritin, which is undetectable by Perl's stain.
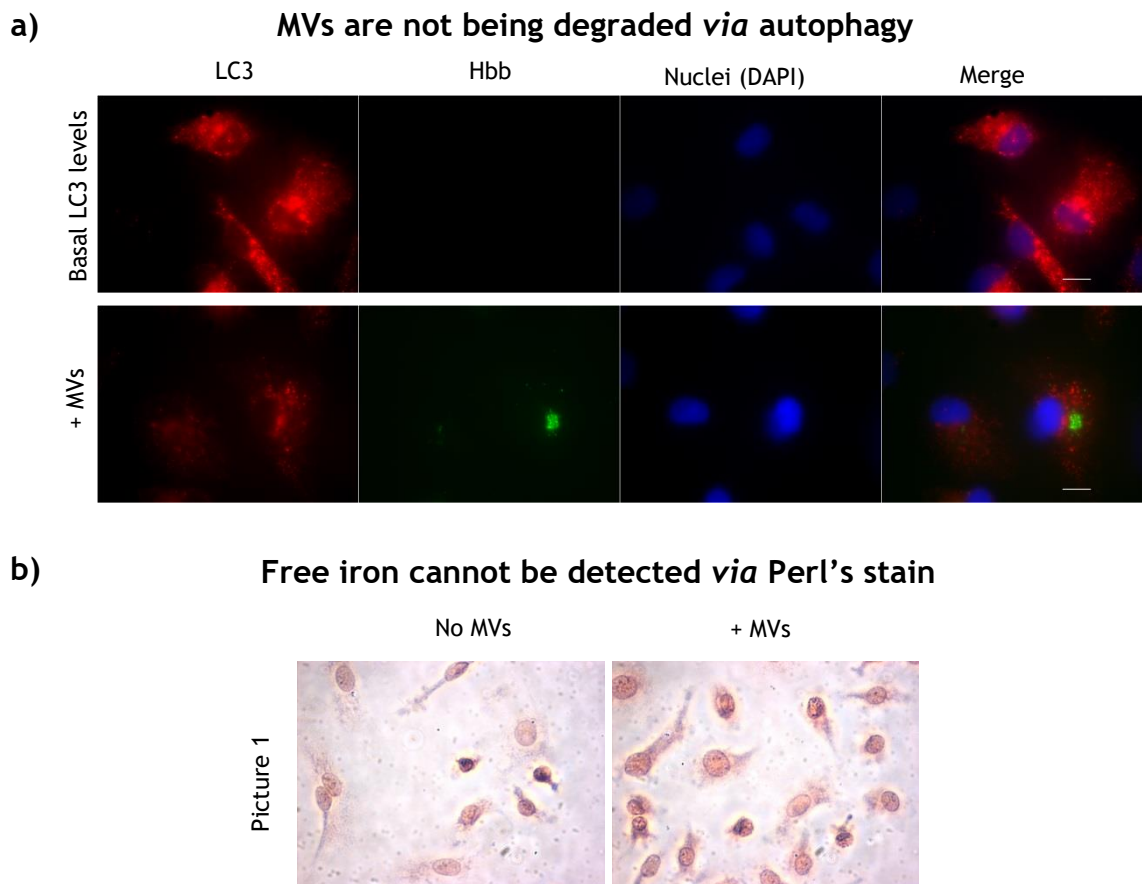
Figure 46: RBC-MVs does not appear to be degraded *via* autophagy and free iron cannot be detected *via* Perl's stain.
a) kIM were incubated with 2.5 µg of RBC-MVs for 24 hours, probed with α-Hbb and α-LC3, then visualised *via* epifluorescence; b) kIM were incubated with 2.5 µg of RBC-MVs for 24 fixed for 10 minutes with ice cold methanol and probed for free iron using Perl's Prussian blue stain. Perl's staining was performed by the Haemotology Department of Gartnaval General Hospital. Scale bar = 10 µm

An additional method of evaluating degradation was performed through the detection of lysosomes. If a macrophage was responding to RBC-MVs by degrading

them, then it might be possible to visualise an increase in lysosome number, or, a distribution similar to RBC-MVs would be observed. Acridine orange (AO) is a live stain that passively diffuses into cells and emits green fluorescence at neutral pH (cytoplasm) and red fluorescence in acidic vacuoles (lysosomes); an advantage to this compound is that it also stains nuclei (Figure **47a**). Overlaying green and red exposures reveals the location of lysosomes and, although there is no difference in number or location of lysosomes in macrophages with or without RBC-MVs, a large vacuole was detected (Figure **47a**, arrow). In addition, the vacuole fluoresces neither green nor red indicating an AO penetration issue. Cells appear to mostly have one vacuole, although some cells do contain two smaller vacuoles. Although this vacuole is present in macrophages with or without RBC-MVs, demonstrating it's not induced, the pattern that RBC-MVs adopt following internalisation (Figure **44a**) suggests they may be present within this vacuole. However, AO is not compatible with IF as it does not persist through fixation or permeabilisation. Therefore, it is not possible to evaluate this hypothesis by combining IF and AO. A potential explanation for this vacuole is that it is a sorting endosome - an endosome that acts as triage before internalised cargo are recycled, degraded or sent to the Golgi[459]. As RAB5 is a marker of sorting endosomes, IF was performed to see if this secondary structure could be observed, and, if it co-localised with RBC-MVs (Figure **47b**). Although RAB5 was readily detected within the cytoplasm, no secondary structure was detected, indicating that this vacuole is unlikely to be a sorting endosome.

a)

Acridine orange reveals a large vacuole

Acridine

Red filter (acidic)   Green filter (neutral)   Merge

No MVs

Single cell enlarged (no MVs)

b)

RAB5 does identify a vacuole

RAB5   Hbb   Nuclei (DAPI)   Merge

Basal Rab5 levels

+ MVs
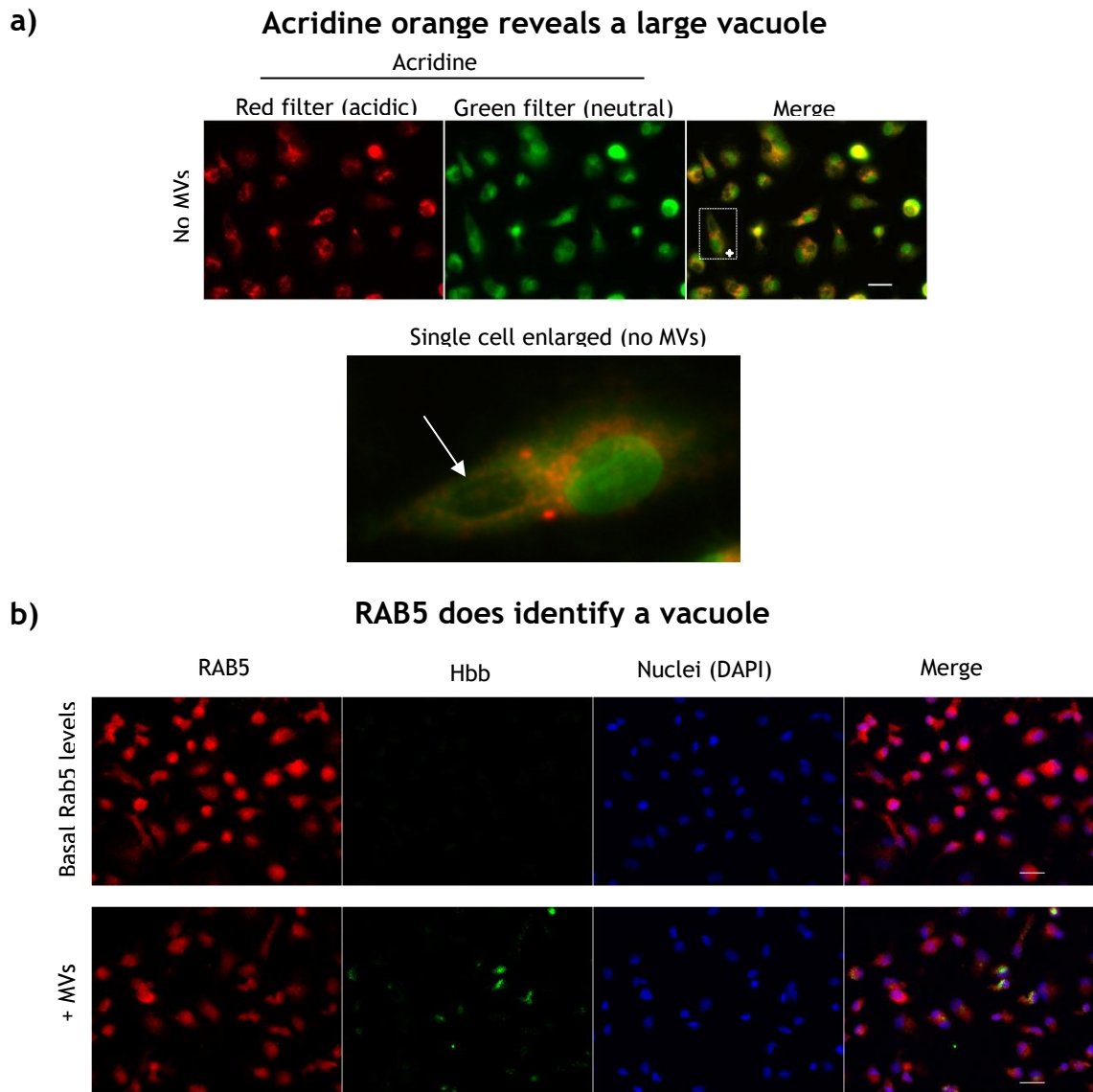
Figure 47: klM contain a large non-acidic vacuole that does not co-localise with sorting endosome markers.

a) klM without RBC-MVs were live stained with 1 µM acridine orange for 15 minutes, washed twice, resuspended in warm PBS and visualised *via* epifluorescence; klM were incubated with 2.5 µg of RBC-MVs for 24 Hrs then probed with α-Hbb and the sorting endosome marker α-RAB5 and visualised *via* epifluorescence. Note, the acridine orange fluoresces at different wavelengths dependent on pH so the reported images were acquired by visualising acridine orange with different filters. Scale bar = 20 µm

While intriguing, the main question to be answered from these experiments was: how do klM respond to RBC-MVs? Therefore, the experiments used to develop an RBC-MV endocytosis model (Figure **38 – 44**) were used to prepare samples ready for unbiased analyses: RNAseq and cytokine profiling. Figure **48a** details the experimental outline, in which macrophages are incubated with RBC-MVs overnight, washed and allowed to process internalised MVs for a further 24 Hrs (Dig). Control time points collected samples from cells without MVs at the same time RBC-MVs were added to macrophages overnight (D0), or, when the overnight

(D1) and Dig (D2) samples were processed. This allowed the comparison of macrophages unexposed to RBC-MVs to macrophages with internalised MVs and those that had processed them – theoretically allowing us to establish how macrophages respond to RBC-MVs (Figure **48a**).

RNA was extracted at each time point as depicted in Figure **48a**. The quality of these samples was assessed by Glasgow Polyomics *via* the calculation of an RNA integrity number (RIN) using an Agilent Bioanalyzer. All samples processed for RNAseq had a RIN of $\geq$ 9.5 (Figure **48b-i**); note one set of samples exhibited degradation (Figure **48b-ii**), so an additional set was prepared. In addition to RIN calculation, RNA quality was tested *via* qPCR of macrophage markers. Although one sample set exhibited low RIN scores (Figure **48b-ii**), when analysed by qPCR there was little difference in the CT value of *ENOX, TYW1* or *B2M* housekeeping genes (Figure **48c**), indicating that while the discarded sample set was not suitable for RNAseq, it was suitable for qPCR analysis. All markers tested by qPCR were present with little variability in expression observed (Figure **48d**). This data indicated the generation of samples suitable for RNAseq, so they were submitted to Glasgow Polyomics for single end sequencing (75 bp).

a) Experimental design schematic
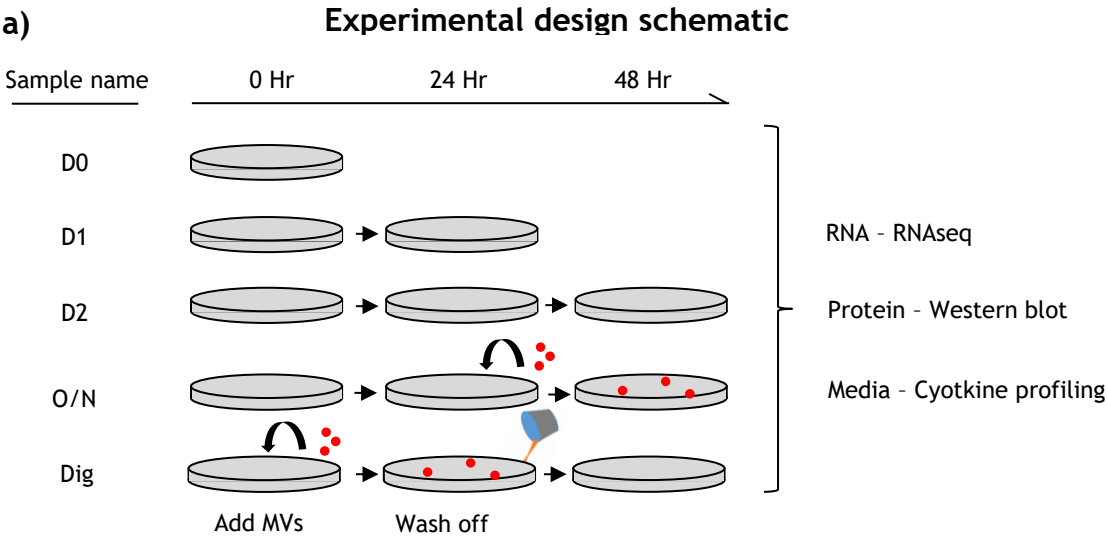
b) Representative electrograms generated *via* bioanalyser

i) "good" quality RNA (RIN:10)

ii) "poor" quality RNA (RIN:6.7)
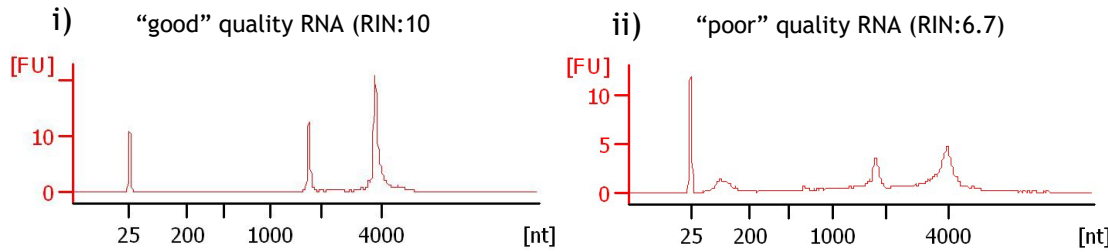
c) There is little difference in expression between Set 1, Set 2 & Set 3

d) There is little difference in expression between Set 1, Set 2 & Set 3

Representative heat map generated *via* Fluidigm
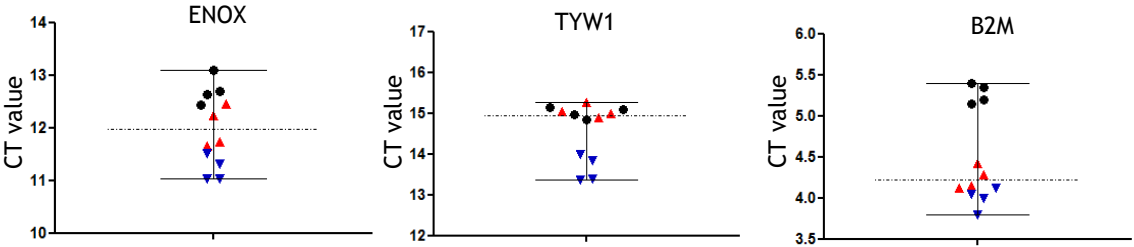
Marker analysis (N=3)
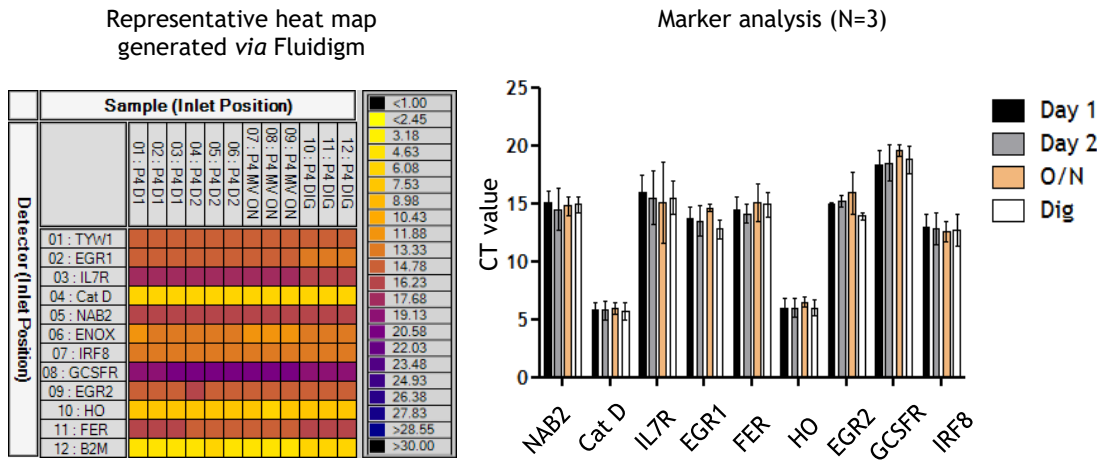
Figure 48: RNAseq experimental design and QC.
a) Schematic detailing the experimental design when generating RNA, protein and media samples to be used for RNAseq, immunoblots and cytokine profiing respectively; b) Representative "good" and "bad" electrograms generated by a Bioanalyser for RNA extracted from macrophages – all samples that had a RIN of $\geq$ 9.5 were sent for RNAseq, those with values $\leq$ 8 were not; c) CT values for three housekeeping genes as generated by qPCR from macrophages plotted as a box plot; d) Heat map generated by the Biomark HD when analysing macrophage samples *via* qPCR; e) Average delta CT values for 8 macrophage markers for each sample from each sample set -*NAB2* = NGFI-A binding protein 2, *CATD* = cathepsin D, *IL-7R* = interleukin 7 receptor, *EGR1* = early growth response 1, *FER* = ferroportin, *HO* = haem oxygenase 1, *EGR2* = early growth response 2, *G-CSFR* = granulocyte-colony stimulating factor receptor, *IRF8* = interferon regulatory factor 8. Note, each sample was run in technical triplicate.

Now that an endocytosis /phagocytosis model had been developed, it was possible to revisit the possibility of e-miRNA functioning within a different cell. Three experimental approaches were taken, luciferase assay, qPCR and IF. pmirGlo is a dual luciferase reporter that contains a sequence complementary to a miRNA of choice within the 3' UTR of firefly luciferase (fLUC); the second luciferase (renilla) is used as a normaliser. Cells that contain miRNA whose sequence is present in fLUC's 3'UTR silence its expression, while cells that don't express that miRNA emit light. Using this methodology, it is possible to establish the functionality of individual miRNA. However, although 5 constructs were successfully cloned and sequenced, it was not possible to perform the assay as all transfection methodologies used (electroporation, lipofection, calcium phosphate or polyethylenimine) resulted in either complete cell death, or failed to transfect klM.

The second methodology utilised qPCR analysis of genes predicted to be targeted by miR-451. This e-miRNA was chosen due to its high abundance, while TargetScan and DIANA were the algorithms used to predict targets[460,461]. To ensure a robust candidate prediction, only target genes predicted by both algorithms (13) were chosen (Figure **49a**); of these, 8 were expressed in the red pulp of the spleen (Tissue Atlas), an area enriched for macrophages with a red cell turnover phenotype. Note that 14-3-3-ζ is a validated target of miR-451, but was predicted by neither algorithm[255]. As silencing of 14-3-3-ζ is reported to lead to erythroid blasts being protected from oxidative stress, a potential benefit to klM internalising material likely containing ROS, this target was also chosen. Target expression and primer specificity were tested by amplifying cDNA from klM and resolving the products on a 2 % agarose gel (Figure **49b**); *PSMB8* and *LYSMD4* were either not expressed, or the primers didn't work, so were not analysed by qPCR. RNA was extracted from klM that had been treated with aRBC-MVs for 48 Hrs (i.e.

digest time point), cDNA prepared and analysed by qPCR. All genes amplified but there was no difference in expression between treated and non-treated cells (Figure **49c**).
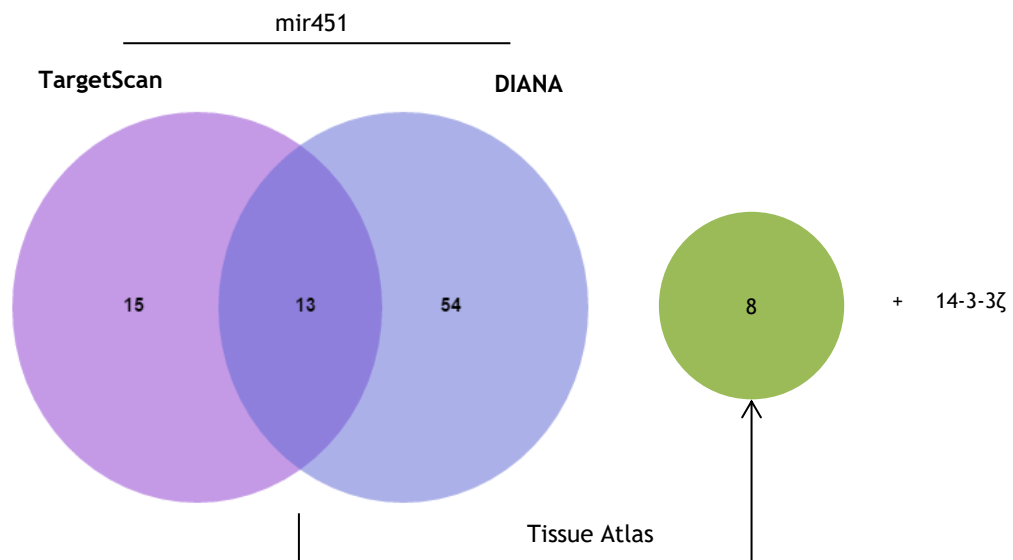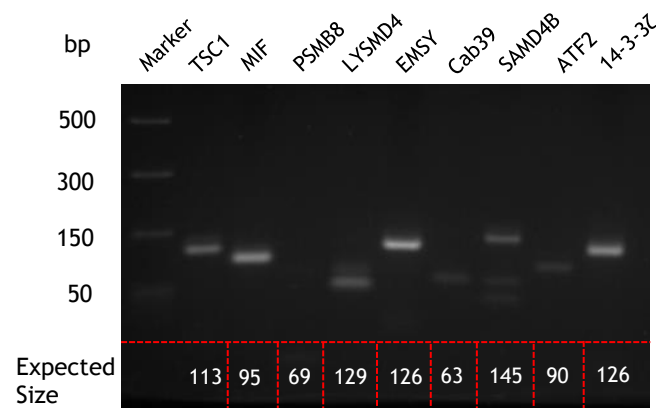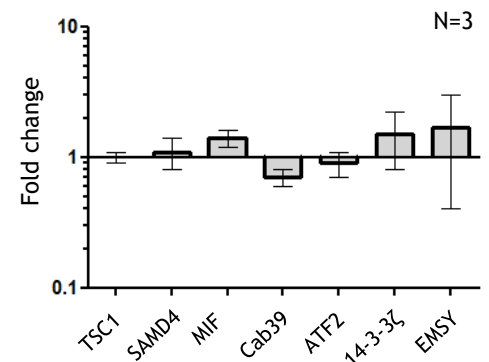
Figure 49: Predicted targets of miR-451 are not downregulated in macrophages that have processed RBC-MVs.

a) mRNA targets of miR-451 were predicted through TargetScan (15) and DIANA (54), targets predicted by both algorithms (13) were assessed for tissue expression *via* Tissue Atlas, targets that are expressed in the spleen (8) were used as candidate genes + 14-3-3-ζ as reported by Yu *et al.*[255]; b) Primers were checked for specificity and gene expression through the amplification of M2 RNA and gel electrophoresis; c) Candidate genes were detected *via* qPCR (universal probe library) and fold change (DIG Vs D2 Figure **48**) calculated using ΔΔCt – genes were normalised against 18s rRNA, *TSC1* = tuberous sclerosis 1, *SAMD4* = sterile alpha motif domain containing 4A, *MIF* = macrophage migration inhibitory factor, *CAB39* = calcium binding protein 39, *ATF2* = activating transcription factor 2, *EMSY* = BRCA2 interacting transcriptional repressor; error bars represent standard deviation.

The final approach employed was to establish if e-miRNA escaped the processing body post internalisation by evaluating AGO2 distribution *via* IF. However, after 24 Hrs, AGO2 was neither more abundant within the cytoplasm of recipient kIM, nor visible in the RBC-MVs that had been internalised (Figure **50a, b**).

a) **AGO2 does not appear to move from MV to cytoplasm**
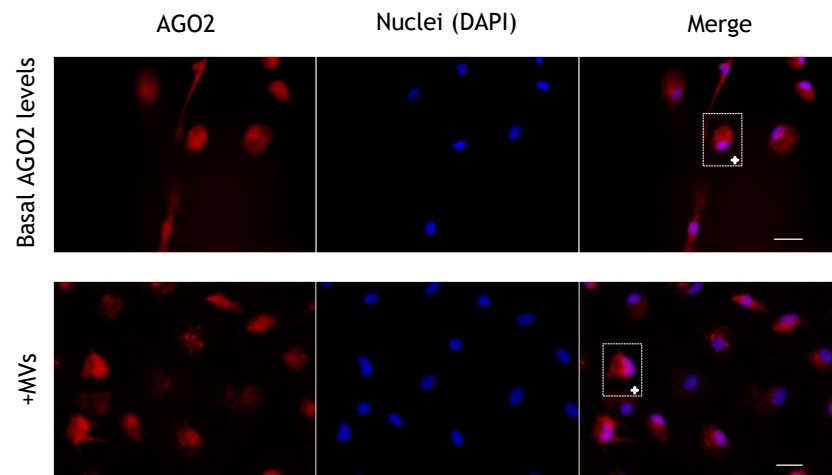
b) **Enlarged from (a)**
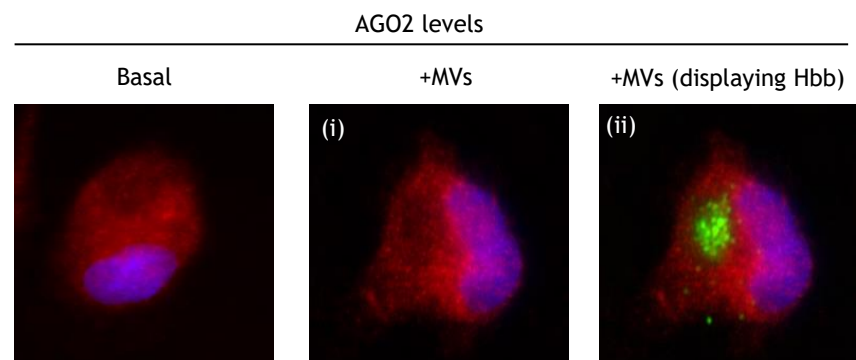
Figure 50: *via* IF it is not clear if AGO2 from RBC-MVs moves into the cytoplasm of kIM following endocytosis / phagocytosis.
a) kIM were incubated with 2.5 µg of RBC-MVs for 24 hours, probed with α-Hbb and α-AGO2 (11A9), then visualised *via* epifluorescence; b) Selected regions from (a) digitally enlarged, (i), (ii) are the same cell, Hbb signal was not displayed in (i) to allow fair comparison of the AGO2 signal between -/+ MV arms. Scale bar = 20 µm

6.3 **Discussion**

The aim of this chapter was to generate an RBC-MV endocytic-phagocytic model, in order to evaluate how macrophages respond to RBC-MV exposure.

6.3.1 **Macrophage generation**

The first stage was to generate macrophages with distinct and relevant phenotypes. As patients require transfusions for a variety of reasons, two main phenotypes were chosen: M1 and M2. As M1 macrophages exhibit an inflammatory phenotype, incubation with RBC-MVs would mimic the transfusion of RBC break down products on patients with underlying inflammation e.g. infection, GVHD etc. While M2 macrophages are more homeostatic, therefore representing patients without underlying inflammation, e.g. surgery patients. Classically activated (M1) macrophages, with a distinct M1 phenotype (Figure **39a**), were generated using widely reported methodologies[451].

The method of generating M2 macrophages within Wheadon lab is to polarise with IL-4. However, this resulted in macrophages that were chimeric (Figure **39b**). In addition, it is reported that IL-4 downregulates CD163, a protein that plays a vital role within red cell biology[462]. For example, within the bone marrow, CD163+ macrophages form blood islands with erythroblasts, allowing RBC maturation, while in splenic/hepatic macrophages, CD163 scavenges extracellular haemoglobin by binding and internalising the haemoglobin-haptoglobin complex[463,464]. Therefore, instead of adhering to an "M2X" system, a polarisation strategy that induced genes essential to erythrocyte biology was pursued. DEX treatment appears to stimulate this phenotype as CD163 is highly expressed (Figure **39c**) and *FER* is ~150-fold upregulated (Figure **40b**) post polarisation. In addition, functional assays within the literature demonstrated that DEX stimulated haemoglobin turnover in monocytes[455], and, increased erythropoiesis when CD34+ stem cells were co-cultured with macrophages[465]. On the other hand, different studies reported deleterious effects of DEX on macrophages, with Gras *et al*. and Haim *et al*. both reporting ~ 40 % cell death[453,454]. However, as an MTT assay (which measures dehydrogenase [NADPH] activity) was used in both studies, it was incorrect by these authors to interpret a loss of metabolic activity as cell death; especially as the phenotype of the macrophage is changing and the metabolic

activity between mM0 and klM macrophages may be different. Indeed, apoptosis assays performed during this studentship showed no indication of DEX-mediated death (Figure **40c**).

Although there is limited information available within the literature, the phenotype described above (CD163^{+}, CD206^{+}, haemoglobin turnover) represents previous information regarding hepatic/splenic macrophages[452]. As hepatic macrophages are reported to scavenge RBC-MVs, the culture methodology described above appears conducive to evaluating how macrophages respond to MVs post transfusion.

6.3.2 Endocytosis assay

As mentioned, the main object of this chapter was to develop an endocytosis model to evaluate how macrophages respond to RBC-MVs. That said, through the generation of this model, additional points of interest/questions were highlighted. While this does not directly affect the question posed above, they are discussed below.

6.3.2.1 How are RBC-MVs internalised?

2.5 µg of RBC-MVs are readily internalised by klM, but do not appear to enter M1 cells and only somewhat into mM0 cells (Figure **41b**). Figure **42a** demonstrates that M1 macrophages are phagocytic and so their inability to internalise RBC-MVs is not due to the cells being defective. In klM, it takes approximately 6 Hrs for MVs to be visually detected (Figure **43a**), while extending incubation periods (24 -72 Hrs) reveals internalisation reaches a maximum at 24 Hrs (Figure **44a**). Taken together, these results suggest a controlled means by which RBC-MVs are internalised and processed. This therefore raises the question, how do klM readily internalise RBC-MVs? Figure **42b** demonstrates that RBC-MV uptake is an active process, suggesting RBC-MVs are internalised *via* receptor-mediated endocytosis. This receptor would have to be absent on M1 macrophages and in low abundance in mM0 as both show limited if any internalisation of RBC-MVs. A candidate receptor is Mer Tyrosine Kinase (MerTK), which has been shown on klM to bind apoptotic cells and apoptotic bodies through recognition of exposed PS[466]. PS exposure is a hallmark of EVs and was demonstrated to be present on the

RBC-MVs used during this project (Chapter **3**). Furthermore, Cohen *et al.* also demonstrated that DEX treatment not only upregulated macrophage MerTK expression, but GM-CSF and IL-4, two cytokines used to polarise cells in this study (Figure **38,39**), downregulated MerTK expression[466]. This potentially explains the differential internalisation pattern observed in Figure **41b** and is discussed below. A means to test this theory would be to block MerTK with a blocking Ab prior to RBC-MV incubation, then evaluate changes in internalisation.

A less specific means of evaluating RBC-MV internalisation is through blocking exposed PS. This has been reported to be a major pathway of EV phagocytosis and blocking PS with Annexin-V has been used successfully by multiple studies to demonstrate this[467,468]. However, this is a candidate based approach, and a pan, unbiased experimental methodology may be more appropriate. For example, the recognition and method of EV internalisation is a topic of interest within the literature and additional compounds (listed in Table **6**) could be used and their effect on internalisation established.

Table 6: Commonly used compounds used to evaluate EV internalisation.

Pathway	Compound	Target	References
Endocytosis	Cytochalasin D	Actin	[469]
CM endocytosis	Dynasore	Dynamin-2	[470]
LRM endocytosis	Flippin	Cholesterol	[469]
Macropinocytosis	EIPA	Sodium / proton exchanger	[471]
Phagocytosis	Annexin-V	Phosphatidylserine	[467,468]

CM, clathrin mediated, LRM, lipid raft mediated, EIPA, 5-(N-ethyl-N-isopropyl)amiloride

6.3.2.2 **During an inflammatory state where do RBC-MVs go?**

As mentioned previously, RBC-MVs are not readily internalised by M1 macrophages. While the differences between klM and M1 macrophages can be used to evaluate how RBC-MVs are internalised, it also raises a clinical question. If a blood unit is transfused to a patient with an underlying inflammatory condition, where do these MVs go? For example, symptoms of aGVHD are varied, but include inflammation and hepatic toxicity[382]. This hepatic toxicity/inflammation may well inhibit the hepatic scavenging of RBC-MVs observed by Willekens *et al.*[392] During this experiment, although most MVs were detected in Kupffer cells (45 %), they

were also detected in other tissues, bone (22.5 %), skin (9.7 %), muscle (5.8 %), spleen (3.4 %), kidney (2.7 %), lung (1.8 %); and 9.1 % remained in the circulation at the time point tested (30 minutes)[392]. Therefore, most RBC-MVs would be free to enter these additional tissues. However, it is important to note that this study offers no concrete evidence that the material being transfused was RBC-MVs. No size markers are offered on the FACs plots, and the method employed by this study to isolate MVs was shown to contain RBC membrane artefacts (Chapter **3**). In addition, the means of labelling "RBC-MVs" is not specific as ^{51}Cr-chromate also labels platelets. This means the observed radioactive signal may well be a mix of RBC artefacts and platelet MVs. This is an important consideration as platelet-derived MVs are reported to be the most numerous, by up to 100-fold, in peripheral blood[431,472].

Only one study, to my knowledge, has looked at the cellular uptake of RBC-MVs and were using endothelial cells as a model. However, this study was researching malaria and as the RBCs used were infected with *P. falciparum,* making comparisons to transfusion, at first glance, debatable. Never the less, Marti *et al*. reported a pro-inflammatory response of endothelial cells to RBC-MVs[421]. Interestingly, this was speculated to be mediated by miR-451 silencing of *CAV-1* or *ATF2,* and this downregulation of *ATF2* was linked to the apoptosis observed in their system. It is important to note, that while this is a malarial system, miR-451 originates from the RBC and not from the parasite. Also, due to their anucleate nature, miR-451 cannot be induced by the parasite, indicating that this is an RBC-MV effect, not a parasite one. As no malarial RBC-MVs were used as controls, it is unclear how much of their observed phenotype is due to *P. falciparum* and how much to RBC-MVs; therefore, some of their findings may well be relevant to the transfusion setting.

6.3.2.3 **What is the purpose of the observed vacuole?**

Comparing the internalisation pattern of RBC-MVs in mM0 and klM reveals a different distribution. In mM0 macrophages, the distribution is diffuse throughout the cytoplasm with no apparent pattern, while in klM, RBC-MVs appear to concentrate at a more defined location within the cytoplasm. Surprisingly, RBC-MVs are not detected at the cell periphery; only at the concentrated areas described above (Figure **41**). As RBC-MVs appear so distinctly localised, one would

expect a gradient to be present: RBC-MVs present at the membrane, recognised by "X" receptor, followed by RBC-MVs found diffusely within the cytoplasm moving towards this area of concentration. Why this is not observed is unclear. It is unlikely that the Hbb positive puncta observed are not RBC-MVs, as they co-localise with BAND3, another RBC-specific marker (Figure **42c**). Uptake *via* micropinocytosis would result in a macropinosome, although this is unlikely to be what occurs here as no lamelliapodia-like projections have been observed at the cell membrane. A potential explanation for the lack of membrane associated RBC-MVs is that they were not surviving the fix and perm methodology. During this studentship, it was noted that macrophages are quite sensitive to external stimuli such as mechanical stress, temperature and buffer tonicity. Therefore, it is entirely possible that the fixation/permeabilisation strategy affected RBC-MV/macrophage interaction.

Interestingly, live staining of macrophages using AO (Figure **47a**) reveals the presence of a large vacuole. Due to the distribution of RBC-MVs observed (Figure **41b**), it is tempting to speculate that they are contained within this vacuole; although the techniques used in this study are not suited to test this hypothesis as they are not compatible with each other. The purpose of this vacuole is unclear as there is no mention within the literature of a single large vacuole being present within macrophages. However, this has been observed by other groups (personal communication Dr Amy Buck, University of Edinburgh); this is important, as it suggests what is being observed is not a peculiarity of our system, but a genuine phenomenon. Note also that this vacuole is visible due to an absence of AO signal, not AO stain (Figure **47a**). As AO passively diffuses and fluoresces regardless of location (pH only affects emission colour), it suggests a penetration issue. However, AO penetration of lysosomes and nuclear membrane is not an issue as AO forms tight red puncta, indicative of lysosomal staining, in addition to staining the nucleus. Consulting the literature does not reveal any explanations for this, AO negative sections can be observed in some figures, but are not discussed by the authors[473]. The only cell type null for AO staining are erythrocytes, although how this is relevant to this vacuole is unclear; especially as the vacuole is present in macrophages not exposed to RBC-MVs. It is unlikely to be a staining time or concentration issue as those used here are widely used within the literature[473,474].

Attempts to characterise this vacuole were unsuccessful. For example, LysoTracker®, a dye similar to AO, failed to stain lysosomes, not just the vacuole. With the thought that RBC-MVs are being turned over in this vacuole, additional markers associated with lysosomes were evaluated. While lysosomal associated membrane protein-1 (LAMP1), lysosomal proteins - cathepsin D and K failed to stain the vacuole, they also did not stain lysosomes. Lysosomes were observed *via* the use of AO (Figure **47a**), so the failure to co-localise these markers with the vacuole is likely to be a technical fault, rather than them being absent. Furthermore, LC3 and RAB5 did not stain this vacuole, indicating that it is neither autophagic or a sorting endosome. Although the reason RBC-MVs disappear after incubation (following wash off) is unclear, it isn't unreasonable to suggest they are being degraded, just not by a classic lysosomal pathway. We investigated whether the RBC-MVs were being degraded by staining for iron deposits. Although Perl's stain failed to detect stored iron (Figure **46b**), additional markers that may be informative would be HO1 or ferroportin. Due to budgetary issues, neither of these markers were evaluated *via* IF.

Another explanation for the loss of Hbb signal following wash off, is that the RBC-MVs are being exported. While this is certainly possible, it seems unlikely that these macrophages would actively take up RBC-MVs, only to excrete them shortly thereafter. Never the less, this hypothesis was examined *via* western blot, where culture media was concentrated using a 100 kDa vivapsin, resolved and probed for Hbb. However, due to the amount of serum present in the media, the blot had too much background to be informative (data not shown). Furthermore, additional data generated (not shown), demonstrated that artificial RBC-MVs were "nude" for RBC markers when analysed by FACs. Meaning that it wasn't possible to evaluate the presence of excreted RBC-MVs within the culture media.

6.3.2.4 **How dynamic are RBC-MV interactions?**

At present, the means of establishing MV internalisation time was IF. Figure **43** demonstrates that it takes approximately 6 Hrs for RBC-MVs to be internalised by klM, however, Willekens *et al*. demonstrated that 90 % of radio-labelled material (purported RBC-MVs) disappeared from circulation 30 minutes post murine transfusion[392]. Why there is a discrepancy is unclear, but there are a couple of considerations: (1) Radioactivity is simply more sensitive than IF, meaning that

Willekens can detect internalisation sooner than 6 Hrs. However, as semi-quantification reveals only ~ 10 % material remains in circulation at 30 minutes, a more likely explanation is that the MVs are simply being internalised faster *in vivo* than *in vitro*. Personal observations of MV stocks reveal that they do not sediment, indicating they are colloidal in nature. Note, although small, as RBC-MVs contain Hbb, they visibly stain the PBS they are stored in pink. The pellet becomes clear after centrifugation, meaning that it is possible to establish RBC-MV sedimentation by eye. In culture, this colloidal suspension means klM interact with MVs as they diffuse to the bottom of a culture plate, *in vivo* one must consider flow. For example, in a human it takes approximately 1 minute for a blood cell to travel around the body. This, coupled with the comparatively narrow diameter of the sinusoidal space, makes it more likely for an MV to interact with a macrophage than in suspension.

One of the most common ways of establishing EV uptake within the literature is to stain them with a membrane dye[456]. As this was not suitable for RBC-MVs (Appendix **17**), real-time internalisation/processing using live imaging could not be performed. Although short time points were used to establish internalisation (Figure **43a**), periods shorter than an overnight incubation following wash off (Figure 8b) were not performed. While this can be performed using IF, live imaging would be a preferable way of establishing RBC-MV processing time as dynamic interactions could be evaluated, rather than static time points. In addition, as noted above, RBC-MVs are not seen at the cell periphery when analysed *via* IF. If the inability to see RBC-MVs at the membrane is a technical artefact, i.e. MVs are fix and perm labile, then this would be circumnavigated *via* a live imaging system. In addition to trying two different membrane markers (PKH26, CellView Jade), CFSE was also used to stain RBC-MVs, although this was found to be inconsistent: sometimes MVs were labelled strongly, others, not at all (data not shown). As these MVs are induced, a potential work around would be to label whole RBCs prior to vesicularisation. However, as discussed previously, a major limitation of labelling MVs prior to uptake is that it may affect how they interact with macrophages.

6.3.2.5 **Why wasn't dose investigated?**

The possibility that transfusion number (dose) positively correlates with any side effects suffered by patients is of clinical interest, however, this has proven difficult to evaluate. It is possible that the experiments described above could be used to evaluate dose, but it is either not possible to definitively prove that a dose effect is occurring, or, establish to what degree. For example, while the experiment in Figure **44a** details no increase in observed signal when extending incubation past 24 Hrs, it does not reveal the mass of MVs internalised/processed. Does the number of MVs internalised respond linearly with time, or does it plateau? A post 24 Hr plateau is what the IF indicates, but it's not unreasonable to suggest that a flux exists between MV internalisation and processing i.e. MVs are processed, as indicated by Figure **44b**, concurrent to uptake and that the signal observed at 24 Hrs is not the same as at 72 Hrs. Establishing the amount of MVs remaining in the media would be the simplest way to infer the amount of MVs internalised, allowing relative uptake across the time points detailed in Figure **43a-44**b to be established. However, means of establishing the amount of MVs remaining in the media have not yet been established at our centre.

With regards to the clinical question, it is possible to add fresh MVs on a daily basis, mimicking multiple transfusions. However, the experiments in Figure **44a** show that increasing the amount of MVs past a certain point has no apparent effect on internalisation, suggesting that daily additions of MVs would not affect uptake. In future, the effect of dose could be pursued by either establishing the amount of MVs internalised, or, performing consecutive wash off experiments.

Nevertheless, while there remains a plethora of questions regarding this endocytic model, a means to evaluate how macrophages respond to RBC-MVs has been generated.

6.3.3 **Assay summary**

In this assay, time points where klM have internalised and processed RBC-MVs has been assessed. Generation of samples at these time points allows the comparison to untreated macrophages, meaning it should be possible to establish early and late responses to MVs. RBC-MVs were generated from the erythrocytes

of an "O-negative" blood donor, meaning these MVs are representative of a transfusion from a "universal donor". Any potential modulation observed is therefore due to an RBC-MV interaction and not an immune response.

Generation of RNA and media samples allows unbiased analyses to be performed to determine how klM respond to a storage artefacts i.e RBC-MVs. Media samples have been snap frozen and stored at -80 °C waiting for cytokine profiling. RNA samples were qualitatively shown to be of high quality by Glasgow Polyomics (Figure **47**) and have been analysed by Illumina sequencing; the results of which discussed in Chapter **7**.

6.3.4 **e-miRNA functioning within klM**

The final experiments within this chapter evaluated whether e-miRNA functioned within klM post-internalisation. However, neither IF nor qPCR indicated that either e-miRNA were entering the cytoplasm (Figure **50b**), or, silencing predictive targets (Figure **49c**). Note, for the qPCR experiment, earlier time points were considered, but the IF failed to show any accumulation of AGO2 over time. Furthermore, future scrutiny of the RNAseq data failed to reveal any of these predictive targets of miR-451 being downregulated. For the IF experiment, a later time point (i.e. digest) may reveal an increase of AGO2 within the cytoplasm, but this was not performed during this study. Failure to detect AGO2 within RBC-MVs is likely due to the same epitope masking encountered in Chapter 4 when trying to evaluate AGO2 in mature erythrocytes

Chapter 7 **RNAseq results**

7.1 **Introduction**

Microvesicles have been shown in multiple studies to not only interact with neighbouring or distal cells, but also transfer miRNA. Transferred miRNA can modulate a host cell's transcriptome, which was of interest to this project as e-miRNA are found within RBC-MVs and could potentially impact on macrophage response when ingested. However, Figure **49** in Chapter 6 demonstrated that the genes predicted to be targeted by selective e-miRNA were not modulated, and, AGO2 did not accumulate in klM following RBC-MV internalisation. Although not conclusive, together, these data indicate the hypothesis of e-miRNA functioning in klM post MV internalisation to be null. Nevertheless, a working RBC-MV endocytosis/phagocytosis model was developed during this study.

This model, in addition to being used to evaluate the transfer of e-miRNA, is also of interest clinically. For example, the RBC-MVs used within this model are very similar to those found within blood units that have undergone long storage periods. These MVs are found within the storage medium of the blood unit and are transfused to a recipient along with the RBCs. The number of MVs present within the blood unit increases the longer the blood is stored, and the effects of transfusing aged blood have been debated within the literature for decades especially in the context of transfusion reactions and why they occur. To simply recapitulate the clinical studies that have been performed, the model generated in Chapter 6 was used to assess the effect of RBC-MVs on klM.

Chapter 6 characterised the macrophages generated *in vitro* as Kupffer-like, the cell type responsible for scavenging transfused MVs in the liver. In addition, data in Chapter 6 also demonstrated that klM were capable of not only internalising, but also processing RBC-MVs. Generating RNA samples from this model allowed a means by which the following unbiased question could be answered:

How do klM respond to RBC-MVs?

This chapter will therefore focus entirely on the analysis of the RNAseq data generated from the samples prepared at the end of Chapter 6.

7.2 **Results**

RNA samples from Chapter 4 were sent for sequencing to Glasgow Polyomics (University of Glasgow). Libraries were prepared from poly(A) purified RNA by polyomics and analysed using Illumina NextSeq 500 sequencers. Alignment and initial analysis was performed by Miss Ana-Maria Nastase (Glasgow Polyomics).

RNAseq reads were aligned using Kallisto V0.43 as per Bray *et al.* while downstream analysis of the Kallisto processed data was performed with DESeq2 as per Love *et al.*[475,476]. Variation between and within data sets was visualised using principle component analysis (PCA). A principal component (PC) can be any factor, e.g. weight, height, patient, treatment etc. The PCA algorithm cycles through all conditions, establishing which PC (factor) causes the most variance within a data set, and which causes the least. For example, PC1 is always the factor causing the most variability within a data set, PC2 causes the second most variability and so forth. Therefore, this methodology allows for any undesirable factors causing data variability to be identified and corrected.

For example, in this project's data set, the most amount of variability comes from a donor effect, as there is 42% variability between samples (Figure **51a**). Although variation between sample set 1 and 2 is low, with most data points clustering together, data set 3 is further right on the x-axis, indicating a higher degree of variation compared to the other sample sets. PC3 analysis, based on sample type rather than sets (donors), is lower than PC1 at 18 % (Figure **51b**). This is presumably caused by a similar distribution of data points on the Y-axis, even between donors. Interestingly, further analysis of Figure **51b** reveals that the control and digest samples are polar opposites on the y-axis, i.e. they are very different to each other. Indeed, using ClustVis to cluster all significantly modulated genes (p=0.04) reveals that control day 0 (CD0) and digest samples (DIG), from all sets, cluster together (Figure **51c**)[477]. PC3 and cluster analysis suggest the time points of interest are CD0 and DIG i.e. macrophages with no MVs compared to macrophages that have processed MVs. Furthermore, PC3 analysis identified a donor effect causing variability, which was controlled using batch correction, allowing data analysis to focus on CD0 Vs DIG; batch correction was performed by Miss Ana-Maria Nastase (Glasgow Polyomics).
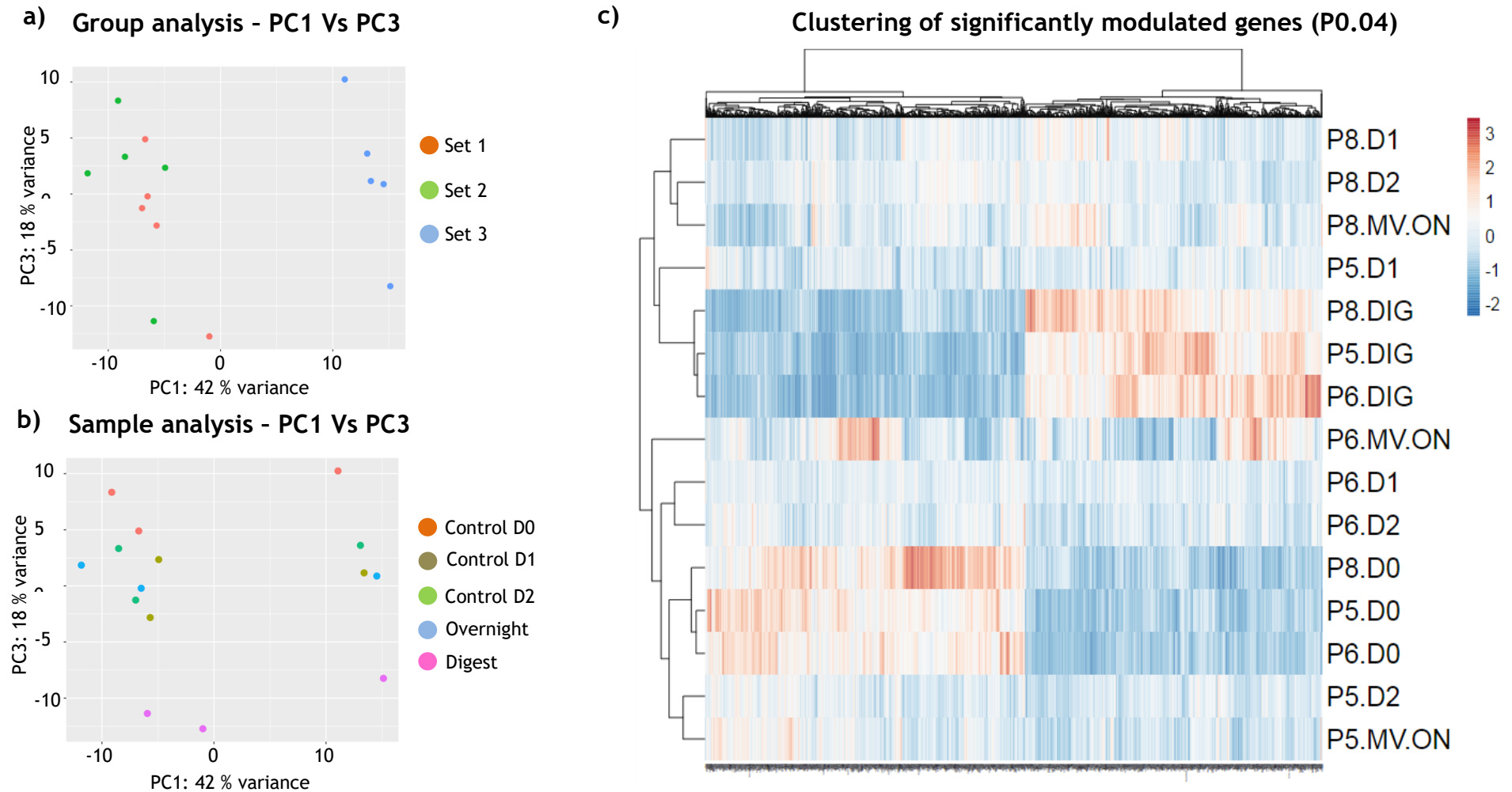
Figure 51: PCA and clustering highlight Control D0 and Digest to be timepoints of interest.
a) PC1 Vs PC3 based on data sets; b) PC1 Vs PC3 based on individual samples; c) clustering analysis of all significantly modulated genes as drawn using ClustVis. Note, PCA was performed by Miss Ana-Maria Nastase at Glasgow Polyomics; P = patient (volunteer), DIG = digest, MV.ON = microvesicles overnight.

To calculate differential expression results, the three individual datasets in Figure **51c** were first averaged to give control day 0, 1 and 2 (CD0-2), macrophages left with microvesicles overnight only (MV-ON) and macrophages that had digested RBC-MVs (DIG). The following data sets were then contrasted for each volunteer: CD0 Vs CD1, CD0 Vs CD2, CD1 Vs CD2, CD0 Vs MV-ON, CD0 Vs DIG, MV-ON Vs DIG, CD1 Vs MV-ON, CD2 Vs DIG and CD2 Vs MV-ON. Differentially expressed genes were filtered against a p-adjusted value of 0.05, leaving only significantly modulated genes (Figure **52a**). For example, comparing CD1 to CD2 reveals no modulation in gene expression. As time is the only difference between these samples, it indicates that there is no drift between 24 and 48 Hrs as gene expression remains the same. Differential expression between CD0/CD1 and CD0/MV-ON was compared, resulting in both comparators sharing the same 56 deregulated genes. Experimentally, at this time point (time nought), media containing the polarisation agent DEX is removed and cells are given fresh media; this occurs in both arms. These shared genes were interpreted as a DEX removal effect, and therefore subtracted from the modulated gene number displayed in Figure **52a**. This indicates that, when comparing between CD0 and CD1, there are 46 differentially expressed genes (102 total genes – 56 shared genes), while there are 149 between CD0 and MV-ON (205-56).

The comparisons with the greatest number of differentially expressed genes are MV-ON versus DIG (477 genes), CD2 versus DIG (391 genes) and CD0 versus DIG (1310 genes). Comparing these genes indicates that there is significant overlap, as indicated by the Venn diagram in Figure **52b**. Due to this overlap, and that both the clustering and PCA indicated the biggest differences were between CD0 versus DIG, these genes were further analysed. Of the 1310 modulated genes, 613 were increased and 584 reduced. The overwhelming majority of genes were protein coding (94%), with the remaining 6% shared between ncRNAs, pseudogenes and "other" (Figure **52c**). Of the 1310 differentially expressed genes, cytoscape analysis revealed 132 genes with poor or no annotation, which corresponds to 10% of the data set. The distribution of gene biotype for un-annotated genes is different to Figure **52c**, with a roughly 50:50 split between protein coding and ncRNA genes (Figure **52d**).
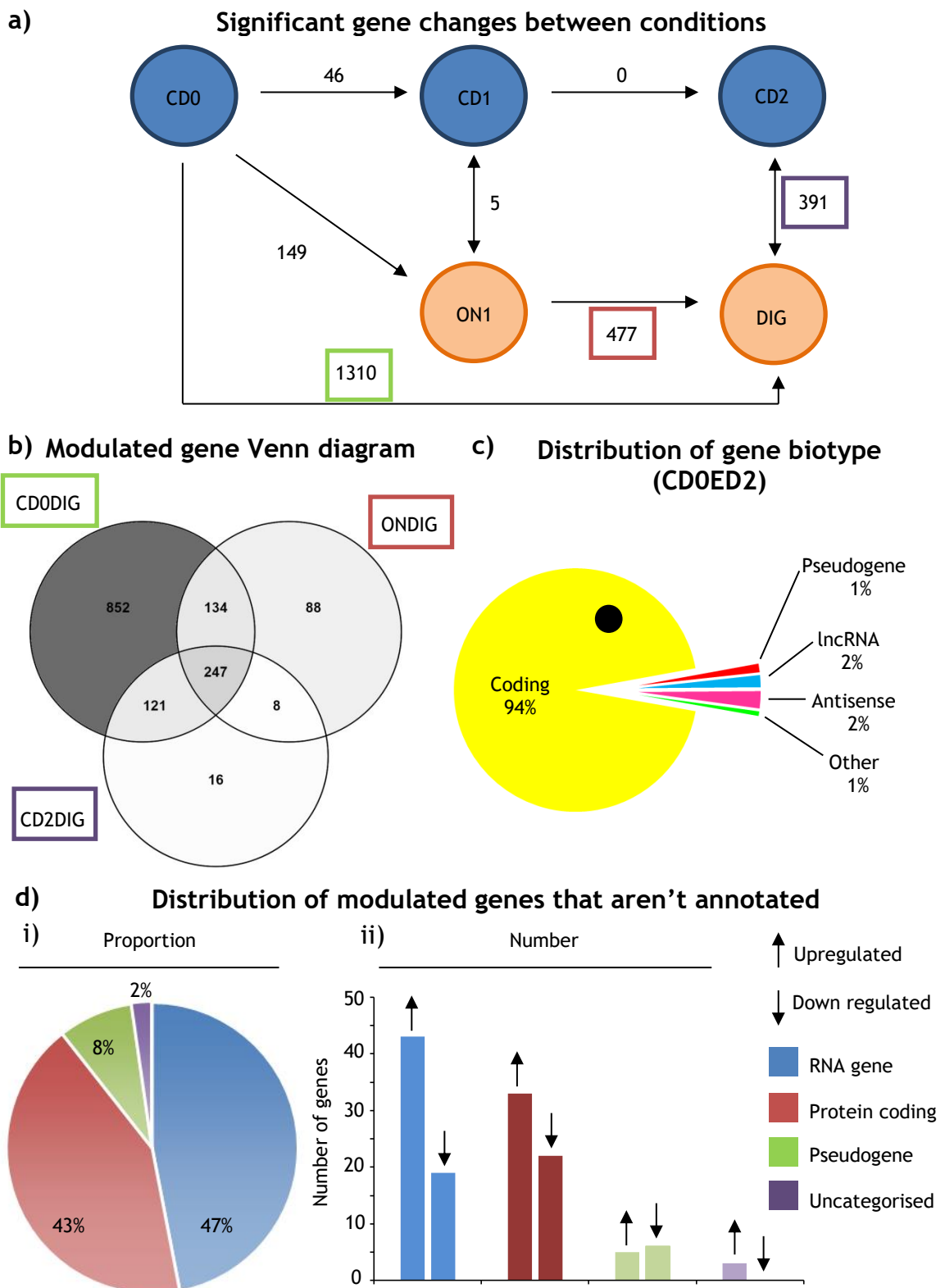
Figure 52: PCA and clustering highlight CD0 and DIG to be timepoints of interest.
a) Differentially expressed genes with a p adjusted value of $\leq$ 0.0.5 were compared between conditions (arrows), number of genes for each comparison is recorded next to each arrow; b) Venn diagram of three different comparitors from a), coloured boxes correspond to the boxes in a), where the gene numbers used in the Venn are taken from; c) Number of genes differentially expressed between CD0 and DIG are counted by biotype then expressed as a proportion of the total number of modulated genes; d) Number of genes differentially expressed between CD0 and DIG that are not annotated, counted by biotype and expressed as a proportion of the total number of modulated genes (i), exact number of expression pattern of these modulated genes (ii).

In order to address the question of how do klM respond to RBC-MVs, gene set enrichment analysis (GSEA) using a generally applicable gene set enrichment (GAGE) methodology was performed[478]. This method was used due to its ability to analyse gene data bi-directionally, that is, its ability to analyse up/down regulated genes simultaneously in the context of a pathway; other GSEA methods do not allow this. GAGE analysis generated gene ontologies (GO) which were depicted as pathways using the Pathview Bioconductor package as per Luo *et al.*[479] In the interest of space, only the top five most significantly deregulated pathways are reported (Figures **53-57**); their relevance are considered in the discussion section.
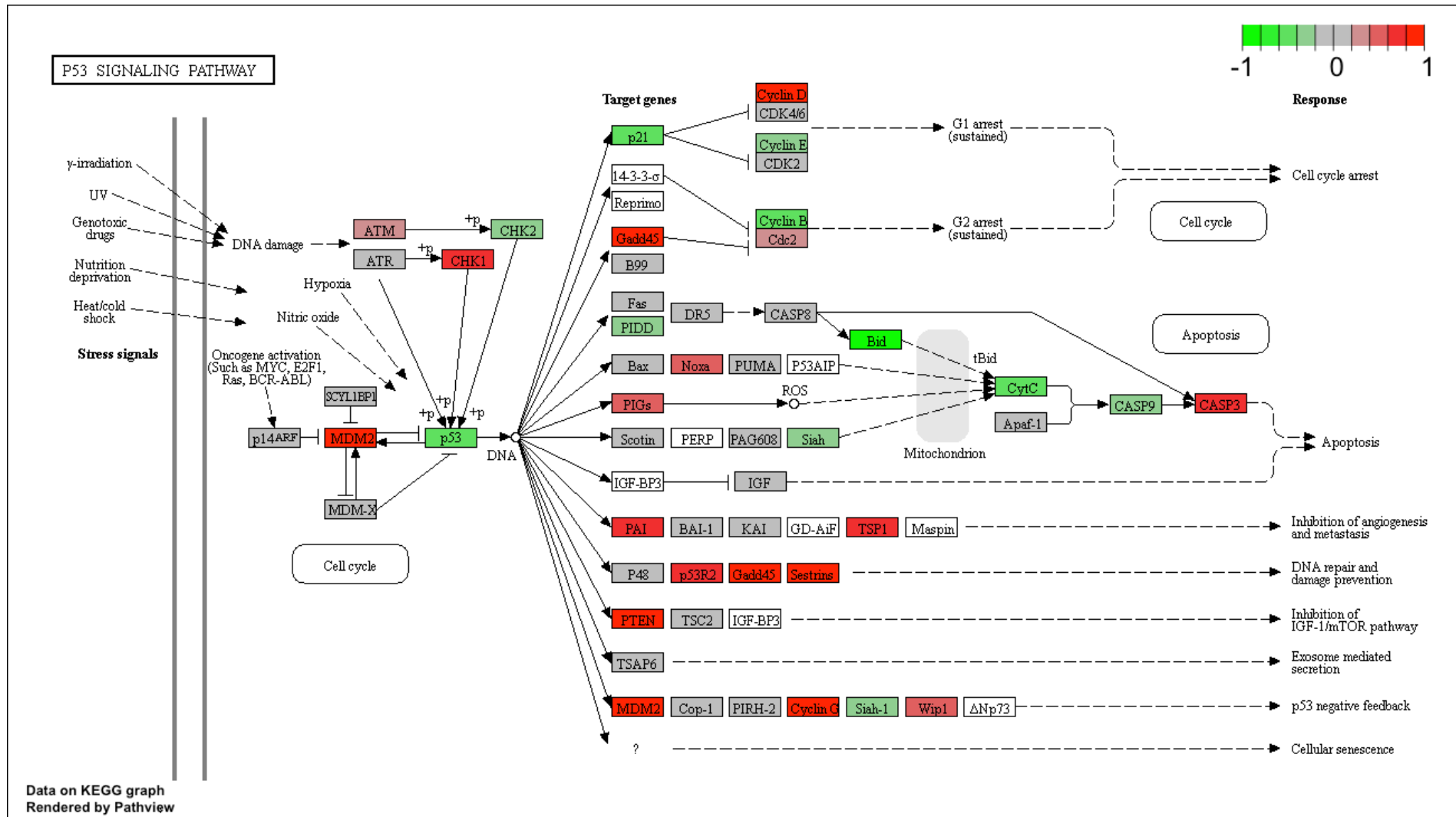
Figure 53: P53 signalling pathway.
Pathway was drawn using the Pathview Bioconductor package by Miss Ana-Maria Nastase of Glasgow Polyomics.
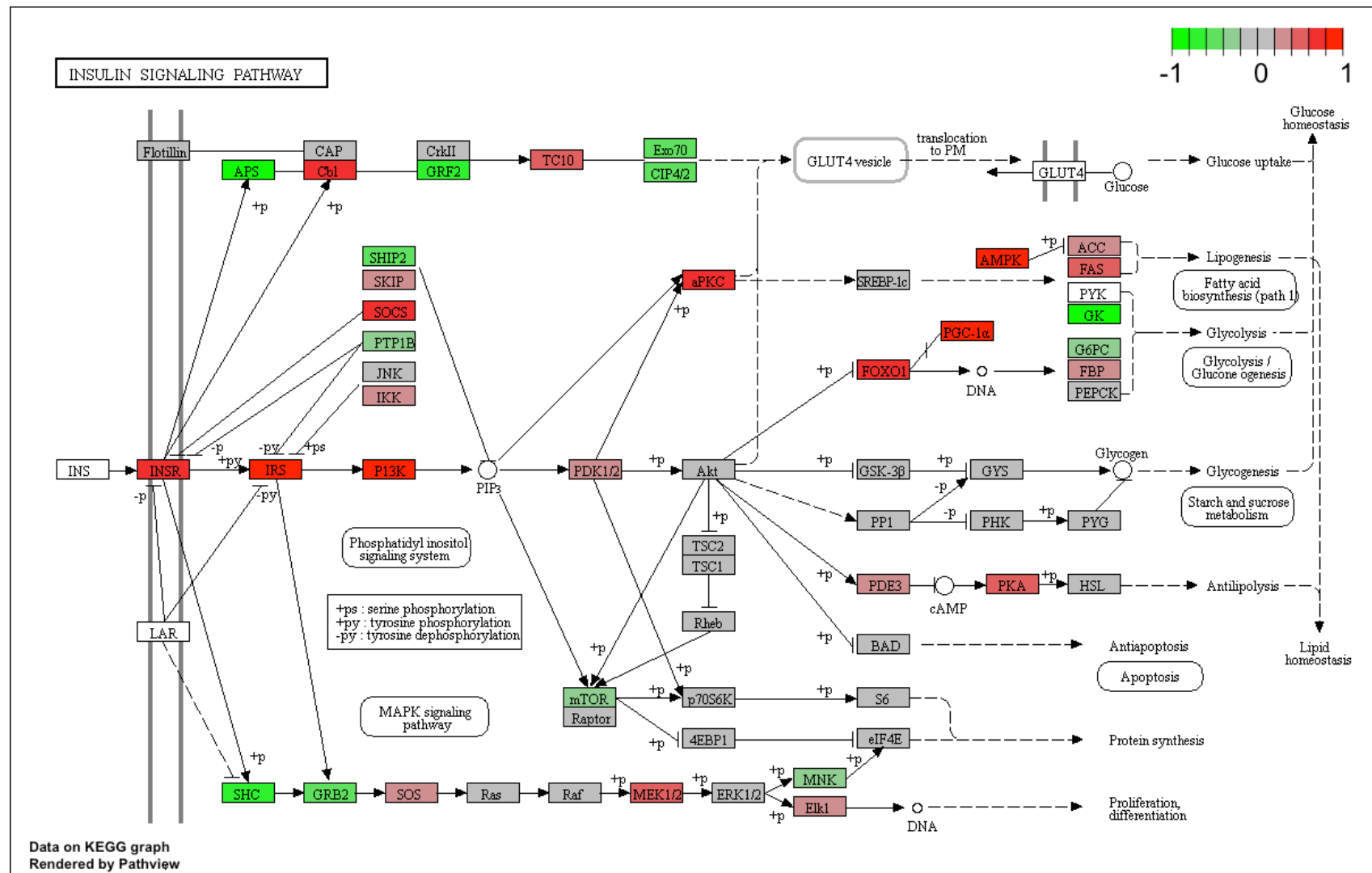
Figure 54: Insulin signalling pathway.
Pathway was drawn using the Pathview Bioconductor package by Miss Ana-Maria Nastase of Glasgow Polyomics.
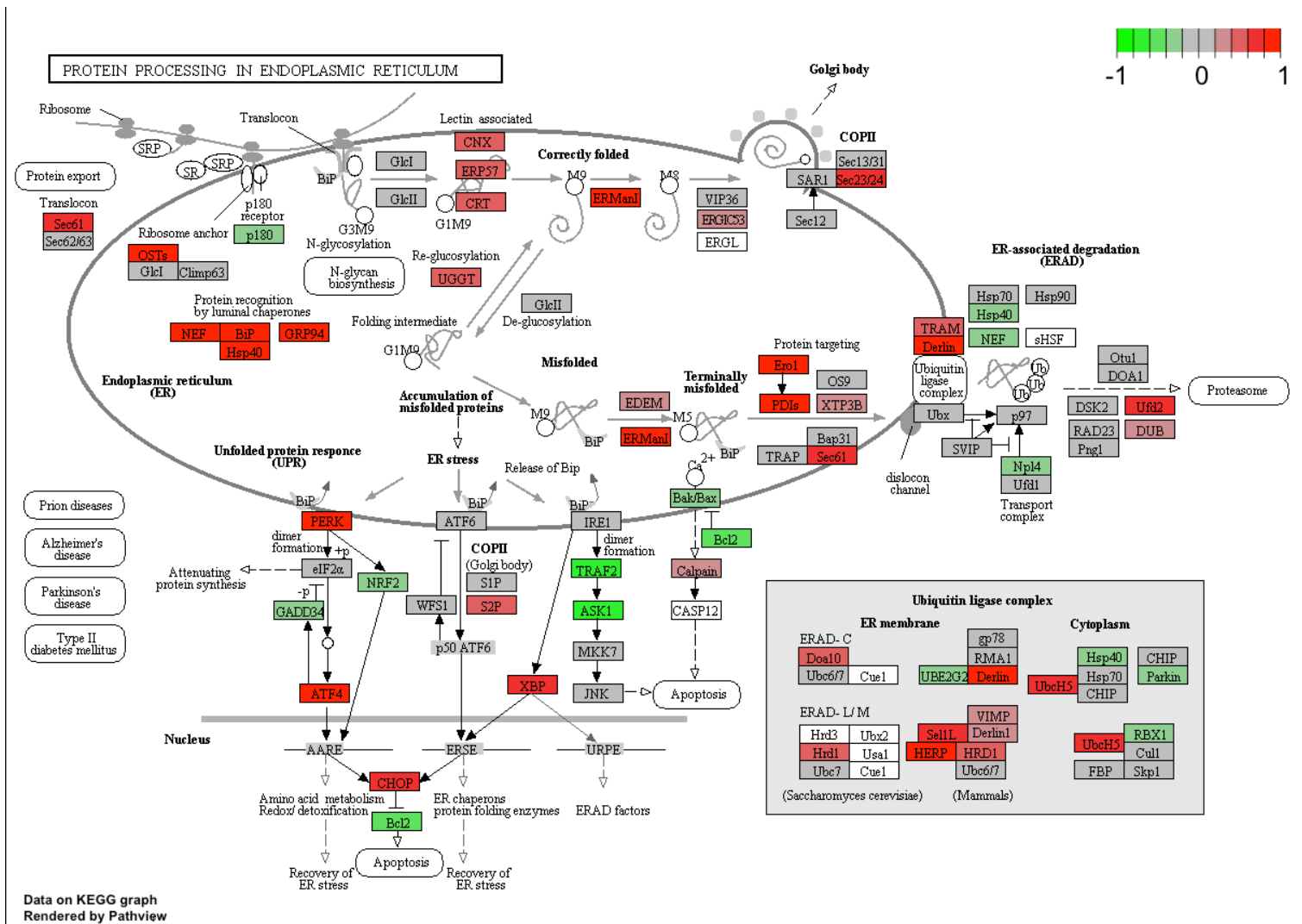
Figure 55: Protein processing in the endoplasmic reticulum pathway.
Pathway was drawn using the Pathview Bioconductor package by Miss Ana-Maria Nastase of Glasgow Polyomics.
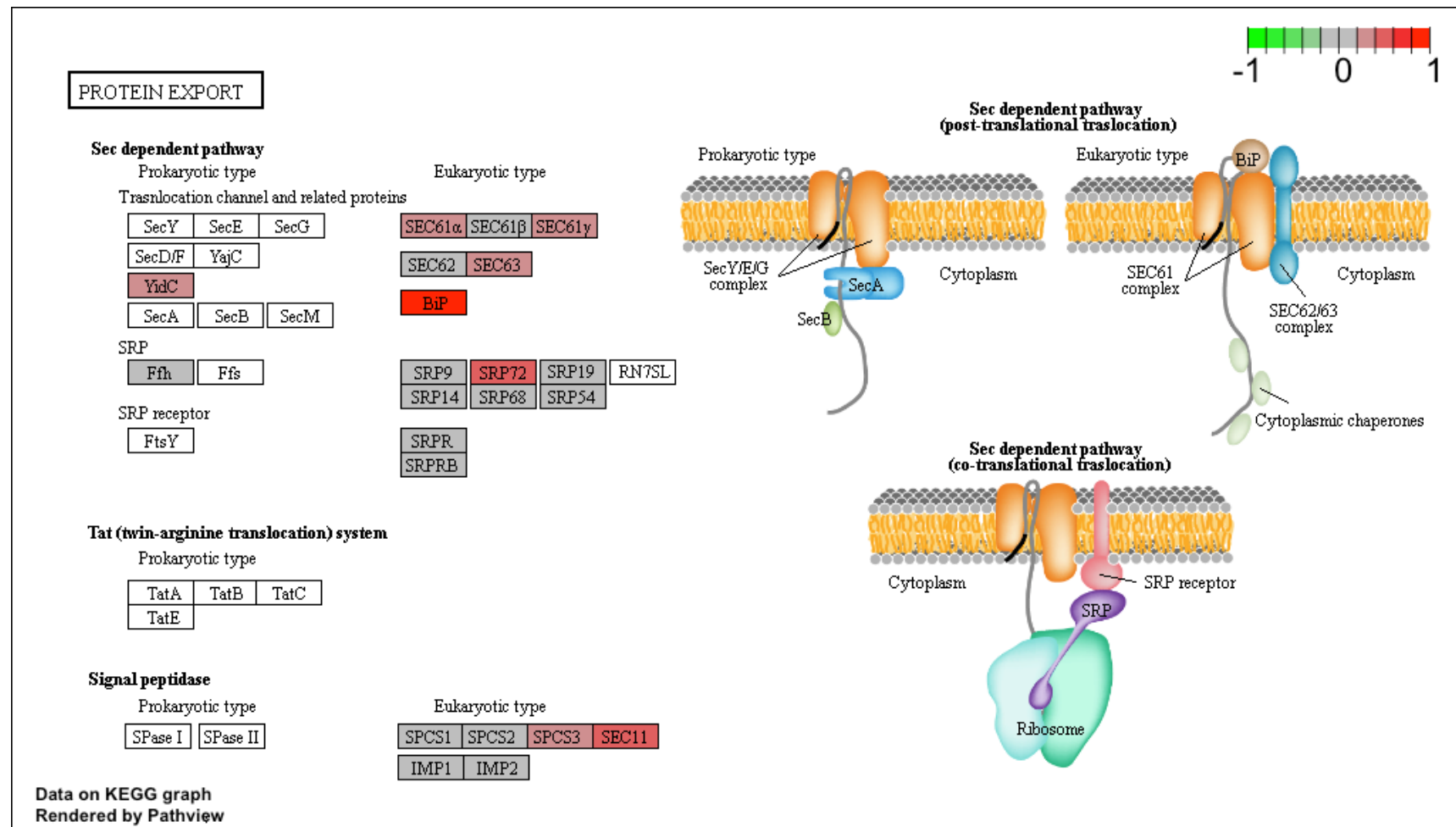
Figure 56: Protein export pathway.
Pathway was drawn using the Pathview Bioconductor package by Miss Ana-Maria Nastase of Glasgow Polyomics.
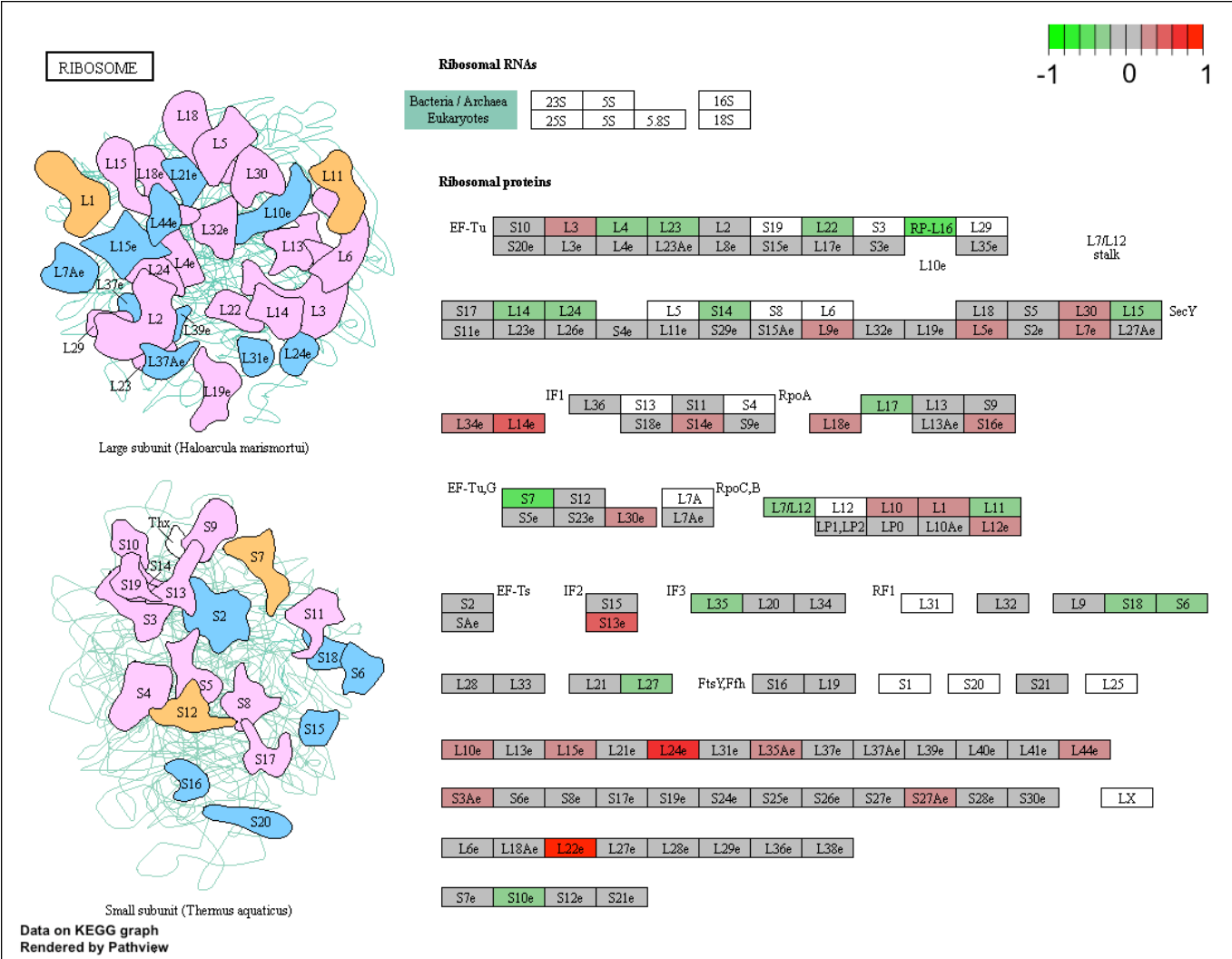
Figure 57: Structure of the ribosome.
Structure was drawn using the Pathview Bioconductor package by Miss Ana-Maria Nastase of Glasgow Polyomics.

Although pathway analysis gives a global indication of how klM are responding to RBC-MVs, it is not perfect. For example, the most dysregulated genes (up- or down-regulated) are not present in the pathways identified above. Arbitrarily using a log2 fold change of ±2, results in 14 genes being up-regulated, 11 down-regulated; of which only CCND3 is present in the pathways listed above (Figure **58a**). This is discussed in depth in Section **8.3**.

With the remaining time available, a small amount of data set validation was performed. As CD163 scavenges extracellular Hbb and is a marker of klM, this target was evaluated further as it was the 9th most upregulated gene in klM[480]. IF reveals that in untreated klM, CD163 appears to form a secondary structure (Figure **58b**). These structures appear limited one per cell and while RBC-MVs do not induce them, they do appear within this structure (Figure **58c**). Indeed, this CD163 pattern appears very similar to what was observed in Chapter 4 when live staining macrophages with acridine orange (AO). AO staining does not persist through fix and perm methodologies meaning it is impossible to co-stain klM with AO and CD163. How CD163 interacts with RBC-MVs is unclear, and unfortunately, due to time constraints, no further investigation was possible.

a) Majority of modulated genes aren't represented by GAGE analysis
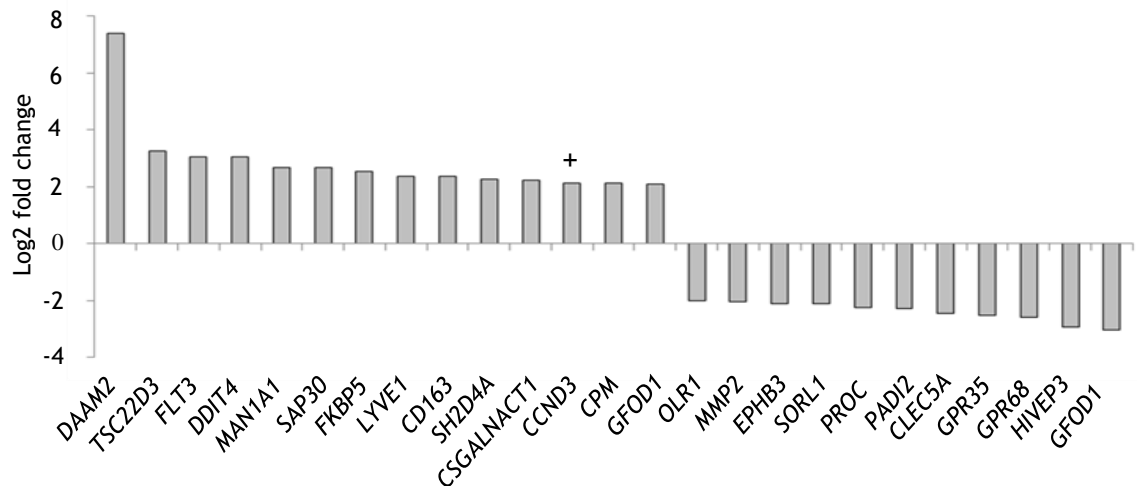
b) RBC-MVs colocalise with CD163
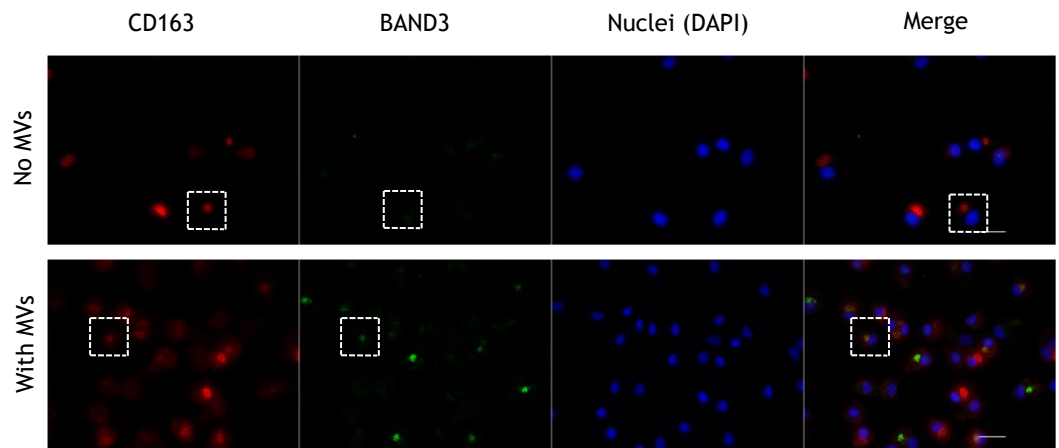
c) Accumulation of CD163 is present in no MV controls
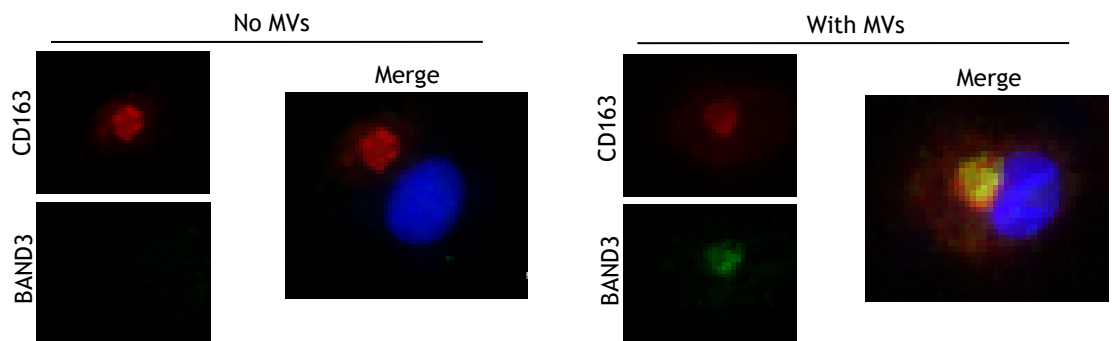
Figure 58: RBC-MVs co-localise with CD163.
a) Genes with a log2 fold change of ≥ 2 or ≤ -2, which represent the most up- and down- regulated genes, are plotted in order of expression on a bar graph, gene highlighted with a + represents the only gene highlighted by GAGE analysis; b) klM were incubated with or with out 2.5 µg of RBC-MVs for 24 hours then probed with αCD163 and αBAND3; broken white boxes indicate areas that were digitally enlarged in c). Scale bar represents 20 µm.

7.3 **Discussion**

The data generated *via* RNAseq can be used for two purposes. Firstly, to evaluate how klM respond to RBC-MVs; and secondly, to evaluate the possibility that e-miRNA from RBC-MVs are regulating the klM transcriptome. First, the question posed during the introduction of this chapter, will be discussed.

How do klM respond to RBC-MVs?

Performing RNAseq enables a more global view of how klM respond to RBC-MVs to be evaluated. From our analysis, we were able to identify key changes in the klM and identify pathways affected for future analyses. One of the key questions we set out to investigate was: Do RBC-MVs (storage breakdown products), have side effects on patients post-transfusion? However, within the confines of this model, there appears little evidence that this is the case. For example, no inflammatory or apoptotic pathways were highlighted through GAGE analysis, indicating there is no immediate negative response to MV exposure (Figures **53-57**). Indeed, the pathways highlighted appear to be more regulatory and important for cellular homeostasis and protein processing, with endoplasmic reticulum protein processing (ERPP)/ protein export two of the most highly modulated pathways. Note, while it is unlikely that RBC-MVs are involved directly in ERPP, a large portion of this pathway that is upregulated is the ubiquitin ligase complex and protein recognition. These are not unique to ERPP, and may well play a role in the disappearance of RBC-MV signal following internalisation and processing.

Cluster of differentiation (CD) markers

The data set was mined further to evaluate, at a mRNA level, any modulation of cluster of differentiation (CD) markers (Figure **59**). CD markers are used extensively in the immunology field to characterise cells with variations in expression and used as a marker for lineage priming and phenotypical changes within cells. Although our profiling indicated that resting klM represent a more M2 phenotype, we first evaluated whether internalisation and processing of RBC-MV induced any M1 inflammatory type responses. CD80/CD86 are classic markers of inflammation, but were undetected within the above data set, indicating no

classic inflammation response. Analysis of the differentially expressed CD markers is challenging as a lot are not classically associated with macrophages and thus are not well studied in this cell type. For example, CD83 although present on macrophages, is classically a DC marker, with most of the functional studies being performed on DCs[481]. The relevance of these studies to macrophages is unclear, but within DCs, it is reportedly induced through TLR signalling and promotes both the pro-inflammatory marker CD86, and the increase of major histocompatability class II proteins[482]. If its function in klM is similar to that within DCs, then its down-regulation in this data set again argues away from an inflammatory response. In addition, CD40, CD274 and CD300c are all reported by the literature to be up-regulated by the bacterial mimic lipopolysaccharide (LPS), suggesting a pro-inflammatory role[483-485]. However, they are down-regulated in the above data set (Figure **59**). LPS, as well as pro-inflammatory cytokines, don't change CD276 expression at a gene level, but are thought to augment pro-inflammatory responses[486,487]; again CD276 is downregulated in this data set (Figure **59**). Taken together, these markers indicate a dampening of any immune response. Indeed, this is borne out by the upregulation of CD72 and CD55, known negative regulators of B and T cells, respectively[488,489]. klM do appear to be responding to RBC-MVs, as indicated by an upregulation of CD70, a marker that positively correlates with macrophage metabolic activity[490]. With such a large upregulation of CD163, klM appear to be entrenching within their klM phenotype, rather than changing it.
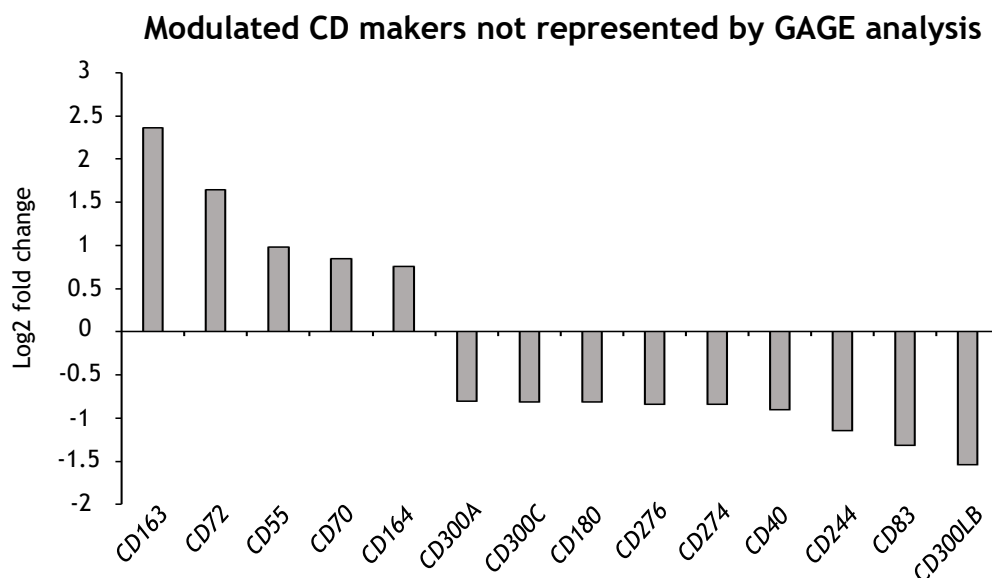
Figure 59: Expression values of all cluster of differentiation (CD) genes.
All modulated CD genes with a p-adjusted value of 0.05 plotted from highest to lowest expression.

Cytokine modulation

As per CD markers, it is also possible to look through the data to see which cytokines are modulated (Figure **60**). However, while a large number of interleukin receptors are modulated, there is little modulation of actual cytokines. In addition, it is difficult to determine what is occurring as cytokines with the same overall effect can have opposite expression patterns. For example, IL-18 is a pro-inflammatory cytokine, which is upregulated, while the two other pro-inflammatory interleukins present, IL-1b/IL-1a, are down-regulated (Figure **60**). No interferons were detected within the data set, but the receptors for class II IFN receptors (IFGR) are, but confusingly, are again contradictory. For example, IFN-γ binds to a membrane receptor comprised of IFNGR1 and IFGR2 subunits[491]. However, IFNGR1 and IFGR2 are up/down-regulated, respectively, in this data set (Figure **60**) meaning that a definitive interpretation regarding a pro or anti-inflammatory effect is impossible. Finally, TNFα is present, which is a strong pro-inflammatory cytokine, but this is also down-regulated (Figure **60**). Taken together, this data does not suggest any large-scale induction of a pro-inflammatory response. There are pro-inflammatory cytokines increasing, but this could be tempered with the parallel down-regulation of other pro-inflammatory cytokines. Interestingly, several of the receptors were up-regulated, indicative that the cells may have increased ability to respond to lower concentrations of the respective cytokines. At the end of culturing the cells for the RNA preparation and RNAseq, the media was collected and snap frozen; these could be used for cytokine profiling in the future. This would allow the establishment of exactly which cytokines are being released, and their concentrations; allowing for a true gauge of inflammatory profile. Due to time and monetary constraints, these samples were not analysed during this project.

Modulated cytokine or cytokine receptors not represented by GAGE
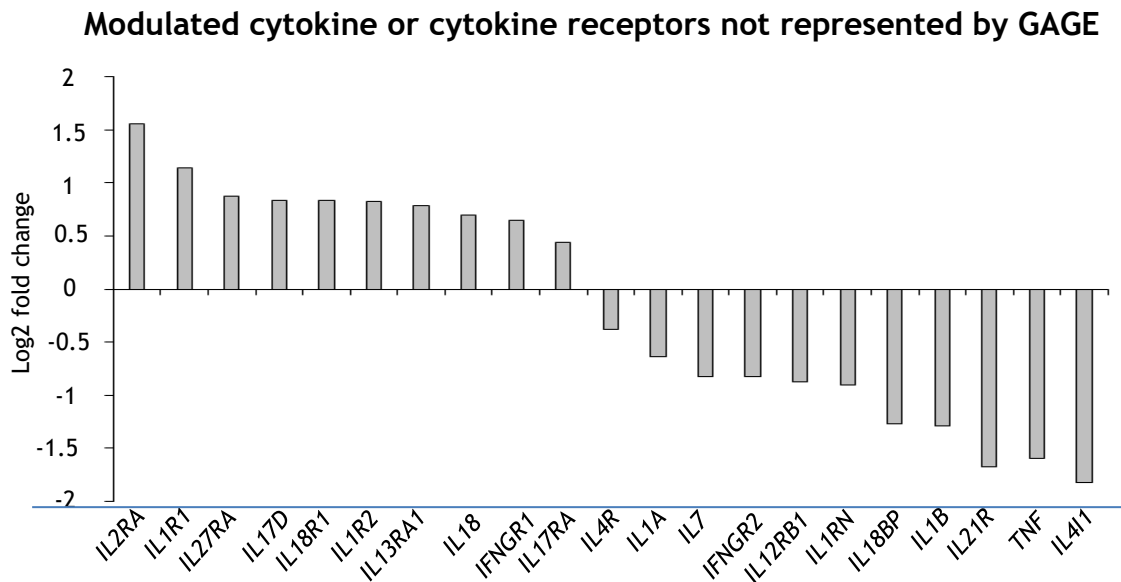
Figure 60: Expression values of cytokine and cytokine receptor genes.
All modulated cytokine or cytokine receptor genes with a p-adjusted value of 0.05 plotted from highest to lowest expression.

Other interesting genes

Simply looking at the most modulated genes to try and establish klM response is also possible (Figure **58a**). *DAAM2* is the most modulated gene with a log2 fold up-regulation of 7.39. Interestingly, *DAAM2* is a formin, which bind actin and play a role in cytoskeletal re-arrangement; something that is required for RBC-MV uptake (Chapter 4, Figure **42b**)[492]. Within macrophages, it has also been reported by multiple studies to play a role in the phagocytosis of *Borrelia*, an interpretation of this is that klM are up-regulating their endo/phagocytic potential[493]. Other than CD163, discussed separately, the remaining genes that are highly modulated do not suggest any additional macrophage response/phenotype that has not already been discussed. For example, *FKBP5* and *TSC22D3* are associated with anti-inflammatory responses within macrophages and are up-regulated within this data set (Figure **58a**)[494]. While *OLR1* and *CLEC5A* are associated with a pro-inflammatory response and are down-regulated (Figure 8a)[495,496]. These genes reinforce the interpretation that there is no pro-inflammatory response present and that klM are more akin to M2 cells than M1, with RBC-MV internalisation and processing not eliciting any M1-like responses. Indeed, the upregulation of *FLT3* in this data set has been associated with enhancing macrophage survival[497], further suggesting no adverse effect of RBC-MV.

<u>CD163</u>

CD163 is one of the most up-regulated genes within this data set. While it has been studied, most papers simply use it as an "M2" marker. *DDIT4* is a suppressor of mTOR activity, which within macrophages, prohibits polarisation[498,499]. In this data set, it is upregulated suggesting polarisation is being inhibited. This, coupled with increased CD163 expression, strongly suggests that treated macrophages are remaining Kupffer-like. Again, suggesting that RBC-MVs are not causing any major changes to the phenotype of the cells, i.e. by adjusting polarisation or inducing inflammation. Indeed, all data discussed so far indicates that this is the case. It is tempting to suggest that any potential pro-inflammatory effects associated with transfusion are not caused by RBC-MVs. However, this is premature, as these conclusions can only be suggested within the context of this *in vitro* model and the scenario *in vivo* may be different due to the complexity and the interplay between different components of the immune system.

While not addressing the initial question, this data set may be suitable for establishing CD163 functionality. IF within Figure **58b** shows that CD163 forms a structure within klM which is independent of RBC-MVs. The distribution of this signal is very similar to that observed by AO staining within Chapter 4, and as discussed previously, has not been reported within macrophages. This raises multiple questions. First, why has this not been reported before, even though IHC analysis has previously been used to detect CD163 successfully in macrophages[500]; note the referenced paper demonstrates CD163 staining for splenic and hepatic macrophages, which is an appropriate comparator to klM. However, detection utilises 3,3'-Diaminobenzidine (DAB) deposition, which is a crude method of staining and masks any subtleties, such as structure, reported by IF. Additional studies have performed CD163 IF, but the signal observed was similar to that by DAB[501,502]. A potential explanation for the discrepancy between Figure **58b** and these studies is the fix and perm methodology utilised. For example, my preliminary work indicates that macrophages are sensitive to fix and perm methodologies. Traditional PFA fixation followed by Triton-X permeabilisation abrogates CD163 structure. It is only maintained when using digitonin, a much milder detergent[503]. The three referenced studies all use paraffin embedded

tissue that is subjected to ethanol rehydration and antigen retrieval, a particularly harsh combination that may have eliminated any nuance.

Interestingly, there is one paper that appears to record CD163 localisation in a similar conformation to that which we demonstrate in Figure **58a**[504]. However, this study was performed by stably expressing different CD163 isoforms in Chinese hamster ovary (CHO) cells, not macrophages. Nonetheless, Moestrup *et al.* demonstrated an apparent cytoplasmic structure that is very similar to that observed in Figure **58b**. To my knowledge, this distribution has not been reported within macrophages, the cell type CD163 is a marker of.

If this structure is not an artefact, what is its purpose? Although it appears to be RBC-MV independent (present in no MV controls), RBC-MVs do appear to localise within this structure, suggesting it plays a role in MV processing. Moestrup *et al.* were the first to report CD163's Hbb scavenging role, although this does not appear to be happening here, as in their study, CD163 is membranous whereas in klM it appears to be localised in the cytoplasmic vacuole[333]. Note that the lack of CD163 at the membrane maybe an artefact as these macrophages were phenotyped as CD163$^+$ *via* FACs (Figure **39b**).

Consulting the literature for CD163 reveals no reports of it forming any secondary structure in macrophages, meaning what is reported in Figure **58b** is novel. CD163 is part of a scavenging receptor cysteine rich (SRCR) superfamily of scavenging receptors, more specifically, type II. There are 9 members within this family, which are categorised by having multiple SRCR domains; CD163 contains 9. Reviewing the literature for the other type II members reveals they are unsurprisingly similar to CD163 in that they are external receptors that recognise specific signals[505]. They are capable of being internalised and forming endosomes, but this always occurs following treatment, and there is no report of any other member forming the secondary structure observed in Figure **58b** natively. Simply comparing to other members within the group has not shed any light on its localisation. If this is genuine, as it appears, then it seems to be a completely novel phenomenon. Although not related to the transfusion question, this does appear interesting and may well be of interest to the wider scientific community. Further work would include establishing what CD163 interacts with *via* pull-downs, establishing which transcript variants (CD163 has 2) are present etc.

<u>Transcriptional regulation by e-miRNA</u>

A hypothesis evaluated during this project was the possibility that e-miRNA could modulate the transcriptome of a recipient cell: in this case, klM. As a first pass, it is possible to mine the RNAseq data to see which down-regulated genes are either predicted to be, or validated targets of, known e-miRNA. To perform this analysis, all genes down-regulated by a log2 value of $\leq$ -2 were compared against the most abundant e-miRNA. Most abundant e-miRNA were defined as, any e-miRNA from the Hamilton lab's erythrocyte sequencing data having a read count of $\geq$ 1x10^4. This resulted in 11 genes (Figure **58a**) being scrutinised by 23 e-miRNA (Figure **61**). First, a prediction methodology using miRDB was performed, but no candidate e-miRNA-gene interactions were identified. As miRNA prediction is poor, a second option was used: miRTarBase V2.0. This is more stringent than miRDB, as all results generated are validated with links to the appropriate study within the literature. This analysis resulted in 2 genes being targeted by 2 e-miRNA: Matrix metaloprotein 2 (*MMP2*) and oxidised low density lipoprotein receptor 1(*OLR1*).
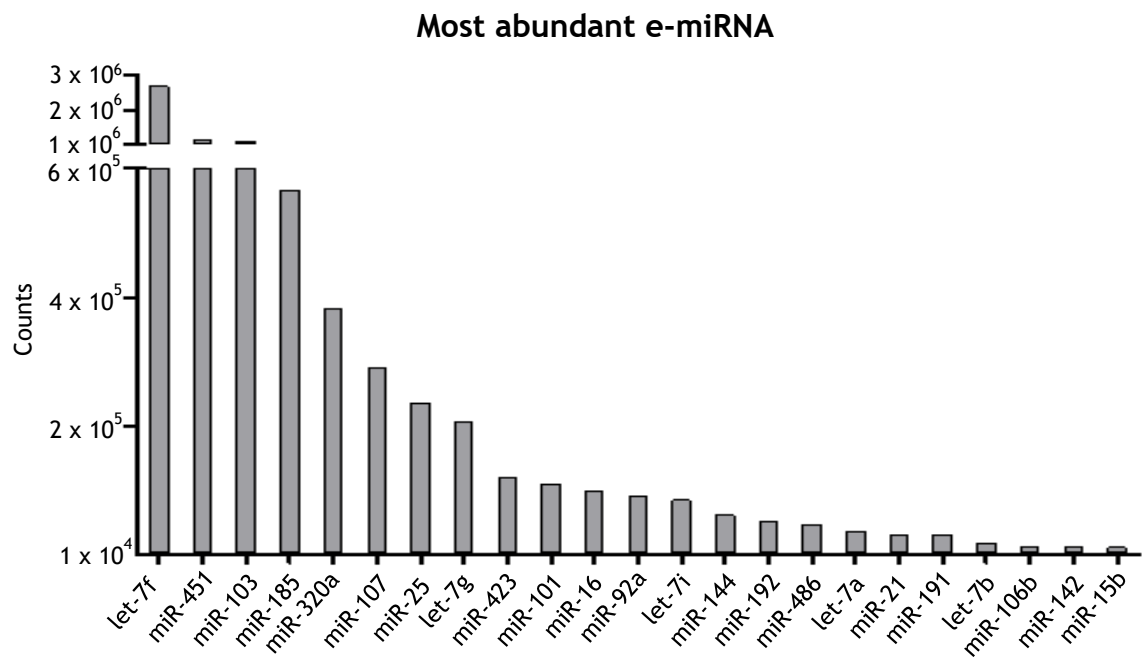
Figure 61: Most abundant e-miRNA.
All e-miRNA with an expression value of $\geq$ 1 x 10^4 counts from the Hamilton lab's sequencing experiment and used to scruitinse the most down-regulated genes from this chapter's data set.

MMP2 has been reported to be regulated by both miR-21 and miR-451[506,507]. A note of caution though, the papers cited in these studies do not show *MMP2* to

be direct targets of these miRs. Indeed, the study by Tanaka *et al.* demonstrated that miR-21 expression positively correlated with *MMP2*, something that is unlikely in our model as *MMP2* is down-regulated[506]. Kang *et al.* did note a reduction in *MMP2* when over-expressing miR-451, but this was in conjunction with three other members of the *AKT* signalling cascade, leading them to believe that *MMP2* downregulation was downstream of *Akt* and not a direct miR-451 target[507]. A suggestion given by the authors was based on Godlewski *et al's.* study that showed *CAB39* to be a direct target of miR-451[508]. However, this target was predicted and tested for in Chapter 4 Figure **49** and was not shown to be modulated upon MV treatment, making it unlikely to be the reason for *MMP2* regulation in this data set. *OLR1* was shown by microarray to be down-regulated by miR-21, but this target was not of interest to the authors so was not further investigated, so its role in regulating *MMP2* remains undefined[509]. Interestingly, the fact that none of these three studies showed direct interactions might be the reason for the discrepancy between miRDB and miRTarBas. miRBD predicts direct targets of miRNAs, while miRTarBase allows for downstream effects to be counted as direct regulation.

<u>Conclusion</u>

Two questions were addressed by this RNAseq data, firstly, the potential transcriptional regulation by e-miRNA, and secondly, how klM respond to RBC-MVs. KlM response is of clinical interest, due to their involvement in transfusion, but there appears to be no adverse effect caused by RBC-MVs. Instead, klM appear to recognise and process them. This lack of inflammatory effect correlates with a recently published paper[510].

Initial work regarding e-miRNA gene regulation did highlight potential candidates. However, upon deeper scrutiny, two of the three targets do not appear relevant to this system. The final gene (*OLR1*) may well be a target for miR-21, but there was insufficient time to test this hypothesis.

In conclusion, the most interesting aspect of this data set is the upregulation of CD163 and the subsequent localisation observed by IF. How it relates to the other modulated genes within this data set may well result in a novel function for CD163. However, this is just one gene, and there are multiple genes highlighted

by this study. For example, *MS4A4A* was not picked up by GAGE analysis but was reported as a novel marker for M2 macrophages only two weeks before this chapter was written[511]. Interestingly, only two years prior Cruse *et al*. demonstrated that in mast cells *MS4A4A* played a role in endocytic recycling, a potential explanation for what is occurring to RBC-MVs[512].

Final discussion

The initial aim of this project was to investigate the possibility that e-miRNA may have a non-canonical role within erythrocytes. However, due to the results in Chapter 2, in addition to studies published during this project, this hypothesis was changed and others formulated. Each chapter contains an in-depth discussion of the results, the reasons for my interpretations, the limits to my interpretations and how it relates to other published work. Therefore, this discussion will act as an executive summary for the overall project and what further work could be performed if desired.

8.1 Function of e-miRNA within erythrocytes

Due to the obvious difficulty in predicting non-canonical miRNA functions, pull downs were performed to see if interacting partners could shed light on any potential function for e-miRNA. However, this methodology failed to identify any proteins, other than a modified AGO2, meaning that the formulation of new hypotheses was not possible. Data generated in Chapter 4 suggests that e-miRNA are lost as cells age – something that was also reported as this work was being performed[400]. This would indicate that e-miRNA having a non-canonical function within erythrocytes was incorrect.

That said, this work did highlight that on occasion (not always seen), AGO2 runs at a higher molecular weight than predicted and none of the published AGO2 post translational modifications readily explain what this modification could be[411,415]. Interestingly, this AGO2 doublet has been observed in other studies, although what causes it is still to be determined. That this is observed in multiple studies demonstrates that this is not a phenomenon specific to erythrocytes, or, a technical abnormality caused in this lab. That one group sequenced it (Meister lab), also indicates that there is an interest in what it could be[411]. However, the Meister lab only managed a sequence coverage of ~6 %, which is a lot less than the ~23 % generated during this study, suggesting it is difficult to sequence this protein. Therefore, different sequencing strategies could be attempted, for example, Edman degradation could be used on trypsinised hmwAGO2, which may enable more complete coverage[513]. Although this modification is not specific to erythrocytes, RBCs could still be used as a model due to the abundance of AGO2

within these cells and the amount that can be easily/cheaply harvested. The relevance of this to the wider scientific community is entirely dependent on what the modification is, and what it signifies. However, in my opinion, this avenue of research would be of interest to the wider scientific community.

8.2 Function of e-miRNA modulating a different cells transcriptome

A specific hypothesis that was tested, was that e-miRNA could regulate the transcriptome of a different cell i.e. macrophages. Although modulation was not seen in macrophages treated with RBC-MVs, this hypothesis was not tested in macrophages that had internalised senescent erythrocytes. However, how much e-miRNA is left within a senescent RBCs? The data in Chapter 4 suggests that while reduced, some e-miRNA are still present; although this presence maybe due to impure fractionation of RBCs. Certainly, it is unlikely that all e-miRNA are lost due to membrane-associated vesicularisation, as Basu *et al*. report some AGO2 associates with the cytoskeleton, something RBC-MVs do not contain[344,422]. Therefore, it is certainly possible that residual e-miRNA persist in senescent RBCs. Is this enriched for a specific e-miRNA, or is it simply an amalgam of all e-miRNA? The hypothesis of e-miRNA acting as a molecular signal is certainly attractive, however, I am undecided on whether I would continue this work. There is no evidence to suggest so far that this hypothesis is valid and using Occam's razor, the most facile explanation for e-miRNA is that they are simply an artefact of maturation.

8.3 Possible side effects of RBC-MVs on transfusion patients

The final area that was investigated during this PhD was the effect of a storage artefact (RBC-MVs) on an appropriate cell type: klM. However, the RNA-seq indicated no inflammatory (pro- or anti-) effect on these cells. It is entirely possible that the model generated simply isn't suitable, although the most recent publications within the medical field report no adverse effects regarding the transfusion of aged blood products, which is in agreement with my data[510,514]. Media samples were taken for cytokine profiling, which is still possible as they are

frozen, although in light of these aforementioned studies it doesn't seem a fruitful avenue to pursue at present.

More interesting are the RNAseq results, both the poorly annotated data and CD163. That CD163 appears to form secondary structures within macrophages and is involved in MV processing is very interesting. A potential method that could be informative would be to express a GFP-CD163 fusion within THP-1 or RAW264.7 cells. While not primary cells, as observed in Chapter **6**, creating a stable cell line would allow the live cell imaging of macrophages, which would be interesting to evaluate in context of phagocytosis. Macrophage biology is clearly an area of interest to the scientific / medical community, so this work would certainly have an audience if more detail could be gained[515].

8.4 Final words

Although I believe there is some genuinely interesting and novel data within this thesis (hmwAGO2, CD163), the majority of this PhD has tested hypotheses that proved to be incorrect. Indeed, one could be mistaken for believing that this thesis represents an elegy to Huxley, who once so aptly said:

"The great tragedy of science – the slaying of a beautiful hypothesis by an ugly fact" – Thomas Huxley

Appendices

Appendix 1: 20 most abundant human e-miRNA

Legend: let-7f, mir-451, mir-103, mir-185, mir-320a, mir-107, mir-25, let-7g, mir-423, mir-101, mir-16, mir-92a, let-7i, mir-144, mir-192, mir-486, let-7a, mir-21, mir-191
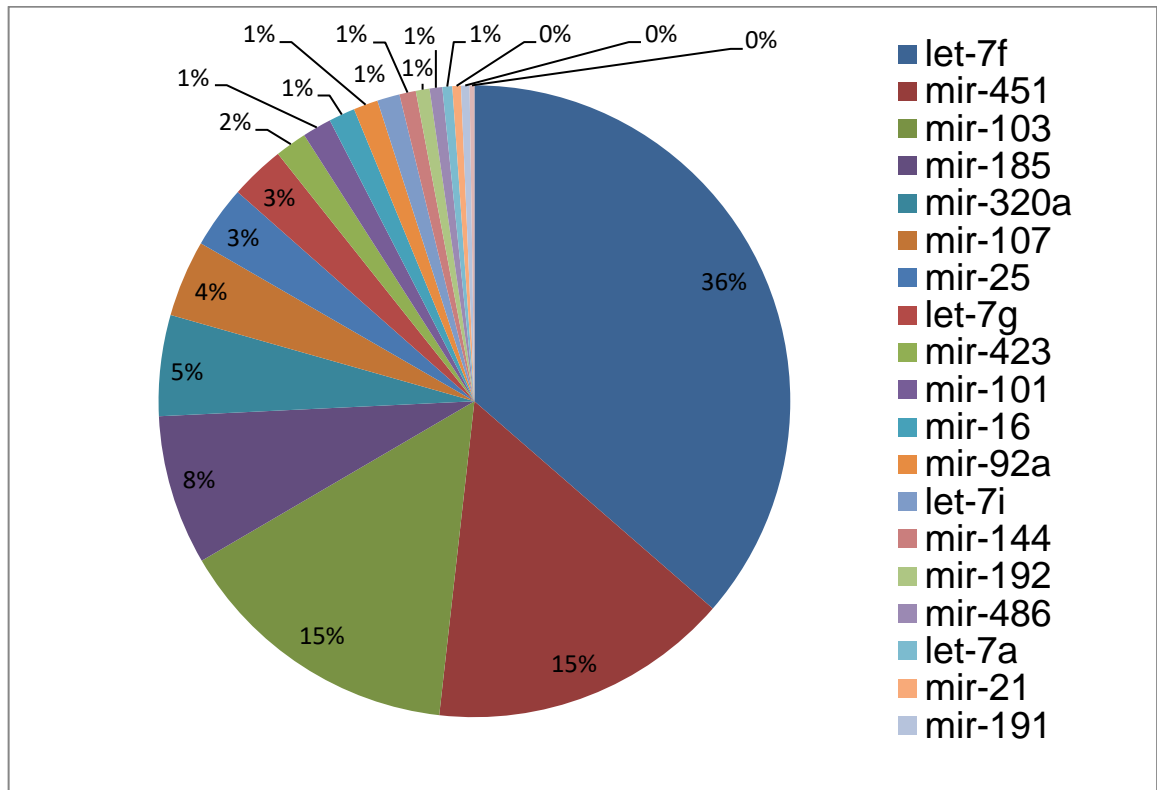
Appendix 2: 20 most abundant bovine e-miRNA

Legend: let-7f, mir-451, mir-103, mir-185, mir-320a, mir-107, mir-25, let-7g, mir-423, mir-101, mir-16, mir-92a, let-7i, mir-144, mir-192, mir-486, let-7a, mir-21, mir-191
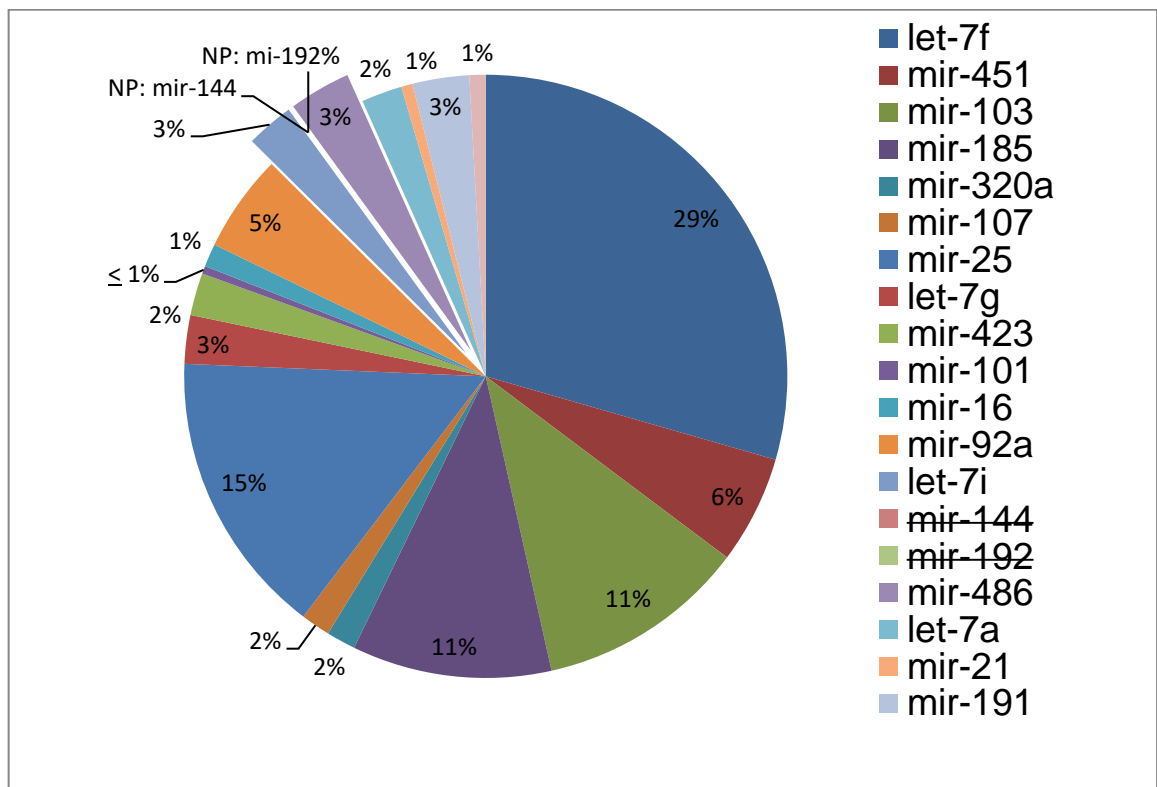
Scored out are not in top 20 human e-miRNA

Appendix 3: 20 most abundant murine e-miRNA
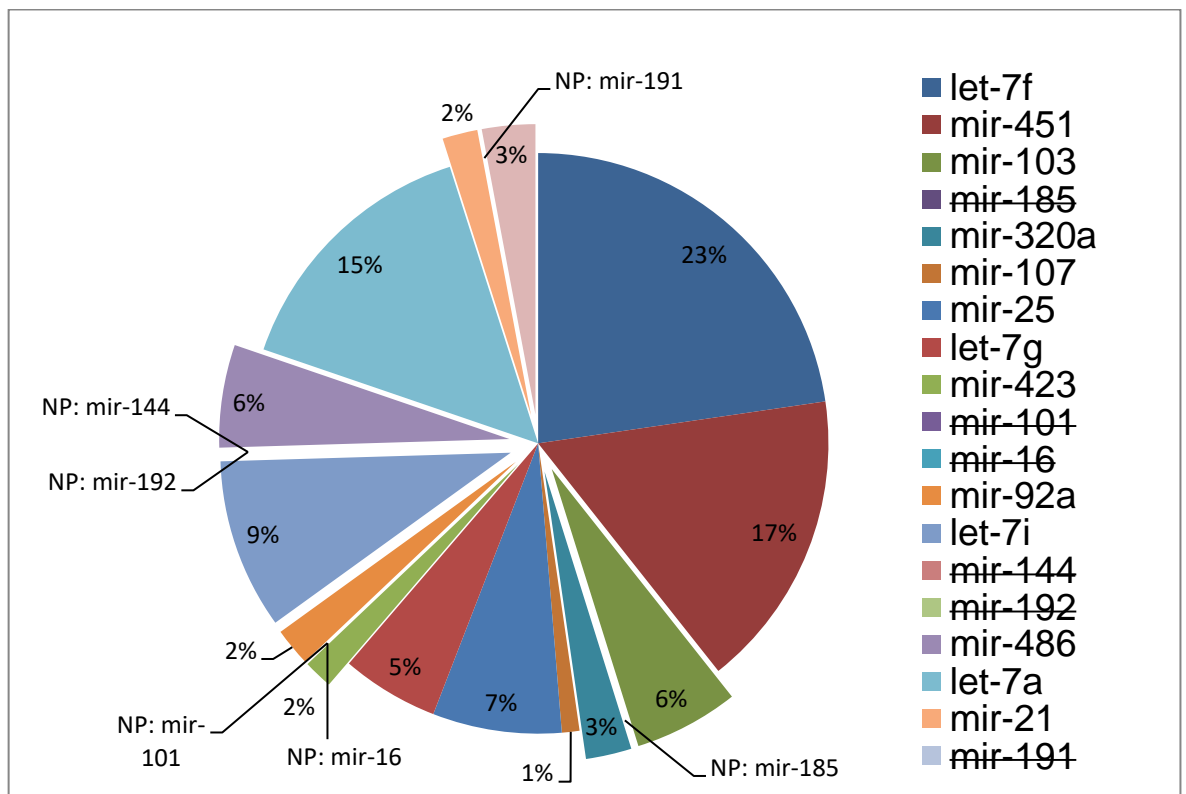
Scored out are not in top 20 human e-miRNA

Appendix 4: 20 most abundant ovine e-miRNA
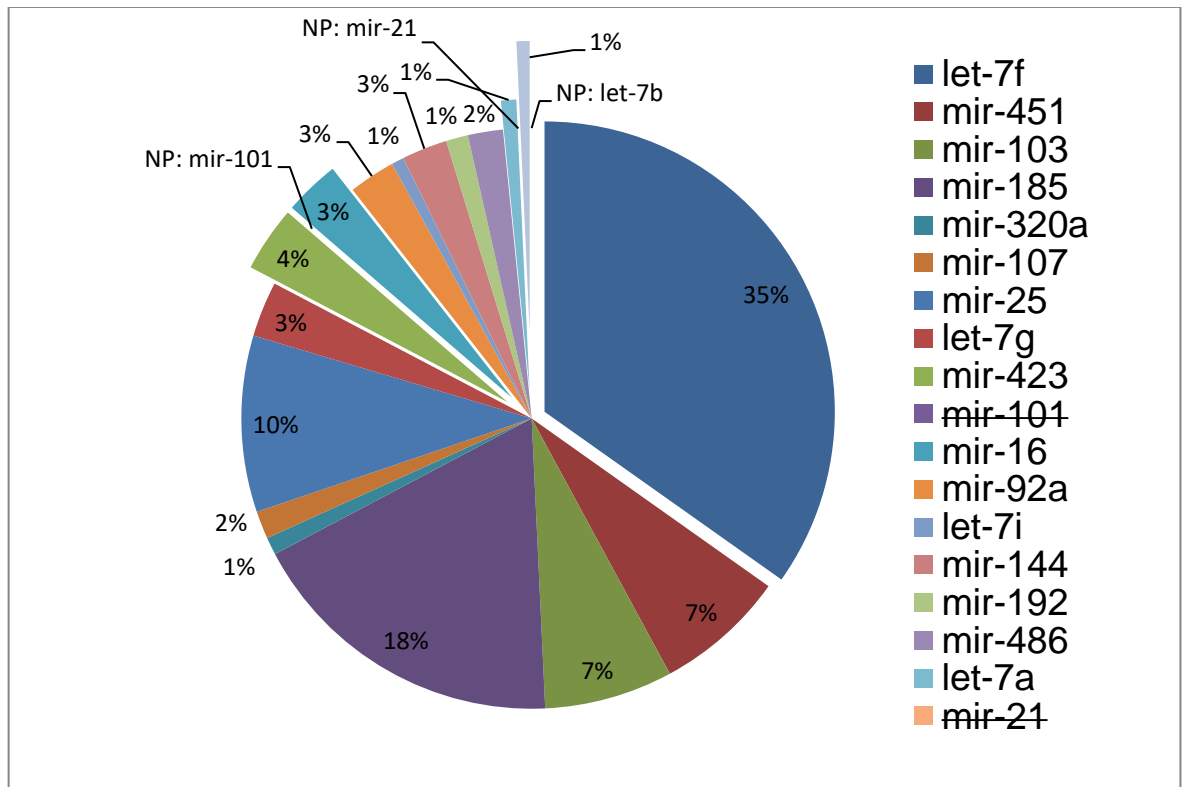
Scored out are not in top 20 human e-miRNA

Appendix 5: Sequences of housekeeping primers

Gene	Forward primer	Reverse primer	Amplicon size (bp)
B2M	TTG TCT TTC AGC AAG GAC TGG	ATG CGG CAT CTT CAA ACC TCC	172
ENOX	GAG CTC GAG GGA ACC TGA TTT	CAC TGG CAC TAC CAA ACT GCA	123
TYW1	ATT GTC ATC AAG ACG CAG GGC	GTT GCG AAT CCC TTC GCT GTT	170

Appendix 6: Primer sequences

Gene	Forward primer	Reverse primer	Amplicon size (bp)	UPL* probe ID
ATF2	TTT GGT CCA GCA CGT AAT GA	CAA ACC CAC TTC TTC ACA GTT TT	90	5
EMSY	CTA AAC TGG TAA CCA CTC CTA CTG G	TGC TAC CAC TCG TAG TTT TCA CAT	126	1
CAB39	GAG TCT TGA AGG CCT GAT GG	CTC CGC CTG TGC TAC CTC	63	55
LYSMD4	AGA AGG GAC TTG GAG GGA AG	ACA ATT CCT CGT GCC TCA TT	129	1
MIF	ACC GCT CCT ACA GCA AGC	CGC GTT CAT GTC GTA ATA GTT G	95	40
PSMB8	CCC TAC CCA CCC CTG TTT	CAC CCA GGG ACT GGA AGA	69	1
SAMD4B	GTC ACT TCT GAA ACG GGT CAC	GGA CTC CTG CTG CCA CTG	145	1
TSC1	ACT GAA GTA CCA GTT GTC GCT AGA	GCC ATT CTC TCG CTC GAA	113	1
14-3-3-ζ	TCC AGG GAC AGA GTC TCA GC	AGC TCA TTT TTA TCC ATG ACT GG	126	74
HO1$^\Delta$	AGG GTG ATA GAA GAG GCC AAG ACT	TTC CAC CGG ACA AAG TTC ATG GC	322	NA
FER$^\Delta$	ACA TAA ACA TGA GCT TCT GAC C	CAA CAA CAA CAA TCC AAT CCC	143	NA
NAB2	TGG GCT CAA GAA TCT GAA CCT	ATT GCC AAC ATC GTC CCA GA	145	NA
Cat-D	GGT GCT CAA GAA CTA CAT GG	ATT CTT CAC GTA GGT GCT GG	195	NA
IL7R	CAA TAT GAG AGT GTT CTA ATG GTC AGC	CCT CAA CTT GCG AGC AGC	162	NA
EGR1	TGA CCG CAG AGT CTT TTC CT	TGG GTT GGT CAT GCT CAC TA	201	NA
EGR2	CTG ACA CTC CAG GTA GCG AG	GTT GAT CAT GCC ATC TCC GGC	235	NA
GCSFR	AAG CAT GTC CCC ACA ACT GTG TC	TGA TTA TGT GCA GGC CTG G	158	NA
IRF8	CCA GGA CTG ATT TGG GAG AA	AGT GGC TGG TTC AGC TTT GT	162	NA

* UPL = universal probe library, Δ primers designed by Vallelian *et al.*[455]

Appendix 7: Capture probes used within this project

Target	Sequence	Oligo origin
miR-16	Bi* - AAA ACG CCA AUA UUU ACG UGC UGC UAA AAA	Synthetic
Let-7b	Bi - AAC AUG GAG AAA UCC AUG UUA ACC ACA CAA CCU ACU ACC UCA UUG UAC CUU UCG AGG UAC AA	Synthetic
Let-7f	Bi - AAA AAA CUA UAC AAU CUA CUA CCU CAA AAA	Synthetic
EB3	Bi - AAA ACA UGC GGA CCA CCA GCU GGU ACU UG	Synthetic
miR-451	UUU GGC AAU GGU AAU GAC UCA A	IVT*
miR-34c	CGU UAG UCG AUU GAU GUG ACG GA	IVT

* IVT = *in vitro* transcription, Bi = biotin

Appendix 8: *Taq*Man® Assays used within this project

Target	Assay ID
miR-92a	000431
miR-451	001105
miR-486	001278

Appendix 9: Removal of leukocytes from platelet free blood using in-house cellulose columns
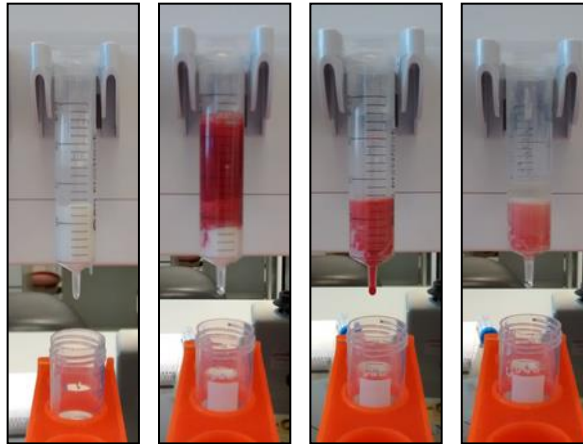
Figure 62: Leukodepletion of platelet ablated / washed RBCs.
(a) A small portion cotton wool pad is placed at the bottom of a 15 mL syringe barrel and 2 g of 1:1 mixed (*w/w*) α-cellulose / Sigma cellulose is layered on top then wetted with RBC wash; (b) 1 mL of platelet ablated compact RBCs is mixed with 10 mL of RBC diluting buffer, layered on top of the packed column and allowed to pass through by gravity filtration; (c) RBCs retained in the filter are removed by passing 15 mL of RBC wash through; (d) some residual RBCs are left within the filter, but the majority are eluted.

Appendix 10: Typical results when analysing processed blood *via* the Hemavet MULTI-TROL™ blood analyser

Cell type	Normal range	Before	After
Neutrophil[1]	1.5 – 8.1	2.27	-
Lymphocyte[1]	1.0 – 4.4	1.80	-
Monocyte[1]	0.1 – 1.0	0.42	-
Eosinophil[1]	0.0 – 0.6	0.32	-
Basophil[1]	0.01 – 0.3	0.01	-
Platelets[1]	150 – 400	209	12
Erythrocytes[2]	3.6 – 6.0	4.16	3.77

1 – thousand cells / μL
2 – million cells / μL

Appendix 11: Antibodies used within this project

Antibody	Company	Experiment type and dilution factor			Conjugate	Raised in	Catalogue #
		WB	IF	FACs[**]			
25F9	eBioscience	NA	NA	1:50	eFluor 660	Mouse	50-0115-41
Actin	Sigma	1:1000	NA	NA	NA	Mouse	A2228
AGO1	Keio University	NA	NA	NA	NA	Rat	NA
AGO2[*] (4G8)	Keio University	1:10, 000	NA	NA	NA	Mouse	NA
AGO2 (11A9)	Millipore	1:1000	1:100	1:100	NA	Rat	MABE253
AGO3 A5	Keio University	NA	NA	NA	NA	Rat	NA
AG03 F6	Keio University	NA	NA	NA	NA	Rat	NA
AGO4	Keio University	NA	NA	NA	NA	Rat	NA
mAGO4	WAKO	NA	NA	NA	NA	Rat	014-22023
Band 3	Santa Cruz	1:250	1:100	NA	NA	Rabbit	SC-20657
CD11b	BD Biosciences	NA	NA	1:50	FITC	Rat	553310
CD41a	BD Biosciences	NA	NA	1:100	APC-Cy7	Mouse	561422
CD80	BD Biosciences	NA	NA	1:50	PE-Cy7	Mouse	561135
CD86	BD Biosciences	NA	NA	1:50	BV421	Mouse	562432
CD163	BD Biosciences	NA	NA	1:50	PerCP-Cy 5.5	Mouse	563887
CD206	BD Biosciences	NA	NA	1:5	PE	Mouse	555954
F4/80	BD Biosciences	NA	NA	1:50	PE	Rat	552958
Gly-A	Sigma	1:1000	NA	NA	NA	Mouse	G7650
Gly-A	BD Biosciences	NA	1:10, 000	1:10, 000	PE	Mouse	340947
GW-182	Santa cruz	NA	1:100	NA	NA	Mouse	SC-56314
Hbb	Santa Cruz	1:500	1:200	NA	NA	Mouse	SC-130320
Human IgG	Sigma	NA	NA	1:1000	FITC	Goat	F9512
Human IgG	BD Bioscience	NA	NA	1:20	V450	Mouse	561299
Rab5	Cell signalling	1:500	NA	NA	NA	Rabbit	#3547
LC3	Cell signalling	1:500	NA	NA	NA	Rabbit	#3868

* anti-AGO1-4 was a kind gift from Mikiko C. Siomi.

Appendix 12: Secondary antibodies and probes used within this project

Probe	Company	Dilution factor	Conjugate	Catalogue #
Annexin	BD biosciences	1:100	FITC	550457
Goat anti-mouse	Dako	1:10,000	HRP	P0447
Goat anti-rabbit	Dako	1:10,000	HRP	P0448
Protein-A	Sigma	1:10, 000	FITC	P5145
Annexin	BD biosciences	1:100	FITC	550457
Goat anti-mouse	Invitrogen	1:2000	Alexa Fluor 594	A-11032
Goat anti-mouse	Invitrogen	1:2000	Alexa Fluor 488	A-11001
Goat anti-rabbit	Invitrogen	1:2000	Alexa Fluor 594	A-11072
Goat anti-rabbit	Invitrogen	1:2000	Alexa Fluor 488	A-11034
Phalloidin	Invitrogen	NA	TRITC	R415

Appendix 13: Acrylamide gel recipes

	Final concentration of resolving gel								Stacking gel
	6 (%)	6.5 (%)	7 (%)	7.5 (%)	8 (%)	10 (%)	12 (%)	15 (%)	5 (%)
30 % bis-Acrylamide	3 mL	3.25 mL	3.5 mL	3.75 mL	4 mL	5 mL	6 mL	7.5 mL	1.67 mL
Milli Q water	6.35 mL	6.1 mL	5.85 mL	5.6 mL	5.35 mL	4.35 mL	3.35 mL	1.85 mL	6 mL
1 M Tris_HCl pH 8.8	5.6 mL	5.6 mL	5.6 mL	5.6 mL	5.6 mL	5.6 mL	5.6 mL	5.6 mL	-
1 M Tris_HCl pH 6.8	-	-	-	-	-	-	-	-	1.25 mL
10 % (w/v) SDS	0.25 mL	0.25 mL	0.25 mL	0.25 mL	0.25 mL	0.25 mL	0.25 mL	0.25 mL	0.15 mL
10 % (w/v) ammonium persulphate	100 μL	100 μL	100 μL	100 μL	100 μL	100 μL	100 μL	100 μL	50 μL
TEMED	20 μL	20 μL	20 μL	20 μL	20 μL	20 μL	20 μL	20 μL	20 μL

Resolving gel volumes sufficient for 3 x 1 mm gels, stacking gel volumes sufficient for 4 x gels

Appendix 14: Sequencing data for excised top band

Accession #	Name	Score	Mass
gi|29171734	protein argonaute-2 isoform 1 [Homo sapiens]	494	97146
gi|11935049	keratin 1 [Homo sapiens]	307	66027
gi|386854	type II keratin subunit protein, partial [Homo sapiens]	259	52757
gi|28317	unnamed protein product [Homo sapiens]	197	59492
gi|119617032	keratin 6B, isoform CRA_a [Homo sapiens]	107	59874
gi|3660145	Chain B, Crystal Structure Of S-Nitroso-Nitrosyl Human Hemoglobin A	105	15865
gi|181402	epidermal cytokeratin 2 [Homo sapiens]	103	65825
gi|6005942	transitional endoplasmic reticulum ATPase [Homo sapiens]	81	89266
gi|4557701	keratin, type I cytoskeletal 17 [Homo sapiens]	78	48076
gi|194387942	unnamed protein product [Homo sapiens]	75	56193
gi|6912352	protein argonaute-1 [Homo sapiens]	74	97152
gi|553734	putative [Homo sapiens]	67	2212
gi|34412	unnamed protein product [Homo sapiens]	66	78029
gi|4929993	Chain A, Module-Substituted Chimera Hemoglobin Beta-Alpha (F133v)	64	15780
gi|193244921	beta globin [Homo sapiens]	64	11477
gi|296863564	Chain A, Crystal Structure Of Mid Domain From Hago2	63	15216
gi|392311616	Chain B, Heterocomplex Of Coil 2b Domains Of Human Intermediate Filament Proteins, Keratin 5 (Krt5) And Keratin 14 (Krt14)	60	15040
gi|435476	cytokeratin 9 [Homo sapiens]	59	62092
gi|386850	keratin K5, partial [Homo sapiens]	58	54478
gi|131412225	keratin, type I cytoskeletal 13 isoform a [Homo sapiens]	50	49527
gi|440575811	alternative protein CSF2RB [Homo sapiens]	47	11638
gi|119567960	hCG1643231, isoform CRA_a [Homo sapiens]	46	18891
gi|186685	keratin type 16 [Homo sapiens]	43	50668
gi|158261511	unnamed protein product [Homo sapiens]	41	49486

Appendix 14 continued

Accession #	Name	Score	Mass
gi|17530177	N-methyl-D-aspartate receptor 3A [Homo sapiens]	37	125538
gi|21758244	unnamed protein product [Homo sapiens]	37	18753
gi|38051823	Plasminogen [Homo sapiens]	32	90526
gi|3183214	RecName: Full=Uncharacterized protein KIAA0087 [Homo sapiens]	26	14928
gi|461397	alpha-1 type XV collagen [Homo sapiens]	20	141842
gi|374095517	RecName: Full=Collagen alpha-2(XI) chain; Flags: Precursor [Homo sapiens]	20	171686
gi|119627102	mitochondrial ribosomal protein L37, isoform CRA_d [Homo sapiens]	17	45548
gi|14164613	sialic acid binding immunoglobulin-like lectin 10 [Homo sapiens]	16	76572
gi|7959353	KIAA1543 protein [Homo sapiens]	15	98004
gi|401664560	hydrocephalus-inducing protein homolog isoform a [Homo sapiens]	14	575528
gi|791002	ARSD [Homo sapiens]	14	65029

Appendix 15: Optimising erythrocyte analysis by SDS-PAGE

(a) Direct lysis
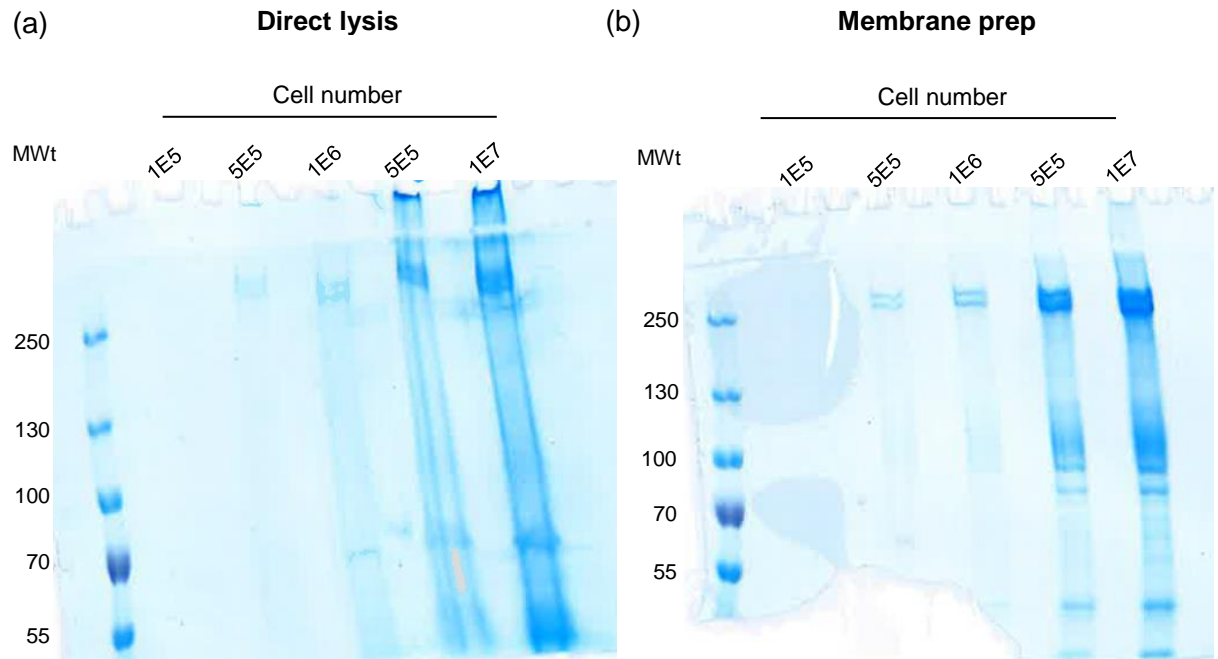
(b) Membrane prep

Figure 63: Electrophoretic profiles of whole RBC and RBC membranes.
Filtered RBCs are pelleted, RBCs washed and enumerated by a Mascot™ Hemavet 950FS, specified cell numbers are either lysed in 1X LDS running buffer, or, membranes prepared as per Section **2.5.4.1** and resolved on a 7.5% acrylamide gel as per Section **2.6.1**. Gels were stained with Coomassie blue as per Section **2.6.3.1**.

Appendix 16: Lipophilic dyes are detrimental to RBC-MVs

a)   **Lipophilic dyes cause RBC-MVs to shrink in size**
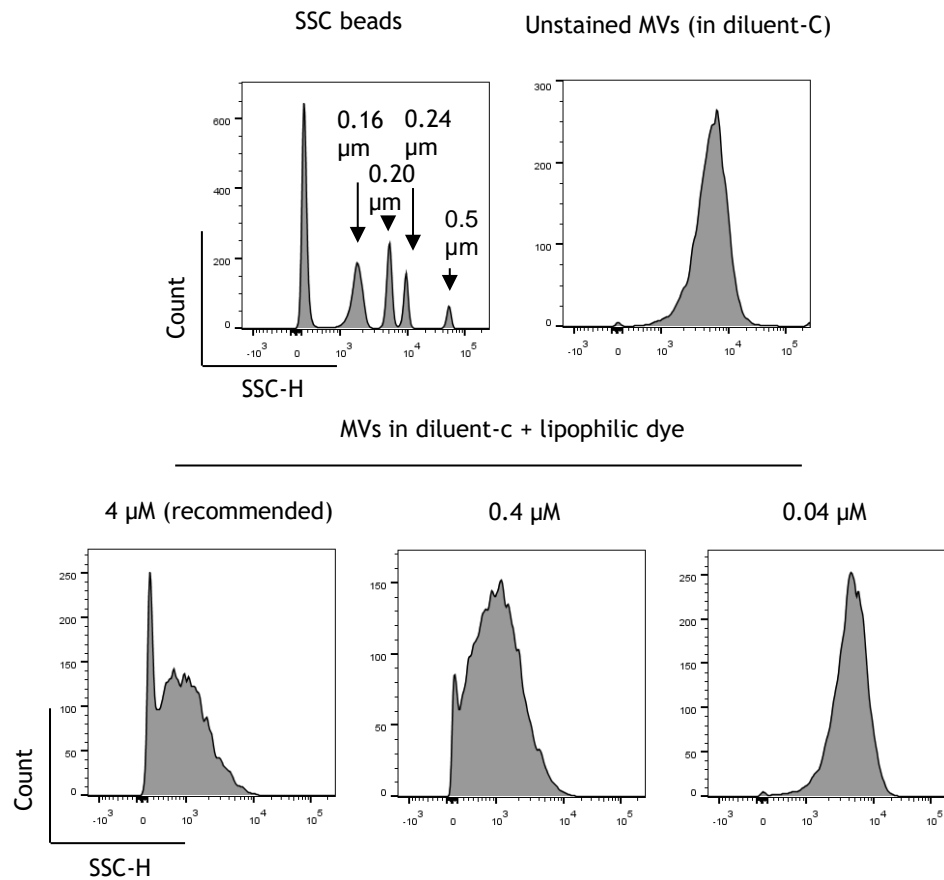
b)   **Overlay of previous data to estimate size**
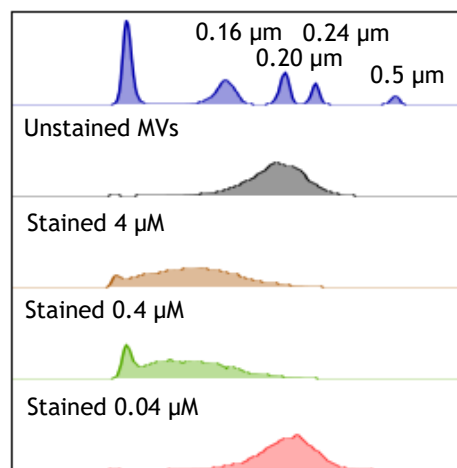
Figure 64: Lipophylic dyes lyse RBC-MVs.
a) Histograms detailing the side scatter (SSC-H) profiles of SSC beads, unstained MVs kit buffer (Diluent C) and MVs stained at different concentrations for 30 minutes; b) Overlay of all histograms from a) to allow ease of comparison.

Appendix 17: Original green "blobs" observed post phagocytosis
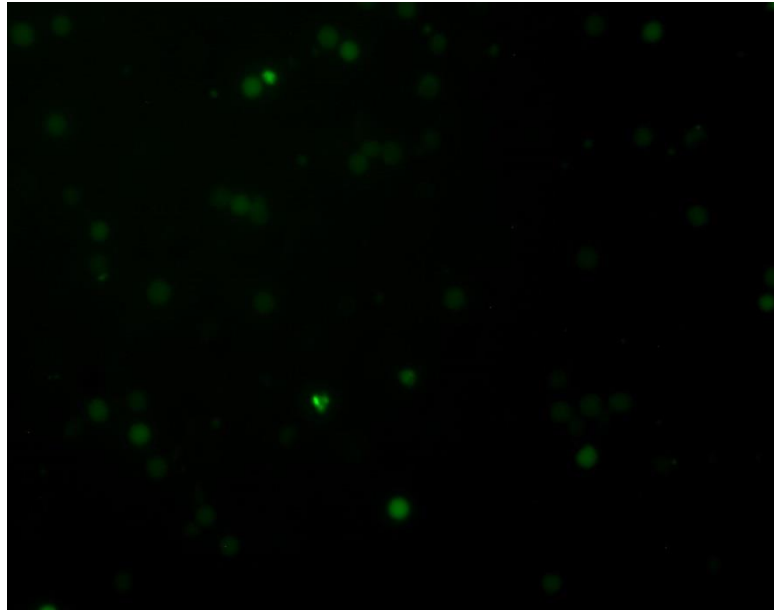
Figure 65: Original "blobs" observed in no RBC-MV prep stained with CFSE.
CFSE labelled "no RBC-MV" in PBS spotted onto a microscope slide and observed under a 40X objective lens.

References

1. FÅHRŒUS., R. The Suspension-stability of the Blood. *Acta Med. Scand.* **55,** 3–7 (2009).
2. WESTERGREN, A. Studies of the Suspension Stability of the Blood in Pulmonary Tuberculosis1. *Acta Med. Scand.* **54,** 247–282 (2009).
3. Fastag, E., Varon, J. & Sternbach, G. Richard Lower: The Origins of Blood Transfusion. *J. Emerg. Med.* **44,** 1146–1150 (2013).
4. Landsteiner, K. *Zur Kenntnis der antifermentativen, lytischen und agglutinierenden Wirkungen des Blutserums und der Lymphe." In: Centralblatt für Bakteriologie, Parasitenkunde und Infektionskrankheiten, Vol. 27, 1900, pp. 357-62. Entire volume offered. by LANDSTEINER, Karl: Jena: Gustav Fischer, 1900. Hardcover, 1st Edition - Scientia Books, ABAA.* **27,** (Jena: Gustav Fischer, 1900).
5. Andral G. Essai d'hématologie pathologique. (1824).
6. Rathjen, T., Nicol, C., McConkey, G. & Dalmay, T. Analysis of short RNAs in the malaria parasite and its red blood cell host. *FEBS Lett.* **580,** 5185–5188 (2006).
7. Hollowayt, B. W. & Ripley, S. H. NUCLEIC ACID CONTENT OF RETICULOCYTES AND ITS RELATION TO UPTAKE OF RADIOACTIVE LEUCINE IN VITRO*.
8. Henras, A. K., Plisson-Chastang, C., O'Donohue, M.-F., Chakraborty, A. & Gleizes, P.-E. An overview of pre-ribosomal RNA processing in eukaryotes. *Wiley Interdiscip. Rev. RNA* **6,** 225–242 (2015).
9. Shine, J. & Dalgarno, L. The 3'-terminal sequence of Escherichia coli 16S ribosomal RNA: complementarity to nonsense triplets and ribosome binding sites. *Proc. Natl. Acad. Sci. U. S. A.* **71,** 1342–6 (1974).
10. Kirchner, S. & Ignatova, Z. Emerging roles of tRNA in adaptive translation, signalling dynamics and disease. *Nat. Rev. Genet.* **16,** 98–112 (2014).
11. Phizicky, E. M. & Hopper, A. K. tRNA biology charges to the front. *Genes Dev.* **24,** 1832–1860 (2010).
12. Ibba, M. & Söll, D. Aminoacyl-tRNA Synthesis. *Annu. Rev. Biochem.* **69,** 617–650 (2000).
13. Ribosome Structure and the Mechanism of Translation. *Cell* **108,** 557–572 (2002).
14. Kung, J. T. Y., Colognori, D. & Lee, J. T. Long Noncoding RNAs: Past, Present, and Future. *Genetics* **193,** 651–669 (2013).
15. Cheng, J. *et al.* Transcriptional Maps of 10 Human Chromosomes at 5-Nucleotide Resolution. *Science (80-.).* **308,** 1149–1154 (2005).
16. Wu, Q. *et al.* Poly A- Transcripts Expressed in HeLa Cells. *PLoS One* **3,** e2803 (2008).
17. Guttman, M. *et al.* Ab initio reconstruction of cell type–specific transcriptomes in mouse reveals the conserved multi-exonic structure of lincRNAs. *Nat. Biotechnol.* **28,** 503–510 (2010).
18. Borsani, G. *et al.* Characterization of a murine gene expressed from the inactive X chromosome. *Nature* **351,** 325–329 (1991).
19. Beltran, M. *et al.* A natural antisense transcript regulates Zeb2/Sip1 gene expression during Snail1-induced epithelial-mesenchymal transition. *Genes Dev.* **22,** 756–769 (2008).
20. Karreth, F. A. *et al.* In Vivo Identification of Tumor- Suppressive PTEN ceRNAs in an Oncogenic BRAF-Induced Mouse Model of Melanoma. *Cell*

147, 382–395 (2011).

21. Wang, X. *et al*. Induced ncRNAs allosterically modify RNA-binding proteins in cis to inhibit transcription. *Nature* **454,** 126–130 (2008).

22. Faghihi, M. A. *et al*. Expression of a noncoding RNA is elevated in Alzheimer's disease and drives rapid feed-forward regulation of ß-secretase. *Nat. Med*. **14,** 723-730 (2008).

23. Jády, B. E. & Kiss, T. A small nucleolar guide RNA functions both in 2'-O-ribose methylation and pseudouridylation of the U5 spliceosomal RNA. *EMBO J*. **20,** 541-51 (2001).

24. Samarsky, D. A., Fournier, M. J., Singer, R. H. & Bertrand, E. The snoRNA box C/D motif directs nucleolar targeting and also couples snoRNA synthesis and localization. *EMBO J*. **17,** 3747-57 (1998).

25. Reichow, S. L., Hamma, T., Ferre-D'Amare, A. R. & Varani, G. The structure and function of small nucleolar ribonucleoproteins. *Nucleic Acids Res*. **35,** 1452–1464 (2007).

26. Ganot, P., Bortolin, M. L. & Kiss, T. Site-specific pseudouridine formation in preribosomal RNA is guided by small nucleolar RNAs. *Cell* **89,** 799–809 (1997).

27. Kiss-László, Z., Henry, Y., Bachellerie, J. P., Caizergues-Ferrer, M. & Kiss, T. Site-specific ribose methylation of preribosomal RNA: a novel function for small nucleolar RNAs. *Cell* **85,** 1077–88 (1996).

28. Kiss, A. M., Jady, B. E., Bertrand, E. & Kiss, T. Human Box H/ACA Pseudouridylation Guide RNA Machinery. *Mol. Cell. Biol*. **24,** 5797–5807 (2004).

29. Matera, A. G., Terns, R. M. & Terns, M. P. Non-coding RNAs: lessons from the small nuclear and small nucleolar RNAs. *Nat. Rev. Mol. Cell Biol*. **8,** 209–220 (2007).

30. Matera, A. G. & Wang, Z. A day in the life of the spliceosome. *Nat. Rev. Mol. Cell Biol*. **15,** 294-294 (2014).

31. Montemayor, E. J. *et al*. Core structure of the U6 small nuclear ribonucleoprotein at 1.7-Å resolution. *Nat. Struct. Mol. Biol*. **21,** 544-551 (2014).

32. Nagai, K. *et al*. Structure and assembly of the spliceosomal snRNPs. Novartis Medal Lecture. *Biochem. Soc. Trans*. **29,** 15-26 (2001).

33. Hall, S. L. & Padgett, R. A. Conserved Sequences in a Class of Rare Eukaryotic Nuclear Introns with Non-consensus Splice Sites. *J. Mol. Biol*. **239,** 357-365 (1994).

34. Senapathy, P., Shapiro, M. B. & Harris, N. L. Splice junctions, branch point sites, and exons: sequence statistics, identification, and applications to genome project. *Methods Enzymol*. **183,** 252–78 (1990).

35. Mowry, K. L. & Steitz, J. A. Identification of the human U7 snRNP as one of several factors involved in the 3' end maturation of histone premessenger RNA's. *Science* **238,** 1682-7 (1987).

36. Kowalski, M. P. & Krude, T. Functional roles of non-coding Y RNAs. *Int. J. Biochem. Cell Biol*. **66,** 20-29 (2015).

37. BELISOVA, A. *et al*. RNA chaperone activity of protein components of human Ro RNPs. *RNA* **11,** 1084-1094 (2005).

38. Chen, X. *et al*. An ortholog of the Ro autoantigen functions in 23S rRNA maturation in D. radiodurans. *Genes Dev*. **21,** 1328–39 (2007).

39. Chen, X. *et al*. The Ro autoantigen binds misfolded U2 small nuclear RNAs and assists mammalian cell survival after UV irradiation. *Curr. Biol*. **13,** 2206–11 (2003).

40. O'Brien, C. A. & Wolin, S. L. A possible role for the 60-kD Ro autoantigen in a discard pathway for defective 5S rRNA precursors. *Genes Dev.* **8,** 2891–903 (1994).
41. Christov, C. P., Gardiner, T. J., Szüts, D. & Krude, T. Functional requirement of noncoding Y RNAs for human chromosomal DNA replication. *Mol. Cell. Biol.* **26,** 6993–7004 (2006).
42. Christov, C. P., Trivier, E. & Krude, T. Noncoding human Y RNAs are overexpressed in tumours and required for cell proliferation. *Br. J. Cancer* **98,** 981–988 (2008).
43. Gardiner, T. J., Christov, C. P., Langley, A. R. & Krude, T. A conserved motif of vertebrate Y RNAs essential for chromosomal DNA replication. *RNA* **15,** 1375–85 (2009).
44. Rutjes, S. A., van der Heijden, A., Utz, P. J., van Venrooij, W. J. & Pruijn, G. J. Rapid nucleolytic degradation of the small cytoplasmic Y RNAs during apoptosis. *J. Biol. Chem.* **274,** 24799–807 (1999).
45. Meiri, E. *et al.* Discovery of microRNAs and other small RNAs in solid tumors. *Nucleic Acids Res.* **38,** 6234–46 (2010).
46. Nicolas, F. E., Hall, A. E., Csorba, T., Turnbull, C. & Dalmay, T. Biogenesis of Y RNA-derived small RNAs is independent of the microRNA pathway. *FEBS Lett.* **586,** 1226–1230 (2012).
47. Luteijn, M. J. & Ketting, R. F. PIWI-interacting RNAs: from generation to transgenerational epigenetics. *Nat. Rev. Genet.* **14,** 523–534 (2013).
48. Kirino, Y. & Mourelatos, Z. Mouse Piwi-interacting RNAs are 2′-O-methylated at their 3′ termini. *Nat. Struct. Mol. Biol.* **14,** 347–348 (2007).
49. Lin, H., Yin, H., Beyret, E., Findley, S. & Deng, W. The role of the piRNA pathway in stem cell self-renewal. *Dev. Biol.* **319,** 479 (2008).
50. Brennecke, J. *et al.* Discrete Small RNA-Generating Loci as Master Regulators of Transposon Activity in Drosophila. *Cell* **128,** 1089–1103 (2007).
51. Saito, K. *et al.* Pimet, the Drosophila homolog of HEN1, mediates 2'-O-methylation of Piwi- interacting RNAs at their 3' ends. *Genes Dev.* **21,** 1603–8 (2007).
52. Izumi, N. *et al.* Identification and Functional Analysis of the Pre-piRNA 3′ Trimmer in Silkworms. *Cell* **164,** 962–973 (2016).
53. Olivieri, D., Senti, K.-A., Subramanian, S., Sachidanandam, R. & Brennecke, J. The Cochaperone Shutdown Defines a Group of Biogenesis Factors Essential for All piRNA Populations in Drosophila. *Mol. Cell* **47,** 954–969 (2012).
54. Nishimasu, H. *et al.* Structure and function of Zucchini endoribonuclease in piRNA biogenesis. *Nature* **491,** 284–287 (2012).
55. Saito, K. *et al.* Specific association of Piwi with rasiRNAs derived from retrotransposon and heterochromatic regions in the Drosophila genome. *Genes Dev.* **20,** 2214–2222 (2006).
56. Gunawardane, L. S. *et al.* A Slicer-Mediated Mechanism for Repeat-Associated siRNA 5' End Formation in Drosophila. *Science (80-.).* **315,** 1587–1590 (2007).
57. Le Thomas, A. *et al.* Piwi induces piRNA-guided transcriptional silencing and establishment of a repressive chromatin state. *Genes Dev.* **27,** 390–399 (2013).
58. Sienski, G., Dönertas, D. & Brennecke, J. Transcriptional Silencing of Transposons by Piwi and Maelstrom and Its Impact on Chromatin State and Gene Expression. *Cell* **151,** 964–980 (2012).

59. Aravin, A. A. *et al.* A piRNA Pathway Primed by Individual Transposons Is Linked to De Novo DNA Methylation in Mice. *Mol. Cell* **31,** 785–799 (2008).

60. Kuramochi-Miyagawa, S. *et al.* DNA methylation of retrotransposon genes is regulated by Piwi family members MILI and MIWI2 in murine fetal testes. *Genes Dev.* **22,** 908–917 (2008).

61. Okamura, K. & Lai, E. C. Endogenous small interfering RNAs in animals. *Nat. Rev. Mol. Cell Biol.* **9,** 673–678 (2008).

62. Czech, B. *et al.* An endogenous small interfering RNA pathway in Drosophila. *Nature* **453,** 798–802 (2008).

63. Ruby, J. G. *et al.* Large-scale sequencing reveals 21U-RNAs and additional microRNAs and endogenous siRNAs in C. elegans. *Cell* **127,** 1193–207 (2006).

64. Chen, L., Dahlstrom, J. E., Lee, S.-H. & Rangasamy, D. Naturally occurring endo-siRNA silences LINE-1 retrotransposons in human cells through DNA methylation. *Epigenetics* **7,** 758–771 (2012).

65. Ameyar-Zazoua, M. *et al.* Argonaute proteins couple chromatin silencing to alternative splicing. *Nat. Struct. Mol. Biol.* **19,** 998–1004 (2012).

66. Fire, A. *et al.* Potent and specific genetic interference by double-stranded RNA in Caenorhabditis elegans. *Nature* **391,** 806–811 (1998).

67. Agrawal, N. *et al.* RNA interference: biology, mechanism, and applications. *Microbiol. Mol. Biol. Rev.* **67,** 657–85 (2003).

68. Napoli, C., Lemieux, C. & Jorgensen, R. Introduction of a Chimeric Chalcone Synthase Gene into Petunia Results in Reversible Co-Suppression of Homologous Genes in trans. *Plant Cell* **2,** 279–289 (1990).

69. van der Krol, A. R., Mur, L. A., Beld, M., Mol, J. N. & Stuitje, A. R. Flavonoid genes in petunia: addition of a limited number of gene copies may lead to a suppression of gene expression. *Plant Cell* **2,** 291–9 (1990).

70. Hamilton, A. J. & Baulcombe, D. C. A species of small antisense RNA in posttranscriptional gene silencing in plants. *Science* **286,** 950–2 (1999).

71. Zamore, P. D., Tuschl, T., Sharp, P. A. & Bartel, D. P. RNAi. *Cell* **101,** 25–33 (2000).

72. Lee, R. C., Feinbaum, R. L. & Ambros, V. The C. elegans heterochronic gene lin-4 encodes small RNAs with antisense complementarity to lin-14. *Cell* **75,** 843–54 (1993).

73. Wightman, B., Ha, I. & Ruvkun, G. Posttranscriptional regulation of the heterochronic gene lin-14 by lin-4 mediates temporal pattern formation in C. elegans. *Cell* **75,** 855–62 (1993).

74. Ruvkun, G. *et al.* The 21-nucleotide let-7 RNA regulates developmental timing in Caenorhabditis elegans. *Nature* **403,** 901–906 (2000).

75. Lee, R. C. & Ambros, V. An Extensive Class of Small RNAs in Caenorhabditis elegans. *Science (80-.).* **294,** 862–864 (2001).

76. Ambros, V. *et al.* A uniform system for microRNA annotation. *RNA* **9,** 277–9 (2003).

77. Bernstein, E. *et al.* Dicer is essential for mouse development. *Nat. Genet.* **35,** 215–217 (2003).

78. Wang, Y., Medvid, R., Melton, C., Jaenisch, R. & Blelloch, R. DGCR8 is essential for microRNA biogenesis and silencing of embryonic stem cell self-renewal. *Nat. Genet.* **39,** 380–385 (2007).

79. Morita, S. *et al.* One Argonaute family member, Eif2c2 (Ago2), is essential for development and appears not to be involved in DNA methylation. *Genomics* **89,** 687–696 (2007).

80. Bartram, M. P. *et al.* Loss of Dgcr8-mediated microRNA expression in the

kidney results in hydronephrosis and renal malformation. *BMC Nephrol.* **16,** 55 (2015).

81. Faller, M. *et al.* DGCR8 recognizes primary transcripts of microRNAs through highly cooperative binding and formation of higher-order structures. *RNA* **16,** 1570–1583 (2010).

82. Wu, Q. *et al.* The RNase III Enzyme DROSHA Is Essential for MicroRNA Production and Spermatogenesis. *J. Biol. Chem.* **287,** 25173–25190 (2012).

83. Klein, U. *et al.* The DLEU2/miR-15a/16-1 Cluster Controls B Cell Proliferation and Its Deletion Leads to Chronic Lymphocytic Leukemia. *Cancer Cell* **17,** 28–40 (2010).

84. van Rooij, E. *et al.* A Family of microRNAs Encoded by Myosin Genes Governs Myosin Expression and Muscle Performance. *Dev. Cell* **17,** 662–673 (2009).

85. Rodriguez, A., Griffiths-Jones, S., Ashurst, J. L. & Bradley, A. Identification of Mammalian microRNA Host Genes and Transcription Units. *Genome Res.* **14,** 1902–1910 (2004).

86. Lee, Y. *et al.* MicroRNA genes are transcribed by RNA polymerase II. *EMBO J.* **23,** 4051–60 (2004).

87. Altuvia, Y. *et al.* Clustering and conservation patterns of human microRNAs. *Nucleic Acids Res.* **33,** 2697–2706 (2005).

88. Hertel, J. *et al.* The expansion of the metazoan microRNA repertoire. *BMC Genomics* **7,** 25 (2006).

89. Babiarz, J. E., Ruby, J. G., Wang, Y., Bartel, D. P. & Blelloch, R. Mouse ES cells express endogenous shRNAs, siRNAs, and other Microprocessor-independent, Dicer-dependent small RNAs. *Genes Dev.* **22,** 2773–85 (2008).

90. Bartel, D. P. MicroRNAs: genomics, biogenesis, mechanism, and function. *Cell* **116,** 281–97 (2004).

91. Auyeung, V. C., Ulitsky, I., McGeary, S. E. & Bartel, D. P. Beyond Secondary Structure: Primary-Sequence Determinants License Pri-miRNA Hairpins for Processing. *Cell* **152,** 844–858 (2013).

92. Han, J. *et al.* The Drosha-DGCR8 complex in primary microRNA processing. *Genes Dev.* **18,** 3016–3027 (2004).

93. Nguyen, T. A. *et al.* Functional Anatomy of the Human Microprocessor. *Cell* **161,** 1374–87 (2015).

94. Quick-Cleveland, J. *et al.* The DGCR8 RNA-binding heme domain recognizes primary microRNAs by clamping the hairpin. *Cell Rep.* **7,** 1994–2005 (2014).

95. Barr, I. *et al.* Ferric, not ferrous, heme activates RNA-binding protein DGCR8 for primary microRNA processing. *Proc. Natl. Acad. Sci. U. S. A.* **109,** 1919–24 (2012).

96. Weitz, S. H., Gong, M., Barr, I., Weiss, S. & Guo, F. Processing of microRNA primary transcripts requires heme in mammalian cells. *Proc. Natl. Acad. Sci.* **111,** 1861–1866 (2014).

97. Zhang, H., Kolb, F. A., Jaskiewicz, L., Westhof, E. & Filipowicz, W. Single Processing Center Models for Human Dicer and Bacterial RNase III. *Cell* **118,** 57–68 (2004).

98. Lee, Y. *et al.* The nuclear RNase III Drosha initiates microRNA processing. *Nature* **425,** 415–419 (2003).

99. Bohnsack, M. T., Czaplinski, K. & Gorlich, D. Exportin 5 is a RanGTP-dependent dsRNA-binding protein that mediates nuclear export of pre-miRNAs. *RNA* **10,** 185–91 (2004).

100. Zeng, Y. & Cullen, B. R. Structural requirements for pre-microRNA binding

and nuclear export by Exportin 5. *Nucleic Acids Res.* **32,** 4776–4785 (2004).

101. Okada, C. *et al.* A High-Resolution Structure of the Pre-microRNA Nuclear Export Machinery. *Science (80-.).* **326,** 1275–1279 (2009).

102. Kutay, U., Bischoff, F. R., Kostka, S., Kraft, R. & Görlich, D. Export of importin alpha from the nucleus is mediated by a specific nuclear transport factor. *Cell* **90,** 1061–71 (1997).

103. Park, J.-E. *et al.* Dicer recognizes the 5′ end of RNA for efficient and accurate processing. *Nature* **475,** 201–205 (2011).

104. Chakravarthy, S., Sternberg, S. H., Kellenberger, C. A. & Doudna, J. A. Substrate-Specific Kinetics of Dicer-Catalyzed RNA Processing. *J. Mol. Biol.* **404,** 392–402 (2010).

105. Lee, Y. *et al.* The role of PACT in the RNA silencing pathway. *EMBO J.* **25,** 522–532 (2006).

106. Fukunaga, R. *et al.* Dicer Partner Proteins Tune the Length of Mature miRNAs in Flies and Mammals. *Cell* **151,** 533–546 (2012).

107. Lee, H. Y. & Doudna, J. A. TRBP alters human precursor microRNA processing in vitro. *RNA* **18,** 2012–2019 (2012).

108. Noland, C. L., Ma, E. & Doudna, J. A. siRNA Repositioning for Guide Strand Selection by Human Dicer Complexes. *Mol. Cell* **43,** 110–121 (2011).

109. Tomari, Y., Matranga, C., Haley, B., Martinez, N. & Zamore, P. D. A Protein Sensor for siRNA Asymmetry. *Science (80-.).* **306,** 1377–1380 (2004).

110. Johnston, M., Geoffroy, M. C., Sobala, A., Hay, R. & Hutvagner, G. HSP90 Protein Stabilizes Unloaded Argonaute Complexes and Microscopic P-bodies in Human Cells. *Mol. Biol. Cell* **21,** 1462–1469 (2010).

111. Schwarz, D. S. *et al.* Asymmetry in the assembly of the RNAi enzyme complex. *Cell* **115,** 199–208 (2003).

112. Ruby, J. G., Jan, C. H. & Bartel, D. P. Intronic microRNA precursors that bypass Drosha processing. *Nature* **448,** 83–86 (2007).

113. Glazov, E. A. *et al.* Repertoire of Bovine miRNA and miRNA-Like Small Regulatory RNAs Expressed upon Viral Infection. *PLoS One* **4,** e6349 (2009).

114. Glazov, E. A. *et al.* A microRNA catalog of the developing chicken embryo identified by a deep sequencing approach. *Genome Res.* **18,** 957–964 (2008).

115. Zhu, Q.-H. *et al.* A diverse set of microRNAs and microRNA-like small RNAs in developing rice grains. *Genome Res.* **18,** 1456–65 (2008).

116. Flynt, A. S., Greimann, J. C., Chung, W.-J., Lima, C. D. & Lai, E. C. MicroRNA Biogenesis via Splicing and Exosome-Mediated Trimming in Drosophila. *Mol. Cell* **38,** 900–907 (2010).

117. Chong, M. M. W. *et al.* Canonical and alternate functions of the microRNA biogenesis machinery. *Genes Dev.* **24,** 1951–1960 (2010).

118. Cole, C. *et al.* Filtering of deep sequencing data reveals the existence of abundant Dicer-dependent small RNAs derived from tRNAs. *RNA* **15,** 2147–2160 (2009).

119. Haussecker, D. *et al.* Human tRNA-derived small RNAs in the global regulation of RNA silencing. *RNA* **16,** 673–695 (2010).

120. Kumar, P., Anaya, J., Mudunuri, S. B. & Dutta, A. Meta-analysis of tRNA derived RNA fragments reveals that they are evolutionarily conserved and associate with AGO proteins to recognize specific RNA targets. *BMC Biol.* **12,** 78 (2014).

121. Hasler, D. *et al.* The Lupus Autoantigen La Prevents Mis-channeling of tRNA Fragments into the Human MicroRNA Pathway. *Mol. Cell* **63,** 110–124

(2016).

122. Ender, C. *et al.* A human snoRNA with microRNA-like functions. *Mol. Cell* **32,** 519–28 (2008).

123. Ono, M. *et al.* Identification of human miRNA precursors that resemble box C/D snoRNAs. *Nucleic Acids Res.* **39,** 3879–91 (2011).

124. Brameier, M., Herwig, A., Reinhardt, R., Walter, L. & Gruber, J. Human box C/D snoRNAs with miRNA like functions: expanding the range of regulatory RNAs. *Nucleic Acids Res.* **39,** 675–86 (2011).

125. Cheloufi, S., Dos Santos, C. O., Chong, M. M. W. & Hannon, G. J. A dicer-independent miRNA biogenesis pathway that requires Ago catalysis. *Nature* **465,** 584–589 (2010).

126. Yoda, M. *et al.* Poly(A)-Specific Ribonuclease Mediates 3′-End Trimming of Argonaute2-Cleaved Precursor MicroRNAs. *Cell Rep.* **5,** 715–726 (2013).

127. Dore, L. C. *et al.* A GATA-1-regulated microRNA locus essential for erythropoiesis. *Proc. Natl. Acad. Sci.* **105,** 3333–3338 (2008).

128. Neilsen, C. T., Goodall, G. J. & Bracken, C. P. IsomiRs – the overlooked repertoire in the dynamic microRNAome. *Trends Genet.* **28,** 544–549 (2012).

129. Han, B. W., Hung, J.-H., Weng, Z., Zamore, P. D. & Ameres, S. L. The 3′-to-5′ Exoribonuclease Nibbler Shapes the 3′ Ends of MicroRNAs Bound to Drosophila Argonaute1. *Curr. Biol.* **21,** 1878–1887 (2011).

130. Wyman, S. K. *et al.* Post-transcriptional generation of miRNA variants by multiple nucleotidyl transferases contributes to miRNA transcriptome complexity. *Genome Res.* **21,** 1450–61 (2011).

131. LUCIANO, D. J., Mirsky, H., Vendetti, N. J. & Maas, S. RNA editing of a miRNA precursor. *RNA* **10,** 1174–1177 (2004).

132. Newman, M. A., Mani, V. & Hammond, S. M. Deep sequencing of microRNA precursors reveals extensive 3′ end modification. *RNA* **17,** 1795–1803 (2011).

133. Burroughs, A. M. *et al.* A comprehensive survey of 3′ animal miRNA modification events and a possible role for 3′ adenylation in modulating miRNA targeting effectiveness. *Genome Res.* **20,** 1398–1410 (2010).

134. Katoh, T. *et al.* Selective stabilization of mammalian microRNAs by 3′ adenylation mediated by the cytoplasmic poly(A) polymerase GLD-2. *Genes Dev.* **23,** 433–8 (2009).

135. Jones, M. R. *et al.* Zcchc11-dependent uridylation of microRNA directs cytokine expression. *Nat. Cell Biol.* **11,** 1157–1163 (2009).

136. Tan, G. C. *et al.* 5′ isomiR variation is of functional and evolutionary importance. *Nucleic Acids Res.* **42,** 9424–9435 (2014).

137. Mercey, O. *et al.* Characterizing isomiR variants within the microRNA-34/449 family. *FEBS Lett.* **591,** 693–705 (2017).

138. Meister, G. Argonaute proteins: functional insights and emerging roles. *Nat. Rev. Genet.* **14,** 447–459 (2013).

139. Lingel, A., Simon, B., Izaurralde, E. & Sattler, M. Nucleic acid 3′-end recognition by the Argonaute2 PAZ domain. *Nat. Struct. Mol. Biol.* **11,** 576–577 (2004).

140. Ma, J.-B. *et al.* Structural basis for 5′-end-specific recognition of guide RNA by the A. fulgidus Piwi protein. *Nature* **434,** 666–670 (2005).

141. Rüdel, S. *et al.* Phosphorylation of human Argonaute proteins affects small RNA binding. *Nucleic Acids Res.* **39,** 2330-2343 (2011).

142. Meister, G. *et al.* Human Argonaute2 Mediates RNA Cleavage Targeted by miRNAs and siRNAs. *Mol. Cell* **15,** 185–197 (2004).

143. Burroughs, A. M. *et al.* Deep-sequencing of human Argonaute-associated small RNAs provides insight into miRNA sorting and reveals Argonaute association with RNA fragments of diverse origin. *RNA Biol.* **8,** 158-77

144. Wang, D. *et al.* Quantitative functions of Argonaute proteins in mammalian development. *Genes Dev.* **26,** 693–704 (2012).

145. Hu, Q. *et al.* DICER- and AGO3-dependent generation of retinoic acid–induced DR2 Alu RNAs regulates human stem cell proliferation. *Nat. Struct. Mol. Biol.* **19,** 1168–1175 (2012).

146. Modzelewski, A. J., Holmes, R. J., Hilz, S., Grimson, A. & Cohen, P. E. AGO4 Regulates Entry into Meiosis and Influences Silencing of Sex Chromosomes in the Male Mouse Germline. *Dev. Cell* **23,** 251-264 (2012).

147. Völler, D. *et al.* Argonaute Family Protein Expression in Normal Tissue and Cancer Entities. *PLoS One* **11,** e0161165 (2016).

148. Frank, F., Sonenberg, N. & Nagar, B. Structural basis for 5′-nucleotide base-specific recognition of guide RNA by human AGO2. *Nature* **465,** 818–822 (2010).

149. Borges, F. & Martienssen, R. A. The expanding world of small RNAs in plants. *Nat. Rev. Mol. Cell Biol.* **16,** 727-741 (2015).

150. Eun, C. *et al.* AGO6 Functions in RNA-Mediated Transcriptional Gene Silencing in Shoot and Root Meristems in Arabidopsis thaliana. *PLoS One* **6,** e25730 (2011).

151. Zilberman, D., Cao, X. & Jacobsen, S. E. ARGONAUTE4 Control of Locus-Specific siRNA Accumulation and DNA and Histone Methylation. *Science (80-.).* **299,** 716–719 (2003).

152. Voinnet, O. Origin, Biogenesis, and Activity of Plant MicroRNAs. *Cell* **136,** 669–687 (2009).

153. Zhu, H. *et al.* Arabidopsis Argonaute10 Specifically Sequesters miR166/165 to Regulate Shoot Apical Meristem Development. *Cell* **145,** 242-256 (2011).

154. Mi, S. *et al.* Sorting of small RNAs into Arabidopsis argonaute complexes is directed by the 5′ terminal nucleotide. *Cell* **133,** 116-27 (2008).

155. Eichhorn, S. W. *et al.* mRNA Destabilization Is the Dominant Effect of Mammalian MicroRNAs by the Time Substantial Repression Ensues. *Mol. Cell* **56,** 104–115 (2014).

156. Guo, H., Ingolia, N. T., Weissman, J. S. & Bartel, D. P. Mammalian microRNAs predominantly act to decrease target mRNA levels. *Nature* **466,** 835-840 (2010).

157. Lewis, B. P., Shih, I., Jones-Rhoades, M. W., Bartel, D. P. & Burge, C. B. Prediction of mammalian microRNA targets. *Cell* **115,** 787-98 (2003).

158. Rehwinkel, J., Behm-Ansmant, I., Gatfield, D. & Izaurralde, E. A crucial role for GW182 and the DCP1:DCP2 decapping complex in miRNA-mediated gene silencing. *RNA* **11,** 1640-7 (2005).

159. Lowell, J. E., Rudner, D. Z. & Sachs, A. B. 3′-UTR-dependent deadenylation by the yeast poly(A) nuclease. *Genes Dev.* **6,** 2088–99 (1992).

160. Braun, J. E., Huntzinger, E., Fauser, M. & Izaurralde, E. GW182 Proteins Directly Recruit Cytoplasmic Deadenylase Complexes to miRNA Targets. *Mol. Cell* **44,** 120-133 (2011).

161. Tucker, M. *et al.* The transcription factor associated Ccr4 and Caf1 proteins are components of the major cytoplasmic mRNA deadenylase in Saccharomyces cerevisiae. *Cell* **104,** 377-86 (2001).

162. Liu, J., Valencia-Sanchez, M. A., Hannon, G. J. & Parker, R. MicroRNA-dependent localization of targeted mRNAs to mammalian P-bodies. *Nat.*

Cell Biol. **7,** 719–23 (2005).

163. Sen, G. L. & Blau, H. M. Argonaute 2/RISC resides in sites of mammalian mRNA decay known as cytoplasmic bodies. *Nat. Cell Biol.* **7,** 633–636 (2005).

164. Bhattacharyya, S. N., Habermacher, R., Martine, U., Closs, E. I. & Filipowicz, W. Relief of microRNA-Mediated Translational Repression in Human Cells Subjected to Stress. *Cell* **125,** 1111–1124 (2006).

165. Yekta, S., Shih, I.-H. & Bartel, D. P. MicroRNA-Directed Cleavage of HOXB8 mRNA. *Science (80-.).* **304,** 594–596 (2004).

166. Llave, C., Xie, Z., Kasschau, K. D. & Carrington, J. C. Cleavage of Scarecrow-like mRNA Targets Directed by a Class of Arabidopsis miRNA. *Science (80-.).* **297,** 2053–2056 (2002).

167. Davis, E. *et al.* RNAi-mediated allelic trans-interaction at the imprinted Rtl1/Peg11 locus. *Curr. Biol.* **15,** 743–9 (2005).

168. Humphreys, D. T., Westman, B. J., Martin, D. I. K. & Preiss, T. MicroRNAs control translation initiation by inhibiting eukaryotic initiation factor 4E/cap and poly(A) tail function. *Proc. Natl. Acad. Sci. U. S. A.* **102,** 16961–6 (2005).

169. Iwasaki, S., Kawamata, T. & Tomari, Y. Drosophila Argonaute1 and Argonaute2 Employ Distinct Mechanisms for Translational Repression. *Mol. Cell* **34,** 58–67 (2009).

170. Richter, J. D. & Sonenberg, N. Regulation of cap-dependent translation by eIF4E inhibitory proteins. *Nature* **433,** 477–480 (2005).

171. Ricci, E. P. *et al.* miRNA repression of translation in vitro takes place during 43S ribosomal scanning. *Nucleic Acids Res.* **41,** 586–598 (2013).

172. Zdanowicz, A. *et al.* Drosophila miR2 Primarily Targets the m7GpppN Cap Structure for Translational Repression. *Mol. Cell* **35,** 881–888 (2009).

173. Mathonnet, G. *et al.* MicroRNA Inhibition of Translation Initiation in Vitro by Targeting the Cap-Binding Complex eIF4F. *Science (80-.).* **317,** 1764–1767 (2007).

174. Gagnon, K. T., Li, L., Chu, Y., Janowski, B. A. & Corey, D. R. RNAi Factors Are Present and Active in Human Cell Nuclei. *Cell Rep.* **6,** 211–221 (2014).

175. Ohrt, T. *et al.* Fluorescence correlation spectroscopy and fluorescence cross-correlation spectroscopy reveal the cytoplasmic origination of loaded nuclear RISC in vivo in human cells. *Nucleic Acids Res.* **36,** 6439–49 (2008).

176. Khudayberdiev, S. A., Zampa, F., Rajman, M. & Schratt, G. A comprehensive characterization of the nuclear microRNA repertoire of post-mitotic neurons. *Front. Mol. Neurosci.* **6,** 43 (2013).

177. Castanotto, D., Lingeman, R., Riggs, A. D. & Rossi, J. J. CRM1 mediates nuclear-cytoplasmic shuttling of mature microRNAs. *Proc. Natl. Acad. Sci. U. S. A.* **106,** 21655–9 (2009).

178. Weinmann, L. *et al.* Importin 8 Is a Gene Silencing Factor that Targets Argonaute Proteins to Distinct mRNAs. *Cell* **136,** 496–507 (2009).

179. Hwang, H.-W., Wentzel, E. A. & Mendell, J. T. A Hexanucleotide Element Directs MicroRNA Nuclear Import. *Science (80-.).* **315,** 97–100 (2007).

180. Tang, R. *et al.* Mouse miRNA-709 directly regulates miRNA-15a/16-1 biogenesis at the posttranscriptional level in the nucleus: evidence for a microRNA hierarchy system. *Cell Res.* **22,** 504–515 (2012).

181. Leucci, E. *et al.* microRNA-9 targets the long non-coding RNA MALAT1 for degradation in the nucleus. *Sci. Rep.* **3,** 2535 (2013).

182. Tan, Y. *et al.* Transcriptional inhibition of Hoxd4 expression by noncoding RNAs in human breast cancer cells. *BMC Mol. Biol.* **10,** 12 (2009).

183. Kim, D. H., Saetrom, P., Snøve, O. & Rossi, J. J. MicroRNA-directed transcriptional gene silencing in mammalian cells. *Proc. Natl. Acad. Sci. U. S. A.* **105,** 16230–5 (2008).

184. Kim, D. H., Villeneuve, L. M., Morris, K. V & Rossi, J. J. Argonaute-1 directs siRNA-mediated transcriptional gene silencing in human cells. *Nat. Struct. Mol. Biol.* **13,** 793–797 (2006).

185. O'Neill, L. A. J., Golenbock, D. & Bowie, A. G. The history of Toll-like receptors — redefining innate immunity. *Nat. Rev. Immunol.* **13,** 453–460 (2013).

186. Lehmann, S. M. *et al.* An unconventional role for miRNA: let-7 activates Toll-like receptor 7 and causes neurodegeneration. *Nat. Neurosci.* **15,** 827–835 (2012).

187. Fabbri, M. *et al.* MicroRNAs bind to Toll-like receptors to induce prometastatic inflammatory response. *Proc. Natl. Acad. Sci.* **109,** E2110–E2116 (2012).

188. He, W. A. *et al.* Microvesicles containing miRNAs promote muscle cell death in cancer cachexia via TLR7. *Proc. Natl. Acad. Sci.* **111,** 4525–4529 (2014).

189. Friedman, R. C., Farh, K. K.-H., Burge, C. B. & Bartel, D. P. Most mammalian mRNAs are conserved targets of microRNAs. *Genome Res.* **19,** 92–105 (2008).

190. Griffiths-Jones lab. miRBase. Available at: http://www.mirbase.org/cgi-bin/query.pl?terms=hsa-miR. (Accessed: 28th September 2017)

191. Guo, L. & Chen, F. A challenge for miRNA: multiple isomiRs in miRNAomics. *Gene* **544,** 1–7 (2014).

192. Jongen-Lavrencic, M., Sun, S. M., Dijkstra, M. K., Valk, P. J. M. & Lowenberg, B. MicroRNA expression profiling in relation to the genetic heterogeneity of acute myeloid leukemia. *Blood* **111,** 5078–5085 (2008).

193. Corsten, M. F. *et al.* MicroRNA-21 Knockdown Disrupts Glioma Growth In vivo and Displays Synergistic Cytotoxicity with Neural Precursor Cell Delivered S-TRAIL in Human Gliomas. *Cancer Res.* **67,** 8994–9000 (2007).

194. Fulci, V. *et al.* Quantitative technologies establish a novel microRNA profile of chronic lymphocytic leukemia. *Blood* **109,** 4944–4951 (2007).

195. Meng, F. *et al.* MicroRNA-21 Regulates Expression of the PTEN Tumor Suppressor Gene in Human Hepatocellular Cancer. *Gastroenterology* **133,** 647–658 (2007).

196. Frankel, L. B. *et al.* Programmed Cell Death 4 (PDCD4) Is an Important Functional Target of the MicroRNA *miR-21* in Breast Cancer Cells. *J. Biol. Chem.* **283,** 1026–1033 (2008).

197. Nair, V. S., Maeda, L. S. & Ioannidis, J. P. A. Clinical Outcome Prediction by MicroRNAs in Human Cancer: A Systematic Review. *JNCI J. Natl. Cancer Inst.* **104,** 528–540 (2012).

198. Vo, N. K., Dalton, R. P., Liu, N., Olson, E. N. & Goodman, R. H. Affinity purification of microRNA-133a with the cardiac transcription factor, Hand2. *Proc. Natl. Acad. Sci.* **107,** 19231–19236 (2010).

199. Sethupathy, P., Megraw, M. & Hatzigeorgiou, A. G. A guide through present computational approaches for the identification of mammalian microRNA targets. *Nat. Methods* **3,** 881–886 (2006).

200. Kordelas, L. *et al.* MSC-derived exosomes: a novel tool to treat therapy-refractory graft-versus-host disease. *Leukemia* (2014). doi:10.1038/leu.2014.41

201. Musunuri, S. *et al.* Increased Levels of Extracellular Microvesicle Markers

and Decreased Levels of Endocytic/Exocytic Proteins in the Alzheimer's Disease Brain. *J. Alzheimer's Dis.* **54,** 1671–1686 (2016).

202. Gould, S. J. & Raposo, G. As we wait: coping with an imperfect nomenclature for extracellular vesicles. *J. Extracell. Vesicles* **2,** 20389 (2013).

203. Johnstone, R. M., Adam, M., Hammond, J. R., Orr, L. & Turbide, C. Vesicle formation during reticulocyte maturation. Association of plasma membrane activities with released vesicles (exosomes). *J. Biol. Chem.* **262,** 9412-20 (1987).

204. Cocucci, E., Racchetti, G. & Meldolesi, J. Shedding microvesicles: artefacts no more. *Trends Cell Biol.* **19,** 43–51 (2009).

205. Colombo, M. *et al.* Analysis of ESCRT functions in exosome biogenesis, composition and secretion highlights the heterogeneity of extracellular vesicles. *J. Cell Sci.* **126,** 5553–5565

206. Ratajczak, J. *et al.* Embryonic stem cell-derived microvesicles reprogram hematopoietic progenitors: evidence for horizontal transfer of mRNA and protein delivery. *Leukemia* **20,** 847–856 (2006).

207. Valadi, H. *et al.* Exosome-mediated transfer of mRNAs and microRNAs is a novel mechanism of genetic exchange between cells. *Nat. Cell Biol.* **9,** 654–659 (2007).

208. Yuan, A. *et al.* Transfer of MicroRNAs by Embryonic Stem Cell Microvesicles. *PLoS One* **4,** e4722 (2009).

209. Ismail, N. *et al.* Macrophage microvesicles induce macrophage differentiation and miR-223 transfer. *Blood* **121,** 984–95 (2013).

210. Montecalvo, A. *et al.* Mechanism of transfer of functional microRNAs between mouse dendritic cells via exosomes. *Blood* **119,** 756–766 (2012).

211. Palma, J. *et al.* MicroRNAs are exported from malignant cells in customized particles. *Nucleic Acids Res.* **40,** 9125-9138 (2012).

212. Tan, X. *et al.* Role of erythrocytes and platelets in the hypercoagulable status in polycythemia vera through phosphatidylserine exposure and microparticle generation. *Thromb. Haemost.* **109,** 1025–1032 (2013).

213. Villarroya-Beltri, C. *et al.* Sumoylated hnRNPA2B1 controls the sorting of miRNAs into exosomes through binding to specific motifs. *Nat. Commun.* **4,** (2013).

214. Ogawa, Y., Taketomi, Y., Murakami, M., Tsujimoto, M. & Yanoshita, R. Small RNA Transcriptomes of Two Types of Exosomes in Human Whole Saliva Determined by Next Generation Sequencing. *Biol. Pharm. Bull.* **36,** 66–75 (2013).

215. Tavian, M. & Peault, B. Embryonic development of the human hematopoietic system. *Int. J. Dev. Biol.* **49,** 243–250 (2005).

216. Lin, C. S., Lim, S. K., D'Agati, V. & Costantini, F. Differential effects of an erythropoietin receptor gene disruption on primitive and definitive erythropoiesis. *Genes Dev.* **10,** 154-64 (1996).

217. Shizuru, J. A., Negrin, R. S. & Weissman, I. L. Hematopoietic Stem and Progenitor Cells: Clinical and Preclinical Regeneration of the Hematolymphoid System. *Annu. Rev. Med.* **56,** 509–538 (2005).

218. Elliott, S., Pham, E. & Macdougall, I. C. Erythropoietins: A common mechanism of action. *Experimental Hematology* **36,** 1573–1584 (2008).

219. Migliaccio, G. *et al.* In Vitro Mass Production of Human Erythroid Cells from the Blood of Normal Donors and of Thalassemic Patients. *Blood Cells, Mol. Dis.* **28,** 169–180 (2002).

220. Eshghi, S., Vogelezang, M. G., Hynes, R. O., Griffith, L. G. & Lodish, H. F.

??4??1 integrin and erythropoietin mediate temporally distinct steps in erythropoiesis: Integrins in red cell development. *J. Cell Biol.* **177,** 871–880 (2007).

221. Foster, S. D., Oram, S. H., Wilson, N. K. & Göttgens, B. From genes to cells to tissues—modelling the haematopoietic system. *Mol. Biosyst.* **5,** 1413 (2009).

222. Wu, H., Liu, X., Jaenisch, R. & Lodish, H. F. Generation of committed erythroid BFU-E and CFU-E progenitors does not require erythropoietin or the erythropoietin receptor. *Cell* **83,** 59-67 (1995).

223. Lodish, H. F. Signalling by the erythropoietin receptor. in *Erythropoiesis and erytropoietins* 155–174 (2009).

224. Ghaffari, S. *et al.* AKT induces erythroid-cell maturation of JAK2-deficient fetal liver progenitor cells and is required for Epo regulation of erythroid-cell differentiation. *Blood* **107,** 1888–1891 (2006).

225. JANDL, J. H., INMAN, J. K., SIMMONS, R. L. & ALLEN, D. W. Transfer of iron from serum iron-binding protein to human reticulocytes. *J. Clin. Invest.* **38,** 161–185 (1959).

226. Suzuki, M. *et al.* GATA factor switching from GATA2 to GATA1 contributes to erythroid differentiation. *Genes to Cells* **18,** 921–933 (2013).

227. Ji, P., Yeh, V., Ramirez, T., Murata-Hori, M. & Lodish, H. F. Histone deacetylase 2 is required for chromatin condensation and subsequent enucleation of cultured mouse fetal erythroblasts. *Haematologica* **95,** 2013-2021 (2010).

228. Koury, S. T., Koury, M. J. & Bondurant, M. C. Cytoskeletal distribution and function during the maturation and enucleation of mammalian erythroblasts. *J. Cell Biol.* **109,** 3005–3013 (1989).

229. Konstantinidis, D. G. *et al.* Signaling and cytoskeletal requirements in erythroblast enucleation. *Blood* **119,** 6118–6127 (2012).

230. Skutelsky, E. & Danon, D. Comparative study of nuclear expulsion from the late erythroblast and cytokinesis. *Exp. Cell Res.* **60,** 427–436 (1970).

231. Hanspal, M., Smockova, Y. & Uong, Q. Molecular identification and functional characterization of a novel protein that mediates the attachment of erythroblasts to macrophages. *Blood* **92,** 2940–50 (1998).

232. BESSIS, M. C. & BRETON-GORIUS, J. Iron metabolism in the bone marrow as seen by electron microscopy: a critical review. *Blood* **19,** 635-63 (1962).

233. Rhodes, M. M., Kopsombut, P., Bondurant, M. C., Price, J. O. & Koury, M. J. Adherence to macrophages in erythroblastic islands enhances erythroblast proliferation and increases erythrocyte production by a different mechanism than erythropoietin. *Blood* **111,** 1700-1708 (2008).

234. Iavarone, A. *et al.* Retinoblastoma promotes definitive erythropoiesis by repressing Id2 in fetal liver macrophages. *Nature* **432,** 1040-1045 (2004).

235. Clark, A. J., Doyle, K. M. & Humbert, P. O. Cell-intrinsic requirement for pRb in erythropoiesis. *Blood* **104,** 1324-1326 (2004).

236. Seki, M. & Shirasawa, H. Role of the reticular cells during maturation process of the erythroblast. 3. The fate of phagocytized nucleus. *Acta Pathol. Jpn.* **15,** 387–405 (1965).

237. Gutierrez, L. *et al.* Homotypic signalling regulates Gata1 activity in the erythroblastic island. *Development* **131,** 3183–3193 (2004).

238. Mortensen, M. *et al.* Loss of autophagy in erythroid cells leads to defective removal of mitochondria and severe anemia in vivo. *Proc. Natl. Acad. Sci.* **107,** 832-837 (2010).

239. Harding, C., Heuser, J. & Stahl, P. Receptor-mediated endocytosis of

transferrin and recycling of the transferrin receptor in rat reticulocytes. *J. Cell Biol.* **97,** 329–339 (1983).

240. CHAPTER V: The reticulocyte maturation in the peripheral blood. *Acta Med. Scand.* **146,** 49–69 (2009).
241. Burka, E. R. RNase activity in erythroid cell lysates. *J. Clin. Invest.* **48,** 1724–1732 (1969).
242. Nagaraj, N. *et al.* Deep proteome and transcriptome mapping of a human cancer cell line. *Mol. Syst. Biol.* **7,** 548 (2011).
243. Macdonald, R. L. & Weir, B. Hematology. in *Cerebral Vasospasm* 44–86 (Elsevier, 2001). doi:10.1016/B978-012464161-7/50005-6
244. Zhan, H. *et al.* MicroRNA deregulation in polycythemia vera and essential thrombocythemia patients. *Blood Cells, Mol. Dis.* **50,** 190–195 (2013).
245. Zhan, M., Miller, C. P., Papayannopoulou, T., Stamatoyannopoulos, G. & Song, C. Z. MicroRNA expression dynamics during murine and human erythroid differentiation. *Exp. Hematol.* **35,** 1015–1025 (2007).
246. Felli, N. *et al.* MicroRNA 223-dependent expression of LMO2 regulates normal erythropoiesis. *Haematologica* **94,** 479–486 (2009).
247. Felli, N. *et al.* MicroRNAs 221 and 222 inhibit normal erythropoiesis and erythroleukemic cell growth via kit receptor down-modulation. *Proc. Natl. Acad. Sci.* **102,** 18081–18086 (2005).
248. Wang, Q. *et al.* MicroRNA miR-24 inhibits erythropoiesis by targeting activin type I receptor ALK4. *Blood* **111,** 588–595 (2008).
249. von Lindern, M., Schmidt, U. & Beug, H. Control of erythropoiesis by erythropoietin and stem cell factor: a novel role for Bruton's tyrosine kinase. *Cell Cycle* **3,** 876–9 (2004).
250. Maguer-Satta, V. *et al.* Regulation of human erythropoiesis by activin A, BMP2, and BMP4, members of the TGFß family. *Exp. Cell Res.* **282,** 110–120 (2003).
251. Li, Y. *et al.* miR-218 inhibits erythroid differentiation and alters iron metabolism by targeting ALAS2 in K562 cells. *Int. J. Mol. Sci.* **16,** 28156–28168 (2015).
252. Lu, J. *et al.* MicroRNA-Mediated Control of Cell Fate in Megakaryocyte-Erythrocyte Progenitors. *Dev. Cell* **14,** 843–853 (2008).
253. Sun, Z. *et al.* miR-150 inhibits terminal erythroid proliferation and differentiation. *Oncotarget* **6,** 43033–43047 (2015).
254. Kim, M. *et al.* MIR144 and MIR451 regulate human erythropoiesis via RAB14. *Br. J. Haematol.* **168,** 583–597 (2015).
255. Yu, D. *et al.* miR-451 protects against erythroid oxidant stress by repressing 14-3-3ζ. *Genes Dev.* **24,** 1620–1633 (2010).
256. Fu, Y. F. *et al.* Mir-144 selectively regulates embryonic {alpha}-hemoglobin synthesis during primitive erythropoiesis. *Blood* **113,** 1340–1349 (2009).
257. Wang, F. *et al.* A regulatory circuit comprising GATA1/2 switch and microRNA-27a/24 promotes erythropoiesis. *Nucleic Acids Res.* **42,** 442–457 (2014).
258. Li, Y. *et al.* The up-regulation of miR-199b-5p in erythroid differentiation is associated with GATA-1 and NF-E2. *Mol. Cells* **37,** 213–9 (2014).
259. Zhu, Y. *et al.* A comprehensive analysis of GATA-1-regulated miRNAs reveals miR-23a to be a positive modulator of erythropoiesis. *Nucleic Acids Res.* **41,** 4129–4143 (2013).
260. Rivkin, N. *et al.* Erythrocyte survival is controlled by microRNA-142. *Haematologica* **102,** 676–685 (2017).
261. Zhang, L., Flygare, J., Wong, P., Lim, B. & Lodish, H. F. miR-191 regulates

mouse erythroblast enucleation by down-regulating Riok3 and Mxi1. *Genes Dev.* **25,** 119–124 (2011).

262. Barde, I. *et al.* A KRAB/KAP1-miRNA Cascade Regulates Erythropoiesis Through Stage-Specific Control of Mitophagy. *Science (80-.).* **340,** 350–353 (2013).

263. Bianchi, E. *et al.* MYB controls erythroid versus megakaryocyte lineage fate decision through the miR-486-3p-mediated downregulation of MAF. *Cell Death Differ.* **22,** 1906–21 (2015).

264. Ma, Y. *et al.* A Feedback Loop Consisting of MicroRNA 23a/27a and the - Like Globin Suppressors KLF3 and SP1 Regulates Globin Gene Expression. *Mol. Cell. Biol.* **33,** 3994–4007 (2013).

265. Li, Y. *et al.* MicroRNA 200a inhibits erythroid differentiation by targeting PDCD4 and THRB. *Br. J. Haematol.* **176,** 50–64 (2017).

266. Wang, F. *et al.* The RNA-binding protein QKI5 regulates primary miR-124-1 processing via a distal RNA motif during erythropoiesis. *Cell Res.* **27,** 416–439 (2017).

267. Zhai, P. F. *et al.* The regulatory roles of MicroRNA-146b-5p and its target platelet-derived growth factor receptor α (PDGFRA) in erythropoiesis and megakaryocytopoiesis. *J. Biol. Chem.* **289,** 22600-22613 (2014).

268. Pase, L. *et al.* miR-451 regulates zebrafish erythroid maturation in vivo via its target gata2. *Blood* **113,** 1794-1804 (2009).

269. Fairbanks, G., Steck, T. L. & Wallach, D. F. H. Electrophoretic analysis of the major polypeptides of the human erythrocyte membrane. *Biochemistry* **10,** 2606-2617 (1971).

270. D'Alessandro, A., Righetti, P. G. & Zolla, L. The red blood cell proteome and interactome: An update. *Journal of Proteome Research* **9,** 144-163 (2010).

271. Liu, S. C., Derick, L. H. & Palek, J. Visualization of the hexagonal lattice in the erythrocyte membrane skeleton. *J. Cell Biol.* **104,** 527-536 (1987).

272. Steck, T. L. The organization of proteins in the human red blood cell membrane. A review. *J. Cell Biol.* **62,** 1–19 (1974).

273. Shotton, D. M., Burke, B. E. & BRANTON, D. The molecular structure of human erythrocyte spectrin. Biophysical and electron microscopic studies. *J. Mol. Biol.* **131,** 303–329 (1979).

274. An, X. *et al.* Identification and functional characterization of protein 4.1R and actin-binding sites in erythrocyte β spectrin: Regulation of the interactions by phosphatidylinositol-4,5-bisphosphate. *Biochemistry* **44,** 10681–10688 (2005).

275. Spectrin: Current understanding of its physical, biochemical, and functional properties. *Life Sci.* **19,** 1–17 (1976).

276. Chasis, J. A. & Mohandas, N. Erythrocyte membrane deformability and stability: Two distinct membrane properties that are independently regulated by skeletal protein associations. *J. Cell Biol.* **103,** 343–350 (1986).

277. Tyler, J. M., Hargreaves, W. R. & Branton, D. Purification of two spectrin-binding proteins: biochemical and electron microscopic evidence for site-specific reassociation between spectrin and bands 2.1 and 4.1. *Proc. Natl. Acad. Sci. U. S. A.* **76,** 5192–6 (1979).

278. Mueller, T. J. & Morrison, M. Glycoconnectin (PAS 2), a membrane attachment site for the human erythrocyte cytoskeleton. *Prog. Clin. Biol. Res.* **56,** 95–116 (1981).

279. Bennett, V. & Baines, A. J. Spectrin and Ankyrin-Based Pathways:

Metazoan Inventions for Integrating Cells Into Tissues. *Physiol Rev* **81,** 1353–1392 (2001).

280. Telen, M. J. Erythrocyte blood group antigens: not so simple after all. *Blood* **85,** 299–306 (1995).
281. Kifor, G., Toon, M. R., Janoshazi, A. & Solomon, A. K. Interaction between red cell membrane band 3 and cytosolic carbonic anhydrase. *J. Membr. Biol.* **134,** 169–179 (1993).
282. Weaver, D. C., Pasternack, G. R. & Marchesi, V. T. The structural basis of ankyrin function. II. Identification of two functional domains. *J Biol Chem* **259,** 6170-5. (1984).
283. Tanner, M. J. The major integral proteins of the human red cell. *Baillieres Clin Haematol* **6,** 333–356 (1993).
284. Poole, J. Red cell antigens on band 3 and glycophorin A. *Blood Rev.* **14,** 31–43 (2000).
285. Dean, L. The Rh blood group. in *Blood Groups and Red Cell Antigens [Internet].* Chapter 7 (2005).
286. Anniss, A. M. & Sparrow, R. L. Expression of CD47 (integrin-associated protein) decreases on red blood cells during storage. *Transfus. Apher. Sci.* **27,** 233–238 (2002).
287. Marfatia, S. M., Lue, R. A., Branton, D. & Chishti, A. H. In vitro binding studies suggest a membrane-associated complex between erythroid p55, protein 4.1, and glycophorin C. *J. Biol. Chem.* **269,** 8631–8634 (1994).
288. Ringrose, J. H. *et al.* Highly Efficient Depletion Strategy for the Two Most Abundant Erythrocyte Soluble Proteins Improves Proteome Coverage Dramatically. doi:10.1021/pr8001029
289. Pandey, K. B. & Rizvi, S. I. Markers of Oxidative Stress in Erythrocytes and Plasma During Aging in Humans. *Oxid. Med. Cell. Longev.* **3,** 2–12 (2010).
290. Cohen, G. & Hochstein, P. Glutathione Peroxidase: The Primary Agent for the Elimination of Hydrogen Peroxide in Erythrocytes. *Biochemistry* **2,** 1420–1428 (1963).
291. Agar, N. S., Sadrzadeh, S. M. H., Hallaway, P. E. & Eaton, J. W. Erythrocyte catalase. A somatic oxidant defense? *J. Clin. Invest.* **77,** 319–321 (1986).
292. Low, F. M., Hampton, M. B. & Winterbourn, C. C. Peroxiredoxin 2 and Peroxide Metabolism in the Erythrocyte. *Antioxid. Redox Signal.* **10,** 1621–1630 (2008).
293. Neelam, S., Kakhniashvili, D. G., Wilkens, S., Levene, S. D. & Goodman, S. R. Functional 20S proteasomes in mature human red blood cells. *Exp. Biol. Med. (Maywood).* **236,** 580–591 (2011).
294. Betz, T., Lenz, M., Joanny, J.-F. & Sykes, C. ATP-dependent mechanics of red blood cells. *Proc. Natl. Acad. Sci.* **106,** 15320–15325 (2009).
295. Kakhniashvili, D. G. The Human Erythrocyte Proteome: Analysis by Ion Trap Mass Spectrometry. *Mol. Cell. Proteomics* **3,** 501–509 (2004).
296. Dinkla, S., Novotný, V. M. J., Joosten, I. & Bosman, G. J. C. G. M. Storage-induced changes in erythrocyte membrane proteins promote recognition by autoantibodies. *PLoS One* **7,** (2012).
297. Pasini, E. M. *et al.* In-depth analysis of the membrane and cytosolic proteome of red blood cells. *Blood* **108,** 791–801 (2006).
298. Bryk, A. H. & Wiśniewski, J. R. Quantitative Analysis of Human Red Blood Cell Proteome. *J. Proteome Res.* **16,** 2752-2761 (2017).
299. van Gestel, R. A. *et al.* Quantitative erythrocyte membrane proteome analysis with Blue-Native/SDS PAGE. *J. Proteomics* **73,** 456–465 (2010).

300. Doss, J. F. *et al.* A comprehensive joint analysis of the long and short RNA transcriptomes of human erythrocytes. *BMC Genomics* **16,** 952 (2015).
301. Lamonte, G. *et al.* Translocation of sickle cell erythrocyte MicroRNAs into Plasmodium falciparum inhibits parasite translation and contributes to malaria resistance. *Cell Host Microbe* **12,** 187–199 (2012).
302. Suzuki, Y. & Sugano, S. Construction of a full-length enriched and a 5'-end enriched cDNA library using the oligo-capping method. *Methods Mol. Biol.* **221,** 73–91 (2003).
303. Watanabe, J., Wakaguri, H., Sasaki, M., Suzuki, Y. & Sugano, S. Comparasite: A database for comparative study of transcriptomes of parasites defined by full-length cDNAs. *Nucleic Acids Res.* **35,** (2007).
304. Wakaguri, H., Suzuki, Y., Sasaki, M., Sugano, S. & Watanabe, J. Inconsistencies of genome annotations in apicomplexan parasites revealed by 5'-end-one-pass and full-length sequences of oligo-capped cDNAs. *BMC Genomics* **10,** 312 (2009).
305. Shemin, D. & Rittenberg, D. THE LIFE SPAN OF THE HUMAN RED BLOOD CELL.
306. Campisi, J. & d'Adda di Fagagna, F. Cellular senescence: when bad things happen to good cells. *Nat. Rev. Mol. Cell Biol.* **8,** 729–740 (2007).
307. Gkouvatsos, K., Papanikolaou, G. & Pantopoulos, K. Regulation of iron transport and the role of transferrin. *Biochimica et Biophysica Acta - General Subjects* **1820,** 188–202 (2012).
308. Ponka, P., Beaumont, C. & Richardson, D. R. Function and regulation of transferrin and ferritin. *Semin. Hematol.* **35,** 35–54 (1998).
309. Ganzoni, A. M., Oakes, R. & Hillman, R. S. Red cell aging in vivo. *J. Clin. Invest.* **50,** 1373–8 (1971).
310. Branch, D. R., Hian, A. L., Carlson, F., Maslow, W. C. & Petz, L. D. Erythrocyte age-fractionation using a Percoll(TM)-Renografin?? density gradient: Application to autologous red cell antigen determinations in recently transfused patients. *Am. J. Clin. Pathol.* **80,** 453–458 (1983).
311. Leif, R. C. *et al.* Two-dimensional impedance studies of BSA buoyant density separated human erythrocytes. *Cytometry* **6,** 13–21 (1985).
312. Warth, J. A. & Rucknagel, D. L. Density ultracentrifugation of sickle cells during and after pain crisis: increased dense echinocytes in crisis. *Blood* **64,** 507–515 (1984).
313. Franco, R. S. *et al.* Changes in the properties of normal human red blood cells during in vivo aging. *Am. J. Hematol.* **88,** 44–51 (2013).
314. Suzuki, T. & Dale, G. L. Biotinylated erythrocytes: in vivo survival and in vitro recovery. *Blood* **70,** 791–5 (1987).
315. Bartosz, G. Aging of the erythrocyte. VII. On the possible causes of inactivation of red cell enzymes. *Mech. Ageing Dev.* **13,** 379–85 (1980).
316. Rifkind, J. M. & Nagababu, E. Hemoglobin redox reactions and red blood cell aging. *Antioxid. Redox Signal.* **18,** 2274–83 (2013).
317. Walder, J. A. *et al.* The interaction of hemoglobin with the cytoplasmic domain of band 3 of the human erythrocyte membrane. *J. Biol. Chem.* **259,** 10238–10246 (1984).
318. Misra, H. P. & Fridovich, I. The generation of superoxide radical during the autoxidation of hemoglobin. *J. Biol. Chem.* **247,** 6960–6962 (1972).
319. Nagababu, E. & Rifkind, J. M. Reaction of hydrogen peroxide with ferrylhemoglobin: Superoxide production and heme degradation. *Biochemistry* **39,** 12503–12511 (2000).
320. Imanishi, H., Nakai, T., Abe, T. & Takino, T. Glutathione metabolism in

red cell aging. *Mech. Ageing Dev.* **32,** 57–62 (1985).

321. Bartosz, G., Tannert, C., Fried, R. & Leyko, W. Superoxide dismutase activity decreases during erythrocyte aging. *Experientia* **34,** 1464 (1978).

322. Low, P. S., Waugh, S. M., Zinke, K. & Drenckhahn, D. The role of hemoglobin denaturation and band 3 clustering in red blood cell aging. *Science (80-.).* **227,** 531–533 (1985).

323. Snyder, L. M. *et al.* Irreversible spectrin-haemoglobin crosslinking in vivo: a marker for red cell senescence. *Br. J. Haematol.* **53,** 379–384 (1983).

324. Kay, M. M. Role of physiologic autoantibody in the removal of senescent human red cells. *J. Supramol. Struct.* **9,** 555-567 (1978).

325. Lutz, H. U. *et al.* Naturally occurring anti-band-3 antibodies and complement together mediate phagocytosis of oxidatively stressed human erythrocytes. *Proc. Natl. Acad. Sci. U. S. A.* **84,** 7368–72 (1987).

326. de Back, D. Z., Kostova, E. B., van Kraaij, M., van den Berg, T. K. & van Bruggen, R. Of macrophages and red blood cells; a complex love story. *Front. Physiol.* **5,** 9 (2014).

327. White, C. *et al.* HRG1 is essential for heme transport from the phagolysosome of macrophages during erythrophagocytosis. *Cell Metab.* **17,** 261–270 (2013).

328. Tenhunen, R., Marver, H. S. & Schmid, R. The enzymatic conversion of heme to bilirubin by microsomal heme oxygenase. *Proc. Natl. Acad. Sci. U. S. A.* **61,** 748–755 (1968).

329. Knutson, M. D., Oukka, M., Koss, L. M., Aydemir, F. & Wessling-Resnick, M. Iron release from macrophages after erythrophagocytosis is up-regulated by ferroportin 1 overexpression and down-regulated by hepcidin. *PNAS* **102,** 1324-1328 (2005).

330. Ganz, T. Macrophages and systemic iron homeostasis. *Journal of Innate Immunity* **4,** 446–453 (2012).

331. Soe-Lin, S., Sheftel, A. D., Wasyluk, B. & Ponka, P. Nramp1 equips macrophages for efficient iron recycling. *Exp. Hematol.* **36,** 929-937 (2008).

332. Soe-Lin, S. *et al.* Nramp1 promotes efficient macrophage recycling of iron following erythrophagocytosis in vivo. *Proc. Natl. Acad. Sci. U. S. A.* **106,** 5960–5 (2009).

333. Kristiansen, M. *et al.* Identification of the haemoglobin scavenger receptor. *Nature* **409,** 198–201 (2001).

334. RIFKIND, R. A. & DANON, D. HEINZ BODY ANEMIA--AN ULTRASTRUCTURAL STUDY. I. HEINZ BODY FORMATION. *Blood* **25,** 885-96 (1965).

335. Rieber, E. E., Shields, C. E., Conrad, M. E. & Crosby, W. H. Some properties of rat erythrocytes after splenectomy and with reimplanted spleens. *Am. J. Physiol.* **212,** 897–900 (1967).

336. NHS. Why give blood | Blood Donation. Available at: https://www.blood.co.uk/why-give-blood/. (Accessed: 29th September 2017)

337. Williamson, L. M. & Cardigan, R. Production and Storage of Blood Components. in *Practical Transfusion Medicine* 259–273 (Blackwell Publishing Ltd). doi:10.1002/9780470988411.ch23

338. Hess, J. R. An update on solutions for red cell storage. *Vox Sanguinis* **91,** 13-19 (2006).

339. Sparrow, R. L. Time to revisit red blood cell additive solutions and storage conditions: A role for 'omics' analyses. *Blood Transfusion* **10,** (2012).

340. Högman, C. F., Hedlund, K. & Zetterström, H. Clinical Usefulness of Red

Cells Preserved in Protein-Poor Mediums. *N. Engl. J. Med.* **299,** 1377–1382 (1978).

341. NAKAO, K., WADA, T., KAMIYAMA, T., NAKAO, M. & NAGANO, K. A Direct Relationship between Adenosine Triphosphate-level and in vivo Viability of Erythrocytes. *Nature* **194,** 877–878 (1962).

342. H??gman, C. F., Hedlund, K. & Sahlestrom, Y. Red Cell Preservation in Protein???Poor Media: III. Protection Against in vitro Hemolysis. *Vox Sang.* **41,** 274–281 (1981).

343. Sparrow, R. L., Sran, A., Healey, G., Veale, M. F. & Norris, P. J. In vitro measures of membrane changes reveal differences between red blood cells stored in saline-adenine-glucose-mannitol and AS-1 additive solutions: A paired study. *Transfusion* **54,** 560–568 (2014).

344. Lutz, H. U., Liu, S. C. & Palek, J. Release of spectrin-free vesicles from human erythrocytes during ATP depletion. I. Characterization of spectrin-free vesicles. *J. Cell Biol.* **73,** 548–560 (1977).

345. Koch, C. G. *et al.* Red blood cell storage: How long is too long? *Annals of Thoracic Surgery* **96,** 1894–1899 (2013).

346. D'Almeida, M. S., Gray, D., Martin, C., Ellis, C. G. & Chin-Yee, I. H. Effect of prophylactic transfusion of stored RBCs on oxygen reserve in response to acute isovolemic hemorrhage in a rodent model. *Transfusion* **41,** 950–956 (2001).

347. Greenwalt, T. J., Bryan, D. J. & Dumaswala, U. J. Erythrocyte Membrane Vesiculation and Changes in Membrane Composition during Storage in Citrate-Phosphate-Dextrose-Adenine-1. *Vox Sang.* **47,** 261–270 (1984).

348. Greenwalt, T. J., McGuinness, C. G. & Dumaswala, U. J. Studies in Red Blood Cell Preservation: 4. Plasma Vesicle Hemoglobin Exceeds Free Hemoglobin. *Vox Sang.* **61,** 14–17 (1991).

349. Latham, J. T., Bove, J. R. & Weirich, F. L. Chemical and hematologic changes in stored CPDA???1 blood. *Transfusion* **22,** 158–159 (1982).

350. Atreya, C., Kannan, M., Mohan, K. V. K. & Kulkarni, S. Membrane array-based differential profiling of platelets during storage for 52 miRNAs associated with apoptosis. *Transfusion* **49,** 1443–1450 (2009).

351. Yu, S. *et al.* Detection of apoptosis-associated microRNA in human apheresis platelets during storage by quantitative real-time polymerase chain reaction analysis. *Blood Transfus.* **12,** 541–547 (2014).

352. Kannan, M. & Atreya, C. Differential profiling of human red blood cells during storage for 52 selected microRNAs. *Transfusion* **50,** 1581–1588 (2010).

353. Pan, B. T., Teng, K., Wu, C., Adam, M. & Johnstone, R. M. Electron microscopic evidence for externalization of the transferrin receptor in vesicular form in sheep reticulocytes. *J. Cell Biol.* **101,** 942–948 (1985).

354. Pan, B. T. & Johnstone, R. M. Fate of the transferrin receptor during maturation of sheep reticulocytes in vitro: Selective externalization of the receptor. *Cell* **33,** 967–978 (1983).

355. Dumaswala, U. J. & Greenwalt, T. J. Human erythrocytes shed exocytic vesicles in vivow. *Transfusion* **24,** 490–492 (1984).

356. Willekens, F. L., Bosch, F. H., Roerdinkholder-Stoelwinder, B., Groenen-Döpp, Y. A. & Werre, J. M. Quantification of loss of haemoglobin components from the circulating red blood cell in vivo. *Eur. J. Haematol.* **58,** 246–50 (1997).

357. Willekens, F. L. A. *et al.* Hemoglobin loss from erythrocytes in vivo results from spleen-facilitated vesiculation. *Blood* **101,** 747–751 (2003).

358. Willekens, F. L. A. *et al*. Erythrocyte vesiculation: A self-protective mechanism? *Br. J. Haematol.* **141,** 549-556 (2008).

359. ALLAN, D., BILLAH, M. M., FINEAN, J. B. & MICHELL, R. H. Release of diacylglycerol-enriched vesicles from erythrocytes with increased intracellular [Ca2+]. *Nature* **261,** 58–60 (1976).

360. Canellini, G. *et al*. Red blood cell microparticles and blood group antigens: an analysis by flow cytometry. *Blood Transfus.* **10 Suppl 2,** 39–45 (2012).

361. Salzer, U. *et al*. Vesicles generated during storage of red cells are rich in the lipid raft marker stomatin. *Transfusion* **48,** 451–462 (2008).

362. Cole, W. F., Rumsby, M. G., Longster, G. H. & Tovey, L. A. The release of erythrocyte membrane antigens to the plasma as membrane microvesicles during the storage of human blood for transfusion [proceedings]. *Biochem. Soc. Trans.* **6,** 1375–8 (1978).

363. Rho, J. *et al*. Magnetic nanosensor for detection and profiling of erythrocyte-derived microvesicles. *ACS Nano* **7,** 11227–11233 (2013).

364. Kriebardis, A. G. *et al*. RBC-derived vesicles during storage: Ultrastructure, protein composition, oxidation, and signaling components. *Transfusion* **48,** 1943–1953 (2008).

365. Eikelboom, J. W., Cook, R. J., Liu, Y. & Heddle, N. M. Duration of red cell storage before transfusion and in-hospital mortality. *Am. Heart J.* **159,** (2010).

366. Vandromme, M. J. *et al*. Transfusion and Pneumonia in the Trauma Intensive Care Unit: An Examination of the Temporal Relationship. *J. Trauma Inj. Infect. Crit. Care* **67,** 97–101 (2009).

367. Hébert, P. C. *et al*. A pilot trial evaluating the clinical effects of prolonged storage of red cells. *Anesth. Analg.* **100,** 1433–1438 (2005).

368. Robinson, S. D. *et al*. Red blood cell storage duration and mortality in patients undergoing percutaneous coronary intervention. *Am. Heart J.* **159,** 876–881 (2010).

369. Koch, C. G. *et al*. Duration of Red-Cell Storage and Complications after Cardiac Surgery. *N. Engl. J. Med.* **358,** 1229–1239 (2008).

370. McKenny, M. *et al*. Age of transfused blood is not associated with increased postoperative adverse outcome after cardiac surgery. *Br. J. Anaesth.* **106,** 643–649 (2011).

371. Baumgartner, J. M. *et al*. Red blood cell supernatant potentiates LPS-induced proinflammatory cytokine response from peripheral blood mononuclear cells. *J. Interferon Cytokine Res.* **29,** 333–338 (2009).

372. Baumgartner, J. M., Silliman, C. C., Moore, E. E., Banerjee, A. & McCarter, M. D. Stored Red Blood Cell Transfusion Induces Regulatory T Cells. *J. Am. Coll. Surg.* **208,** 110–119 (2009).

373. Sadallah, S., Eken, C. & Schifferli, J. A. Erythrocyte-derived ectosomes have immunosuppressive properties. *J. Leukoc. Biol.* **84,** 1316-1325 (2008).

374. Sweeney, J., Kouttab, N. & Kurtis, J. Stored red blood cell supernatant facilitates thrombin generation. *Transfusion* **49,** 1569–1579 (2009).

375. Zimring, J. C. *et al*. A novel mouse model of red blood cell storage and posttransfusion in vivo survival. *Transfusion* **49,** 1546–1553 (2009).

376. Hod, E. A. *et al*. Transfusion of red blood cells after prolonged storage produces harmful effects that are mediated by iron and inflammation. *Blood* **115,** 4284–4292 (2010).

377. Zecher, D., Cumpelik, A. & Schifferli, J. A. Erythrocyte-derived microvesicles amplify systemic inflammation by thrombin-dependent activation of complement. *Arterioscler. Thromb. Vasc. Biol.* **34,** 313–320

(2014).

378. Vlaar, A. P. J. *et al.* Supernatant of aged erythrocytes causes lung inflammation and coagulopathy in a 'two-hit' in vivo syngeneic transfusion model. *Anesthesiology* **113,** 92–103 (2010).

379. Silliman, C. C. *et al.* Plasma and lipids from stored packed red blood cells cause acute lung injury in an animal model. *J. Clin. Invest.* **101,** 1458-1467 (1998).

380. Bleakley, M. & Riddell, S. R. Molecules and mechanisms of the graft-versus-leukaemia effect. *Nat. Rev. Cancer* **4,** 371–380 (2004).

381. Gooley, T. A. *et al.* Reduced Mortality after Allogeneic Hematopoietic-Cell Transplantation. *N. Engl. J. Med.* **363,** 2091–2101 (2010).

382. Lee, S. J., Vogelsang, G. & Flowers, M. E. D. Chronic graft-versus-host disease. *Biology of Blood and Marrow Transplantation* **9,** 215-233 (2003).

383. Ferrara, J. L., Levine, J. E., Reddy, P. & Holler, E. Graft-versus-host disease. *The Lancet* **373,** 1550-1561 (2009).

384. Nestel, F. P., Price, K. S., Seemayer, T. A. & Lapp, W. S. Macrophage priming and lipopolysaccharide-triggered release of tumor necrosis factor alpha during graft-versus-host disease. *J. Exp. Med.* **175,** 405-13 (1992).

385. Koyama, M. *et al.* Recipient nonhematopoietic antigen-presenting cells are sufficient to induce lethal acute graft-versus-host disease. *Nat. Med.* **18,** 135–142 (2011).

386. Shlomchik, W. D. Prevention of Graft Versus Host Disease by Inactivation of Host Antigen-Presenting Cells. *Science (80-.).* **285,** 412-415 (1999).

387. Carlson, M. J. *et al.* In vitro-differentiated TH17 cells mediate lethal acute graft-versus-host disease with severe cutaneous and pulmonary pathologic manifestations. *Blood* **113,** 1365-74 (2009).

388. Nikolic, B., Lee, S., Bronson, R. T., Grusby, M. J. & Sykes, M. Th1 and Th2 mediate acute graft-versus-host disease, each with distinct end-organ targets. *J. Clin. Invest.* **105,** 1289-1298 (2000).

389. Sunul, H. & Erguven, N. Transfusion-associated graft-versus-host disease. *Transfus. Apher. Sci.* **49,** 331–333 (2013).

390. Bratosin, D. *et al.* Cellular and molecular mechanisms of senescent erythrocyte phagocytosis by macrophages. A review. *Biochimie* **80,** 173-95 (1998).

391. Hornig, R. & Lutz, H. U. Band 3 protein clustering on human erythrocytes promotes binding of naturally occurring anti-band 3 and anti-spectrin antibodies. *Exp. Gerontol.* **35,** 1025-44 (2000).

392. Willekens, F. L. A. *et al.* Liver Kupffer cells rapidly remove red blood cell-derived vesicles from the circulation by scavenger receptors. *Blood* **105,** 2141–2145 (2005).

393. Lozzio, C. B. & Lozzio, B. B. Human chronic myelogenous leukemia cell-line with positive Philadelphia chromosome. *Blood* **45,** 321-34 (1975).

394. Schneider, U., Schwenk, H. U. & Bornkamm, G. Characterization of EBV-genome negative "null" and "T" cell lines derived from children with acute lymphoblastic leukemia and leukemic transformed non-Hodgkin lymphoma. *Int. J. cancer* **19,** 621-6 (1977).

395. SCHERER, W. F., SYVERTON, J. T. & GEY, G. O. Studies on the propagation in vitro of poliomyelitis viruses. IV. Viral multiplication in a stable strain of human malignant epithelial cells (strain HeLa) derived from an epidermoid carcinoma of the cervix. *J. Exp. Med.* **97,** 695-710 (1953).

396. Beutler, E., West, C. & Blume, K. G. The removal of leukocytes and platelets from whole blood. *J. Lab. Clin. Med.* **88,** 328-33 (1976).

397. Dodge, T; Mitchell, C; Hanahan, D. The preparation and chemical characteristics of hemoglobin-free ghosts of human erythrocytes. *Arch. Biochem. Biophys.* **100,** 119–130 (1963).

398. Deitrick, R. W. Intravascular haemolysis in the recreational runner. *Br J Sp Med* **25,** (1991).

399. Jannot, G., Vasquez-Rifo, A. & Simard, M. J. Argonaute Pull-Down and RISC Analysis Using 2'-O-Methylated Oligonucleotides Affinity Matrices. in 233–249 (Humana Press, 2011). doi:10.1007/978-1-61779-046-1_16

400. Azzouzi, I. *et al.* Deep sequencing and proteomic analysis of the microRNA-induced silencing complex in human red blood cells. *Exp. Hematol.* **43,** 382–392 (2015).

401. Fabian, M. R. *et al.* Mammalian miRNA RISC Recruits CAF1 and PABP to Affect PABP-Dependent Deadenylation. *Mol. Cell* **35,** 868–880 (2009).

402. Flotho, A. & Melchior, F. Sumoylation: A Regulatory Protein Modification in Health and Disease. *Annu. Rev. Biochem.* **82,** 357–385 (2013).

403. Geiss-Friedlander, R. & Melchior, F. Concepts in sumoylation: a decade on. *Nat. Rev. Mol. Cell Biol.* **8,** 947–956 (2007).

404. Sahin, U., Lapaquette, P., Andrieux, A., Faure, G. & Dejean, A. Sumoylation of Human Argonaute 2 at Lysine-402 Regulates Its Stability. *PLoS One* **9,** e102957 (2014).

405. Qi, H. H. *et al.* Prolyl 4-hydroxylation regulates Argonaute 2 stability. *Nature* **455,** 421–424 (2008).

406. Leung, A. K. L. *et al.* Poly(ADP-Ribose) Regulates Stress Responses and MicroRNA Activity in the Cytoplasm. *Mol. Cell* **42,** 489–499 (2011).

407. Rybak, A. *et al.* The let-7 target gene mouse lin-41 is a stem cell specific E3 ubiquitin ligase for the miRNA pathway protein Ago2. *Nat. Cell Biol.* **11,** 1411–1420 (2009).

408. McKenzie, A. J. *et al.* KRAS-MEK Signaling Controls Ago2 Sorting into Exosomes. *Cell Rep.* **15,** 978–987 (2016).

409. Golden, R. J. *et al.* An Argonaute phosphorylation cycle promotes microRNA-mediated silencing. *Nature* **542,** 197–202 (2017).

410. Zeng, Y., Sankala, H., Zhang, X. & Graves, P. R. Phosphorylation of Argonaute 2 at serine-387 facilitates its localization to processing bodies. *Biochem. J.* **413,** 429–436 (2008).

411. Völler, D., Reinders, J., Meister, G. & Bosserhoff, A.-K. Strong reduction of AGO2 expression in melanoma and cellular consequences. *Br. J. Cancer* **109,** 3116–3124 (2013).

412. Wellek, B., Hahn, H. & Opferkuch, W. Quantitative contributions of IgG, IgM and C3 to erythrophagocytosisand rosette formation by peritoneal macrophages, and anti-opsoninactivity of dextran sulfate 500. *Eur. J. Immunol.* **5,** 378–382 (1975).

413. Sambrano, G. R., Parthasarathy, S. & Steinbergt, D. Recognition of oxidatively damaged erythrocytes by a macrophage receptor with specificity for oxidized low density lipoprotein. *Med. Sci.* **91,** 3265–3269 (1994).

414. Sambrano, G. R., Terpstra, V. & Steinberg, D. Independent mechanisms for macrophage binding and macrophage phagocytosis of damaged erythrocytes. Evidence of receptor cooperativity. *Arterioscler. Thromb. Vasc. Biol.* **17,** 3442–8 (1997).

415. Rüdel, S., Flatley, A., Weinmann, L., Kremmer, E. & Meister, G. A multifunctional human Argonaute2-specific monoclonal antibody. *RNA* **14,** 1244–53 (2008).

416. Mebius, R. E. & Kraal, G. Structure and function of the spleen. *Nat. Rev. Immunol.* **5,** 606-616 (2005).
417. Hermanský, F., Poch, T. & Lodrová, V. Peroxidase and pseudoperoxidase reactions in relation to sudanophilia. *Histochemistry* **53,** 89–95 (1977).
418. Leblond, P. F. & Shoucri, R. Calculation of surface area and volume of human erythrocytes from scanning electron micrographs. *J. Microsc.* **113,** 161–70 (1978).
419. Ferret, E., Evrard, C., Foucal, A. & Gervais, P. Volume changes of isolated human K562 leukemia cells induced by electric field pulses. *Biotechnol. Bioeng.* **67,** 520–528 (2000).
420. Azuma-Mukai, A. *et al.* Characterization of endogenous human Argonautes and their miRNA partners in RNA silencing. *Proc. Natl. Acad. Sci. U. S. A.* **105,** 7964–9 (2008).
421. Mantel, P.-Y. *et al.* Infected erythrocyte-derived extracellular vesicles alter vascular function via regulatory Ago2-miRNA complexes in malaria. *Nat. Commun.* **7,** 12727 (2016).
422. Basu, A. *et al.* Proteome analysis of the triton-insoluble erythrocyte membrane skeleton. *J. Proteomics* **128,** 298–305 (2015).
423. Pfeffer, S. R., Huima, T. & Redman, C. M. Biosynthesis of Spectrin and Its Assembly into the Cytoskeletal System of Friend Erythroleukemia Cells.
424. Bosch, F. H. *et al.* Characteristics of red blood cell populations fractionated with a combination of counterflow centrifugation and Percoll separation. *Blood* **79,** 254–60 (1992).
425. Alexander, M. *et al.* Exosome-delivered microRNAs modulate the inflammatory response to endotoxin. *Nat. Commun.* **6,** 7321 (2015).
426. van der Meijden, P. E. J. *et al.* Platelet- and erythrocyte-derived microparticles trigger thrombin generation via factor XIIa. *J. Thromb. Haemost.* **10,** 1355–1362 (2012).
427. Rubin, O. *et al.* Red blood cell-derived microparticles isolated from blood units initiate and propagate thrombin generation. *Transfusion* **53,** 1744–1754 (2013).
428. Jy, W., Johansen, M. E., Bidot, C., Horstman, L. L. & Ahn, Y. S. Red cell-derived microparticles (RMP) as haemostatic agent. *Thromb. Haemost.* **110,** 751–760 (2013).
429. Spronk, H. M. H., ten Cate, H. & van der Meijden, P. E. J. Differential roles of tissue factor and phosphatidylserine in activation of coagulation. *Thromb. Res.* **133 Suppl 1,** S54-6 (2014).
430. Koshiar, R. L., Somajo, S., Norström, E. & Dahlbäck, B. Erythrocyte-derived microparticles supporting activated protein C-mediated regulation of blood coagulation. *PLoS One* **9,** (2014).
431. Berckmans, R. J. *et al.* Cell-derived microparticles circulate in healthy humans and support low grade thrombin generation. *Thromb. Haemost.* **85,** 639–46 (2001).
432. Pattanapanyasat, K. *et al.* Flow cytometric quantitation of red blood cell vesicles in thalassemia. *Cytometry* **57B,** 23–31 (2004).
433. Witwer, K. W. *et al.* Standardization of sample collection, isolation and analysis methods in extracellular vesicle research. *J. Extracell. Vesicles* **2,** 20360 (2013).
434. Allan, D., Thomas, P. & Limbrick, A. R. The isolation and characterization of 60 nm vesicles ('nanovesicles') produced during ionophore A23187-induced budding of human erythrocytes. *Biochem. J.* **188,** 881–7 (1980).
435. SZATANEK, R., BARAN, J., SIEDLAR, M. & BAJ-KRZYWORZEKA, M. Isolation

of extracellular vesicles: Determining the correct approach (Review). *Int. J. Mol. Med.* **36,** 11–17 (2015).

436. Deem, S., Berg, J. T., Kerr, M. E. & Swenson, E. R. Effects of the RBC membrane and increased perfusate viscosity on hypoxic pulmonary vasoconstriction. *J. Appl. Physiol.* **88,** 1520–8 (2000).

437. Tiffert, T. & Lew, V. L. Dynamic morphology and cytoskeletal protein changes during spontaneous inside-out vesiculation of red blood cell membranes. *Pflugers Arch. Eur. J. Physiol.* **466,** 2279–2288 (2014).

438. Guest, M. M., Bond, T. P., Cooper, R. G. & Derrick, J. R. Red Blood Cells: Change in Shape in Capillaries. *Science (80-.).* **142,** 1319–1321 (1963).

439. Fischer, T. & Schmid-Schönbein, H. Tank Tread Motion of Red Cell Membranes in Viscometric Flow: Behavior of Intracellular and Extracellular Markers (with Film). in *Red Cell Rheology* 347–361 (Springer Berlin Heidelberg, 1978). doi:10.1007/978-3-642-67059-6_26

440. Fischer, T. M., Stöhr-Lissen, M. & Schmid-Schönbein, H. The red cell as a fluid droplet: tank tread-like motion of the human erythrocyte membrane in shear flow. *Science* **202,** 894–6 (1978).

441. Nantakomol, D. *et al.* The absolute counting of red cell-derived microparticles with red cell bead by flow rate based assay. *Cytom. Part B - Clin. Cytom.* **76,** 191–198 (2009).

442. Gerotziafas, G. T. *et al.* The acceleration of the propagation phase of thrombin generation in patients with steady-state sickle cell disease is associated with circulating erythrocyte-derived micro particles. *Thromb. Haemost.* **107,** 1044–1052 (2012).

443. Grisendi, G. *et al.* Detection of microparticles from human red blood cells by multiparametric flow cytometry. *Blood Transfus.* **13,** 274–280 (2015).

444. Sewify, E. M., Sayed, D., Abdel Aal, R. F., Ahmad, H. M. & Abdou, M. A. Increased circulating red cell microparticles (RMP) and platelet microparticles (PMP) in immune thrombocytopenic purpura. *Thromb. Res.* **131,** e59–e63 (2013).

445. Larson, M. C., Woodliff, J. E., Hillery, C. A., Kearl, T. J. & Zhao, M. Phosphatidylethanolamine is externalized at the surface of microparticles. *Biochim. Biophys. Acta - Mol. Cell Biol. Lipids* **1821,** 1501–1507 (2012).

446. Almizraq, R., Tchir, J. D. R., Holovati, J. L. & Acker, J. P. Storage of red blood cells affects membrane composition, microvesiculation, and in vitro quality. *Transfusion* **53,** 2258–2267 (2013).

447. Prudent, M. *et al.* Differences between calcium-stimulated and storage-induced erythrocyte-derived microvesicles. *Transfus. Apher. Sci.* **53,** 153–158 (2015).

448. Rubin, O., Crettaz, D., Canellini, G., Tissot, J.-D. & Lion, N. Microparticles in stored red blood cells: an approach using flow cytometry and proteomic tools. *Vox Sang.* **95,** 288–297 (2008).

449. Guyatt, G. H. *et al.* GRADE: an emerging consensus on rating quality of evidence and strength of recommendations. *BMJ* **336,** 924–6 (2008).

450. Alexander, P. E. *et al.* Transfusion of fresher vs older red blood cells in hospitalized patients: a systematic review and meta-analysis. *Blood* **127,** 400–410 (2016).

451. Mia, S., Warnecke, A., Zhang, X.-M., Malmström, V. & Harris, R. A. An optimized Protocol for Human M2 Macrophages using M-CSF and IL-4/IL-10/TGF-*β* Yields a Dominant Immunosuppressive Phenotype. *Scand. J. Immunol.* **79,** 305–314 (2014).

452. Gordon, S., Plüddemann, A. & Martinez Estrada, F. Macrophage

heterogeneity in tissues: phenotypic diversity and functions. *Immunol. Rev.* **262,** 36–55 (2014).

453. Haim, Y. O., Unger, N. D., Souroujon, M. C., Mittelman, M. & Neumann, D. Resistance of LPS-activated bone marrow derived macrophages to apoptosis mediated by dexamethasone. *Sci. Rep.* **4,** 4323 (2015).

454. Porcheray, F. *et al.* Macrophage activation switching: an asset for the resolution of inflammation. *Clin. Exp. Immunol.* **142,** 481–9 (2005).

455. Vallelian, F. *et al.* Glucocorticoid Treatment Skews Human Monocyte Differentiation into a Hemoglobin- Clearance Phenotype with Enhanced Heme-Iron Recycling and Antioxidant Capacity. (2010). doi:10.1182/blood-2010-04-277319

456. Franzen, C. A. *et al.* Characterization of uptake and internalization of exosomes by bladder cancer cells. *Biomed Res. Int.* **2014,** 619829 (2014).

457. Huang, J. & Brumell, J. H. Bacteria–autophagy interplay: a battle for survival. *Nat. Rev. Microbiol.* **12,** 101–114 (2014).

458. Poss, K. D. & Tonegawa, S. Heme oxygenase 1 is required for mammalian iron reutilization. *Proc. Natl. Acad. Sci. U. S. A.* **94,** 10919–24 (1997).

459. Grant, B. D. & Donaldson, J. G. Pathways and mechanisms of endocytic recycling. *Nat. Rev. Mol. Cell Biol.* **10,** 597–608 (2009).

460. Lewis, B. P., Burge, C. B. & Bartel, D. P. Conserved Seed Pairing, Often Flanked by Adenosines, Indicates that Thousands of Human Genes are MicroRNA Targets. *Cell* **120,** 15–20 (2005).

461. Maragkakis, M. *et al.* DIANA-microT web server: elucidating microRNA functions through target prediction. *Nucleic Acids Res.* **37,** W273-6 (2009).

462. Crawford, R. M., Finbloom, D. S., Ohara, J., Paul, W. E. & Meltzer, M. S. B cell stimulatory factor-1 (interleukin 4) activates macrophages for increased tumoricidal activity and expression of Ia antigens. *J. Immunol.* **139,** 135–41 (1987).

463. Fabriek, B. O. *et al.* The macrophage CD163 surface glycoprotein is an erythroblast adhesion receptor. *Blood* **109,** 5223-5229 (2007).

464. Graversen, J. H., Madsen, M. & Moestrup, S. K. CD163: a signal receptor scavenging haptoglobin-hemoglobin complexes from plasma. *Int. J. Biochem. Cell Biol.* **34,** 309-14 (2002).

465. Falchi, M. *et al.* Dexamethasone targeted directly to macrophages induces macrophage niches that promote erythroid expansion. *Haematologica* **100,** 178–187 (2015).

466. Zizzo, G., Hilliard, B. A., Monestier, M. & Cohen, P. L. Efficient Clearance of Early Apoptotic Cells by Human Macrophages Requires M2c Polarization and MerTK Induction. *J. Immunol.* **189,** 3508-3520 (2012).

467. Meckes, D. G. *et al.* Human tumor virus utilizes exosomes for intercellular communication. *Proc. Natl. Acad. Sci.* **107,** 20370-20375 (2010).

468. Keller, S. *et al.* Systemic presence and tumor-growth promoting effect of ovarian carcinoma released exosomes. *Cancer Lett.* **278,** 73–81 (2009).

469. Svensson, K. J. *et al.* Exosome Uptake Depends on ERK1/2-Heat Shock Protein 27 Signaling and Lipid Raft-mediated Endocytosis Negatively Regulated by Caveolin-1. *J. Biol. Chem.* **288,** 17713–17724 (2013).

470. Hazan-Halevy, I. *et al.* Cell-specific uptake of mantle cell lymphoma-derived exosomes by malignant and non-malignant B-lymphocytes. *Cancer Lett.* **364,** 59-69 (2015).

471. Tian, T. *et al.* Exosome Uptake through Clathrin-mediated Endocytosis and Macropinocytosis and Mediating miR-21 Delivery. *J. Biol. Chem.* **289,** 22258-22267 (2014).

472. DAVEY, M. G. & LANDER, H. THE LABELLING OF HUMAN PLATELETS WITH RADIOCHROMATE. *Aust. J. Exp. Biol. Med. Sci.* **41,** 581–93 (1963).

473. Pierzyńska-Mach, A., Janowski, P. A. & Dobrucki, J. W. Evaluation of acridine orange, LysoTracker Red, and quinacrine as fluorescent probes for long-term tracking of acidic vesicles. *Cytom. Part A* **85,** 729–737 (2014).

474. Moriyama, Y., Takano, T. & Ohkuma, S. Acridine Orange as a Fluorescent Probe for Lysosomal Prot on Pump1. *Commun. J. Biochem* **92,** 1333–1336 (1982).

475. Bray, N. L., Pimentel, H., Melsted, P. & Pachter, L. Near-optimal probabilistic RNA-seq quantification. *Nat. Biotechnol.* **34,** 525–527 (2016).

476. Love, M. I., Huber, W. & Anders, S. Moderated estimation of fold change and dispersion for RNA-seq data with DESeq2. *Genome Biol.* **15,** 550 (2014).

477. Metsalu, T. & Vilo, J. ClustVis: a web tool for visualizing clustering of multivariate data using Principal Component Analysis and heatmap. *Nucleic Acids Res.* **43,** W566–W570 (2015).

478. Luo, W., Friedman, M. S., Shedden, K., Hankenson, K. D. & Woolf, P. J. GAGE: generally applicable gene set enrichment for pathway analysis. *BMC Bioinformatics* **10,** 161 (2009).

479. Luo, W. & Brouwer, C. Pathview: an R/Bioconductor package for pathway-based data integration and visualization. *Bioinformatics* **29,** 1830–1831 (2013).

480. Kristiansen, M. *et al.* Identification of the haemoglobin scavenger receptor. *Nature* **409,** 198–201 (2001).

481. Cao, W., Lee, S. H. & Lu, J. CD83 is preformed inside monocytes, macrophages and dendritic cells, but it is only stably expressed on activated dendritic cells. *Biochem. J.* **385,** 85–93 (2005).

482. Tze, L. E. *et al.* CD83 increases MHC II and CD86 on dendritic cells by opposing IL-10–driven MARCH1-mediated ubiquitination and degradation. *J. Exp. Med.* **208,** 149–165 (2011).

483. Dong, L., Wang, S., Chen, M., Li, H. & Bi, W. The Activation of Macrophage and Upregulation of CD40 Costimulatory Molecule in Lipopolysaccharide-Induced Acute Lung Injury. *J. Biomed. Biotechnol.* **2008,** 1–6 (2008).

484. Rodriguez-Garcia, M. *et al.* Expression of PD-L1 and PD-L2 on human macrophages is up-regulated by HIV-1 and differentially modulated by IL-10. *J. Leukoc. Biol.* **89,** 507–515 (2011).

485. Simhadri, V. R., Mariano, J. L., Gil-Krzewska, A., Zhou, Q. & Borrego, F. CD300c is an Activating Receptor Expressed on Human Monocytes. *J. Innate Immun.* **5,** 389–400 (2013).

486. Zhang, G. *et al.* Soluble CD276 (B7-H3) is released from monocytes, dendritic cells and activated T cells and is detectable in normal human serum. *Immunology* **123,** 538–546 (2008).

487. Zhang, G. *et al.* B7-H3 Augments the Inflammatory Response and Is Associated with Human Sepsis. *J. Immunol.* **185,** 3677–3684 (2010).

488. Adachi, T., Wakabayashi, C., Nakayama, T., Yakura, H. & Tsubata, T. CD72 negatively regulates signaling through the antigen receptor of B cells. *J. Immunol.* **164,** 1223–9 (2000).

489. Liu, J. *et al.* The complement inhibitory protein DAF (CD55) suppresses T cell immunity in vivo. *J. Exp. Med.* **201,** 567–77 (2005).

490. Winkels, H. *et al.* CD70 limits atherosclerosis and promotes macrophage function. *Thromb. Haemost.* **117,** 164–175 (2016).

491. Sadler, A. J. & Williams, B. R. G. Interferon-inducible antiviral effectors.

Nat. Rev. Immunol. **8,** 559–568 (2008).

492. Mellor, H. The role of formins in filopodia formation. *Biochim. Biophys. Acta - Mol. Cell Res.* **1803,** 191–200 (2010).

493. Naj, X., Hoffmann, A.-K., Himmel, M. & Linder, S. The Formins FMNL1 and mDia1 Regulate Coiling Phagocytosis of Borrelia burgdorferi by Primary Human Macrophages. *Infect. Immun.* **81,** 1683–1695 (2013).

494. Chinenov, Y., Coppo, M., Gupte, R., Sacta, M. A. & Rogatsky, I. Glucocorticoid receptor coordinates transcription factor-dominated regulatory network in macrophages. *BMC Genomics* **15,** 656 (2014).

495. Kume, N. *et al.* Inducible expression of LOX-1, a novel receptor for oxidized LDL, in macrophages and vascular smooth muscle cells. *Ann. N. Y. Acad. Sci.* **902,** 323-7 (2000).

496. Wortham, B. W. *et al.* Cutting Edge: CLEC5A Mediates Macrophage Function and Chronic Obstructive Pulmonary Disease Pathologies. *J. Immunol.* **196,** 3227–3231 (2016).

497. Nicholls, S. E., Winter, S., Mottram, R., Miyan, J. A. & Whetton, A. D. Flt3 ligand can promote survival and macrophage development without proliferation in myeloid progenitor cells. *Exp. Hematol.* **27,** 663–72 (1999).

498. Byles, V. *et al.* The TSC-mTOR pathway regulates macrophage polarization. *Nat. Commun.* **4,** 2834 (2013).

499. Gharibi, B., Ghuman, M. & Hughes, F. J. DDIT4 regulates mesenchymal stem cell fate by mediating between HIF1α and mTOR signalling. *Sci. Rep.* **6,** 36889 (2016).

500. Lau, S. K., Chu, P. G. & Weiss, L. M. CD163: A Specific Marker of Macrophages in Paraffin-Embedded Tissue Samples. *Am. J. Clin. Pathol.* **122,** 794-801 (2004).

501. Azad, A. K. *et al.* γ-Tilmanocept, a New Radiopharmaceutical Tracer for Cancer Sentinel Lymph Nodes, Binds to the Mannose Receptor (CD206). *J. Immunol.* **195,** 2019–2029 (2015).

502. Gadd, V. L. *et al.* Portal, but not lobular, macrophages express matrix metalloproteinase-9: association with the ductular reaction and fibrosis in chronic hepatitis C. *Liver Int.* **33,** 569–579 (2013).

503. Gebelein, C. G. & Carraher, C. E. *Polymeric materials in medication.* (Plenum Press, 1985).

504. Nielsen, M. J., Madsen, M., Møller, H. J. & Moestrup, S. K. The macrophage scavenger receptor CD163: endocytic properties of cytoplasmic tail variants. *J. Leukoc. Biol.* **79,** 837–845 (2006).

505. Martínez, V. G., Moestrup, S. K., Holmskov, U., Mollenhauer, J. & Lozano, F. The conserved scavenger receptor cysteine-rich superfamily in therapy and diagnosis. *Pharmacol. Rev.* **63,** 967–1000 (2011).

506. Moriyama, T. *et al.* MicroRNA-21 modulates biological functions of pancreatic cancer cells including their proliferation, invasion, and chemoresistance. *Mol. Cancer Ther.* **8,** 1067–1074 (2009).

507. Nan, Y. *et al.* MiRNA-451 plays a role as tumor suppressor in human glioma cells. *Brain Res.* **1359,** 14–21 (2010).

508. Godlewski, J. *et al.* MicroRNA-451 Regulates LKB1/AMPK Signaling and Allows Adaptation to Metabolic Stress in Glioma Cells. *Mol. Cell* **37,** 620–632 (2010).

509. Gabriely, G. *et al.* MicroRNA 21 Promotes Glioma Invasion by Targeting Matrix Metalloproteinase Regulators. *Mol. Cell. Biol.* **28,** 5369–5380 (2008).

510. Heddle, N. M. *et al.* Effect of Short-Term vs. Long-Term Blood Storage on Mortality after Transfusion. *N. Engl. J. Med.* **375,** 1937–1945 (2016).

511. Sanyal, R. *et al.* MS4A4A: a novel cell surface marker for M2 macrophages and plasma cells. *Immunol. Cell Biol.* **95,** 611–619 (2017).
512. Cruse, G. *et al.* The CD20 homologue MS4A4 directs trafficking of KIT toward clathrin-independent endocytosis pathways and thus regulates receptor signaling and recycling. *Mol. Biol. Cell* **26,** 1711–1727 (2015).
513. Walsh, K. A., Ericsson, L. H., Parmelee, D. C. & Titani, K. ADVANCES IN PROTEIN SEQUENCING. *Ann. Rev. Biochem* 5–261 (1981).
514. Cooper, D. J. *et al.* Age of Red Cells for Transfusion and Outcomes in Critically Ill Adults. *N. Engl. J. Med.* NEJMoa1707572 (2017). doi:10.1056/NEJMoa1707572
515. Wynn, T. A., Chawla, A. & Pollard, J. W. Macrophage biology in development, homeostasis and disease. *Nature* **496,** 445–455 (2013).